The role of 14q32 microRNAs in vascular remodelling

Welten, S.M.J.

The role of 14q32 microRNAs in vascular remodelling

Sabine Welten

Cover: Immunofluorescent staining of aortic sprouts in murine aortic ring assay
Printing: Ridderprint BV, The Netherlands
ISBN: 978-94-6299-526-0

The role of 14q32 microRNAs in vascular remodelling

Proefschrift

ter verkrijging van
de graad van Doctor aan de Universiteit Leiden,
op gezag van Rector Magnificus prof. mr. C.J.J.M. Stolker,
volgens besluit van het College voor Promoties
te verdedigen op 9 maart 2017
klokke 16.15 uur

door

Sabine Marlies Janine Welten

Geboren te Amsterdam in 1988

Promotor:	Prof. dr. P.H.A. Quax
Co-promotor:	Dr. A.Y. Nossent
Leden Promotiecommissie:	Prof. dr. H.C.J. Eikenboom Prof. dr. J.W. Jukema Prof. dr. M.J.T.H. Goumans Prof. dr. C.J.M. de Vries (AMC, Amsterdam) Dr. R.A. Boon (Goethe Universität, Frankfurt am Main)

The research described in this thesis was supported by the Netherlands Institute for Regenerative Medicine (NIRM, FES0908) and was performed at the department of Vascular Surgery, Leiden University Medical Center, Leiden, The Netherlands.

Table of contents

Part IV

Chapter 1

General introduction and outline of thesis

General Introduction

The vasculature consists of all the blood vessels that supply our organs with oxygen and nutrients. In addition, waste products are removed from our organs via these blood vessels. The vasculature is able to respond to certain stimuli. For example, if there is an increase in demand for oxygen, certain new blood vessels can arise. Unfortunately, blood vessels can also become clogged due to the build-up of cholesterol and fat within the vessel wall. The response of the vasculature to certain stimuli is called vascular remodelling. In this thesis, we investigate the effect of small molecules, called microRNAs, on different processes of vascular remodelling.

Vascular remodelling

The vasculature is an active organ which is capable of sensing and adapting to environmental stimuli such as hemodynamic changes. Vascular remodelling is the structural alteration of the vessel wall, which involves cell growth, cell death, cell migration and extracellular matrix rearrangements, driven by environmental changes[1]. This can be either adaptive (e.g increased neovascularization upon ischemia) or maladaptive (e.g. atherosclerosis and restenosis). The arterial wall consists of three layers, namely the tunica intima containing endothelial cells, the tunica media consisting mainly of smooth muscle cells and the tunica adventitia which is the outer layer containing fibroblasts and extracellular matrix that is rich in collagen. The endothelium plays a prominent part in vascular remodelling, as it is located at the inner layer of the vasculature and capable of sensing changes in blood flow, inflammatory mediators, cytokines and chemokines. Activated endothelium can subsequently lead to changes in the tunica media and tunica adventitia, driving vascular remodelling.

Angiogenesis and arteriogenesis

Angiogenesis and arteriogenesis are both mechanisms of neovascularisation through which blood vessels arise that can restore blood flow after an ischemic event. Angiogenesis describes the sprouting of capillaries from pre-existing blood vessels, driven by ischemic and hypoxic signals[2]. Upon ischemia, the transcription factor hypoxia inducible factor 1α (HIF1α) becomes available and drives transcription of pro-angiogenic factors such as vascular endothelial growth factor (VEGF). In response to VEGF, vascular permeability increases. Proteases such as the urokinase plasminogen activator (uPA) and matrix metalloproteinases (MMPs) degrade the extracellular matrix and release growth factors such as bFGF and VEGF which are embedded within the ECM[3, 4]. Subsequently, endothelial migration is facilitated by tip and stalk cells, which form the native, tube like structures (Figure 1A). Tip cells contain filopodia that sense chemotactic guidance cues (such as ephrins and semaphorins). Stalk cells following the tip cells will proliferate and form a lumen through which blood can be transported. Fusion of tip cells with other capillary networks is aided by recruited myeloid cells, allowing for perfusion of the neovessel[4]. Finally, pericytes are being recruited to provide support to the newly formed capillaries by laying down a basement membrane. Angiogenesis is not always beneficial, as it can facilitate tumour growth and metastasis[5] as well as accelerate atherosclerosis[6].

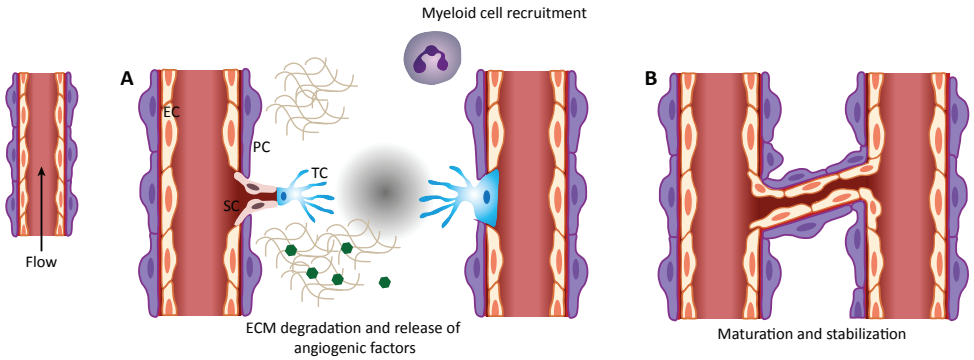

Figure 1. During ischemia, pro-angiogenic factors such as VEGF cause vascular permeability. Degradation of the basement membrane is followed by loosening of endothelial cell (EC) junctions and pericyte (PC) contact. Next, tip cells (TC) will sprout from the existing blood vessel (**A**). Proteases cause degradation of the extracellular matrix, releasing growth factors (in green) embedded within the matrix. Tip cells extend their filopodia to detect chemotactic guidance cues and adhere to the extracellular matrix to migrate. Stalk cells (SC) follow these tip cells and form a lumen. Fusion of tip cells with other capillary networks is aided by recruited myeloid cells. (**B**). Blood can now flow through the neovessel, allowing for re-establishment of the basement membrane and endothelial cell junctions, recruitment of pericytes and maturation of the newly formed capillary network.

In arteriogenesis, pre-existing arteriolar anastomoses enlarge to form collateral arteries. Collateral artery formation is driven by changes in shear stress rather than oxygen levels[7]. Mature collateral vessels can compensate flow deficits caused by major arterial obstructions, whereas the formation of new capillaries by angiogenesis is often not sufficient to restore blood flow and oxygen levels in the affected area. Under normal conditions, there is only a minimal net flow in the arteriolar anastomoses, due to a high resistance within these anastomoses. However, a sudden occlusion of a major artery results in an increased pressure gradient over the anastomoses. Blood flow is redistributed through the pre-existent collateral arterioles, which increases the fluid shear stress to the vascular wall. Increased shear stress activates endothelial cells, which upregulate the expression of cell adhesion molecules (such as VCAM-1) on their surface. The endothelium produces cytokines, such as MCP-1, and releases nitric oxide (NO). The expression of adhesion molecules and release of cytokines lead to the attraction, adhesion and invasion of monocytes into the collateral wall[8, 9]. Several inflammatory cell types have been demonstrated to play a role in arteriogenesis; monocytes and NK cells are thought to play a role in the early phases of collateral artery growth, whereas a variety of T-cell subsets have been found to play a role in a subsequent later phase[10].

After infiltration and maturation of monocytes into macrophages, these cells will produce additional growth factors and cytokines, contributing to the inflammatory environment of the arterioles. Matrix metalloproteinases (MMPs) produced by macrophages, will degrade the extracellular matrix, creating space for the expansion of growing collaterals. Smooth muscle cells are now activated and will start to proliferate. In addition, remodelling of the adventitial layer is established through activation and proliferation of fibroblasts, the expression of growth factors and extracellular proteolysis. Finally, enlargement of the collateral artery diameter is established and blood flow to distal tissues is (partially) restored (Figure 2)[8].

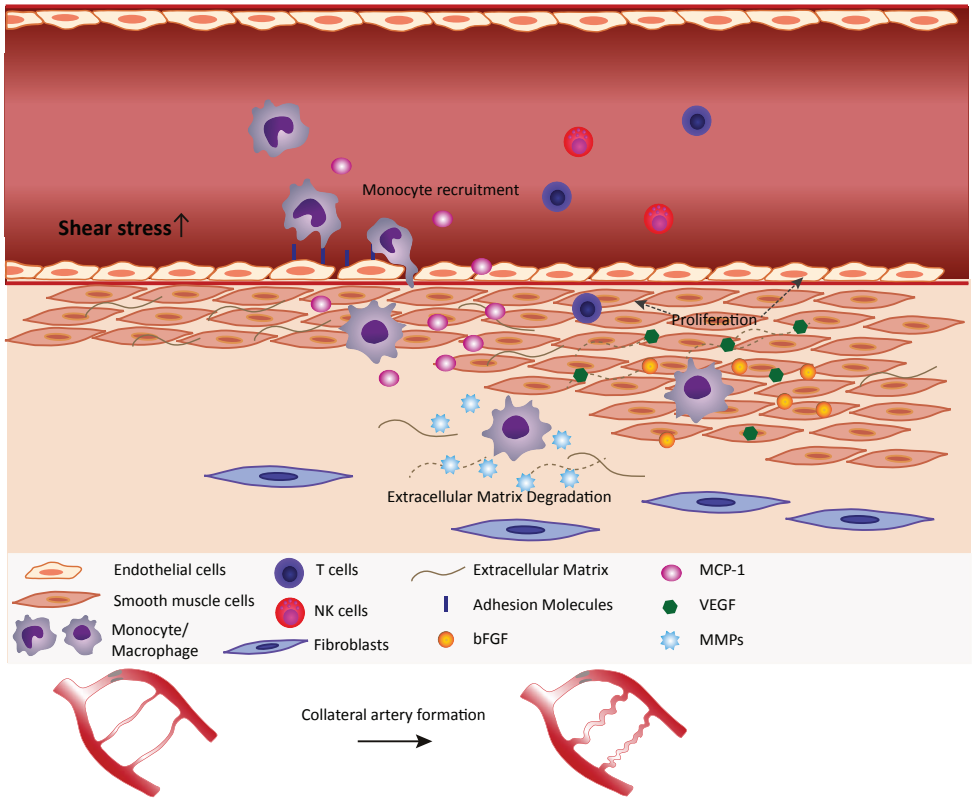

Figure 2. Upon increased shear stress, endothelial cells are activated and the expression of adhesion molecules is upregulated. Cytokines released by the endothelium will attract and recruit inflammatory cells, such as monocytes, to the vessel wall. Once invaded into the vessel wall, monocytes will differentiate into macrophages and release growth factors, matrix metalloproteinases (MMPs) and cytokines. Subsequently, other inflammatory cells are recruited, extracellular matrix is degraded by MMPs and smooth muscle cells, endothelial cells and fibroblasts will start to proliferate, resulting in collateral growth.

Atherosclerosis and post-interventional restenosis

The most common cause underlying cardiovascular diseases is atherosclerosis, the build-up of plaques in the inner walls of the arteries. Atherosclerosis is a chronic, multifactorial disease in which multiple inflammatory processes and changes in cholesterol homeostasis play a role.[11] The formation of early fatty streaks starts at sites of damaged or activated endothelium caused by for example dyslipidemia, disturbed flow or hypertension. The activated endothelium increases expression of adhesion molecules such as VCAM-1 and selectins. Circulating monocytes subsequently adhere and infiltrate into the arterial wall. Monocytes will then differentiate into macrophages, which are able to take up lipids via their scavenger receptors, contributing to the formation of foam cells and early atherosclerotic lesions[12]. The continued influx and activation of inflammatory cells such as monocytes, T cells and mast cells results in the progression of atherosclerosis[13, 14]. The recognition of modified lipids (such as oxidized LDL), parts of damaged cells, or modified matrix components by immune cells, by pattern recognition receptors such as Toll-like receptors (TLRs) results in a chronic inflammatory state of the affected vessel area. Additionally, the release of cytokines and growth factors stimulates smooth muscle cells, which start to proliferate and migrate into the intima.

Here, smooth muscle cells will produce collagen and other extracellular matrix components, forming a fibrous cap[15]. Over time, cellular apoptosis can lead to the formation of a necrotic core containing cellular debris and cholesterol crystals. Atherosclerotic plaques can remain stable and asymptomatic for years as long as the lesions contain a thick fibrous cap and lumen area is preserved[16]. However, progression in growth of the atherosclerotic plaque will eventually lead to narrowing of the lumen, limiting blood flow and oxygen supply towards distal tissues. Moreover, unstable lesions containing a large necrotic core and thin fibrous cap are prone to rupture. Plaque rupture will expose the pro-thrombotic necrotic core to the blood, causing platelet aggregation, the formation of blood clots and result in occlusive thrombus formation[17]. These thrombi can cause an ischemic stroke or myocardial infarction and thus require surgical intervention to re-open the vessel or thrombolytic therapy to dissolve the blood clot and restore blood flow (Figure 3).

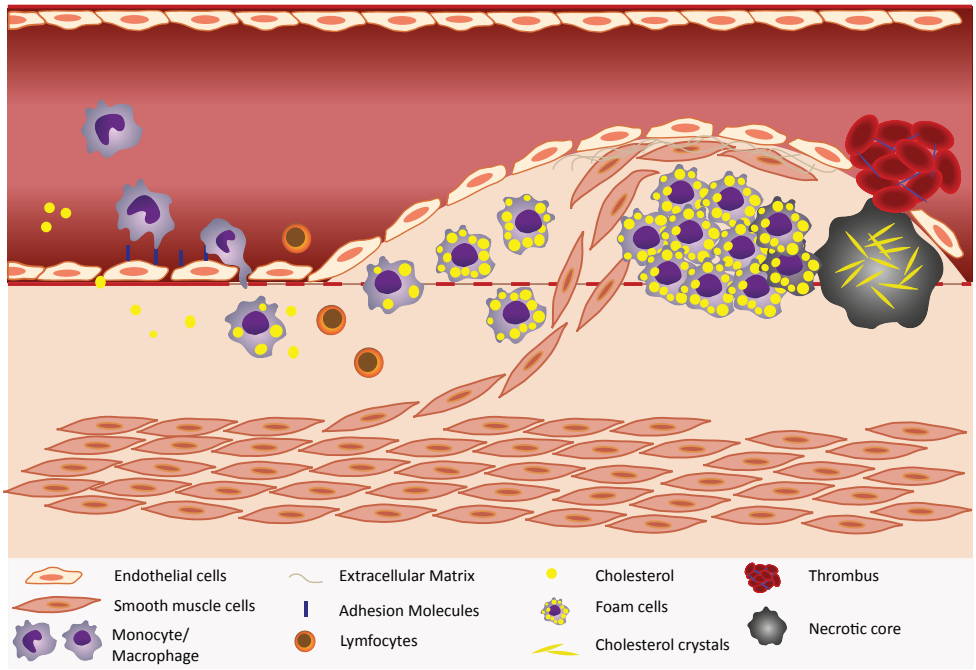

Figure 3. Formation of an atherosclerotic plaque from left to right. Influx of LDL cholesterol into the vessel wall leads to activation of the endothelium and upregulation of adhesion molecules. Subsequently, monocytes and other inflammatory cells are recruited to the vessel wall and migrate into the intima. Within the intima, macrophages will take up lipids via their scavenger receptors and contribute to the formation of fatty streaks. Plaque progression continues with the migration and proliferation of smooth muscle cells which start to produce collagen and extracellular matrix. A stable plaque contains a thick fibrous cap and is rich in smooth muscle cells, whereas unstable plaques are rich in foam cells and have a weak fibrous cap, making it prone to rupture. Upon rupture, thrombus formation occurs, which can lead to complications.

Endovascular interventions, such as balloon angioplasty with or without stenting, can be performed to restore blood flow arteries occluded by atherosclerotic lesions. Unfortunately, success of this strategy is limited by the fact that a significant number of patients experiences renewed obstruction of the re-opened vessels. Vascular damage inflicted by balloon angioplasty generates a local inflammatory reaction, resulting in restenosis of the artery. Restenosis consists of both intimal hyperplasia

and accelerated atherosclerosis[18]. Intimal hyperplasia is characterized by rearrangements of the extracellular matrix, proliferation and migration of smooth muscle cells and inflammation. On top of that, accelerated atherosclerosis is observed under hypercholesterolemic conditions, which results in the uptake of lipids by macrophages in the vessel wall and the subsequent formation of foam cells.

In vivo mouse models for vascular remodelling

The contribution of different molecules, growth factors or cells to vascular remodelling can be studied using experimental mouse models. Here, I discuss those mouse models that were used in this thesis.

Both angiogenesis and arteriogenesis can be studied using models in which hind limb ischemia is induced. Single ligation of the left femoral artery in C57BL/6 mice is often used to study factors that are regulated during neovascularization. Generally, C57BL/6 mice have a good angiogenic and arteriogenic response and blood flow is restored within 7 days after single ligation of the femoral artery. Therefore, intervention studies are done in a model for hind limb ischemia where double ligation of the left femoral artery is performed, as this model provides a substantial therapeutic window which is optimal for testing new therapeutic approaches. In the adductor muscle, increased shear stress over pre-existent arterioles leads to arteriogenesis, whereas in the distal gastrocnemius and soleus muscles, local ischemia induces angiogenesis.

Different models are used to study atherosclerosis formation in mice. One such model is the carotid collar model. In this model, a semi-constrictive collar is placed around the carotid arteries of hypercholesterolemic ApoE$^{-/-}$ mice. Low shear stress and disturbed flow proximal to the site of collar placement results in endothelial activation and to atherosclerotic lesion formation. Already four weeks after collar placement, these lesions can be evaluated for numerous parameters, such as necrotic core, collagen content, smooth muscle cells, inflammatory cells, etc.

The femoral artery cuff model is a suitable model to study post-interventional neointimal hyperplasia. In this model a non-constrictive collar is placed around the femoral artery of mice. The use of this model in either normocholesterolemic C57BL/6 mice or hypercholesterolemic mice allow us to study the contribution of smooth muscle cells, macrophages and other inflammatory cells to this process.

Non-coding RNAs

Non coding RNAs include all functional RNA molecules that are not transcribed and translated into functional proteins. This class of RNA molecules includes, amongst others, transfer RNAs (tRNAs), ribosomal RNAs (rRNAs), small nuclear RNAs (snRNAs), small nucleolar RNAs (snoRNAs), small interfering RNAs (siRNAs), microRNAs, and long non-coding RNAs (lncRNAs). Most of these RNAs are involved in the regulation of other RNAs, such as snRNAs, which regulate splicing and snoRNAs, which modify rRNAs. Other RNAs are involved in gene regulation, called RNA interference (RNAi). These RNAs include microRNAs, siRNAs and lncRNAs[19].

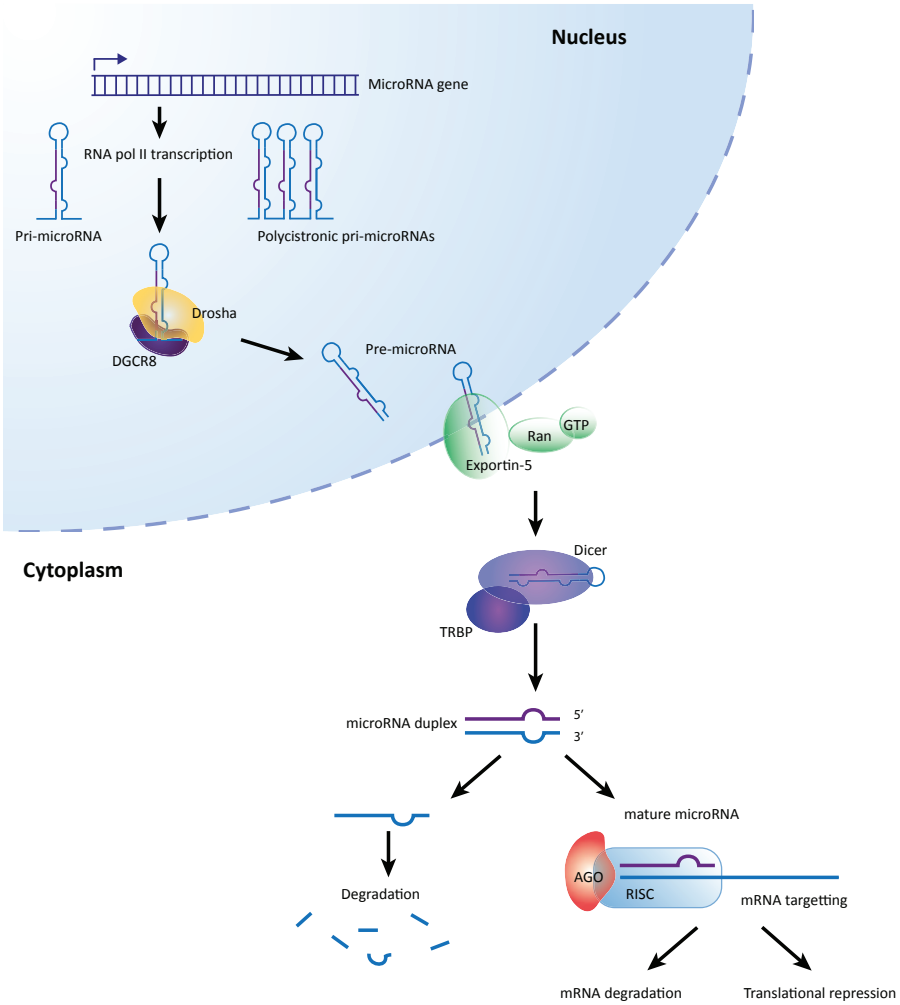

Figure 4. Biogenesis of microRNAs. Primary microRNAs are transcribed from individual microRNA genes, from introns of protein coding genes or from polycistronic transcripts by RNA polymerase II. These pri-microRNAs are processed by Drosha to form pre-microRNAs of approximately 70-100 nucleotides long. After transportation by Exportin-5 to the cytoplasm, pre-microRNAs are cleaved by Dicer into microRNA duplexes. One of the mature microRNA strands is then incorporated into the RISC complex, whereas the other strand is degraded or loaded into its own RICS complex. Mature microRNAs regulate gene expression via translational repression or mRNA degradation of their target mRNA.

MicroRNAs and their role in vascular remodelling

MicroRNAs are short endogenous RNA molecules of ~22 nucleotides long that regulate gene expression. MicroRNA genes are located either intergenic or intragenic (within introns of coding or noncoding genes). Some microRNAs have their own promoters and are expressed independently, while other microRNAs are organized in clusters and share the same transcriptional regulation[20]. MicroRNA genes are transcribed as primary microRNAs (pri-microRNAs) by RNA polymerase II and form stem-loop structures (Figure 4)[21]. These pri-microRNAs enter a nuclear complex consisting of Drosha (RNAse III enzyme) and cofactor DGCR8, where they are cleaved to form pre-microRNAs of about 70 nucleotides long[22]. Pre-microRNAs are transported to the cytoplasm by Exportin-5, where

they are processed by the enzyme Dicer into mature microRNA duplexes. From this microRNA duplex, one strand (the guide strand)is generally preferred for association with an Argonaute (AGO) protein and incorporation into the RNA induced silencing complex (RISC), whereas the other strand (the passenger strand) is rapidly removed and degraded[23]. However, accumulating evidence suggests that the passenger strand can also be loaded into the RICS[24, 25]. Mature microRNAs guide the RISC complex to target sites in the 3' untranslated region of their target mRNAs. Binding of a microRNA to the 3' UTR of a target mRNA can either lead to degradation of the mRNA or lead to translational repression of the mRNA target[26]. Messenger RNA degradation is usually seen in plant cells and takes place when microRNA binding occurs with perfect complementarity to the mRNA target. Either way, binding of a microRNA to the 3' UTR of a target mRNA leads to downregulation of the expression of that gene. The first 2 to 8 nucleotides from the 5' portion of a microRNA, is important for target recognition and is referred to as the seed sequence of the microRNA[26].

During development, many microRNAs are expressed in a tissue specific manner, suggesting the involvement of microRNAs in determining and maintaining tissue identity[27]. Each microRNA has the ability to regulate hundreds of targets and by doing so, specific microRNAs can regulate complex, multifactorial physiological processes such as vascular remodelling. The development and progression of cardiovascular disease has been linked to the dysregulation of many individual microRNAs and multiple microRNAs have been found to be modulators of atherosclerosis, lipoprotein metabolism, inflammation and vascular remodelling[28]. For example, the miR-33 family consisting of miR-33a/b, targets the cholesterol transporter ABCA1 and inhibition of miR-33a/b reduced *in vivo* progression of atherosclerotic plaque formation[29]. The miR-17-92 gene cluster has a well described role in angiogenesis, as well as arteriogenesis[30, 31]. In addition, microRNAs from this cluster contribute to atherosclerosis and neointima formation[32, 33].

The 14q32 non-coding RNA cluster

The 14q32 genomic region is located on human chromosome 14, chromosome 12F1 in mice. This region hosts one of the largest microRNA clusters in the genome, containing 54 microRNAs and is highly conserved in mammals[43]. Extensive hypomethylation of the 14q32 locus was observed in human atherosclerotic plaques, which resulted in upregulation of 14q32 microRNAs and suggesting a role for epigenetic modulation of the 14q32 microRNA cluster in atherosclerosis[44].
In addition, the human 14q32 locus contains three lncRNAs and 41 snoRNAs (Figure 5). MEG3, one of the 14q32 lncRNAs, is upregulated in endothelial cells under hypoxia[37]. Deletion of MEG3 in mice (MEG3$^{-/-}$ mice) leads to increased VEGF expression and cortical microvessel density in these animals[45].
The 14q32 snoRNAs are orphan snoRNAs of the C/D box subtype and can be divided into three highly related copy-sets, namely SNORD112 (1 copy), SNORD113 (9 copies) and SNORD114 (31 copies).

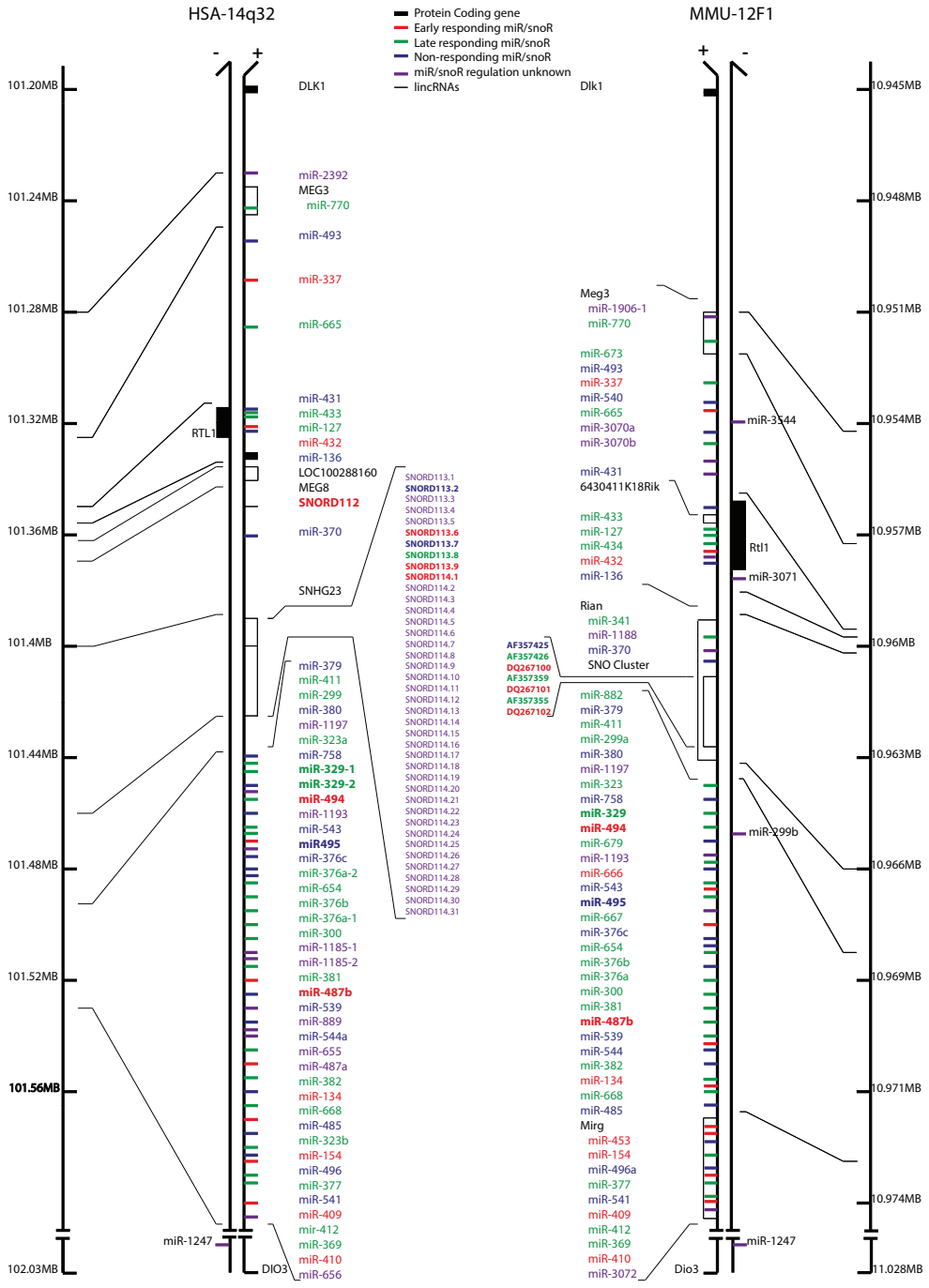

Figure 5. A schematic overview of the human 14q32 and murine 12F1 locus. In humans, the 14q32 locus contains 54 microRNAs, 3 lncRNAs (MEG3, MEG8 and SNHG23) and 41 snoRNAs to date. In mice, the cluster contains 61 microRNAs, 2 lcnRNAs (Meg3 and Rian) and 7 snoRNAs. Colors indicate whether murine microRNAs were early (red), late (green) or non-responders (blue) after hind limb ischemia in mice. Coding (thick bars) and noncoding (thin bars) genes are indicated in black.

Outline of this thesis

The aim of this thesis is to investigate the role of 14q32 microRNAs in vascular remodelling, as well as to identify microRNAs as new therapeutic targets for the treatment of cardiovascular diseases.

The first part of this thesis focuses on the role of microRNAs in vascular remodelling and in particular that of microRNAs from the 14q32 cluster, by studying their involvement in arteriogenesis and angiogenesis, atherosclerosis and restenosis.

Chapter 2 reviews the multifactorial nature of microRNAs in the vasculature, emphasizing the multiple roles microRNAs can have in different forms of vascular remodelling. Often, the effect of microRNA manipulation is ascribed to regulation of a single target gene. However, it should be taken into account that microRNAs are able to target numerous genes and modulation of a single microRNA can have diverse effects in different disease models.

Chapter 3 describes the use of a Reversed Target Prediction (RTP) strategy to identify microRNAs that affect arteriogenesis and angiogenesis. In this chapter, we report the role of 14q32 microRNAs miR-329, miR-487b, miR-494 and miR-495 in post-ischemic blood flow recovery. Upregulation of microRNAs from the 14q32 cluster was observed after single ligation of the femoral artery, following three different expression patterns (Figure 5). Selecting microRNAs from each expression pattern (miR-329 as a late responder, miR-487b and miR-494 as early responders and miR-495 as non-responder), we demonstrated increased blood flow recovery and neovascularization after inhibition of these microRNAs using Gene Silencing Oligonucleotides (GSOs) in an hind limb ischemia model.

In **Chapter 4**, we made use of the same RTP strategy to identify microRNAs that could affect atherosclerosis. Again, the 14q32 cluster was predicted to target genes that influence atherosclerosis. We observed increased expression of 14q32 microRNA miR-494 in unstable human atherosclerotic plaques compared to stable lesions. Inhibition of miR-494 in the carotid collar model for atherosclerosis resulted in reduced lesion formation, while plaque stability was increased. Multiple target genes of miR-494 were upregulated both *in vitro* and *in vivo*.

In **Chapter 5** the role of 14q32 microRNAs in post-interventional vascular remodelling or restenosis is investigated. Restenosis consist of intimal hyperplasia and accelerated atherosclerosis. Non-constrictive cuffs were placed around the femoral artery of mice to induce intimal hyperplasia. Accelerated atherosclerosis was induced in hypercholesterolemic ApoE mice by placing semi-constrictive collars around both carotid arteries. GSOs against miR-329, miR-494 and miR-495 were used to inhibit these microRNAs in both experimental models for restenosis. GSO-495 treated animals showed decreased intimal hyperplasia compared to control animals after cuff placement, whereas GSO-329 and GSO-494 treatment had less profound effects on intimal hyperplasia. In the accelerated atherosclerosis model, GSO-495 treatment resulted in smaller atherosclerotic lesions which had smaller necrotic cores and increased collagen content.

The second part of this thesis investigates the (post)transcriptional regulation of 14q32 microRNA expression.

Chapter 6 focuses on Myocyte Enhancer Factor 2a (MEF2a) in post-ischemic neovascularization. A recent study showed transcriptional regulation of the 14q32 region by MEF2a[46]. Therefore, we hypothesized that inhibition of MEF2a could improve post-ischemic neovascularization via inhibition of 14q32 microRNAs. Indeed, GSO-Mef2a treatment led to improved blood flow recovery and increased arteriogenesis and angiogenesis after hind limb ischemia in mice. Moreover, reduced expression of 14q32 microRNAs miR-329 and miR-494 was observed in these animals, which could partially explain the observed effects. However, we could not confirm transcriptional regulation of 14q32 microRNAs by Mef2a, but we did show that Mef2a could act as RNA binding protein, regulating the expression of 14q32 microRNAs at the post-transcriptional level.
In **Chapter 7**, we zoom in on the differential expression of 14q32 microRNAs observed after ischemia. By evaluating the expression levels of pri-microRNAs, pre-microRNAs and mature microRNAs after induction of ischemia, we found clues that the differential regulation of these microRNAs occurs from pre-microRNA to mature microRNA processing. Using Stable Isotope Labelling of Amino Acids (SILAC), followed by RNA pull down and Mass Spectrometry on 3T3 cells under serum starvation, we determined which RNA-Binding Proteins (RBPs) are responsible for the differential post-transcriptional regulation of 14q32 microRNAs. We identified CIRBP and HADHB as post-transcriptional regulators of 14q32 microRNA miIR-329 expression under ischemia.

In the third and last part of this thesis, the expression of microRNAs in subcutaneous adipose tissue of critical limb ischemia patients is discussed and the potential use of microRNAs as biomarker to predict the risk of amputation in these patients is evaluated. In the past, microRNAs have been reported as suitable biomarkers for the diagnosis and prognosis of cardiovascular disease including acute myocardial infarction, heart failure and peripheral arterial disease. Moreover, their small size protects them from endogenous RNase activity, which contributes to the high stability of microRNAs.
In **Chapter 8** we determined local microRNA expression in subcutaneous and perivascular adipose tissues of critical limb ischemia patients that underwent major amputation compared to healthy controls. Whereas most microRNAs were downregulated in amputation samples, eight microRNAs were upregulated in these patients. Six out of eight upregulated microRNAs belong to the 14q32 microRNA cluster. We show that increased expression of these six 14q32 microRNAs can be used as biomarkers to identify CLI patients at risk of major amputation.

The results of all studies described in this thesis, as well as future perspectives, are discussed in **Chapter 9**. Figure 6 summarizes the outline of this thesis.

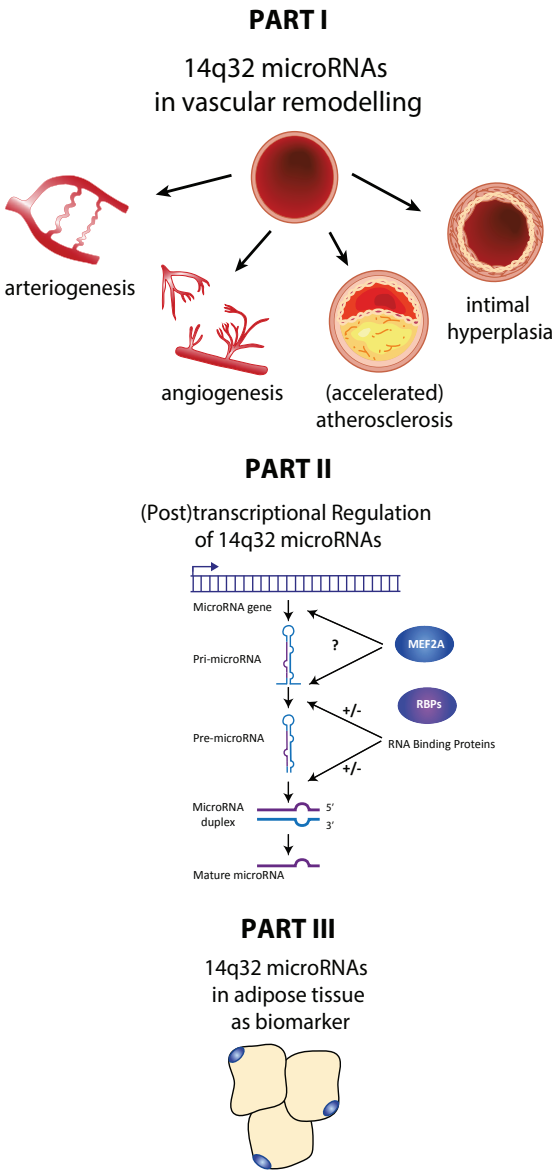

Figure 6. Graphical summary of the thesis outline. Part I of this thesis investigates the role of 14q32 microRNAs in different processes of vascular remodelling, namely arteriogenesis and angiogenesis, (accelerated) atherosclerosis and intimal hyperplasia (restenosis). Part II discusses several (post)transcriptional mechanisms that could regulate 14q32 microRNA expression. In Part III, microRNA expression in adipose tissue of critical limb ischemia patients is studied and the possible use of 14q32 microRNAs as biomarker for identification of critical limb ischemia patients at risk of amputation is evaluated.

Reference List

1. Gibbons GH, Dzau VJ. The emerging concept of vascular remodeling. *N Engl J Med* 1994 May 19;330(20):1431-8.
2. Risau W. Mechanisms of angiogenesis. *Nature* 1997 Apr 17;386(6626):671-4.
3. Carmeliet P. Mechanisms of angiogenesis and arteriogenesis. *Nat Med* 2000 Apr;6(4):389-95.
4. Adams RH, Alitalo K. Molecular regulation of angiogenesis and lymphangiogenesis. *Nat Rev Mol Cell Biol* 2007 Jun;8(6):464-78.
5. Folkman J. Angiogenesis in cancer, vascular, rheumatoid and other disease. *Nat Med* 1995 Jan;1(1):27-31.
6. Moreno PR, Purushothaman KR, Fuster V, Echeverri D, Truszczynska H, Sharma SK, et al. Plaque neovascularization is increased in ruptured atherosclerotic lesions of human aorta: implications for plaque vulnerability. *Circulation* 2004 Oct 5;110(14):2032-8.
7. Ito WD, Arras M, Scholz D, Winkler B, Htun P, Schaper W. Angiogenesis but not collateral growth is associated with ischemia after femoral artery occlusion. *Am J Physiol* 1997 Sep;273(3 Pt 2):H1255-H1265.
8. van Oostrom MC, van Oostrom O., Quax PH, Verhaar MC, Hoefer IE. Insights into mechanisms behind arteriogenesis: what does the future hold? *J Leukoc Biol* 2008 Dec;84(6):1379-91.
9. Buschmann I, Schaper W. Arteriogenesis Versus Angiogenesis: Two Mechanisms of Vessel Growth. *News Physiol Sci* 1999 Jun;14:121-5.
10. van Weel, V, Toes RE, Seghers L, Deckers MM, de Vries MR, Eilers PH, et al. Natural killer cells and CD4+ T-cells modulate collateral artery development. *Arterioscler Thromb Vasc Biol* 2007 Nov;27(11):2310-8.
11. Hansson GK. Inflammation, atherosclerosis, and coronary artery disease. *N Engl J Med* 2005 Apr 21;352(16):1685-95.
12. Galkina E, Ley K. Immune and inflammatory mechanisms of atherosclerosis (*). *Annu Rev Immunol* 2009;27:165-97.
13. Bot I, de Jager SC, Zernecke A, Lindstedt KA, van Berkel TJ, Weber C, et al. Perivascular mast cells promote atherogenesis and induce plaque destabilization in apolipoprotein E-deficient mice. *Circulation* 2007 May 15;115(19):2516-25.
14. Hansson GK. Inflammatory mechanisms in atherosclerosis. *J Thromb Haemost* 2009 Jul;7 Suppl 1:328-31.
15. Gomez D, Owens GK. Smooth muscle cell phenotypic switching in atherosclerosis. *Cardiovasc Res* 2012 Jul 15;95(2):156-64.
16. Finn AV, Nakano M, Narula J, Kolodgie FD, Virmani R. Concept of vulnerable/unstable plaque. *Arterioscler Thromb Vasc Biol* 2010 Jul;30(7):1282-92.
17. Bentzon JF, Otsuka F, Virmani R, Falk E. Mechanisms of plaque formation and rupture. *Circ Res* 2014 Jun 6;114(12):1852-66.
18. Bennett MR. In-stent stenosis: pathology and implications for the development of drug eluting stents. *Heart* 2003 Feb;89(2):218-24.
19. Elia L, Condorelli G. RNA (Epi)genetics in cardiovascular diseases. *J Mol Cell Cardiol* 2015 Jul 20.
20. Bartel DP. MicroRNAs: genomics, biogenesis, mechanism, and function. *Cell* 2004 Jan 23;116(2):281-97.
21. Lee Y, Kim M, Han J, Yeom KH, Lee S, Baek SH, et al. MicroRNA genes are transcribed by RNA polymerase II. *EMBO J* 2004 Oct 13;23(20):4051-60.
22. Lee Y, Ahn C, Han J, Choi H, Kim J, Yim J, et al. The nuclear RNase III Drosha initiates microRNA processing. *Nature* 2003 Sep 25;425(6956):415-9.
23. Krol J, Loedige I, Filipowicz W. The widespread regulation of microRNA biogenesis, function and decay. *Nat Rev Genet* 2010 Sep;11(9):597-610.
24. Yang X, Du WW, Li H, Liu F, Khorshidi A, Rutnam ZJ, et al. Both mature miR-17-5p and passenger strand miR-17-3p target TIMP3 and induce prostate tumor growth and invasion. *Nucleic Acids Res* 2013 Nov;41(21):9688-704.
25. Schober A, Nazari-Jahantigh M, Wei Y, Bidzhekov K, Gremse F, Grommes J, et al. MicroRNA-126-5p promotes endothelial proliferation and limits atherosclerosis by suppressing Dlk1. *Nat Med* 2014 Apr;20(4):368-76.
26. Doench JG, Sharp PA. Specificity of microRNA target selection in translational repression. *Genes Dev* 2004 Mar 1;18(5):504-11.
27. Wienholds E, Kloosterman WP, Miska E, Alvarez-Saavedra E, Berezikov E, de BE, et al. MicroRNA expression in zebrafish embryonic development. *Science* 2005 Jul 8;309(5732):310-1.
28. Jamaluddin MS, Weakley SM, Zhang L, Kougias P, Lin PH, Yao Q, et al. miRNAs: roles and clinical applications in vascular disease. *Expert Rev Mol Diagn* 2011 Jan;11(1):79-89.
29. Rayner KJ, Sheedy FJ, Esau CC, Hussain FN, Temel RE, Parathath S, et al. Antagonism of miR-33 in mice promotes reverse cholesterol transport and regression of atherosclerosis. *J Clin Invest* 2011 Jul;121(7):2921-31.
30. Bonauer A, Carmona G, Iwasaki M, Mione M, Koyanagi M, Fischer A, et al. MicroRNA-92a controls angiogenesis and functional recovery of ischemic tissues in mice. *Science* 2009 Jun 26;324(5935):1710-3.
31. Landskroner-Eiger S, Qiu C, Perrotta P, Siragusa M, Lee MY, Ulrich V, et al. Endothelial miR-17 approximately 92 cluster negatively regulates arteriogenesis via miRNA-19 repression of WNT signaling. *Proc Natl Acad Sci* 2015 Oct 13;112(41):12812-7.
32. Wu W, Xiao H, Laguna-Fernandez A, Villarreal G, Jr., Wang KC, Geary GG, et al. Flow-Dependent Regulation of Kruppel-Like Factor 2 Is Mediated by MicroRNA-92a. *Circulation* 2011 Aug 2;124(5):633-41.
33. Iaconetti C, Polimeni A, Sorrentino S, Sabatino J, Pironti G, Esposito G, et al. Inhibition of miR-92a increases endothelial proliferation and migration in vitro as well as reduces neointimal proliferation in vivo after vascular injury. *Basic Res Cardiol* 2012 Sep;107(5):296.
34. Rizki G, Boyer LA. Lncing epigenetic control of transcription to cardiovascular development and disease. *Circ Res* 2015 Jul 3;117(2):192-206.

35. Mercer TR, Mattick JS. Structure and function of long noncoding RNAs in epigenetic regulation. *Nat Struct Mol Biol* 2013 Mar;20(3):300-7.
36. Rinn JL, Chang HY. Genome regulation by long noncoding RNAs. *Annu Rev Biochem* 2012;81:145-66.
37. Michalik KM, You X, Manavski Y, Doddaballapur A, Zornig M, Braun T, et al. Long noncoding RNA MALAT1 regulates endothelial cell function and vessel growth. *Circ Res* 2014 Apr 25;114(9):1389-97.
38. Uchida S, Dimmeler S. Long noncoding RNAs in cardiovascular diseases. *Circ Res* 2015 Feb 13;116(4):737-50.
39. Kiss T. Small nucleolar RNA-guided post-transcriptional modification of cellular RNAs. *EMBO J* 2001 Jul 16;20(14):3617-22.
40. Filipowicz W, Pogacic V. Biogenesis of small nucleolar ribonucleoproteins. *Curr Opin Cell Biol* 2002 Jun;14(3):319-27.
41. Michel CI, Holley CL, Scruggs BS, Sidhu R, Brookheart RT, Listenberger LL, et al. Small nucleolar RNAs U32a, U33, and U35a are critical mediators of metabolic stress. *Cell Metab* 2011 Jul 6;14(1):33-44.
42. Brandis KA, Gale S, Jinn S, Langmade SJ, Dudley-Rucker N, Jiang H, et al. Box C/D small nucleolar RNA (snoRNA) U60 regulates intracellular cholesterol trafficking. *J Biol Chem* 2013 Dec 13;288(50):35703-13.
43. Benetatos L, Hatzimichael E, Londin E, Vartholomatos G, Loher P, Rigoutsos I, et al. The microRNAs within the DLK1-DIO3 genomic region: involvement in disease pathogenesis. *Cell Mol Life Sci* 2013 Mar;70(5):795-814.
44. Aavik E, Lumivuori H, Leppanen O, Wirth T, Hakkinen SK, Brasen JH, et al. Global DNA methylation analysis of human atherosclerotic plaques reveals extensive genomic hypomethylation and reactivation at imprinted locus 14q32 involving induction of a miRNA cluster. *Eur Heart J* 2015 Apr 21;36(16):993-1000.
45. Gordon FE, Nutt CL, Cheunsuchon P, Nakayama Y, Provencher KA, Rice KA, et al. Increased expression of angiogenic genes in the brains of mouse meg3-null embryos. *Endocrinology* 2010 Jun;151(6):2443-52.
46. Snyder CM, Rice AL, Estrella NL, Held A, Kandarian SC, Naya FJ. MEF2A regulates the Gtl2-Dio3 microRNA mega-cluster to modulate WNT signaling in skeletal muscle regeneration. *Development* 2013 Jan 1;140(1):31-42.

Part I

14q32 microRNAs in vascular remodelling

Chapter 2

The multifactorial nature of microRNAs is vascular remodelling

Cardiovasc Res 2016 May 1;110(1):6-22

SMJ Welten[1,2*]

EAC Goossens[1,2*]

PHA Quax[1,2†]

AY Nossent[1,2†]

[*]Authors contributed equally to this work

[†] Authors contributed equally to this work

[1]Department of Surgery and [2]Einthoven Laboratory for Experimental Vascular Medicine,
Leiden University Medical Center, Leiden, the Netherlands

[3]Department of Biochemistry and Pharmacology, Odense University Hospital, Odense, Denmark

[4]Idera Pharmaceuticals, Cambridge, MA, United States of America

Abstract

Vascular remodelling is a multifactorial process which involves both adaptive and maladaptive changes of the vessel wall through amongst others, cell proliferation and migration, but also apoptosis and necrosis of the various cell types in the vessel wall. Vascular remodelling can be beneficial e.g. during neovascularization after ischemia, as well as pathological e.g. during atherosclerosis and aneurysm formation. In recent years, it has become clear that microRNAs are able to target many genes that are involved in vascular remodelling processes and either can promote or inhibit structural changes of the vessel wall. Since many different processes of vascular remodelling are regulated by similar mechanisms and factors, both positive and negative vascular remodelling can be affected by the same microRNAs. A large number of microRNAs has been linked to various aspects of vascular remodelling and indeed, several of these microRNAs regulate multiple vascular remodelling processes, including both the adaptive processes angiogenesis and arteriogenesis as well as maladaptive processes of atherosclerosis, restenosis and aneurysm formation. Here, we discuss the multifactorial role of microRNAs and microRNA clusters that were reported to play a role in multiple forms of vascular remodelling and are clearly linked to cardiovascular disease. The microRNAs reviewed are miR-126, miR-155 and the microRNA gene clusters 17-92, 23/24/27, 143/145 and 14q32. Understanding the contribution of these microRNAs to the entire spectrum of vascular remodelling processes is important, especially as these microRNAs may have great potential as therapeutic targets for treatment of various cardiovascular diseases.

Introduction

MicroRNAs

MicroRNAs are a class of endogenous noncoding RNA molecules of approximately 22 nucleotides in length. MicroRNAs inhibit translation of mRNAs into proteins by binding to specific sites in the 3'untranslated region (3'UTR) of their target mRNAs. Rather than completely silencing their target gene, binding of a microRNA leads to modest target downregulation. However, a single microRNA is able to downregulate the expression of numerous target genes, and by doing so, that single microRNA can regulate complex, multifactorial physiological processes[1]. MicroRNAs have been shown to play an important role in human diseases, including cardiovascular disease (CVD). In this review, we describe the multifactorial nature of microRNAs in the regulation of vascular remodelling, by discussing the different target genes and regulatory mechanisms that have been described for these microRNAs. Although many microRNAs play a role in some aspects of vascular remodelling, we focused on those microRNAs that to play a role in multiple forms of vascular remodelling ánd are clearly linked to CVD. The individual microRNAs miR-126 and miR-155, the microRNA gene clusters 17-92, 23/24/27, 143/145, and the largest known microRNA gene cluster 14q32, all met these criteria (Figure 1). An overview of confirmed target genes for these microRNAs is given in Table 1 and 2.

Vascular remodelling

Vascular remodelling comprises beneficial adaptive responses of the vessel wall to changes in hemodynamic forces, vasoactive stimuli or growth factors, but also maladaptive responses that can lead to CVD[2]. Thus, vascular remodelling can be divided into adaptive and maladaptive processes regarding vessel wall structure and blood supply towards downstream tissues[3]. For this review, we focused on neovascularization on the one hand and on atherosclerosis, post-interventional restenosis and aneurysm formation on the other. All of these processes are orchestrated by microRNAs[3].

When studying the role of microRNAs in these processes, there are several microRNAs that have been very well described. For example, one of the most promising microRNAs as therapeutic target for the treatment of atherosclerotic disease is miR-33a/b, (discussed below), as it controls cholesterol metabolism, a crucial mechanism in CVD. The phenotype of smooth muscle cells (SMCs), either contractile or proliferative, is also imperative for vascular remodelling and neointima formation. Several microRNAs, including miR-133, miR-125b, miR-26a, miR-663 and miR-1, have been shown to control SMC phenotype and function[4-8].

In aneurysm formation, the miR-29 family has been shown to play a major role by targeting genes that are involved in extracellular matrix homeostasis. Inhibition of miR-29b in two murine abdominal aortic aneurysm (AAA) models increased expression of genes encoding for collagen and elastin and reduced expression of matrix metalloproteinases, resulting in decreased aneurysm progression in these mice[9]. Similarly, miR-21 regulated AAA expansion through targeting of PTEN[10].

Therapeutic potential of microRNAs

Several microRNAs that gave promising results as therapeutic targets in murine models of CVD are now being studied in larger animal models. A relevant example is the miR-33 family, consisting of miR-33a and miR-33b. Both miR-33a and miR-33b regulate the expression of cholesterol transporter ABCA1, which mediates the efflux of cholesterol[11]. Inhibition or deficiency of miR-33a reduced progression of plaques and raised HDL levels in atherosclerotic mouse models[11-13]. Since rodents lack miR-33b, extrapolation of these results to a human situation was not straightforward. Systemic inhibition of miR-33a/b in African green monkeys, which do express miR-33b, led to increased expression of ABCA1 in the liver of treated animals and increased plasma HDL levels[14]. The authors also observed regulation of other genes involved in fatty acid oxidation and fatty acid synthesis, leading to a decrease in plasma VLDL levels, an effect that was not observed in mice[14]. Moreover, no overt toxicity was observed in animals treated with anti-miRs, supporting the development of anti-miR-33 therapeutics for treatment of atherosclerosis.

Janus phenomenon

However, caution is wanted when intervening in individual processes of vascular remodelling. This is best illustrated by the Janus phenomenon, named after the two-faced Roman deity Janus. The Janus phenomenon was first described by Epstein et al., who noticed that interventions used to stimulate arteriogenesis also increased atherosclerosis and vice versa[18]. The phenomenon is explained by the fact that there is a strong overlap in the mechanisms that underlie the various forms of vascular remodelling. One of the important mechanisms shared in vascular remodelling are the inflammatory responses. Since microRNAs can target numerous genes that may be involved in many processes, modulation of one microRNA could influence more than one form of vascular remodelling. This could be positive, for example when targeting a single microRNA inhibits various forms of maladaptive remodelling simultaneously. However, an unwanted effect could be that anti-atherogenic microRNAs also have anti-arteriogenic effects due to common pathways in atherosclerosis and arteriogenesis. The Janus phenomenon is a major drawback for many novel therapeutics designed to modulate vascular remodelling and must also be taken into account when exploring the therapeutic potential of microRNAs.

Therefore, we chose to discuss those microRNAs, miR-126, miR-155 and microRNA gene clusters 17-92, 23/24/27, 143/145 and 14q32, that play a confirmed role in multiple forms of vascular remodelling ánd are clearly linked to CVD.

Non-standard Abbreviations and Acronyms	
3'UTR	3'untranslated region
AAA	Abdominal aortic aneurysm
AAV	Adeno-associated virus
AngII	Angiotensin II
CAD	Coronary artery disease
CVD	Cardiovascular disease
EC	Endothelial cell
HDL	High density lipoprotein
IA	Intracranial aneurysm
LNA	Locked nucleic acid
miR	MicroRNA
MO	Morpholino
MP/MV	Microparticle/Microvesicle
MSC	Mesenchymal stem cell
oxLDL	Oxidized low density lipoprotein
PBMC	Peripheral blood mononuclear cell
siRNA	Small interfering RNA
TLR	Toll-like receptor
(V)LDL	(very) low density lipoprotein
(V)SMC	(vascular) smooth muscle cell
Abbreviations of NCBI-Annotated Target Genes	
ABCA1	ATP-binding cassette transporter A1
ACAT1	Acyl-CoA cholesterol acyltransferase-1
ACE	Angiotensin converting enzyme
ANGPTL3	Angiopoietin-like 3
ARF6	ADP ribosylation factor 6
AT1R	Angiotensin II type 1 receptor
BCL2 / 6	B-cell lymphoma 2 / 6
bFGF	Basic fibroblast growth factor
BIC	B cell integration cluster
BMP4	Bone morphogenetic protein 4
CCL2/MCP1	Monocyte chemoattractant protein 1
CD146	Cluster of differentiation 146 (melanoma cell adhesion molecule)
CDK4	Cyclin dependent kinase 4
CPT1α	Carnitine palmitoyl transferase 1α
CXCL12/SDF1	Stromal derived factor-1
CXCR4	Chemokine (C-X-C motif) receptor 4
DGAT2	Diacylglycerol O-acyltransferase 2
DLK1	NOTCH1 inhibitor delta-like 1 homolog
E2F1	E2F transcription factor 1
EFNB2	Ephrin B2
eNOS	Endothelial nitric oxide synthase
ERK1/2	Extracellular-signal-related kinase 1/2
ETS-1	V-ets avian erythroblastosis virus E26 oncogene homolog 1
FGFGR2	Fibroblast growth factor receptor 2
FLT1	VEGF receptor fms-related tyrosine kinase 1
FOXO3 / 4	Forkhead box O 3 / 4
FSR2	Fibroblast growth factor receptor substrate 2
FZD4	Frizzled class receptor 4
GATA2	GATA Binding Protein 2
GPAM	glycerol-3-phosphate acyltransferase 1 mitochondrial
HIF1α / HIF2α	Hypoxia inducible factor 1 / 2, alpha subunit
HKII	Hexokinase II
HMGB1	HMG box-transcription protein 1
HMOX1	Heme oxygenase 1
ICAM1	Intracellular cell adhesion molecule 1
IGF1	Insulin-like growth factor 1

IL33	Interleukin 33
INSIG1	Insulin induced gene 1
IRS1 / 2	Insulin receptor substrate 1 / 2
ITGβ8	Integrin β 8
JAK1	Janus Kinase 1
KLF2 / 4 / 5	Krüppel-like factor 2 / 4 / 5
LPL	Lipoprotein lipase
LRP6	LDL receptor related protein 6
MCP1/CCL2	Monocyte chemoattractant protein 1
MEF2a	Myocyte enhancer factor 2
MEG3	Maternally expressed gene 3
MIF	Macrophage migration inhibitory factor
MKK4	Mitogen-Activated Protein Kinase Kinase 4
MMP1 / 3	Matrix metalloproteinase 1 / 3
MRTFA	Myocardin related transcription factor A
Myd88	myeloid differentiation primary response gene
PAK4	p21-activated kinase 4
PIK3R2	Phosphoinositide-3-kinase, regulatory subunit 2
PPARγ	Proliferator-activator receptor gamma
PPP2R2A	Protein phosphatase 2 regulatory subunit B, alpha
RGS16	Regulator of G protein signalling 16
SDF1/CXCL12	Stromal derived factor-1
SEMA6A / 6D / 3B	Semaphorin 6A / 6D / 3B
SMAD3	SMAD family member 3
SOCS1 / 5	Suppressor of cytokine signalling 1 / 5
SPRED1	Sprouty-related, EVH1 domain containing 1
SREBPs	Sterol regulatory element-binding proteins
SRF	Serum response factor
TAB2	TGF-β activated kinase1/MAP3K7 binding protein 2
TGFβ(2)	Transforming growth factor beta (2)
TGFβR2	TGFβ receptor 2
TIMP3	Tissue inhibitor of metalloproteinase 3
TLR4	Toll like receptor 4
TNF-α	Tumor necrosis factor alpha
TRIF	TIR-domain-containing adapter-inducing interferon-β
uPA	urokinase-type plasminogen activator
VCAM1	Vascular cell adhesion molecule 1
VE-cadherin	Vascular endothelial cadherin
VEGF	Vascular endothelial growth factor

Table 1. Non standard abbreviations and acronyms.

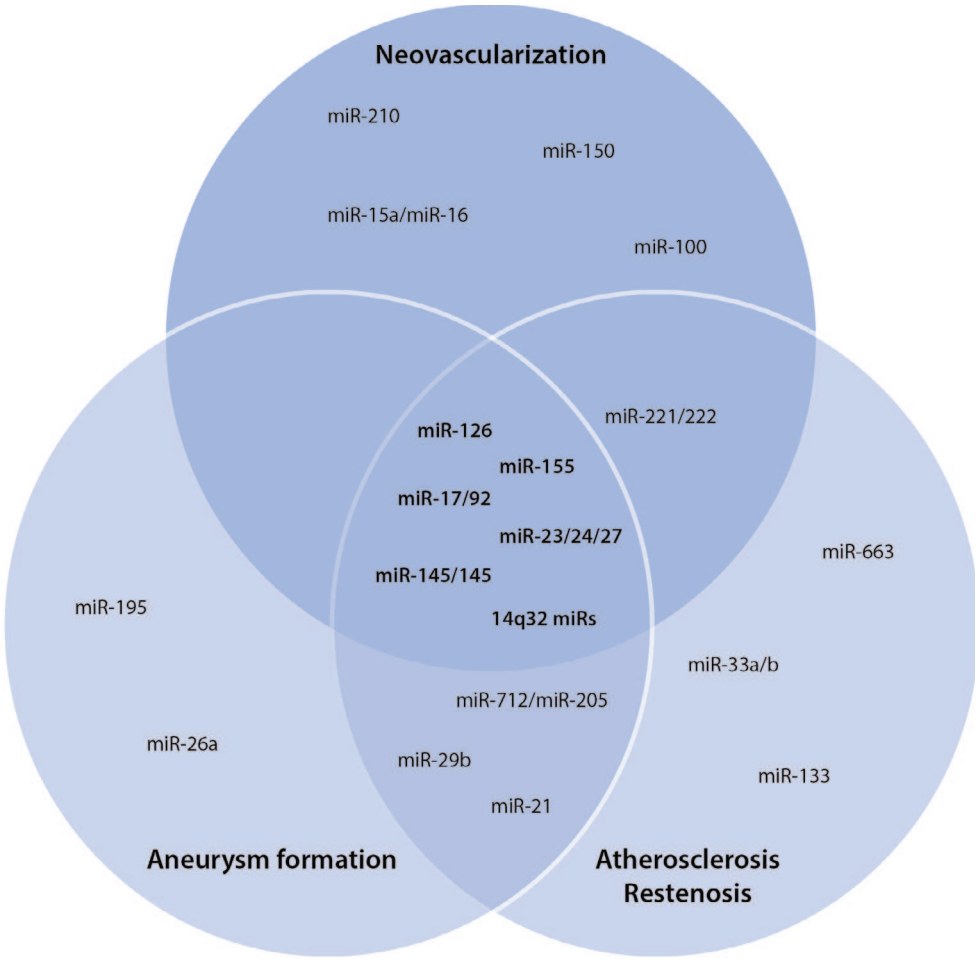

Figure 1. The top 5 microRNAs reported to play a role in each of the following vascular remodelling processes, atherosclerosis and restenosis formation, aneurysm formation and neovascularization, are shown. MicroRNAs that were reported to play a role in multiple forms of these processes were selected for this review and shown here in bold.

miR-126

MiR-126 is one of the most abundantly expressed microRNAs in endothelial cells (ECs)[15]. The miR-126 gene is located on human chromosome 9 and gives rise to two mature microRNAs, miR-126-3p and miR-126-5p. Generally, the role of miR-126 in vascular remodelling as described in the literature corresponds to miR-126-3p (Figure 2). MiR-126 is also abundantly expressed in platelets, suggesting a role for miR-126 in vascular homeostasis and inflammation[16]. Platelets are a major source of circulating miR-126[17]. Consequently, levels of circulating miR-126 are influenced by the use of platelet inhibitors, such as aspirin[17]. The delivery of miR-126 by platelet microparticles (MPs) to primary human macrophages was reported recently and miR-126 derived from these platelet MPs influences macrophage gene expression and function[18]. Levels of miR-126 are differentially expressed in plasma samples of patients with coronary artery disease (CAD)[19].

Neovascularization

The first studies from 2008 that investigated the role of miR-126 in EC function demonstrated that miR-126 targets VCAM1[20]. Increased expression of adhesion molecules such as VCAM1 and increased leukocyte adherence to ECs are necessary for the initiation of angiogenesis. Both mechanisms are stimulated by inhibition of miR-126[20]. In HUVECs, inhibition of miR-126 led to increased proliferation and migration[21]. Furthermore, injection of miR-126 inhibitors into zebrafish embryos affected blood vessel integrity, as was demonstrated by collapsed lumens and compromised endothelial tube organization[21].Studies in mice showed that inhibition of miR-126 decreased recovery after myocardial infarction and impaired angiogenic capacity in a hind limb ischemia model[22-24]. These effects were partially mediated via inhibitors of VEGF-signalling, namely SPRED1 and PIK3R2[21-23]. Both Spred1 and Pik3r2 are upregulated in absence of miR-126, causing an increase in vascular permeability and leakage[21, 23]. MiR-126 was also shown to target CXCL12[25]. Silencing miR-126 induced CXCL12 expression which enhanced migration of $CD34^+$ progenitor cells *in vitro* and increased the number of circulating bone marrow-derived progenitor cells after hind limb ischemia *in vivo*[25, 26].

In addition, exosomes from human $CD34^+$ cells, which are rich in miR-126, have great angiogenic capacity both *in vitro* and *in vivo*[27]. Mocharla *et al.* showed that $CD34^+$ peripheral blood mononuclear cells (PBMCs) secrete microvesicles and exosomes that are enriched with miR-126[28]. These microvesicles and exosomes are taken up by ECs and facilitate the proangiogenic effects of miR-126[28].

Atherosclerosis

Atherosclerotic plaque progression is often accompanied by apoptosis of (vascular) cells in the plaque[29]. During apoptosis, ECs release microvesicles that are enriched with miR-126[25]. Delivery of miR-126 to recipient vascular cells inhibits the progression of atherosclerosis, presumably via suppression of RGS16, which is a negative regulator of CXCR4. Subsequent upregulation of CXCR4 led to the production of CXCL12. This reduced lesion formation by decreasing the number of macrophages and apoptotic cells in the plaque and increasing the recruitment of endothelial progenitor cells for repair in a mouse model for atherosclerosis[25]. Vesicle-independent transfer of miR-126 from ECs

to SMCs was also reported, increasing miR-126 levels in SMCs (Figure 2). Decreased expression of miR-126 target genes FOXO3, BCL2 and IRS1 led to increased proliferation of SMCs[30]. Subjecting ECs to laminar shear stress or miR-126 inhibition abolished these effects. In miR-126$^{-/-}$ mice, neointima formation was attenuated compared to wildtype mice after ligation of the left common carotid artery[30]. Recently, the contribution of miR-126-5p to atherosclerosis formation was demonstrated by Schober *et al.*[31]. Hypercholesterolemic miR-126$^{-/-}$ApoE$^{-/-}$ and miR-126$^{+/+}$ApoE$^{-/-}$ mice were subjected to endothelial denudation. After 14 and 28 days, lesion area was increased in miR-126$^{-/-}$ApoE$^{-/-}$ mice compared to control animals[31]. Moreover, endothelial recovery of the carotid lumen was impaired in miR-126$^{-/-}$ApoE$^{-/-}$ animals due to reduced EC proliferation[31]. In these animals, expression of multiple miR-126-5p predicted target genes was increased, whereas expression of known miR-126-3p targets was not[31]. The authors confirmed targeting of DLK1 by miR-126-5p and demonstrated that inhibition of miR-126-5p increased Dlk1 expression and reduced EC proliferation[31]. To identify the specific role of miR-126-3p and miR-126-5p in endothelial repair, denuded arteries of ApoE$^{-/-}$ mice were treated with either miR-126-3p-, miR-126-5p- or control-miR inhibitors. Treatment with anti-miR-126-5p, but not anti-miR-126-3p, significantly increased the lesion area and impaired endothelial recovery and EC proliferation[31]. In untreated ApoE$^{-/-}$ mice, disturbed flow led to decreased miR-126-5p levels and increased Dlk1 mRNA and protein levels in the carotid artery, whereas miR-126-3p levels were unaltered[31]. The authors proposed that miR-126-5p plays a role in regulating EC proliferation at non-predilection sites, whereas miR-126-3p presumably regulates the replicative capacity of ECs at predilection sites[31]. Finally, in human atherosclerotic lesions miR-126-5p levels were found to inversely correlate with DLK1 expression and the number of lesional macrophages and positively correlated with EC proliferation, suggesting an atheroprotective effect of increased miR-126-5p levels in humans[31].

Aneurysm

Although miR-126 is upregulated in AAA and upregulation correlated with decreased TNF-α expression, the exact function of miR-126 in AAA pathogenesis is still unknown[32]. In plasma of patients with AAA, miR-126 was significantly downregulated compared to plasma of healthy volunteers, but not compared to patients with CAD[32].

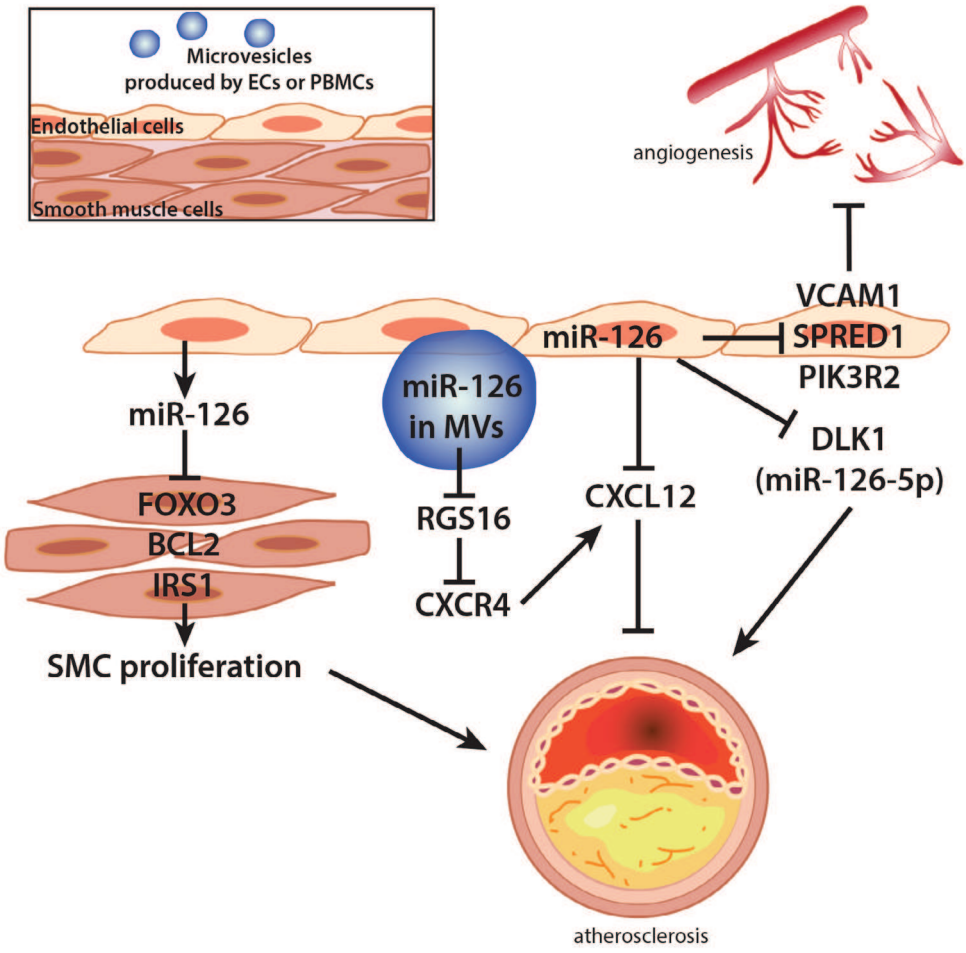

Figure 2. The role of endothelial miR-126 in vascular remodelling. MiR-126 regulates angiogenesis and vascular integrity via targeting of VCAM1 and targeting the inhibitors of VEGF signalling;SPRED1and PIK3R2. Via microvesicle-mediated delivery from ECs to neighbouring vascular cells, miR-126 inhibits RGS16, an inhibitor of CXCR4, resulting in the expression of CXCL12 and reducing atherosclerosis. Paracrine secretion of miR-126 from ECs to SMCs leads to inhibition of FOXO3, BCL2 and IRS1 target genes and increases proliferation of SMCs, which contributes to the atherogenic actions of miR-126. In addition, miR-126-5p suppresses the NOTCH1 inhibitor DLK1, thereby limiting atherosclerosis. Arrows indicate upregulation. Capped lines indicate inhibition. MV; microvesicle, EC; endothelial cell, SMC; smooth muscle cell. PBMCs; peripheral blood mononuclear cells. For full target gene names, see Table 1.

miR-155

The miR-155 gene is located within an exon of the non-coding RNA BIC on human chromosome 21. MiR-155 is highly expressed by activated B and T cells, but also by monocytes and macrophages[33, 34]. In addition, miR-155 is expressed in ECs and SMCs[35].

MiR-155 is upregulated in macrophages via TLR ligands, such as LPS[34]. MiR-155 exerts pro-inflammatory effects via targeting of the anti-inflammatory SOCS1[36]. In contrast, anti-inflammatory effects of miR-

155 signalling have also been described via targeting of TAB2[37] (Figure 3).

In 2012, Corsten *et al.* described a role for miR-155 in CVD, demonstrating upregulation of miR-155 during the acute inflammatory phase of viral myocarditis[38]. Systemic inhibition of miR-155 reduced cardiac monocyte/macrophage infiltration, decreased T lymphocyte activation and reduced myocardial damage in a mouse model of acute viral myocarditis[38].

Neovascularization

MiR-155 is co-expressed with AT1R in HUVECs and SMCs, where it represses AT1R expression[39]. Interestingly, a single nucleotide polymorphism (+1166 A/C), which is associated with CVD, was found to disrupt a miR-155 target site in the 3'UTR of AT1R[39]. Overexpression of miR-155 reduced migration of HUVECs in response to Angiotensin II (AngII) via targeting of the AT1R.

ETS-1 has two potential binding sites for miR-155 in its 3'UTR and is another target of miR-155 in HUVECs[35]. ETS-1 and its downstream target genes VCAM1, MCP1 and FLT1 were induced in HUVECs upon stimulation with AngII. Overexpression of miR-155 abrogated this effect[35].

Recent work by Pankratz *et al.* demonstrated that miR-155 exerts both antiangiogenic and proarteriogenic functions after induction of hind limb ischemia in mice[40, 41]. MiR-155 was upregulated seven days after femoral artery ligation in mice. Inhibition of miR-155 in HUVECs resulted in increased EC proliferation and tube formation[40]. These results were confirmed in aortic ring assays, as well as in *in vivo* matrigel plug assays using miR-155$^{-/-}$ mice. In miR-155$^{-/-}$ ECs, expression of AT1R was increased. AT1R expression could be manipulated by overexpression or inhibition of miR-155 in both human and murine ECs. The authors concluded that the antiangiogenic properties of miR-155 are mediated via AT1R[40] (Figure 2). Despite the antiangiogenic properties of miR-155, blood flow recovery after hind limb ischemia was impaired in miR-155$^{-/-}$ mice. MiR-155 deficiency decreased migration of bone-marrow derived macrophages. MiR-155$^{-/-}$ macrophages showed significantly reduced expression levels of proarteriogenic cytokines and chemokines upon LPS stimulation, compared to wildtype cells. SOCS1 was identified as a potential mediator, as this was the most upregulated target gene in miR-155$^{-/-}$ BMDMs. Knockdown of SOCS1 indeed reversed the effects of miR-155 deficiency on proarteriogenic cytokine production[40].

Atherosclerosis

Expression of miR-155 was upregulated in human atherosclerotic plaques, predominantly in pro-inflammatory macrophages[42, 43]. However, circulating levels of miR-155 were significantly lower in patients with CAD compared to healthy volunteers[19]. In several studies, treatment of macrophages with oxidized LDL and IFN-γ led to upregulation of miR-155, whereas suppression of miR-155 by oxLDL treatment has also been reported[42, 44-46]. Nazari-Jahantigh *et al.* demonstrated that miR-155 targets BCL6, a transcription factor that attenuates pro-inflammatory NF-kB signalling and directly represses CCL2. Leukocyte-specific deletion of miR-155 decreased Ccl2 signalling and reduced atherosclerotic plaque formation in ApoE$^{-/-}$ mice[42]. Recently, Tian *et al.* showed that miR-155 targets HMGB1, which supresses MIF and increases uptake of oxLDL by macrophages[47]. Elevated miR-155 levels enhanced oxLDL induced foam cell formation by targeting HMGB1. Systemic inhibition of miR-155 in ApoE$^{-/-}$ mice resulted in smaller atherosclerotic plaques that contained less lipid-laden macrophages[47]. However,

opposite findings on the role of miR-155 in atherosclerosis have also been reported. LDL-R$^{-/-}$ mice transplanted with miR-155$^{-/-}$ bone marrow developed larger lesions compared to mice transplanted with wildtype bone marrow[48]. Increased numbers of macrophages and neutrophils were present in these lesions as well as increased numbers of granulocytes and inflammatory monocytes in the circulation[48]. Apparently, miR-155 can have opposite effects in macrophages, being either pro- or anti-inflammatory (Figure 3).

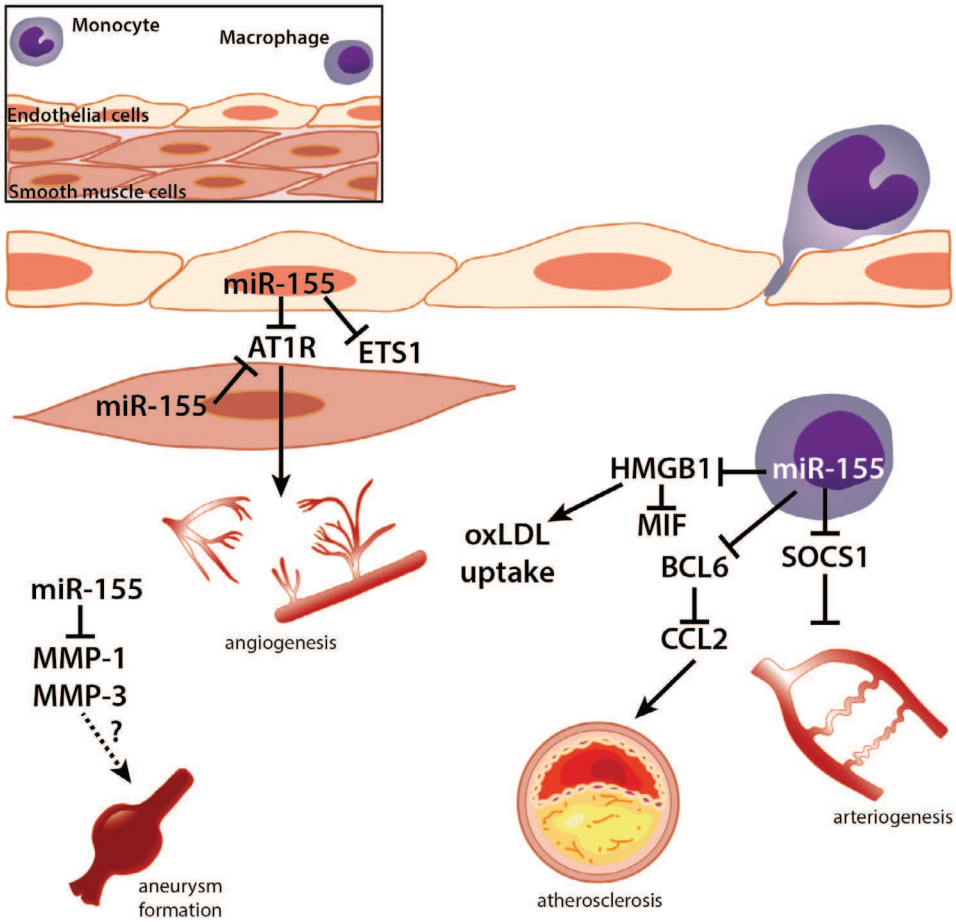

Figure 3. The inflammatory miR-155 in vascular remodelling. MiR-155 is co-expressed with AT1R in HUVECs and SMCs and inhibits expression of AT1R in these cells. ETS1 transcription factor is also targeted by miR-155 in HUVECs. Via these targets, miR-155 affects angiogenesis. In addition, miR-155 has been demonstrated to affect arteriogenesis. This effect is mediated by inhibition of SOCS1 in macrophages, resulting in upregulation of proarteriogenic cytokines. MiR-155 in atherosclerotic plaques is predominantly expressed in (pro-inflammatory) macrophages, where it suppresses the transcription factor BCL6. In addition, miR-155 targets HMGB1, increasing oxLDL uptake by macrophages. MiR-155 reduces matrix metalloproteinases MMP-1 and MMP-3, which could reduce matrix degradation and progression of aneurysm formation. Arrows indicate upregulation. Capped lines indicate inhibition. The dashed line indicates possible interactions that have not been confirmed yet. (HUV)EC; (human umbilical venous) endothelial cell, SMC; smooth muscle cell. For full target gene names, see Table 1.

Aneurysm

MiR-155 is significantly upregulated in AAA tissue[32]. However, expression of miR-155 was lower in plasma of patients with AAA compared to plasma levels of healthy controls ánd of patients with CAD[32]. In models for rheumatoid arthritis, overexpression of miR-155 led to downregulation of MMP1 and MMP3[49]. This suggests that overexpression of miR-155 in AAA may function as an endogenous rescue mechanism that inhibits matrix degradation and progression of aneurysm formation[49].

miR-17-92 cluster

The miR-17-92 gene cluster is located within intron 3 of the C13orf25 gene on human chromosome 13 and encodes six individual microRNAs, namely miR-17, miR-18a, miR-19a, miR-20a, miR-19b-1 and miR-92a[50] (Figure 4). Recently, it was shown that expression of the miR-17-92 cluster in ECs is stimulated by VEGF, via activation of the Erk/Elk1 pathway[51]. Upon stimulation, expression of miR-17-92 contributed to endothelial proliferation and angiogenic sprouting *in vitro* and physiological angiogenesis *in vivo*[51].

Neovascularization

In 2009, Bonauer *et al.* showed that miR-92a is highly expressed in human ECs and overexpression of miR-92a in ECs blocked sprouting in a three-dimensional angiogenesis model. *In vivo* inhibition of miR-92a increased the number of perfused vessels in matrigel plugs and improved blood flow recovery after hind limb ischemia[52]. ITGA5 was identified as a direct target of miR-92a[52]. To elucidate the specific function of the other members of the miR-17-92 cluster in angiogenesis, Doebele *et al.* overexpressed or blocked individual members of the cluster both *in vitro* and *in vivo*[53]. *In vitro* inhibition of all miR-17-92 members, except miR-19, resulted in increased sprouting of EC spheroids[53]. Combined inhibition of miR-17 and miR-20a was shown to promote angiogenesis in matrigel plugs *in vivo,* whereas inhibition of other members showed trends but no significant effects on angiogenesis[53]. Expression of JAK1 was reduced at mRNA and protein level upon miR-17 overexpression and inhibition of JAK1 using siRNAs was shown to reduce *in vitro* angiogenesis. Using luciferase assays, JAK1 was confirmed as a direct target of miR-17[53].

The contribution of the miR-17-92 cluster to physiological and pathological arteriogenesis was studied by Landskroner-Eiger *et al.*[54]. Endothelial specific knockout of miR-17-92 in mice showed that these animals had more pre-existent collateral arterioles. Consequently, these animals showed improved blood flow recovery after ischemia. MiR-19a targets components of WNT signalling, namely FZD4 and LRP6. Inhibition of miR-19a improved post-ischemic blood flow recovery[54].

Expression of the miR-17-92 cluster is repressed by HDAC9 in ECs[55]. Inhibition of HDAC9 reduced neovascularization *in vitro* and *in vivo*. Inhibition of HDAC9, using either a broad spectrum HDAC inhibitor or siRNAs against HDAC9, increased expression of the miR-17-92 cluster, suggesting that the antiangiogenic effects of HDAC9 inhibition are mediated through the miR-17-92 cluster. Indeed, inhibition of miR-17-20a combined, but not of miR-17 alone, completely rescued the reduced sprouting and network formation in HDAC9 deficient ECs[55].

Atherosclerosis

Several studies showed that miR-17-92 cluster members are regulated by changes in shear stress[56, 57]. Upregulation of miR-19a by laminar shear stress has an antiproliferative effect on ECs via targeting of Cyclin D1[57]. MiR-92a expression was reduced in HUVECs that were subjected to atheroprotective laminar shear stress, leading to upregulation of KLF2[58]. Expression of KLF2 targets eNOS and thrombomodulin were decreased upon miR-92a overexpression[58].

MicroRNA expression profiling in HUVECs revealed upregulation of miR-92a upon low shear stress conditions and the presence of oxLDL[59]. Accordingly, miR-92a expression was higher in the vasculature of both mice and humans in atheroprone regions with low shear stress[59]. MiR-92a inhibition reduced atherosclerosis formation in hypercholesterolemic $LDLR^{-/-}$ mice. Expression of target genes Klf2 and Klf4 was increased upon anti-miR-92a treatment. The authors identified SOCS5 as a novel target of miR-92a, which is involved in the regulation of endothelial inflammation[58]. Furthermore, circulating ICAM-1 levels were reduced in anti-miR-92a treated animals. These results suggest that upregulation of miR-92a by oxLDL in atheroprone regions promotes endothelial dysfunction and atherosclerosis formation[59].

Interestingly, inhibition of miR-92a in rats reduced neointima formation in carotid arteries after vascular injury[60]. MiR-92a inhibition increased EC proliferation and migration, improving reendothelialization after balloon injury or arterial stenting. Expression of KLF4 and MKK was upregulated by miR-92a inhibition[60]. MiR-92a is a promising therapeutic target to reduce atherosclerosis development and post-interventional restenosis.

Aneurysm

Two members of the 17-92 cluster, miR-20a and miR-92a, were significantly upregulated in ECs of AAA tissue, but a causative role has yet to be confirmed[32].

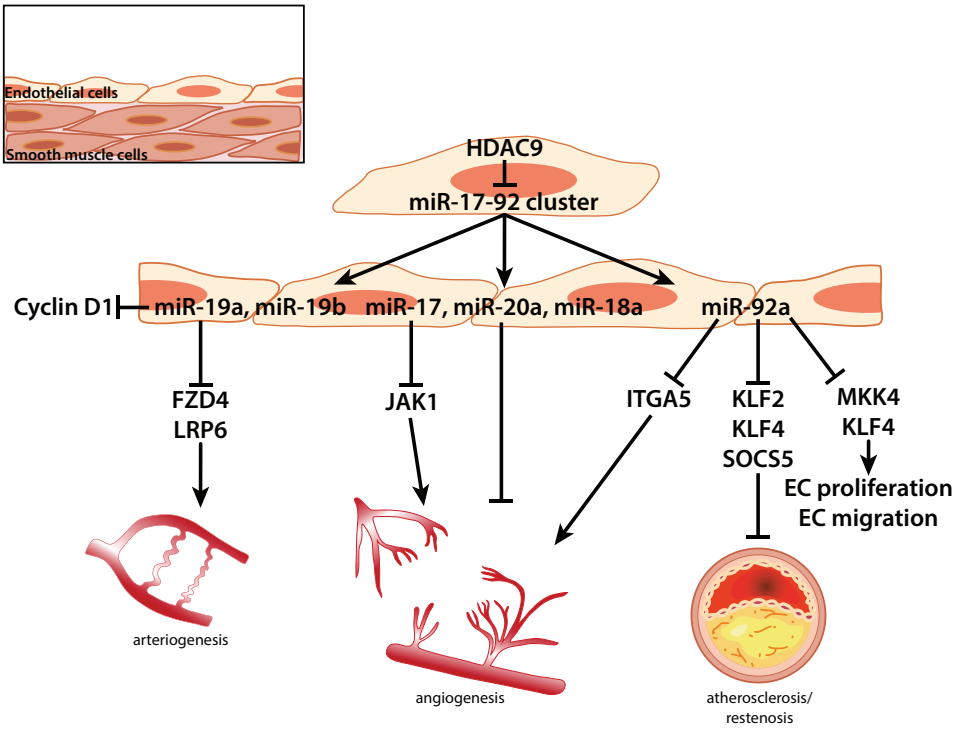

Figure 4. The role of the miR-17-92 cluster in vascular remodelling. MiR-17-92 cluster members regulate angiogenesis via suppression of several target genes. MiR-17 reduces expression of JAK1. ITGA5 is targeted by miR-92a. In addition, miR-92a targets KLF2, KLF4 and SOCS5, promoting atherosclerosis formation. Proliferation and migration of endothelial cells is regulated by targeting of MKK4 and KLF4 by miR-92a. MiR-19a has an antiproliferative effect in ECs via suppression of Cyclin D1. Other target genes of miR-19a include FZD4 and LRP6, regulators of WNT signalling. Targeting of these genes by miR-19a affects collateral artery formation and bloodflow recovery after ischemia. Arrows indicate upregulation. Capped lines indicate inhibition. EC; endothelial cell. For full target gene names, see Table 1.

miR-23/24/27 family

The miR-23/24/27 family consists of two separate microRNA gene clusters. The mouse intergenic miR-23a-27a-24-2 cluster lies on chromosome 8; in humans this cluster is located on chromosome 19. The miR-23b-27b-24-1 cluster has an intronic location on mouse chromosome 13, chromosome 9 in humans[61, 61, 62]. Members of the miR-23/24/27 family are highly expressed in vascularized tissues and ECs[63] (Figure 5). Laminar flow and unidirectional shear stress increase the expression of miR-23b, miR-27a/b and miR-24 in ECs[56, 64, 65]. Increased expression of miR-23b and miR-27b by pulsatile shear flow was found to correlate with EC growth arrest. The expression of cell cycle gene E2F1 was downregulated by miR-23b and miR-27b[56]. Moreover, phosphorylation of the Rb protein was blocked by miR-23b. Decreased Rb phosphorylation reduces EC proliferation and inhibits cell cycle progression[56]. Anti-miR-23b, but not anti-miR-27, treatment of HUVECs resulted in partial reversal of shear stress induced growth arrest[55].

Neovascularization

Knockdown of miR-23a/b and miR-27a/b decreased *in vitro* EC sprouting and *ex vivo* aortic ring sprouting[62]. Anti-angiogenic genes SEMA6A, SEMA6D and SPROUTY2 are targeted by miR-23a/b and miR-27a/b , as shown by luciferase gene reporter assays[62]. Urbich *et al.* showed that i*n vivo* angiogenesis was also affected upon inhibition of miR-27a/b. Anti-miR-27a/b treatment decreased the number of perfused vessels in matrigel plugs[66]. Moreover, inhibition of miR-27a/b impaired vasculogenesis in zebrafish embryos. *In vitro* experiments showed additional targeting of SEMA3B but *in vivo,* only SEMA6A was a target of miR-27a/b[66]. Young *et al.* showed that miR-27a also targets VE-cadherin, both *in vitro* and *in vivo*[67].

MiR-24 is expressed in cardiac ECs[68]. The expression of miR-24 is induced upon hypoxia and miR-24 is enriched in cardiac ECs compared to other cardiac cells after cardiac ischemia[68, 69]. Overexpression of miR-24 in HUVECs increased apoptosis and impaired tube formation, sprouting, migration and proliferation[68]. The endothelium-enriched transcription factors GATA2 and PAK4 were validated as targets of miR-24. Inhibition of miR-24 increased vascularity and decreased myocardial infarct size in mice[68]. Another confirmed target gene for miR-24 in ECs is NDST1. Inhibition of NDST1 by miR-24 decreased sulfation of HSPGs and subsequently the binding affinity of HSPGs for VEGFA. MiR-24 mediated suppression of NDST1 lowered VEGFR2 levels and reduced EC responsiveness to VEGFA[70]. Via these mechanisms, miR-24 affects EC responsiveness to VEGFA. MiR-24 also affected apoptosis, proliferation and function of SMCs, partially through HMOX1[69].

Atherosclerosis, restenosis and lipid metabolism

The effects of miR-24 and 27b as described here are predominantly on lipid metabolism, which will ultimately also influence atherosclerosis[71-73]. MiR-24 and miR-27b are upregulated in livers of high-fat diet (HFD) fed mice[71, 72]. Inhibition of miR-24 in HFD fed mice reduced plasma triglyceride levels and lipid accumulation in the liver, but did not affect plasma cholesterol levels. This effect was mediated via increased expression of INSIG1 in the liver and subsequent decreased expression of SREBPs and other lipogenic genes[72].

MiR-27b targets several additional lipogenic genes, including PPARγ, ANGPTL3 and GPAM. However, direct binding of miR-27b to the 3'UTR of the mRNAs of these genes was not demonstrated[71]. Upregulation of hepatic miR-27b was observed in HFD $ApoE^{-/-}$ mice and expression of miR-27b target genes Angptl3 and Gpam was reduced[71]. Experiments performed in the THP-1 human monocyte cell line showed that miR-27a/b regulates cholesterol homeostasis[73]. MiR-27a/b targeting of ABCA1 affected apoA1-mediated cholesterol efflux in macrophages[73]. Lipid uptake was also affected by miR-27a/b, as was shown by reduced oxLDL binding to macrophages after miR-27a/b overexpression. This was mediated by miR-27a/b target gene LPL. Finally, cholesteryl-ester formation was reduced by miR-27a/b via targeting of ACAT1[73].

The contribution of miR-23b to SMC phenotypic switching upon vascular injury was recently reported by Iaconetti *et al.*[74]. Expression of miR-23b was reduced after carotid injury in rats. Increased proliferation and migration of SMCs was observed upon miR-23b inhibition, whereas overexpression of miR-23b led to reduced proliferation and migration[74]. Overexpression of miR-23b resulted in decreased neointima formation in rat carotid arteries after balloon angioplasty and target genes uPA, SMAD3 and FOXO4

were downregulated in these animals[74].

Aneurysm

MicroRNA expression profiling revealed decreased expression of the miR-23b/miR-24-1 cluster, in human intracranial aneurysmal (IA) samples[75, 76]. In murine AAA models, the miR-23b-27b-24 cluster is also downregulated. MiR-24 was most significantly downregulated, leading to upregulation of the inflammatory target gene CHI3L1[77]. *In situ* hybridization showed localization of miR-24 in adventitial macrophages of aneurysmal aortic mouse tissue. MiR-24 co-localized with CHI3L1 in activated macrophages, where CHI3L1 drives inflammatory gene expression[78]. Modulation of miR-24 levels in murine AAA models using either pre-miR-24 or anti-miR-24 led to reduced and increased AAA formation respectively[77]. In summary, miR-23b-24-27b family members are downregulated in human IA samples and murine AAA models and modulation of miR-24 influences aortic inflammation, thereby contributing to AAA development[75-77]. This renders the miR-23-24-27 family a potentially interesting therapeutic target for AAA treatment.

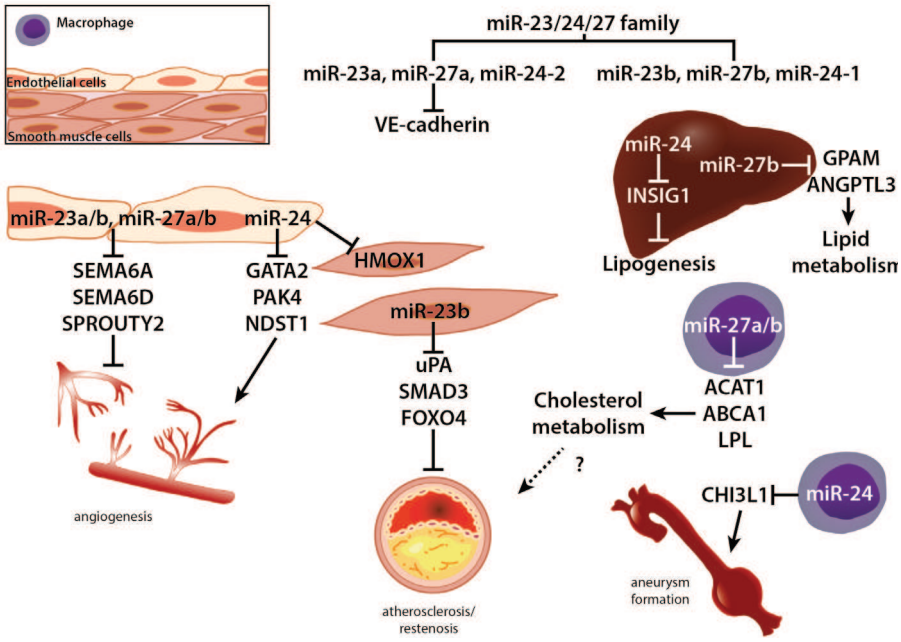

Figure 5. Different roles in vascular remodelling for microRNAs of the miR-23/24/27 family. The miR-23/24/27 family consists of two miR clusters, namely the miR-23a-27a-24-2 cluster and the miR-23b-27b-24-1 cluster. MiR-23a/b and miR-27a/b target the anti-angiogenic genes SEMA6A, SEMA6D and SPROUTY2. In addition, miR-27a inhibits expression of VE-cadherin. MiR-24 inhibits proliferation, migration and sprouting of HUVECs via the endothelium-enriched transcription factor GATA2, PAK4 and NDST1. Moreover, miR-24 affects SMC apoptosis, proliferation and function via HMOX1. Expression of miR-23b in SMCs was found to target uPA, SMAD3 and FOXO4, which results in decreased proliferation and migration of SMCs. Overexpression of miR-23b decreases neointima formation upon balloon injury in rats. Members of the miR-23/24/27 family also play an important role in lipid metabolism. Cholesterol metabolism is affected by miR-27a/b through suppression of ACAT1, ABCA1 and LPL in macrophages. In the liver, miR-27b targets the lipogenic genes GPAM and ANGPTL3, whereas miR-24 suppresses expression of INSIG1. Of the miR-23/24/27 family members, only miR-24 has been described to affect AAA formation. MiR-24 is expressed in macrophages in the adventitia of murine aneurysmal tissue, where it is co-localized with and inhibits expression of the CHI3L1 gene. Arrows indicate upregulation. Capped lines indicate inhibition. The dashed lines indicates an interaction that has not been confirmed yet. (HUV)EC; (human umbilical venous) endothelial cell, SMC; smooth muscle cell. For full target gene names, see Table 1.

miR-143/145 cluster

The miR-143/145 gene cluster contains two highly conserved microRNAs, which are located on human chromosome 5. In 2007, these microRNAs were first described as downregulated in rat carotid arteries after induction of balloon injury[78]. Restoration of miR-143 and miR-145 expression levels using an adenoviral vector reduced neointima formation upon balloon injury in rat carotids[79, 80]. MiR-145 is the most abundantly expressed microRNA in healthy rat carotid arteries, where it is predominantly localized in SMCs[81]. During SMC differentiation from multipotent stem cells, high transcript levels of miR-143 and miR-145 are observed[82]. Upregulation of these microRNAs allows for SMC differentiation, whereas their expression is downregulated upon proliferation[82]. Together, these microRNAs play an important role in the differentiation and proliferation of SMCs. Differentiation of SMCs is induced via SRF, Myocardin and myocardin-related transcription factors, but can also be induced via the Jag-1/ Notch signalling pathway[83, 84]. These factors also regulate the transcription of the miR-143/145 cluster, further promoting differentiation of SMCs[83, 84] (Figure 6, upper panel). Expression of contractile genes is mediated via (amongst other factors) KLF4, which is directly targeted by miR-145[82]. Inhibition of KLF4 by miR-145 increases expression of SMC markers [82]. MiR-143 can directly inhibit proliferation of SMCs via targeting of ELK1[84].

In accordance with these findings, Boettger *et al.* described that miR-143/145 deficient mice have a thinner arterial medial layer and a decreased blood pressure[85]. In general, the miR-143/145 cluster has proven essential for SMC function and controls the phenotypic switch of contractile SMCs towards synthetic VSMCs[79, 81, 82, 85] (Figure 6, upper panel).

Neovascularization

MiR-145 inhibits tumour angiogenesis via targeting of IGF1, the IRS1 pathway and its downstream genes N-RAS and VEGF-A[86, 87]. MiR-143 was found to inactivate AKT, which is a downstream signalling molecule in the IGF1 receptor pathway and thereby regulates angiogenesis and tumorigenesis[88]. Inactivation of AKT by miR-143 resulted in decreased protein levels of HIF-1α and reduced VEGFA expression[88]. In neuroblastoma samples, miR-145 expression was also downregulated, which was inversely correlated with HIF-2α expression[89]. The authors showed that miR-145 can directly target HIF-2α and suppress angiogenesis, which was demonstrated by tube formation of neuroblastoma cells[89].

Although these findings relate mainly to pathological angiogenesis, many fundamental mechanisms are shared with physiological angiogenesis, such as receptor signalling cascades (e.g. HIF-1α), proliferation and migration of vascular cells and tube formation[90]. Indeed, Wang *et al.* found that miR-145 was transiently downregulated *in vivo* following coronary artery occlusion in mice and *in vitro* upon hypoxia treatment of cardiac fibroblasts[91]. Inhibition of miR-145 increased infarct scar size at 7 and 28 days after myocardial infarction in mice. However, reduced differentiation of cardiac fibroblasts towards myofibroblasts, and not decreased angiogenesis, most likely mediated these effects[91]. The authors demonstrated that transfection with miR-145 increased the number of α-SMA positive cells in fibroblast cultures, thus inducing transdifferentiation of fibroblasts into myofibroblasts. KLF5 is

a direct target of miR-145. Transfection with miR-145 decreased expression of KLF5 and increased Myocardin expression. These data suggest that miR-145 mediates differentiation of cardiac fibroblasts to myofibroblasts through the KLF5-Myocardin pathway[91].

Work by Climent *et al.* suggests that miR-143 and miR-145 are transferred from SMCs to ECs via membrane protrusions[92]. TGFβ induces the transfer of miR-143/145, as inhibition of either the TGFβ pathway or TGFβR2 reduced miR-143/145 transfer towards ECs[92]. Overexpression of miR-143 and miR-145 in ECs reduced proliferation and the ability to form capillary-like structures on matrigel[92]. The authors identified HKII and ITGβ8 as direct targets of miR-143/145 that modulate the angiogenic potential of ECs[92] (Figure 6).

Atherosclerosis and restenosis

MiR-143/145$^{-/-}$ mice develop spontaneous neointimal lesions in the femoral arteries at older age[85]. Angiotensin converting enzyme (ACE) was identified as a target for miR-143/145. Increased expression of ACE in miR-143/145$^{-/-}$ mice resulted in increased AngII levels, which subsequently contributed to the synthetic phenotype of miR-143/145$^{-/-}$ SMCs[85]. ApoE$^{-/-}$ mice treated with SMC-specific lentiviral miR-145 showed a reduction in plaque size and an increase in atherosclerotic plaque stability[93]. This is in line with the finding that overexpression of miR-145 decreased neointima formation in balloon injured arteries by modulation of KLF5 expression[80]. However, reduced neointima formation after carotid artery ligation in miR-143/145$^{-/-}$ mice has also been reported[94]. The authors explained this by the fact that the SMCs in their knockout model were already deficient in miR-145 at the onset of injury, whereas in the overexpression model, miR-145 expression was normal at the onset of the experiment[94].

In humans, miR-145 levels were significantly lower in plaques than in atherosclerosis-free regions[93]. Cholesterol loading of mouse aortic SMCs resulted in downregulation of SMC markers, whereas expression of macrophage markers was increased[95]. Expression of miR-143 and miR-145, as well as the expression of SRF and Myocardin, were downregulated[95]. Cholesterol loading, via downregulation of the miR-143/145/SRF/Myocardin axis, causes reprogramming of SMCs towards a macrophage like phenotype[95]. Moverover, statin treatment, which is the most common form of anti-atherosclerotic therapy today, increases expression of miR-143/145 in ECs[96].

In addition to intercellular transfer of miR-143/145 from SMCS to ECs, transport of miR-143/145 in the opposite direction has also been described[92]. Increases in laminar shear stress lead to upregulation of KLF2, which subsequently induces transcription of the miR-143/145 cluster in ECs[96]. Upregulation of miR-145 in ECs was shown to repress JAM-A, which reduces leukocyte recruitment and infiltration and thus atherosclerosis formation[97]. KLF2 also triggered release of EC derived MVs, which transfer miR-143/145 from ECs to SMCs. Injection of MVs that are rich in miR-143/145 in HFD fed mice, led to a reduction of plaque formation[96]. In contrast, miR-143/145$^{-/-}$ mice developed smaller atherosclerotic lesions compared to LDLR$^{-/-}$ controls[98]. Plaques of miR-143/145$^{-/-}$ mice contained less macrophages and analysis of plasma cholesterol levels revealed decreased VLDL and LDL fractions. ABCA1 was confirmed as miR-145 target in this study, but this was not reflected by increased HDL levels in miR-143/145$^{-/-}$ mice[98].

Aneurysm

MiR-145 was downregulated in IA tissues[75]. Elia *et al.* demonstrated that both miR-143 and miR-145 were reduced in human thoracic aorta aneurysms, which correlated with SMC function[79, 99]. In AAA however, expression levels of miR-145 and miR-143 were similar to those in normal abdominal aortic tissues[32].

Homozygous miR-143/145$^{-/-}$ mice showed structural defects in the SMC layer of the aorta[74]. Additionally, the SMCs in the media of aortas from miR-143/145$^{-/-}$ mice had a dedifferentiated phenotype, demonstrated by increased migration and proliferation and an increased protein synthesis[74].

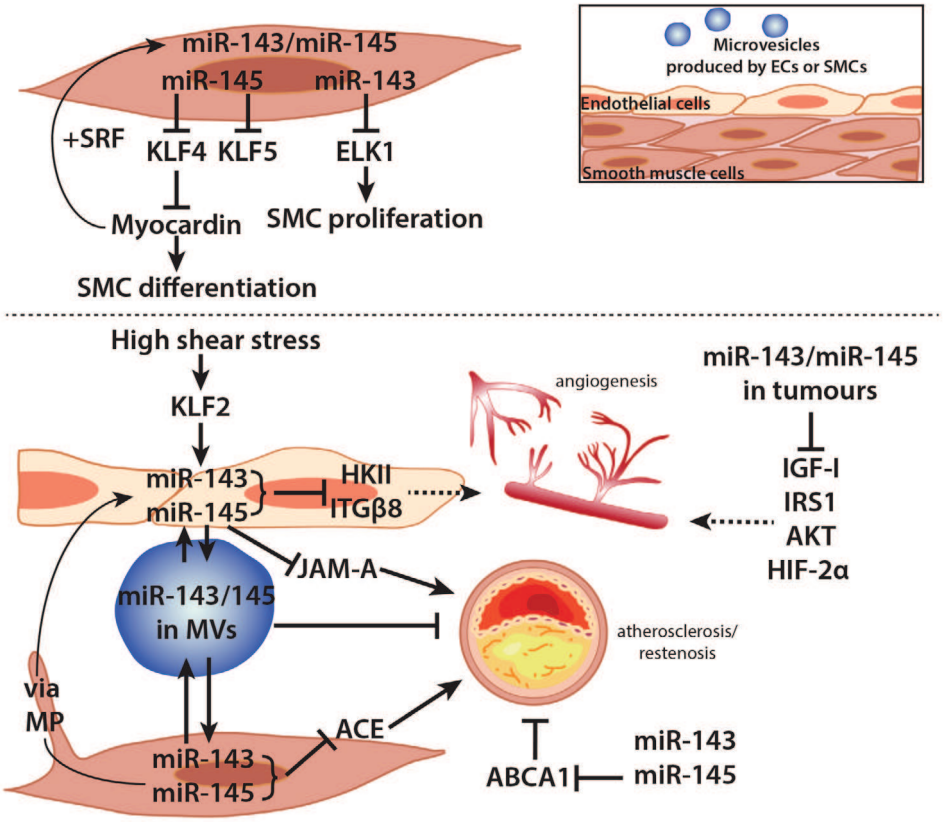

Figure 6. The miR-143/145 cluster in vascular remodelling. MiR-143 and miR-145 control SMC phenotype. Differentiation of SMCs is regulated by SRF, Myocardin and myocardin-related transcription factors (MRTFs). Via a feedback loop, these factors also regulate expression of the miR-143/miR-145 cluster itself (upper panel). Inhibition of KLF4 and KLF5 by miR-145 results, via Myocardin, in SMC differentiation and myofibroblast transdifferentiation, whereas targeting of ELK1 by miR-143 inhibits proliferation of SMCs. TGFβ and BMP4 are also able to activate expression of the miR-143/miR-145 cluster (not shown here). In addition, high shear stress, via KLF2, increases expression of miR-143/miR-145 in ECs (figure 4, lower panel).
In tumours, miR-145 suppresses IGF1 and the IRS1 pathway, affecting angiogenesis. In addition, miR-145 targets HIF2α and suppresses angiogenesis. MiR-143 targets AKT, thereby decreasing HIF1α and VEGFA expression. Transfer of miR-143/145 from VSMCs to ECs via membrane protrusions (MP) decreases the expression of HKII and ITGβ8 and via this mechanism presumably modulates angiogenesis. Intercellular transfer of miR-143/145 via MVs has also been described. MVs rich in miR-143/145 inhibit atherosclerotic plaque formation. ACE is another target of miR-143/145 which affects atherosclerosis. Arrows indicate upregulation. Capped lines indicate inhibition. The dashed lines indicate interactions that have not been confirmed yet. MP; membrane protrusion, MV; microvesicle, EC; endothelial cell , SMC; smooth muscle cell. For full target gene names, see Table 1.

14q32 microRNA gene cluster

The 14q32 microRNA cluster is the largest known mammalian microRNA gene cluster, located on human chromosome 14 and mouse chromosome 12. The cluster consists of 54 microRNAs in humans and 61 in mice[100, 101] (Figure 7). It is assumed that transcription of the 14q32 microRNA gene cluster is controlled by the long noncoding RNA MEG3, also located on human chromosome 14, as deletion of MEG3 leads to downregulation of 14q32 microRNAs, as was shown in MEG3$^{-/-}$ mice[102]. MEG3$^{-/-}$ embryos have increased expression of VEGF pathway genes and increased cortical microvessel density[102].

Neovascularization

Using a reverse target prediction analysis, where we looked for putative microRNA binding sites in the 3'UTRs of a set of nearly 200 neovascularization genes, our research group observed enrichment of binding sites for 14q32 microRNAs in the 3' UTRs of these genes. Microarray analyses performed on adductor muscle tissue of mice that underwent single ligation of the femoral artery as a model for effective neovascularization showed upregulation of 14q32 microRNAs following three different expression patterns[101]. We observed so called early responders, microRNAs whose expression was upregulated 24 hours after induction of ischemia, late responders whose expression was upregulated from 72 hours after ischemia induction and non-responders. Inhibition of early responders miR-487b, miR-494, late responder miR-329 and non-responder miR-495 led to increased neovascularization and an improved blood flow recovery after hind limb ischemia in mice. Inhibition of miR-329, miR-487b and miR-495 increased proliferation of human umbilical arterial ECs[101]. *In vivo,* inhibition of miR-329 led to upregulation of target genes TLR4, VEGFA, FGFR2 and MEF2A, whereas TLR4, VEGFA, ARF6, EFNB2 and FGFR2 were upregulated upon inhibition of miR-494. Using dual luciferase reporter gene assays, direct binding of miR-494 to the 3'UTRs of VEGFA, EFNB2 and FGFR2 was demonstrated. MiR-329 directly targets MEF2a and although VEGFA was regulated by miR-329, this was an indirect effect[101]. MiR-495 directly targets the 3'UTR of CCL2 and via this mechanism, proliferation and apoptosis of HUVECs is affected[103]. Inhibition of miR-329, miR-487b, miR-494 and miR-495 also increased sprouting in aortic ring assays[101]. Wang *et al.* showed that miR-329 is a negative regulator of angiogenesis by targeting CD146, which functions as co-receptor for VEGFR2. Inhibition of miR-329 increased angiogenesis in this study, both *in vitro* and *in vivo*[104].

In a model for cerebral ischemia, 14q32 miR-376b-5p also regulates angiogenesis. Expression of miR-376b-5p was decreased following middle cerebral artery occlusion (MCAO) in rats and miR-376b-5p inhibited angiogenesis *in vivo*, as well as in HUVEC cultures, via targeting of the HIF-1α mediated VEGFA/Notch-1 signalling pathway [105]. In another study, 14q32 microRNA miR-377 was identified as the most significantly downregulated microRNA in hypoxia-treated mesenchymal stem cells (MSCs) in rats[106]. Knockdown of miR-377 in HUVECs promoted angiogenesis *in vitro*, via direct targeting of VEGFA. To elucidate whether hypoxia-associated miR-377 regulated MSC induced myocardial angiogenesis in ischemic hearts, the authors transduced rat MSCs with lentiviral vectors in order to overexpress or suppress miR-377 expression. MSCs with lentiviral miR-377, anti-miR-377 or empty vector were then injected into ischemic rat hearts after ligation of the left anterior descending coronary artery.

Inhibition of miR-377 in MSCs enhanced angiogenesis, decreased the area of fibrosis and improved cardiac function of these animals[106].

Atherosclerosis

MicroRNA expression profiling in symptomatic versus asymptomatic human atherosclerotic plaques, showed upregulated expression of 14q32 microRNA miR-127[107]. Our group also investigated expression of 14q32 microRNAs in stable versus unstable plaques of patients who underwent carotid endarterectomy surgery. We observed upregulation of 14q32 miR-494 in unstable atherosclerotic plaques. Inhibition of miR-494 led to reduced plaque formation in mice, while plaque stability was increased[108]. Moreover, total plasma cholesterol and VLDL fractions were decreased in these animals. Inhibition of miR-494 led to upregulation of target genes TGFB2, TIMP3 and IL33.

In addition,14q32 microRNA miR-136 was upregulated in human atherosclerotic plaques . This microRNA is also highly expressed in synthetic SMCs *in vitro*[109]. MiR-136 targets PPP2R2A, resulting in increased ERK1/2 phosphorylation and increased proliferation of SMCs. The authors proposed that via this mechanism, miR-136 contributes to abnormal proliferation of SMCs, which is often observed in atherosclerosis[109].

In a study performed by Ramirez *et al.*, the 14q32 microRNA miR-758 regulated ABCA1 in macrophages. Transfection of J774-macrophages with miR-758 reduced cholesterol efflux[110]. MiR-758 levels were furthermore regulated by dietary cholesterol *in vivo*. High dietary fat repressed miR-758 expression in the liver as well as in peritoneal macrophages, whereas ABCA1 levels were increased[110]. In another study, miR-758 levels were upregulated in hypercholesterolemic human plaques compared to normocholesterolemic plaques[111]. ABCA1 mRNA levels were also increased in hypercholesterolemic patients, whereas protein levels were similar to normocholesterolemic patients, suggesting strong posttranscriptional regulation of ABCA1 by miR-758. These human data suggest a role for miR-758 as ABCA1 modulator in human atherosclerotis[111].

A role for the 14q32 microRNA miR-370 in lipid metabolism and atherosclerosis was first described by Iloupoulos *et al.,* mainly via direct targeting of CPT1α, an important enzyme in fatty acid β-oxidation[112]. Other lipogenic genes such as SREBP-1c and DGAT2 were also regulated by miR-370. Using transfection experiments with sense and antisense miR-370, this regulation was mediated indirectly via miR-122[112]. Finally, extensive hypomethylation of the 14q32 locus was observed in human atherosclerotic plaques, which resulted in upregulation of several 14q32 microRNAs[113]. These findings suggest a role for epigenetic modulation of the 14q32 microRNA cluster in atherosclerosis[113].

Aneurysm

MiR-487b is involved in hypertension-induced outward remodelling of the aorta. Chronic hypertension induced via AngII infusion led to significant upregulation of miR-487b in the aortae of rats[114]. MiR-487b was predominantly expressed in the adventitia and co-localized with the vasoactive IRS1. Using luciferase reporter gene assays, miR-487b was shown to directly target the IRS1 3'UTR, both in rats and humans. MiR-487b downregulated expression of IRS1 in aortae of hypertensive rats, both at mRNA and protein level[114].

Although further research into this extraordinarily large microRNA cluster is necessary, it is clear that the 14q32 microRNAs play important but diverse roles in the multiple processes of vascular remodelling, opening up new possibilities for prevention, detection and treatment of CVD[115] (Figure 7).

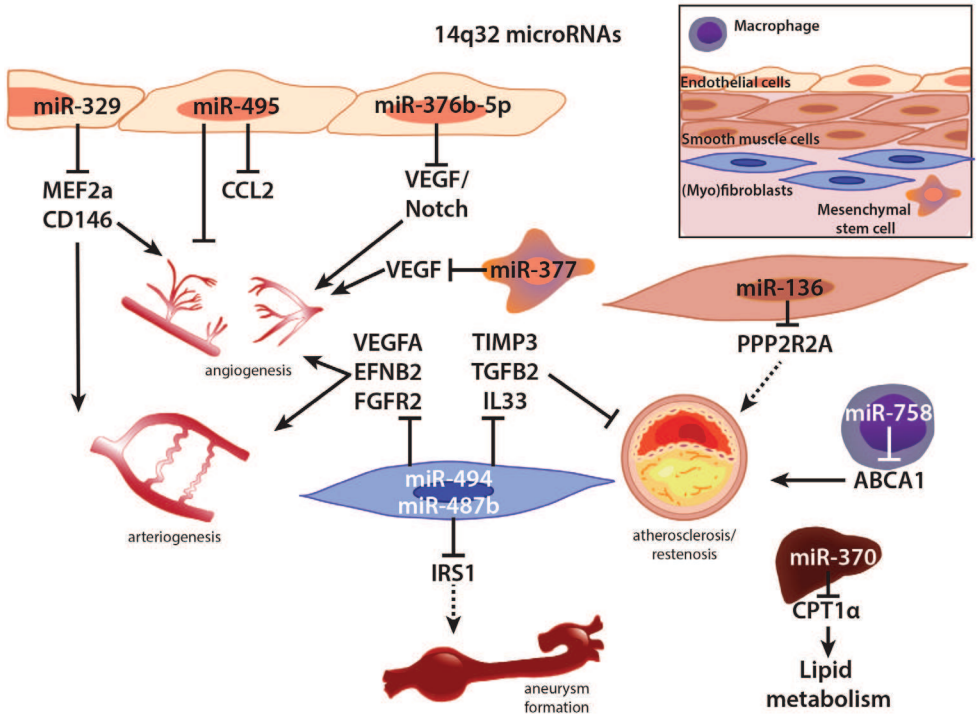

Figure 7. Roles for 14q32 miRs in vascular remodelling. MiR-329 inhibits angiogenesis and arteriogenesis via targeting of the co-receptor for VEGFR2, CD136 and MEF2a. Arteriogenesis and angiogenesis are also inhibited by miR-494, which suppresses VEGFA, EFNB2 and FGFR2. MiR-495 inhibits both arteriogenesis and angiogenesis. Proliferation and migration of HUVECs is affected by miR-495, via targeting of CCL2. VEGF signalling is further influenced through targeting of the HIF1α mediated VEGF/Notch signalling pathway by miR-376-5p and via direct targeting of VEGF by miR-377. MiR-494 also influences atherosclerosis, through the inhibition of several target genes namely TIMP3, TGFβ2 and IL33. MiR-136 is upregulated in human atherosclerotic plaques, where it targets PPP2R2A. Furthermore, cholesterol metabolism is affected by miR-758 through suppression of ABCA1 and by miR-370 via direct targeting of CPT1α. MiR-487b in highly expressed in the adventitia of rat aortae during chronic hypertension. Here, miR-487b targets IRS1, where it is thought to contribute to outward remodelling of the aorta. Arrows indicate upregulation. Capped lines indicate inhibition. MV; microvesicle, (HUV)EC; (human umbilical venous) endothelial cell , SMC; smooth muscle cell layer. For full target names, see Table 1.

Circulating microRNAs

Several of the microRNAs discussed in this review are also expressed in the circulation and could be used as biomarkers for vascular remodelling and cardiovascular disease. For example, circulating miR-155 was expressed at significantly lower levels in CAD patients compared to healthy volunteers[19]. Likewise, circulating levels of miR-126, miR-17, miR-92a were decreased in these patients[19, 115]. Several miRs, including miR-126, were significantly increased in plasma of patients with insufficient collateral artery function[116]. Furthermore, circulating levels of several 14q32 microRNAs, including miR-134,

miR-328, miR-370, miR-487a and miR-480 may have a diagnostic value for acute myocardial infarction, coronary artery disease and cardiac death[117-121]. 14q32 miR-487b was increased in circulating leukocytes of patients with acute ischemic stroke[122]. Other 14q32 microRNAs, including miR-665 and miR-541 have been reported to play a role in heart failure and cardiac hypertrophy, respectively[123, 124] Nevertheless, these findings need to be confirmed in large prospective cohort studies to determine the potential use of these microRNAs as biomarkers for CVD.

Future perspectives

In this review, we have described the multifactorial nature of microRNAs in vascular remodelling, as demonstrated by their role in multiple remodelling processes. Adaptive remodelling, such as arteriogenesis and angiogenesis, is stimulated by miR-126 and by the miR-23/24/27 family. Correspondingly, these microRNAs inhibit pathological remodelling, including atherosclerosis and restenosis. MiR-17/92, the 14q32 miRs and miR-143/145 induce pathological remodelling, while they inhibit adaptive remodelling (except miR-143/145, for which different effects on pathological remodelling have been described). MiR-155 was found to inhibit angiogenesis but stimulated arteriogenesis and was also reported to play contradicting roles in atherosclerosis formation.
The role of these microRNAs in the molecular mechanisms leading to aneurysm formation however, are still poorly described; except for miR-24 and miR-487b, the microRNAs discussed here were only described to be differentially regulated in aneurysms, and a causative role has yet to be elucidated (Figure 8). As mentioned in the introduction, a single microRNA is able to target numerous genes and can regulate complex (patho)physiological processes. Often in literature, a single target gene is validated to explain the observed *in vivo* and *in vitro* effects upon microRNA modulation. However, it is far more plausible that the observed effects are caused by modulation of many genes involved in these (patho)physiological processes rather than one gene. Since microRNAs only modestly downregulate the expression of their target genes, it can be difficult to confirm significant changes in target gene expression. Nevertheless, the multifactorial nature of microRNAs in both adaptive and maladaptive vascular remodelling offers great opportunities for development of future therapeutics for treatment and prevention of CVD. In conclusion, the multifactorial effects on vascular remodelling observed for the microRNAs discussed here, will hopefully stimulate the continued efforts to explore the potential of microRNAs as therapeutic target.

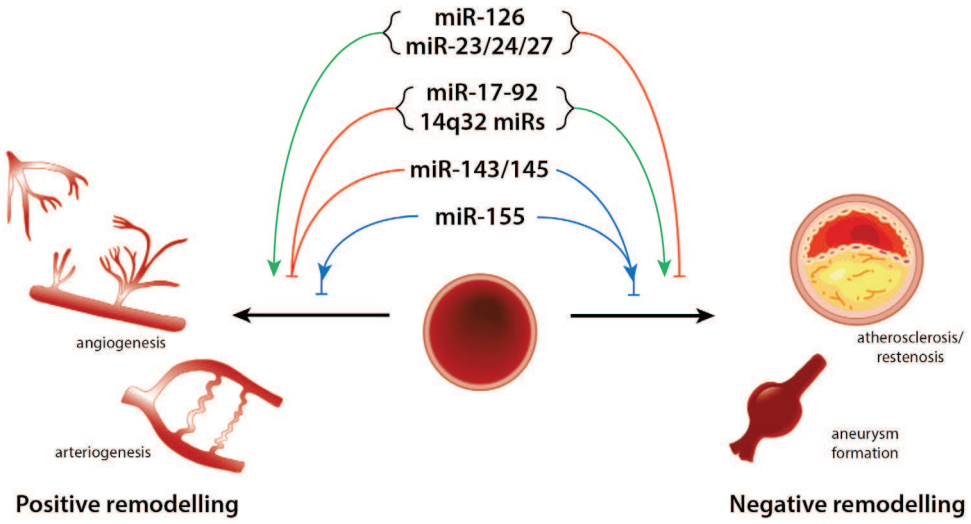

Figure 8. Graphical abstract. Several vascular microRNAs can influence multiple processes of vascular remodelling. MiR-126 is both pro-angiogenic as well as anti-atherosclerotic, like the miR-23-24-27 family. On the other hand, the 17-92 microRNA cluster and 14q32 miRs are anti-angiogenic but pro-atherosclerotic. For miR-155 and miR-143/145, both pro- and anti-angiogenic functions have been reported, as well as pro- and anti-atherosclerotic roles. Green arrows indicate a stimulatory function, whereas red arrows represent an inhibitory function. Blue arrows are used when both stimulatory as well as inhibitory roles have been reported.

MicroRNA		Confirmed Targets	Biological process affected
miR-126		VCAM1[20], SPRED1 and PIK3R2[21-23]	Angiogenesis, vascular integrity
		SDF1/CXCL12[25, 26]	Migration of $CD34^+$ progenitor cells
		RGS16[25]	Recruitment of Sca-1+ endothelial progenitor cells, atherosclerosis
		FOXO3, BCL2 and IRS1[30]	VSMC turnover
		DLK1 (miR-126-5p)[31]	Endothelial repair, atherosclerosis
miR-155		SOCS1[36]	Proinflammatory signalling
		TAB2[37]	Anti-inflammatory signalling
		PU.1[38]	Monocyte/macrophage infiltration, T lymphocyte activation
		AT1R[39], ETS-1[35]	HUVEC activation and migration
		AT1R[40], SOCS1[40]	Angiogenesis, Arteriogenesis
		BCL6, CCL2[42]	Atherosclerosis
		HMGB1[47]	Foam cell formation
		MMP1 and MMP3[49]	Matrix degradation
miR-23-24-27	miR-23 and miR-27	SEMA6A, SEMA6D, SPROUTY2[62]	EC sprouting, angiogenesis
	miR-23b	E2F1[56]	Rb phosphorylation, EC growth arrest
		uPA, SMAD3, FOXO4[74]	VSMC phenotypic switching
	miR-24	GATA2, PAK4[68]	Vascularity, cardiac function and infarct size after myocardial infarction
		NDST1[70]	HSPG sulfation and affinity of HSPGs for VEGF, endothelial cell responsiveness to VEGFA
		HMOX1[69]	SMC apoptosis and proliferation
		INSIG1[72]	Lipid accumulation and plasma triglyceride levels
		CHI3L1[77]	Inflammation, AAA formation
	miR-27a	VE-cadherin[67]	Vascular leakage
	miR-27b	ABCA1, LPL, ACAT1[73]	Cholesterol efflux, lipid uptake and cholesteryl ester formation
miR-17-92	miR-17-92	TSP1, CTGF[125]	Tumour angiogenesis
	miR-17/20	JAK1[53]	Angiogenesis
	miR-19a	CyclinD1[57]	EC proliferation
		FZD4 and LRP6[54]	WNT signalling, arteriogenesis
	miR-92a	KLF2, KLF4, SOCS5[59]	Endothelial homeostasis, atherosclerosis
		ITGA5[52]	Blood flow recovery after ischemia and LV function after myocardial infarction
		KLF4 and MKK[60]	EC proliferation and migration
miR-143/145	miR-143/145	HKII, ITGβ8[92]	Angiogenesis, vessel stability
		ACE[85]	Atherosclerosis
	miR-143	ELK1[84]	VSMC proliferation
		AKT[88]	Angiogenesis, tumorigenesis
	miR-145	IGF-I, IRS1[86, 87]	Tumour angiogenesis
		HIF2α[89]	Angiogenesis
		KLF5[91]	Transdifferentiation of fibroblasts to myofibroblasts, neointima formation
		KLF4[82]	VSMC differentiation
		JAMA1[97]	Leukocyte recruitment
		ABCA1[98]	Cholesterol efflux
14q32 miRs	miR-329	MEF2a[101], CD146[104]	Angiogenesis, Arteriogenesis, EC proliferation
	miR-494	VEGFA, EFNB2, FGFR2[101]	Angiogenesis, Arteriogenesis, myofibroblast proliferation
		TIMP3, TGFB2, IL33[108]	Atherosclerosis
	miR-376b-5p	HIF1a/VEGF signalling pathway[105]	Angiogenesis
	miR-377	VEGFA[106]	Angiogenesis
	miR-136	PPP2R2A[109]	VSMC proliferation
	miR-758	ABCA1[110]	Cholesterol efflux
	miR-370	CPT1α[112]	Fatty acid β oxidation
	miR-487b	IRS1[114]	Outward remodelling of the aorta

Table 2. Overview of confirmed target genes for microRNAs discussed.

References

1. Rajewsky N. microRNA target predictions in animals. Nat Genet 2006;38 Suppl:S8-13.
2. Gibbons GH, Dzau VJ. The emerging concept of vascular remodeling. N Engl J Med 1994;330:1431-1438.
3. Wei Y, Schober A, Weber C. Pathogenic arterial remodeling: the good and bad of microRNAs. Am J Physiol Heart Circ Physiol 2013;304:H1050-H1059.
4. Torella D, Iaconetti C, Catalucci D, Ellison GM, Leone A, Waring CD, et al. MicroRNA-133 controls vascular smooth muscle cell phenotypic switch in vitro and vascular remodeling in vivo. Circ Res 2011;109:880-893.
5. Villeneuve LM, Kato M, Reddy MA, Wang M, Lanting L, Natarajan R. Enhanced levels of microRNA-125b in vascular smooth muscle cells of diabetic db/db mice lead to increased inflammatory gene expression by targeting the histone methyltransferase Suv39h1. Diabetes 2010;59:2904-2915.
6. Leeper NJ, Raiesdana A, Kojima Y, Chun HJ, Azuma J, Maegdefessel L, et al. MicroRNA-26a is a novel regulator of vascular smooth muscle cell function. J Cell Physiol 2011;226:1035-1043.
7. Liu K, Ying Z, Qi X, Shi Y, Tang Q. MicroRNA-1 regulates the proliferation of vascular smooth muscle cells by targeting insulin-like growth factor 1. Int J Mol Med 2015;36:817-824.
8. Li P, Zhu N, Yi B, Wang N, Chen M, You X, et al. MicroRNA-663 regulates human vascular smooth muscle cell phenotypic switch and vascular neointimal formation. Circ Res 2013;113:1117-1127.
9. Maegdefessel L, Azuma J, Toh R, Merk DR, Deng A, Chin JT, et al. Inhibition of microRNA-29b reduces murine abdominal aortic aneurysm development. J Clin Invest 2012;122:497-506.
10. Maegdefessel L, Azuma J, Toh R, Deng A, Merk DR, Raiesdana A, et al. MicroRNA-21 blocks abdominal aortic aneurysm development and nicotine-augmented expansion. Sci Transl Med 2012;4:122ra22.
11. Najafi-Shoushtari SH, Kristo F, Li Y, Shioda T, Cohen DE, Gerszten RE, et al. MicroRNA-33 and the SREBP host genes cooperate to control cholesterol homeostasis. Science 2010;328:1566-1569.
12. Rayner KJ, Sheedy FJ, Esau CC, Hussain FN, Temel RE, Parathath S, et al. Antagonism of miR-33 in mice promotes reverse cholesterol transport and regression of atherosclerosis. J Clin Invest 2011;121:2921-2931.
13. Rayner KJ, Suarez Y, Davalos A, Parathath S, Fitzgerald ML, Tamehiro N, et al. MiR-33 contributes to the regulation of cholesterol homeostasis. Science 2010;328:1570-1573.
14. Rayner KJ, Esau CC, Hussain FN, McDaniel AL, Marshall SM, van Gils JM, et al. Inhibition of miR-33a/b in non-human primates raises plasma HDL and lowers VLDL triglycerides. Nature 2011;478:404-407.
15. Kuehbacher A, Urbich C, Zeiher AM, Dimmeler S. Role of Dicer and Drosha for endothelial microRNA expression and angiogenesis. Circ Res 2007;101:59-68.
16. Gatsiou A, Boeckel JN, Randriamboavonjy V, Stellos K. MicroRNAs in platelet biogenesis and function: implications in vascular homeostasis and inflammation. Curr Vasc Pharmacol 2012;10:524-531.
17. de Boer HC, van Solingen C, Prins J, Duijs JM, Huisman MV, Rabelink TJ, et al. Aspirin treatment hampers the use of plasma microRNA-126 as a biomarker for the progression of vascular disease. Eur Heart J 2013;34:3451-3457.
18. Laffont B, Corduan A, Rousseau M, Duchez AC, Lee CH, Boilard E, et al. Platelet microparticles reprogram macrophage gene expression and function. Thromb Haemost 2015;115.
19. Fichtlscherer S, De Rosa S, Fox H, Schwietz T, Fischer A, Liebetrau C, et al. Circulating microRNAs in patients with coronary artery disease. Circ Res 2010;107:677-684.
20. Harris TA, Yamakuchi M, Ferlito M, Mendell JT, Lowenstein CJ. MicroRNA-126 regulates endothelial expression of vascular cell adhesion molecule 1. Proc Natl Acad Sci U S A 2008;105:1516-1521.
21. Fish JE, Santoro MM, Morton SU, Yu S, Yeh RF, Wythe JD, et al. miR-126 regulates angiogenic signaling and vascular integrity. Dev Cell 2008;15:272-284.
22. van Solingen C., Seghers L, Bijkerk R, Duijs JM, Roeten MK, van Oeveren-Rietdijk AM, et al. Antagomir-mediated silencing of endothelial cell specific microRNA-126 impairs ischemia-induced angiogenesis. J Cell Mol Med 2009;13:1577-1585.
23. Wang S, Aurora AB, Johnson BA, Qi X, McAnally J, Hill JA, et al. The endothelial-specific microRNA miR-126 governs vascular integrity and angiogenesis. Dev Cell 2008;15:261-271.
24. Katare R, Rawal S, Munasinghe PE, Tsuchimochi H, Inagaki T, Fujii Y, et al. Ghrelin Promotes Functional Angiogenesis in a Mouse Model of Critical Limb Ischemia Through Activation of Proangiogenic MicroRNAs. Endocrinology 2015:en20151799.
25. Zernecke A, Bidzhekov K, Noels H, Shagdarsuren E, Gan L, Denecke B, et al. Delivery of microRNA-126 by apoptotic bodies induces CXCL12-dependent vascular protection. Sci Signal 2009;2:ra81.
26. van Solingen C., de Boer HC, Bijkerk R, Monge M, van Oeveren-Rietdijk AM, Seghers L, et al. MicroRNA-126 modulates endothelial SDF-1 expression and mobilization of Sca-1(+)/Lin(-) progenitor cells in ischaemia. Cardiovasc Res 2011;92:449-455.
27. Sahoo S, Klychko E, Thorne T, Misener S, Schultz KM, Millay M, et al. Exosomes from human CD34(+) stem cells mediate their proangiogenic paracrine activity. Circ Res 2011;109:724-728.
28. Mocharla P, Briand S, Giannotti G, Dorries C, Jakob P, Paneni F, et al. AngiomiR-126 expression and secretion from circulating CD34(+) and CD14(+) PBMCs: role for proangiogenic effects and alterations in type 2 diabetics. Blood 2013;121:226-236.

29. Stoneman VE, Bennett MR. Role of apoptosis in atherosclerosis and its therapeutic implications. Clin Sci (Lond) 2004;107:343-354.
30. Zhou J, Li YS, Nguyen P, Wang KC, Weiss A, Kuo YC, et al. Regulation of vascular smooth muscle cell turnover by endothelial cell-secreted microRNA-126: role of shear stress. Circ Res 2013;113:40-51.
31. Schober A, Nazari-Jahantigh M, Wei Y, Bidzhekov K, Gremse F, Grommes J, et al. MicroRNA-126-5p promotes endothelial proliferation and limits atherosclerosis by suppressing Dlk1. Nat Med 2014;20:368-376.
32. Kin K, Miyagawa S, Fukushima S, Shirakawa Y, Torikai K, Shimamura K, et al. Tissue- and plasma-specific MicroRNA signatures for atherosclerotic abdominal aortic aneurysm. J Am Heart Assoc 2012;1:e000745.
33. Turner M, Vigorito E. Regulation of B- and T-cell differentiation by a single microRNA. Biochem Soc Trans 2008;36:531-533.
34. O'Connell RM, Taganov KD, Boldin MP, Cheng G, Baltimore D. MicroRNA-155 is induced during the macrophage inflammatory response. Proc Natl Acad Sci U S A 2007;104:1604-1609.
35. Zhu N, Zhang D, Chen S, Liu X, Lin L, Huang X, et al. Endothelial enriched microRNAs regulate angiotensin II-induced endothelial inflammation and migration. Atherosclerosis 2011;215:286-293.
36. Lu LF, Thai TH, Calado DP, Chaudhry A, Kubo M, Tanaka K, et al. Foxp3-dependent microRNA155 confers competitive fitness to regulatory T cells by targeting SOCS1 protein. Immunity 2009;30:80-91.
37. Ceppi M, Pereira PM, Dunand-Sauthier I, Barras E, Reith W, Santos MA, et al. MicroRNA-155 modulates the interleukin-1 signaling pathway in activated human monocyte-derived dendritic cells. Proc Natl Acad Sci U S A 2009;106:2735-2740.
38. Corsten MF, Papageorgiou A, Verhesen W, Carai P, Lindow M, Obad S, et al. MicroRNA profiling identifies microRNA-155 as an adverse mediator of cardiac injury and dysfunction during acute viral myocarditis. Circ Res 2012;111:415-425.
39. Sethupathy P, Borel C, Gagnebin M, Grant GR, Deutsch S, Elton TS, et al. Human microRNA-155 on chromosome 21 differentially interacts with its polymorphic target in the AGTR1 3' untranslated region: a mechanism for functional single-nucleotide polymorphisms related to phenotypes. Am J Hum Genet 2007;81:405-413.
40. Pankratz F, Bemtgen X, Zeiser R, Leonhardt F, Kreuzaler S, Hilgendorf I, et al. MicroRNA-155 Exerts Cell-Specific Antiangiogenic but Proarteriogenic Effects During Adaptive Neovascularization. Circulation 2015;131:1575-1589.
41. Welten SM, Quax PH, Nossent AY. Letter Regarding Article, "MicroRNA-155 Exerts Cell-Specific Antiangiogenic but Proarteriogenic Effects During Adaptive Neovascularization". Circulation 2015;132:e375.
42. Nazari-Jahantigh M, Wei Y, Noels H, Akhtar S, Zhou Z, Koenen RR, et al. MicroRNA-155 promotes atherosclerosis by repressing Bcl6 in macrophages. J Clin Invest 2012;122:4190-4202.
43. Raitoharju E, Lyytikainen LP, Levula M, Oksala N, Mennander A, Tarkka M, et al. miR-21, miR-210, miR-34a, and miR-146a/b are up-regulated in human atherosclerotic plaques in the Tampere Vascular Study. Atherosclerosis 2011;219:211-217.
44. Huang RS, Hu GQ, Lin B, Lin ZY, Sun CC. MicroRNA-155 silencing enhances inflammatory response and lipid uptake in oxidized low-density lipoprotein-stimulated human THP-1 macrophages. J Investig Med 2010;58:961-967.
45. Zhu GF, Yang LX, Guo RW, Liu H, Shi YK, Wang H, et al. miR-155 inhibits oxidized low-density lipoprotein-induced apoptosis of RAW264.7 cells. Mol Cell Biochem 2013;382:253-261.
46. Yang K, He YS, Wang XQ, Lu L, Chen QJ, Liu J, et al. MiR-146a inhibits oxidized low-density lipoprotein-induced lipid accumulation and inflammatory response via targeting toll-like receptor 4. FEBS Lett 2011;585:854-860.
47. Tian FJ, An LN, Wang GK, Zhu JQ, Li Q, Zhang YY, et al. Elevated microRNA-155 promotes foam cell formation by targeting HBP1 in atherogenesis. Cardiovasc Res 2014;103:100-110.
48. Donners MM, Wolfs IM, Stoger LJ, van der Vorst EP, Pottgens CC, Heymans S, et al. Hematopoietic miR155 deficiency enhances atherosclerosis and decreases plaque stability in hyperlipidemic mice. PLoS One 2012;7:e35877.
49. Stanczyk J, Pedrioli DM, Brentano F, Sanchez-Pernaute O, Kolling C, Gay RE, et al. Altered expression of MicroRNA in synovial fibroblasts and synovial tissue in rheumatoid arthritis. Arthritis Rheum 2008;58:1001-1009.
50. Concepcion CP, Bonetti C, Ventura A. The microRNA-17-92 family of microRNA clusters in development and disease. Cancer J 2012;18:262-267.
51. Chamorro-Jorganes A, Lee MY, Araldi E, Landskroner-Eiger S, Fernandez-Fuertes M, Sahraei M, et al. VEGF-Induced Expression of miR-17~92 Cluster in Endothelial Cells is Mediated by ERK/ELK1 Activation and Regulates Angiogenesis. Circ Res 2015.
52. Bonauer A, Carmona G, Iwasaki M, Mione M, Koyanagi M, Fischer A, et al. MicroRNA-92a controls angiogenesis and functional recovery of ischemic tissues in mice. Science 2009;324:1710-1713.
53. Doebele C, Bonauer A, Fischer A, Scholz A, Reiss Y, Urbich C, et al. Members of the microRNA-17-92 cluster exhibit a cell-intrinsic antiangiogenic function in endothelial cells. Blood 2010;115:4944-4950.
54. Landskroner-Eiger S, Qiu C, Perrotta P, Siragusa M, Lee MY, Ulrich V, et al. Endothelial miR-17 approximately 92 cluster negatively regulates arteriogenesis via miRNA-19 repression of WNT signaling. Proc Natl Acad Sci 2015;112:12812-12817.
55. Kaluza D, Kroll J, Gesierich S, Manavski Y, Boeckel JN, Doebele C, et al. Histone deacetylase 9 promotes angiogenesis by targeting the antiangiogenic microRNA-17-92 cluster in endothelial cells. Arterioscler Thromb Vasc Biol 2013;33:533-543.
56. Wang KC, Garmire LX, Young A, Nguyen P, Trinh A, Subramaniam S, et al. Role of microRNA-23b in flow-regulation of Rb phosphorylation and endothelial cell growth. Proc Natl Acad Sci U S A 2010;107:3234-3239.

57. Qin X, Wang X, Wang Y, Tang Z, Cui Q, Xi J, et al. MicroRNA-19a mediates the suppressive effect of laminar flow on cyclin D1 expression in human umbilical vein endothelial cells. Proc Natl Acad Sci U S A 2010;107:3240-3244.
58. Wu W, Xiao H, Laguna-Fernandez A, Villarreal G, Jr., Wang KC, Geary GG, et al. Flow-Dependent Regulation of Kruppel-Like Factor 2 Is Mediated by MicroRNA-92a. Circulation 2011;124:633-641.
59. Loyer X, Potteaux S, Vion AC, Guerin CL, Boulkroun S, Rautou PE, et al. Inhibition of microRNA-92a prevents endothelial dysfunction and atherosclerosis in mice. Circ Res 2014;114:434-443.
60. Iaconetti C, Polimeni A, Sorrentino S, Sabatino J, Pironti G, Esposito G, et al. Inhibition of miR-92a increases endothelial proliferation and migration in vitro as well as reduces neointimal proliferation in vivo after vascular injury. Basic Res Cardiol 2012;107:296.
61. Bang C, Fiedler J, Thum T. Cardiovascular importance of the microRNA-23/27/24 family. Microcirculation 2012;19:208-214.
62. Zhou Q, Gallagher R, Ufret-Vincenty R, Li X, Olson EN, Wang S. Regulation of angiogenesis and choroidal neovascularization by members of microRNA-23~27~24 clusters. Proc Natl Acad Sci U S A 2011;108:8287-8292.
63. Neth P, Nazari-Jahantigh M, Schober A, Weber C. MicroRNAs in flow-dependent vascular remodelling. Cardiovasc Res 2013;99:294-303.
64. Weber M, Baker MB, Moore JP, Searles CD. MiR-21 is induced in endothelial cells by shear stress and modulates apoptosis and eNOS activity. Biochem Biophys Res Commun 2010;393:643-648.
65. Ni CW, Qiu H, Jo H. MicroRNA-663 upregulated by oscillatory shear stress plays a role in inflammatory response of endothelial cells. Am J Physiol Heart Circ Physiol 2011;300:H1762-H1769.
66. Urbich C, Kaluza D, Fromel T, Knau A, Bennewitz K, Boon RA, et al. MicroRNA-27a/b controls endothelial cell repulsion and angiogenesis by targeting semaphorin 6A. Blood 2012;119:1607-1616.
67. Young JA, Ting KK, Li J, Moller T, Dunn L, Lu Y, et al. Regulation of vascular leak and recovery from ischemic injury by general and VE-cadherin-restricted miRNA antagonists of miR-27. Blood 2013;122:2911-2919.
68. Fiedler J, Jazbutyte V, Kirchmaier BC, Gupta SK, Lorenzen J, Hartmann D, et al. MicroRNA-24 regulates vascularity after myocardial infarction. Circulation 2011;124:720-730.
69. Fiedler J, Stohr A, Gupta SK, Hartmann D, Holzmann A, Just A, et al. Functional MicroRNA Library Screening Identifies the HypoxaMiR MiR-24 as a Potent Regulator of Smooth Muscle Cell Proliferation and Vascularization. Antioxid Redox Signal 2013.
70. Kasza Z, Fredlund FP, Tamm C, Eriksson AS, O'Callaghan P, Heindryckx F, et al. MicroRNA-24 suppression of N-deacetylase/N-sulfotransferase-1 (NDST1) reduces endothelial cell responsiveness to vascular endothelial growth factor A (VEGFA). J Biol Chem 2013;288:25956-25963.
71. Vickers KC, Shoucri BM, Levin MG, Wu H, Pearson DS, Osei-Hwedieh D, et al. MicroRNA-27b is a regulatory hub in lipid metabolism and is altered in dyslipidemia. Hepatology 2013;57:533-542.
72. Ng R, Wu H, Xiao H, Chen X, Willenbring H, Steer CJ, et al. Inhibition of microRNA-24 expression in liver prevents hepatic lipid accumulation and hyperlipidemia. Hepatology 2014;60:554-564.
73. Zhang M, Wu JF, Chen WJ, Tang SL, Mo ZC, Tang YY, et al. MicroRNA-27a/b regulates cellular cholesterol efflux, influx and esterification/hydrolysis in THP-1 macrophages. Atherosclerosis 2014;234:54-64.
74. Iaconetti C, De Rosa S, Polimeni A, Sorrentino S, Gareri C, Carino A, et al. Down-regulation of miR-23b induces phenotypic switching of vascular smooth muscle cells in vitro and in vivo. Cardiovasc Res 2015;107:522-533.
75. Jiang Y, Zhang M, He H, Chen J, Zeng H, Li J, et al. MicroRNA/mRNA profiling and regulatory network of intracranial aneurysm. BMC Med Genomics 2013;6:36.
76. Liu D, Han L, Wu X, Yang X, Zhang Q, Jiang F. Genome-wide microRNA changes in human intracranial aneurysms. BMC Neurol 2014;14:188.
77. Maegdefessel L, Spin JM, Raaz U, Eken SM, Toh R, Azuma J, et al. miR-24 limits aortic vascular inflammation and murine abdominal aneurysm development. Nat Commun 2014;5:5214.
78. Ji R, Cheng Y, Yue J, Yang J, Liu X, Chen H, et al. MicroRNA expression signature and antisense-mediated depletion reveal an essential role of MicroRNA in vascular neointimal lesion formation. Circ Res 2007;100:1579-1588.
79. Elia L, Quintavalle M, Zhang J, Contu R, Cossu L, Latronico MV, et al. The knockout of miR-143 and -145 alters smooth muscle cell maintenance and vascular homeostasis in mice: correlates with human disease. Cell Death Differ 2009;16:1590-1598.
80. Cheng Y, Liu X, Yang J, Lin Y, Xu DZ, Lu Q, et al. MicroRNA-145, a novel smooth muscle cell phenotypic marker and modulator, controls vascular neointimal lesion formation. Circ Res 2009;105:158-166.
81. Zhang C. MicroRNA-145 in vascular smooth muscle cell biology: a new therapeutic target for vascular disease. Cell Cycle 2009;8:3469-3473.
82. Cordes KR, Sheehy NT, White MP, Berry EC, Morton SU, Muth AN, et al. miR-145 and miR-143 regulate smooth muscle cell fate and plasticity. Nature 2009;460:705-710.
83. Boucher JM, Peterson SM, Urs S, Zhang C, Liaw L. The miR-143/145 cluster is a novel transcriptional target of Jagged-1/Notch signaling in vascular smooth muscle cells. J Biol Chem 2011;286:28312-28321.
84. Davis-Dusenbery BN, Chan MC, Reno KE, Weisman AS, Layne MD, Lagna G, et al. down-regulation of Kruppel-like factor-4 (KLF4) by microRNA-143/145 is critical for modulation of vascular smooth muscle cell phenotype by transforming growth factor-beta and bone morphogenetic protein 4. J Biol Chem 2011;286:28097-28110.
85. Boettger T, Beetz N, Kostin S, Schneider J, Kruger M, Hein L, et al. Acquisition of the contractile phenotype by murine arterial smooth muscle cells depends on the Mir143/145 gene cluster. J Clin Invest 2009;119:2634-2647.

86. Zou C, Xu Q, Mao F, Li D, Bian C, Liu LZ, et al. MiR-145 inhibits tumor angiogenesis and growth by N-RAS and VEGF. Cell Cycle 2012;11:2137-2145.
87. La Rocca G., Shi B, Badin M, De Angelis T., Sepp-Lorenzino L, Baserga R. Growth inhibition by microRNAs that target the insulin receptor substrate-1. Cell Cycle 2009;8:2255-2259.
88. Qian X, Yu J, Yin Y, He J, Wang L, Li Q, et al. MicroRNA-143 inhibits tumor growth and angiogenesis and sensitizes chemosensitivity to oxaliplatin in colorectal cancers. Cell Cycle 2013;12:1385-1394.
89. Zhang H, Pu J, Qi T, Qi M, Yang C, Li S, et al. MicroRNA-145 inhibits the growth, invasion, metastasis and angiogenesis of neuroblastoma cells through targeting hypoxia-inducible factor 2 alpha. Oncogene 2014;33:387-397.
90. Anand S, Cheresh DA. Emerging Role of Micro-RNAs in the Regulation of Angiogenesis. Genes Cancer 2011;2:1134-1138.
91. Wang YS, Li SH, Guo J, Mihic A, Wu J, Sun L, et al. Role of miR-145 in cardiac myofibroblast differentiation. J Mol Cell Cardiol 2014;66:94-105.
92. Climent M, Quintavalle M, Miragoli M, Chen J, Condorelli G, Elia L. TGFbeta Triggers miR-143/145 Transfer From Smooth Muscle Cells to Endothelial Cells, Thereby Modulating Vessel Stabilization. Circ Res 2015;116:1753-1764.
93. Lovren F, Pan Y, Quan A, Singh KK, Shukla PC, Gupta N, et al. MicroRNA-145 targeted therapy reduces atherosclerosis. Circulation 2012;126:S81-S90.
94. Xin M, Small EM, Sutherland LB, Qi X, McAnally J, Plato CF, et al. MicroRNAs miR-143 and miR-145 modulate cytoskeletal dynamics and responsiveness of smooth muscle cells to injury. Genes Dev 2009;23:2166-2178.
95. Vengrenyuk Y, Nishi H, Long X, Ouimet M, Savji N, Martinez FO, et al. Cholesterol loading reprograms the microRNA-143/145-myocardin axis to convert aortic smooth muscle cells to a dysfunctional macrophage-like phenotype. Arterioscler Thromb Vasc Biol 2015;35:535-546.
96. Hergenreider E, Heydt S, Treguer K, Boettger T, Horrevoets AJ, Zeiher AM, et al. Atheroprotective communication between endothelial cells and smooth muscle cells through miRNAs. Nat Cell Biol 2012;14:249-256.
97. Schmitt MM, Megens RT, Zernecke A, Bidzhekov K, van den Akker NM, Rademakers T, et al. Endothelial junctional adhesion molecule-a guides monocytes into flow-dependent predilection sites of atherosclerosis. Circulation 2014;129:66-76.
98. Sala F, Aranda JF, Rotllan N, Ramirez CM, Aryal B, Elia L, et al. MiR-143/145 deficiency attenuates the progression of atherosclerosis in Ldlr-/-mice. Thromb Haemost 2014;112:796-802.
99. Boon RA, Dimmeler S. MicroRNAs and aneurysm formation. Trends Cardiovasc Med 2011;21:172-177.
100. Benetatos L, Hatzimichael E, Londin E, Vartholomatos G, Loher P, Rigoutsos I, et al. The microRNAs within the DLK1-DIO3 genomic region: involvement in disease pathogenesis. Cell Mol Life Sci 2013;70:795-814.
101. Welten SM, Bastiaansen AJ, de Jong RC, de Vries MR, Peters EA, Boonstra MC, et al. Inhibition of 14q32 MicroRNAs miR-329, miR-487b, miR-494, and miR-495 increases neovascularization and blood flow recovery after ischemia. Circ Res 2014;115:696-708.
102. Gordon FE, Nutt CL, Cheunsuchon P, Nakayama Y, Provencher KA, Rice KA, et al. Increased expression of angiogenic genes in the brains of mouse meg3-null embryos. Endocrinology 2010;151:2443-2452.
103. Liu D, Zhang XL, Yan CH, Li Y, Tian XX, Zhu N, et al. MicroRNA-495 regulates the proliferation and apoptosis of human umbilical vein endothelial cells by targeting chemokine CCL2. Thromb Res 2015;135:146-154.
104. Wang P, Luo Y, Duan H, Xing S, Zhang J, Lu D, et al. MicroRNA 329 suppresses angiogenesis by targeting CD146. Mol Cell Biol 2013;33:3689-3699.
105. Li LJ, Huang Q, Zhang N, Wang GB, Liu YH. miR-376b-5p regulates angiogenesis in cerebral ischemia. Mol Med Rep 2014;10:527-535.
106. Wen Z, Huang W, Feng Y, Cai W, Wang Y, Wang X, et al. MicroRNA-377 regulates mesenchymal stem cell-induced angiogenesis in ischemic hearts by targeting VEGF. PLoS One 2014;9:e104666.
107. Cipollone F, Felicioni L, Sarzani R, Ucchino S, Spigonardo F, Mandolini C, et al. A unique microRNA signature associated with plaque instability in humans. Stroke 2011;42:2556-2563.
108. Wezel A, Welten SM, Razaway W, Lagraauw, de Vries MR, Goossens E.A.C., et al. Inhibition of microRNA-494 reduces atherosclerotic lesion development and increases plaque stability. Ann Surg 2015.
109. Zhang CF, Kang K, Li XM, Xie BD. MicroRNA-136 Promotes Vascular Muscle Cell Proliferation Through the ERK1/2 Pathway by Targeting PPP2R2A in Atherosclerosis. Curr Vasc Pharmacol 2014.
110. Ramirez CM, Davalos A, Goedeke L, Salerno AG, Warrier N, Cirera-Salinas D, et al. MicroRNA-758 regulates cholesterol efflux through posttranscriptional repression of ATP-binding cassette transporter A1. Arterioscler Thromb Vasc Biol 2011;31:2707-2714.
111. Mandolini C, Santovito D, Marcantonio P, Buttitta F, Bucci M, Ucchino S, et al. Identification of microRNAs 758 and 33b as potential modulators of ABCA1 expression in human atherosclerotic plaques. Nutr Metab Cardiovasc Dis 2014.
112. Iliopoulos D, Drosatos K, Hiyama Y, Goldberg IJ, Zannis VI. MicroRNA-370 controls the expression of microRNA-122 and Cpt1alpha and affects lipid metabolism. J Lipid Res 2010;51:1513-1523.
113. Aavik E, Lumivuori H, Leppanen O, Wirth T, Hakkinen SK, Brasen JH, et al. Global DNA methylation analysis of human atherosclerotic plaques reveals extensive genomic hypomethylation and reactivation at imprinted locus 14q32 involving induction of a miRNA cluster. Eur Heart J 2014.
114. Nossent AY, Eskildsen TV, Andersen LB, Bie P, Bronnum H, Schneider M, et al. The 14q32 MicroRNA-487b Targets the Antiapoptotic Insulin Receptor Substrate 1 in Hypertension-Induced Remodeling of the Aorta. Ann Surg 2013.
115. Dimmeler S, Yla-Herttuala S. 14q32 miRNA cluster takes center stage in neovascularization. Circ Res 2014;115:680-682.

116. Hakimzadeh N, Nossent AY, van der Laan AM, Schirmer SH, de Ronde MW, Pinto-Sietsma SJ, et al. Circulating MicroRNAs Characterizing Patients with Insufficient Coronary Collateral Artery Function. PLoS One 2015;10:e0137035.
117. He F, Lv P, Zhao X, Wang X, Ma X, Meng W, et al. Predictive value of circulating miR-328 and miR-134 for acute myocardial infarction. Mol Cell Biochem 2014;394:137-144.
118. Hoekstra M, van der Lans CA, Halvorsen B, Gullestad L, Kuiper J, Aukrust P, et al. The peripheral blood mononuclear cell microRNA signature of coronary artery disease. Biochem Biophys Res Commun 2010;394:792-797.
119. Li C, Fang Z, Jiang T, Zhang Q, Liu C, Zhang C, et al. Serum microRNAs profile from genome-wide serves as a fingerprint for diagnosis of acute myocardial infarction and angina pectoris. BMC Med Genomics 2013;6:16.
120. Matsumoto S, Sakata Y, Nakatani D, Suna S, Mizuno H, Shimizu M, et al. A subset of circulating microRNAs are predictive for cardiac death after discharge for acute myocardial infarction. Biochem Biophys Res Commun 2012;427:280-284.
121. Wang J, Pei Y, Zhong Y, Jiang S, Shao J, Gong J. Altered serum microRNAs as novel diagnostic biomarkers for atypical coronary artery disease. PLoS One 2014;9:e107012.
122. Jickling GC, Ander BP, Zhan X, Noblett D, Stamova B, Liu D. microRNA expression in peripheral blood cells following acute ischemic stroke and their predicted gene targets. PLoS One 2014;9:e99283.
123. Mohnle P, Schutz SV, Schmidt M, Hinske C, Hubner M, Heyn J, et al. MicroRNA-665 is involved in the regulation of the expression of the cardioprotective cannabinoid receptor CB2 in patients with severe heart failure. Biochem Biophys Res Commun 2014;451:516-521.
124. Liu F, Li N, Long B, Fan YY, Liu CY, Zhou QY, et al. Cardiac hypertrophy is negatively regulated by miR-541. Cell Death Dis 2014;5:e1171.
125. Dews M, Homayouni A, Yu D, Murphy D, Sevignani C, Wentzel E, et al. Augmentation of tumor angiogenesis by a Myc-activated microRNA cluster. Nat Genet 2006;38:1060-1065.

Chapter 3-I

Inhibition of 14q32 MicroRNAs miR-329, miR-487b, miR-494 and miR-495 Increases Neovascularization and Blood Flow Recovery after Ischemia

Circ Res 2014 Sep 26;115:696-708

SMJ Welten[1,2*]

AJNM Bastiaansen[1,2*]

RCM de Jong[1,2]

MR de Vries[1,2]

HAB Peters[1,2]

MC Boonstra[1]

SP Sheikh[3]

N La Monica[4]

ER Kandimalla[4]

PHA Quax[1,2]

AY Nossent[1,2]

[*]Authors contributed equally to this work

[1]Department of Surgery and [2]Einthoven Laboratory for Experimental Vascular Medicine,
Leiden University Medical Center, Leiden, the Netherlands

[3]Department of Biochemistry and Pharmacology, Odense University Hospital, Odense, Denmark

[4]Idera Pharmaceuticals, Cambridge, MA, United States of America

Abstract

Rationale: Effective neovascularization is crucial for recovery after cardiovascular events.

Objective: As microRNAs regulate expression of up to several hundred target genes, we set out to identify microRNAs that target genes in all pathways of the multifactorial neovascularization process. Using www.targetscan.org, we performed a reverse target prediction analysis on a set of 197 genes involved in neovascularization. We found enrichment of binding sites for 27 microRNAs in a single microRNA gene cluster. MicroArray analyses showed upregulation of 14q32 microRNAs during neovascularization in mice following single femoral artery ligation.

Methods and Results: Gene Silencing Oligonucleotides were used to inhibit four 14q32 microRNAs, miR-329, miR-487b, miR-494 and miR-495, one day prior to double femoral artery ligation. Blood flow recovery was followed by Laser Doppler Perfusion Imaging. All 4 GSOs clearly improved blood flow recovery after ischemia. Mice treated with GSO-495 or GSO-329 showed increased perfusion already after 3 days (30% perfusion vs. 15% in control) and those treated with GSO-329 showed a full recovery of perfusion after 7 days (vs. 60% in control). Increased collateral artery diameters (arteriogenesis) were observed in adductor muscles of GSO-treated mice, as well as increased capillary densities (angiogenesis) in the ischemic soleus muscle. In vitro, treatment with GSOs led to increased sprout formation and increased arterial endothelial cell proliferation, as well as to increased arterial myofibroblast proliferation.

Conclusion: The 14q32 microRNA gene cluster is highly involved in neovascularization. Inhibition of 14q32 microRNAs miR-329, miR-487b, miR-494 and miR-495 provides a promising tool for future therapeutic neovascularization.

Introduction

Neovascularization is the body's natural repair mechanism to restore blood flow to ischemic tissues after a cardiovascular event. Neovascularization is comprised of arteriogenesis and angiogenesis. Arteriogenesis is defined by the maturation of pre-existing collateral arterioles into mature collateral arteries[1]. Arteriogenesis takes place upstream of the ischemic area and is driven by increases in shear stress, rather than ischemia. When a nearby artery becomes occluded, blood is forced through collateral arterioles. The increases in flow, shear stress and circumferential stretch activate the arteriolar wall and trigger an inflammatory response that leads to rearrangement of the extracellular matrix and outward remodeling of the arteriole. Angiogenesis is defined by the sprouting of new capillaries from existing blood vessels in the microcirculation[2]. Angiogenesis is driven solely by ischemia. Via, amongst others, the Hypoxia-Inducible Factor 1α (HIF1α), ischemia leads to upregulation of pro-angiogenic growth factors, triggering nearby vascular endothelial cells (ECs) to form sprouts towards the ischemic area. Ischemia also induces gene transcription of pro-inflammatory chemokines and cytokines which trigger a local inflammatory reaction. As to arteriogenesis, inflammation is crucial to angiogenesis too, facilitating extracellular matrix rearrangement, cell growth and proliferation.

Both arteriogenesis and angiogenesis are highly multifactorial processes and yet clinical trials aiming to induce neovascularization in patients with occlusive arterial disease have so far only focused on single-factor therapeutics, such as growth factors (for example Vascular Endothelial Growth Factor A (VEGFA) and basic Fibroblast Growth Factor (bFGF)). Unfortunately, these trials were less successful than anticipated[1, 3, 4]. Growth factors only target one of multiple processes required for efficient neovascularization. Therefore, there is a need for novel pro-arterio- and pro-angiogenic factors that can act as master switches in neovascularization.

MicroRNAs (miRs) are endogenous RNA molecules that down-regulate expression of their target genes[5]. MiRs do not completely silence their target genes, but rather down-tune their expression. However, because each miR has multiple, up to several hundred, target genes, changes in miR expression can have a major impact. Inhibition of a single miR can thus lead to activation of entire multifactorial physiological processes.

Several studies have been published on the effects of miR inhibition on neovascularization, but in general, the focus of these studies lies with angiogenesis alone, not arteriogenesis[6-14]. In the present study, we exploited the master switch character of miRs in order to identify miRs that play a regulatory role in neovascularization as a whole, including both angiogenesis and arteriogenesis. We performed a 'reverse target prediction' analysis (RTP) on a set of nearly 200 genes involved in all facets of angiogenesis and arteriogenesis, aiming to identify miRs that can target multiple neovascularization genes. We found enrichment of putative target sites for 27 miRs that are all located in one large miR gene cluster. This miR gene cluster consists of over 50 miRs, highly conserved in mammals, that are transcribed from one polycystronic site on the imprinted DLK1-region on the long arm of human chromosome 14 (14q32; chromosome 12F1 in mice) (Figure 1).

The 14q32 miR gene cluster was first discovered in 2004, by Seitz et al[15]. Using in silico DNA-sequence analyses, Seitz and colleagues were able to predict 46 of the currently known 54 human 14q32 miR

genes (61 in mice). The cluster is highly conserved in mammals, but not in other vertebrates or in invertebrates. Although many miRs are transcribed from polycistronic miR gene clusters, the 14q32 cluster is among the largest known miR gene clusters in any species. The facts that the cluster is so specifically conserved in mammals and that it is located in a strictly regulated, imprinted region of the genome, hint at its biological importance. Indeed, almost all 14q32 miRs have been implicated in human disease, many of them in cardiovascular disease[16]. Interestingly, most 14q32 miRs are predicted to regulate focal adhesion and ECM interactions, both crucial in vascular remodelling. Knockout of the cluster, via knockout of the Meg3 locus[17, 18], led to over-expression of several pro-angiogenic genes, including Vegfa and Dll4, and drastically increased vascular capillary density in mouse embryos[19]. A recent study showed that the cluster is under transcriptional control of a binding site for the Myocyte Enhancer Factor 2A (MEF2A)[20], a transcription factor known to influence vascular remodelling[21, 22].
We show here that inhibition of individual 14q32 miRs leads to improvements in post-ischemic blood flow recovery in vivo.

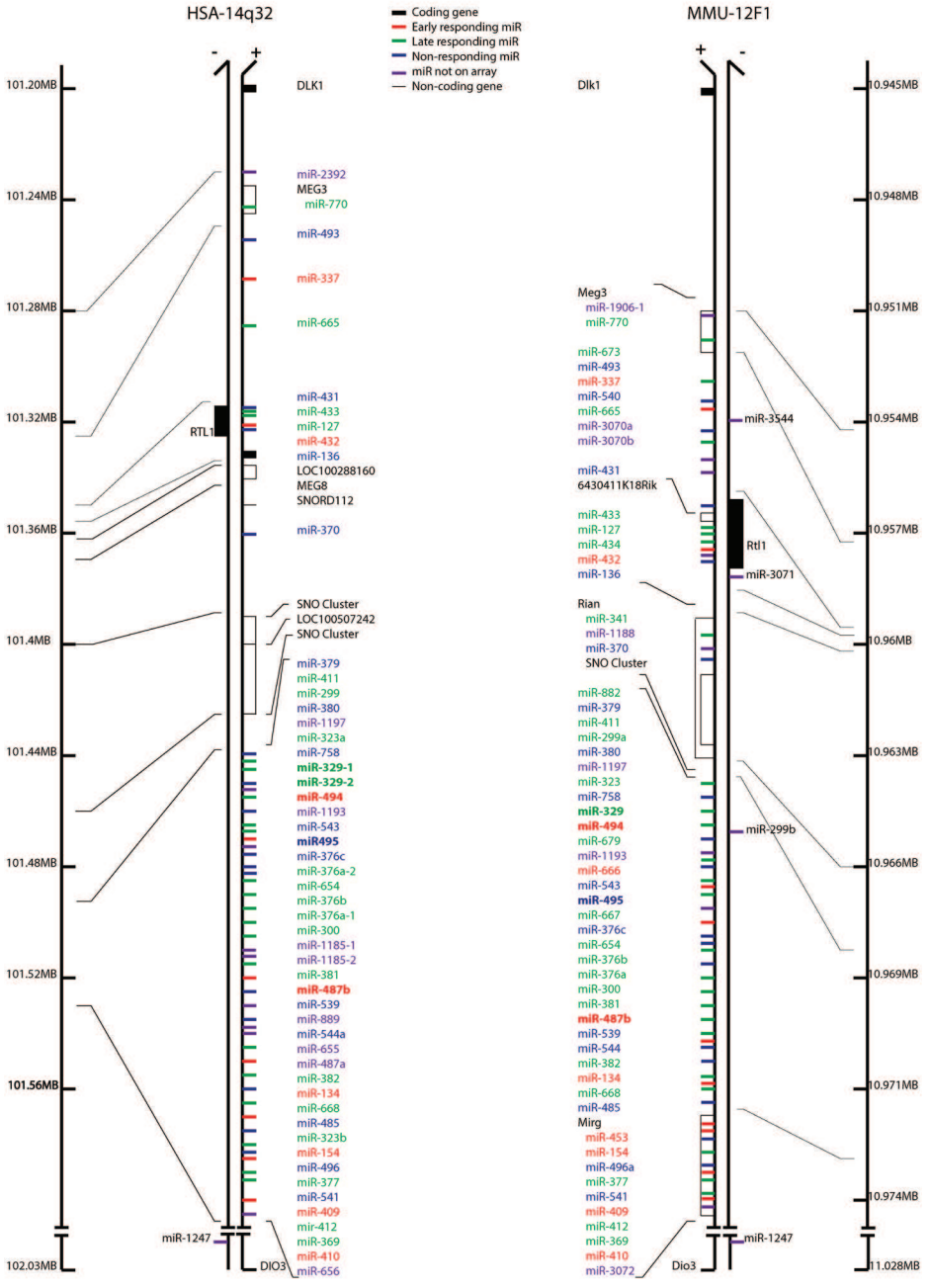

Figure 1. A schematic overview of the human 14q32 and murine 12F1 loci. Colors indicate whether the murine miRs were early (red), late (green) or non-responders (blue) after hind limb ischemia induced by single ligation of the femoral artery in healthy C57Bl/6 mice. 14q32 miRs that were not included in the microArray are indicated in purple and coding (thick bars) and non-coding genes (thin bars) are indicated in black. Human base positions are numbered according to assembly GRCh37.p13, murine base positions according to GRCm38.p2.

Methods

Reverse Target Prediction

To identify miRs that are involved in arterio- and angiogenesis, an in silico reverse target prediction (RTP) was performed. A selection was made of 127 genes known from literature and previous studies within our group to play important roles in arterio- and angiogenesis (Table S1A). To ensure the master switch character of the identified miRs, we selected target genes covering all aspects of vascular remodeling; endothelial activation, smooth muscle cell proliferation, extracellular matrix rearrangement, chemo- and cytokines and their receptors, growth factors and their receptors, the natural killer complex, pro-arteriogenic and pro-angiogenic transcription factors and signaling molecules (Table S1A). We then used www.targetscan.org to, for each individual gene, generate a list of all miRs predicted to target these 127 genes. Each list, no restrictions were applied, was copied into a spreadsheet and for each miR we simply counted the number of times it was present in the file.

To confirm the relevance of our findings, we selected an additional 70 genes that we found upregulated, using microArray analysis, at the site of active arteriogenesis, the adductor muscle group, in C57Bl/6 mice subjected to single ligation of the left femoral artery (Table S2A). We repeated the RTP for these 70 genes and looked for similarities in identified miRs between the two reverse target predictions (for 14q32 miRs, Table S3).

Both RTPs were performed looking for miR binding sites in human target genes to ensure clinical relevance. Conservation between human and murine target sites was checked to confirm the validity of our murine model of hind limb ischemia (for 14q32miRs, Table S4).

The procedure of the RTPs is schematically summarized in Supplemental Figure S1.

MicroRNA Inhibitors

AntagomiRs were designed with perfect reverse complementarity to the mature target miR sequence and purchased from VBC Biotech (Vienna, Austria). AntagomiRs were made up of a single-stranded O-methyl-modified RNA strand with 5'-end and 3'-end phosporothioate linkages and a 3'-end cholesterol tail.

Gene Silencing Oligonucleotides (GSOs) were designed with perfect reverse complementarity to the mature target miR sequence and synthesized at Idera Pharmaceuticals (Cambridge, MA, USA)[23]. As a negative control, a scrambled sequence was used, designed not to target any known murine miR. GSOs were made up of two single-stranded O-methyl-modified DNA strands, linked together at their 5' ends by a phosphorothioate-linker. Shielding the 5'-end of the single-stranded oligonucleotides prevents activation of the innate immune system via Toll-like Receptors; the double DNA strand increases specificity for the target miR.

Sequences of all antagomiRs and GSOs used are given in Table S5 (Supplemental Data).

Hind Limb Ischemia Models

Healthy adult male C57Bl/6 mice, aged 8 to 12 weeks (Charles River and Harlan) were housed in groups of 4 or 5 mice with free access to tap water and regular chow. All experiments were approved by the committee on animal welfare of the Leiden University Medical Center (Leiden, The Netherlands).

For miR-inhibition experiments, mice were given a bolus injection of 1 mg (~40mg/kg) GSO in PBS or PBS alone via the tail vein (i.v.), 1 day prior to femoral artery ligation.

Mice were anesthetized by intraperitoneal (i.p.) injection of midazolam (8 mg/kg, Roche Diagnostics), medetomidine (0.4 mg/kg, Orion) and fentanyl (0.08 mg/kg, Janssen Pharmaceuticals). Unilateral hind limb ischemia was induced by electrocoagulation of the left femoral artery proximal to the superficial epigastric arteries alone (single ligation: model for effective arteriogenesis), or combined with electrocoagulation of the distal femoral artery proximal to the bifurcation of the popliteal and saphenous artery24 (double ligation: model for severe Peripheral Arterial Disease). After surgery, anaesthesia was antagonized with flumazenil (0.7 mg/kg, Fresenius Kabi), atipamezole (3.3 mg/kg, Orion) and buprenorphine (0.2 mg/kg, MSD Animal Health).

Blood flow recovery to the paw was measured over time using Laser Doppler Perfusion Imaging (LDPI) (Moore Instruments). Mice were anaesthetized by i.p. injection of midazolam (8 mg/kg) and medetomidine (0.4 mg/kg). Mice were place in a double-glazed pot, perfused with water at 37°C for 5 minutes prior to each measurement. After LDPI, anesthesia was antagonized by subcutaneous injection of flumazenil (0.7 mg/kg) and atipamezole (3.3 mg/kg). LDPI measurements in the treated paw were

normalized to measurements of the untreated paw, as internal control.
Analgesic fentanyl (0.08 mg/kg) was administered subcutaneously after the final LDPI measurement and mice were sacrificed. The adductor, gastrocnemius and soleus muscles were harvested and either snap-frozen on dry ice or fixed in 4% PFA.

Additional Materials and Methods are provided in the Supplemental Data.

Results

Reverse Target Prediction

We performed two reverse target prediction analyses. In the initial RTP, we included 127 genes that are known to be involved in neovascularization from both literature and our own studies (Online Table I-A). As anticipated, we observed enrichment of putative binding sites for several miRs that were previously reported to influence post-ischemic neovascularization, including miR-17/92a[9] (29 and 21 putative target genes, respectively), miR-106b/93/258, 14 (29, 29 and 21 putative target genes respectively), the miR-15a family[10, 11, 25] (26 putative target genes), miR-503[13] (11 putative target genes) and miR-100[7] (2 putative target genes) but not, for example, miR-126[6]. However, more outspoken was the enrichment of putative binding sites for 27 miRs from the 14q32 miR gene cluster, including miR-329, miR-494 and miR-495 (20, 31 and 44 putative target genes, respectively). All findings of RTP1 are given in Online Tables I-B and I-C.
In the second RTP, we included 70 additional genes that we found upregulated in the early stages of vascular remodeling in murine tissue after hind limb ischemia induced by single ligation of the femoral artery, a model for effective neovascularization (Online Table II-A). We again observed enrichment of binding sites for miR-17/92 (8 and 4 putative target genes, respectively), miR-106/93/25 (8, 8 and 4 putative target genes respectively), the miR-15a family (3 putative target genes), miR-503 (5 putative target genes) and miR-100 (1 putative target genes). Furthermore, enrichment of binding sites for 26 of the initial 27 identified 14q32 miRs was recovered, including miR-329, miR-494 and miR-495 (10, 8 and 7 putative target genes, respectively). All findings of RTP2 are given in Online Table II-B. The findings for 14q32 miRs in RTP1 and RTP2 are summarized in Online Table III.
We used human target gene sequences in both RTPs and checked for conservation between human and murine target sites. The 14q32 miR gene cluster is highly conserved between mammals and we found that many, but not all, putative target sites are conserved as well (Online Table IV).

MicroArray

We performed microarray analyses of miR expression profiles on the same murine tissue samples used for mRNA microarray analyses. At 24 hours after hind limb ischemia (single femoral artery ligation), 14q32 miR-494 was the second-most significantly regulated microRNA of all microRNAs, after miR-883a-5p. MiR-494 was rapidly upregulated at 24 hours and at 72 hours; expression normalized after 7 days (Online Figure I-C). When we looked at other 14q32 miRs, we observed that more than half the cluster members were upregulated during effective neovascularization. When we include the opposite strands known to have microRNA functions as well, thirteen 14q32 miRs were already upregulated 24 hours after ischemia (early-responders); 39 14q32 miRs were first upregulated 72 hours after ischemia

(late responders); 23 14q32 miRs were not regulated at all (non-responders); eleven 14q32 miRs were not on the microArray (Online Table VI).
For further studies, we chose to investigate one 14q32 miR from each responder group, that all were predicted to target multiple neovascularization genes. We selected miR-494 (early-responder), miR-329 (late responder) and miR-495 (non-responder). MiR-487b was the second most significantly upregulated 14q32 miR (early-responder). Although it was not identified in either RTP, we did previously report that miR-487b plays an important role in outward remodeling of the aorta[26] and therefore we also included miR-487b in our further studies. Expression of these four 14q32 miRs was measured in various murine tissues using rt/qPCR (Online Figure II).
Regulation of these four 14q32 miRs, of miRs previously linked to neovascularization and of the Top-9 non-14q32 miRs identified in RTP1 and RTP2 are shown in Online Figure I.

Gene Silencing Oligonucleotides

We compared the efficacy and specificity of Gene Silencing Oligonucleotides[23] to the more commonly used antagomiRs, using cultures of primary human umbilical arterial myofibroblasts. At a concentration of 10ng/µl, both antagomiRs and GSOs proved equally potent in inhibiting expression of their target miR in myofibroblasts. Also, both types of miR-inhibitors showed a high specificity for their target miR (Figure 2A & B). However, at higher concentrations (15ng/µl), signs of cytotoxicity were observed (Online Figure IV). These effects were subtle for GSOs, but very outspoken for antagomiRs. Therefore, we performed our further in vitro studies using GSOs only, at a concentration of 10 ng/µl.

In Vivo MiR Inhibition

We used rt/qPCR to confirm down-regulation of the targeted 14q32 miRs in the adductor muscles of GSO-treated mice. All four GSOs achieved knockdown of their target miR at day 3 after surgery, corresponding to day 4 after injection, compared to the GSO-control. At day 7 after surgery, day 8 after GSO injection, expression of miR-495 had normalized, but miR-329 and miR-494 were still downregulated. MiR-487b showed very low expression levels at day 7, even in GSO-control treated animals, potentially masking the inhibitory effects of GSO-487b. However, miR-487b expression was still repressed at day 17 (Figure 2C).

GSO Biodistribution

To investigate the bio-distribution of GSOs after i.v. injection with or without the induction of hindlimb ischemia, IRD-800-labelled GSO-329 was visualized after injection. Already within one hour after injection, high dye-intensities could be measured throughout the entire mouse (Figure 3A) Uptake of GSOs was clearly visible in all organs and tissues, including blood vessels (aorta and vena cava, but not in the brain, which was then used to normalize dye-intensities as a measure of tissue-uptake (Figure 3J). Although present, the dye-signal in both the adductor and calf muscles was very weak (Figures 3C, 3E and 3G). However in animals subjected to hindlimb ischemia 24 hours after GSO injection, sacrificed at 48 hours after injection, major uptake of GSOs was observed in both the adductor and calf muscles, but only in the operated paw (Figures 3B, 3D, 3F and 3H). Although GSOs were readily taken

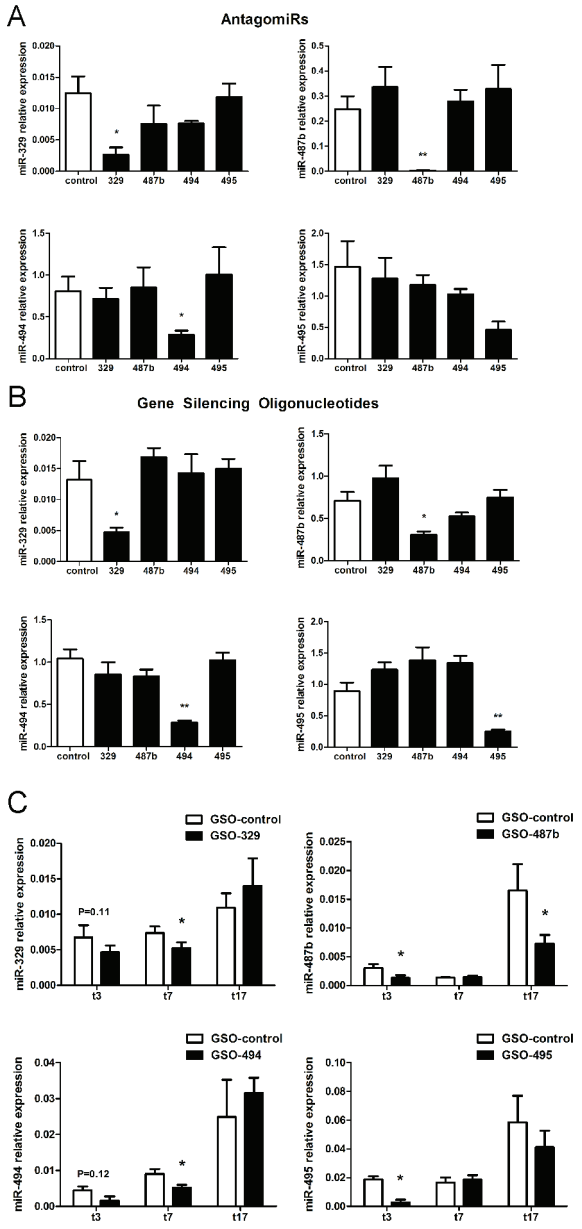

Figure 2. MiR inhibition in primary human arterial myofibroblasts and in adductor muscle tissue of mice subjected to Hind Limb Ischemia. (A) Inhibition of individual 14q32 miRs in myofibroblasts for 48 hours by antagomiRs (10ng/µl). (B) Inhibition of individual 14q32 miRs in myofibroblasts for 48hrs by GSOs (10ng/µl). Mean expression levels, from at least 3 independent experiments, relative to miR-103 are shown here ± SEM. *$p < 0.05$, **$p < 0.01$. (C) Expression of 14q32 miRs in adductor muscle tissue of C57Bl/6 mice treated with GSO-329, GSO-487b, GSO-494 and GSO 495 or GSO-control (1mg/mouse) at 3, 7 and 17 days after double ligation of the left femoral artery. Per group, adductor muscle tissue of 2 (day 3), 9 (day 7) and 10 (day 17) mice was used. Mean expression levels relative to let-7C are shown here ± SEM. *$p<0.05$.

up into the liver, the feces at 48 hours did not contain any label. However, both kidneys and urine at 48 hours gave very high dye intensities, indicating that GSOs are cleared predominantly via the kidneys. Although intensities dropped slightly in most organs at 48 hours compared to one hour after injection, dye intensities were still high throughout the body after 48 hours, indicating slow clearance, which supports the prolonged inhibition of microRNAs that we observed in the adductor muscle of mice subjected to hindlimb ischemia.

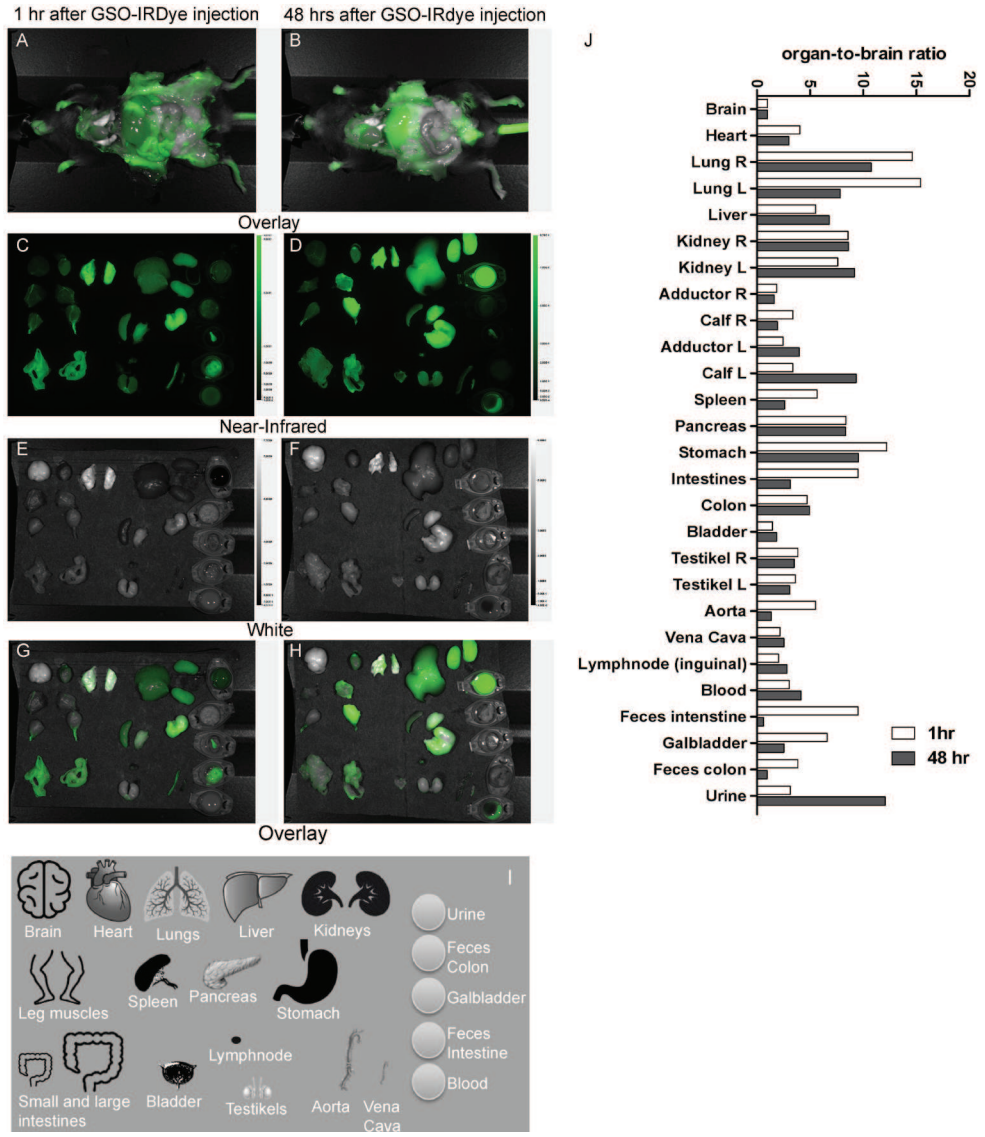

Figure 3. Tissue uptake and biodistribution of GSOs. Uptake of IDye800CW labelled GSO-329 at 1hour (left panels) and 48 hours (right panels) after i.v. injection. Overlay images of whole animals (A and B) and near-infrared (C and D), white (E and F) and overlay (G and H) of individual organs showing uptake of GSOs by various organs. (I) Schematic representation of organs shown in panels C-H. (J) near-infrared fluorescence of individual organs relative to fluorescence of the brain.

Blood Flow Recovery In Vivo

Mice were given a bolus injection of 1mg GSO in PBS, or PBS alone, via the tail vein. The next day, they were subjected to double ligation of the left femoral artery, a model for severe peripheral artery disease. Blood flow recovery to the paw was followed by LDPI up to 17 days after hind limb ischemia. Mice in all groups appeared healthy and no significant weight loss was observed. All four treatment groups, GSO-329, GSO-487b, GSO-494 and GSO-495, showed drastically improved blood flow recovery compared to both the PBS and the GSO-control groups (Figures 4A-D). There were no significant differences between the PBS and GSO-control groups. Mice that received either GSO-329 or GSO-495 showed an increase in perfusion compared to GSO-control as early as 3 days after induction of ischemia. The increase in perfusion persisted over time in both groups and mice treated with GSO-329 even made a full recovery in paw perfusion within an astounding seven days after induction of ischemia, compared to approximately 60% recovery in GSO-control treated mice (Figures 4A and 4E). Mice treated with GSO-495 or GSO-494 had nearly fully recovered perfusion after ten days followed by mice treated with GSO-487b at two weeks. The GSO-control and PBS groups did not make full recoveries before being sacrificed at day 17.

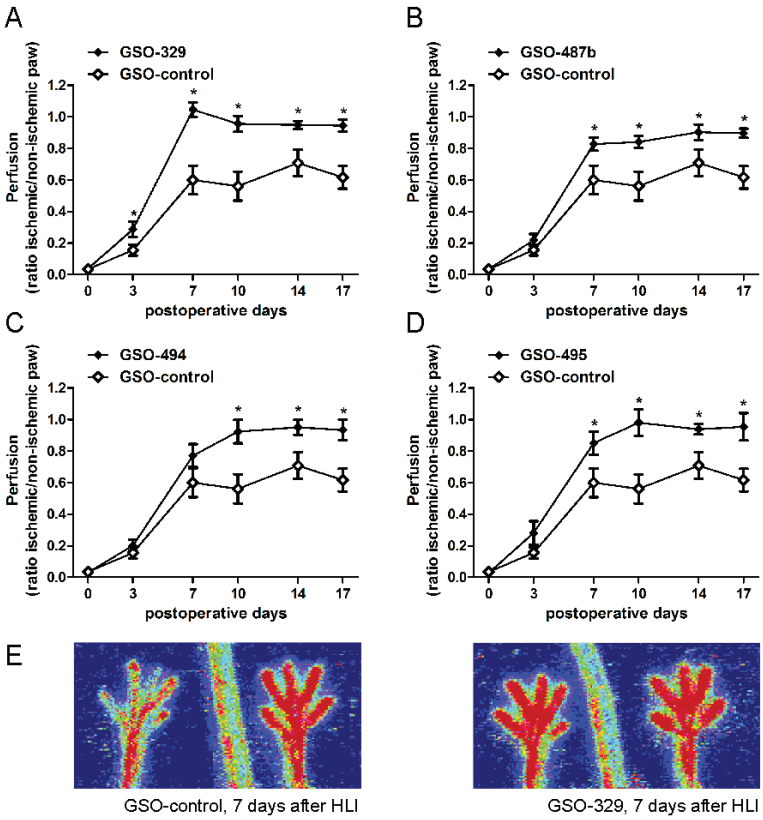

Figure 4. Blood flow recovery after in vivo 14q32 miR inhibition. (A-D) Quantification of LDPI measurements over time in mice (11/group) treated with GSOs (1 mg/mouse). Data are calculated as the ratio of the ischemic over the non-ischemic paw and presented as mean ± SEM. (E) Representative LDPI images of paws 7 days after induction of HLI in the left limb of mice treated with either GSO-control or GSO-329. *p<0.05.

Collateral Artery Diameter Increase

In addition to the increased blood flow recovery observed in animals treated with GSO-329, GSO-487b, GSO-494 and GSO-495, we determined the number and diameter of arterioles by analyzing α-SMA positive vessels in the adductor muscles of GSO-treated mice sacrificed 7 days after double ligation of the left femoral artery. Collateral arteries form from pre-existing arterioles. Therefore, we were not surprised that the number of collateral arteries between the left and right paw either within groups, or between groups, were similar in all groups, except for GSO-487b (Figure 5A). However, we did observe increases in arteriole diameters between the left and right adductor muscles compared to the GSO control for mice treated with GSO-487b (3-fold, p=0.02). Arteriole diameters also appeared increased in mice treated with GSO-329 (2.6-fold, p=0.09), GSO-494 (1.9-fold, p=0.3) and GSO-495 (2.3 fold, p=0.3), indicating GSO-induced increases in arteriogenesis (Figure 5B). When we quantified both arterioles with a diameter smaller and a diameter larger than 20µm we observed a significant decrease in the number of small arterioles in the left compared to the right paw of mice treated with GSO-329 and GSO-487b (Figure 5C) and a trend towards an increase in the number of large collaterals for all four GSOs (Figure 5D), clearly indicating remodeling of small collateral arterioles into larger collateral arteries.

Accumulation of macrophages around the remodeling arterioles is visualized in Online Figure V.

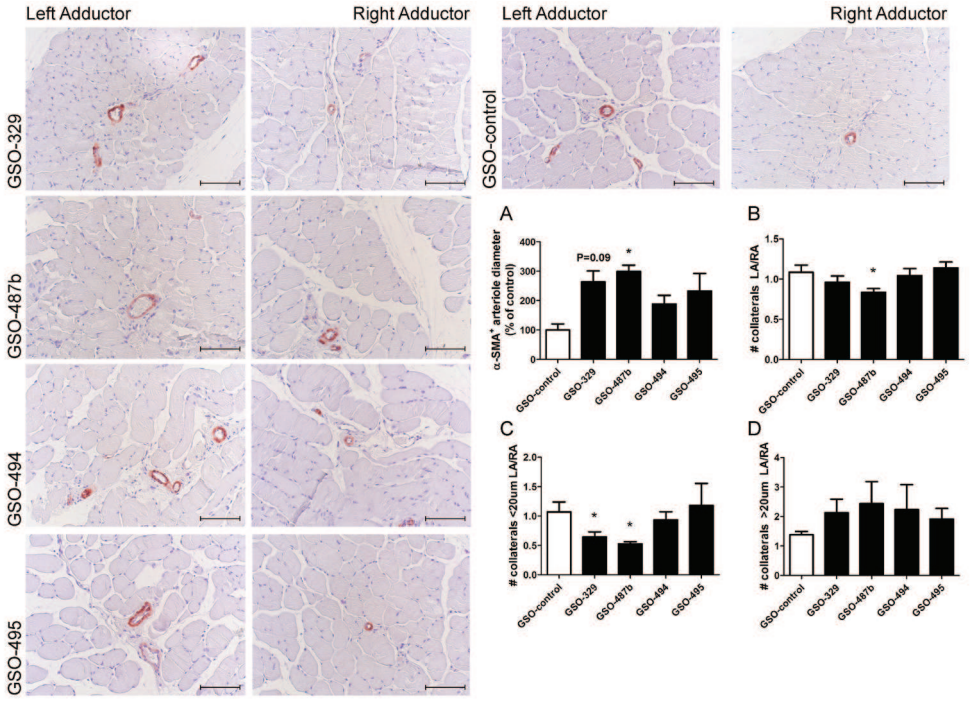

Figure 5. In vivo arteriogenesis after 14q32 miR inhibition. Representative images of α-SMA staining in right (untreated) and left (ligated femoral artery) adductor muscle tissues of mice treated with GSOs and (A) quantification of the increase in diameter of α-SMA+ arterioles, relative to the increase in mice treated with GSO-control. Number of (B) total, (C) small (diameter < 20µm) and (D) large (diameter > 20 µm) collateral arterioles. Per group, left and right adductor muscles of 9 mice were included. From each muscle, 8 sections were used and from each section, 1 representative photograph was used. The scale bar represents 100 µm. Data are presented as mean ± SEM. *p<0.05.

Increase in Capillary Density

The left (ischemic) and right (normoxic) soleus muscles of GSO-treated mice, sacrificed 7 days after double ligation of the left femoral artery, were stained for CD31 to visualize capillary formation. Increases in capillary formation compared to mice treated with GSO control were observed in the left solei of mice treated with GSO-329 (5-fold), GSO-487b (4-fold) and GSO-495 (4-fold). Capillary formation also appeared increased in the left solei of mice treated with GSO-494 (2.5-fold), but this was not significant (Figure 6).

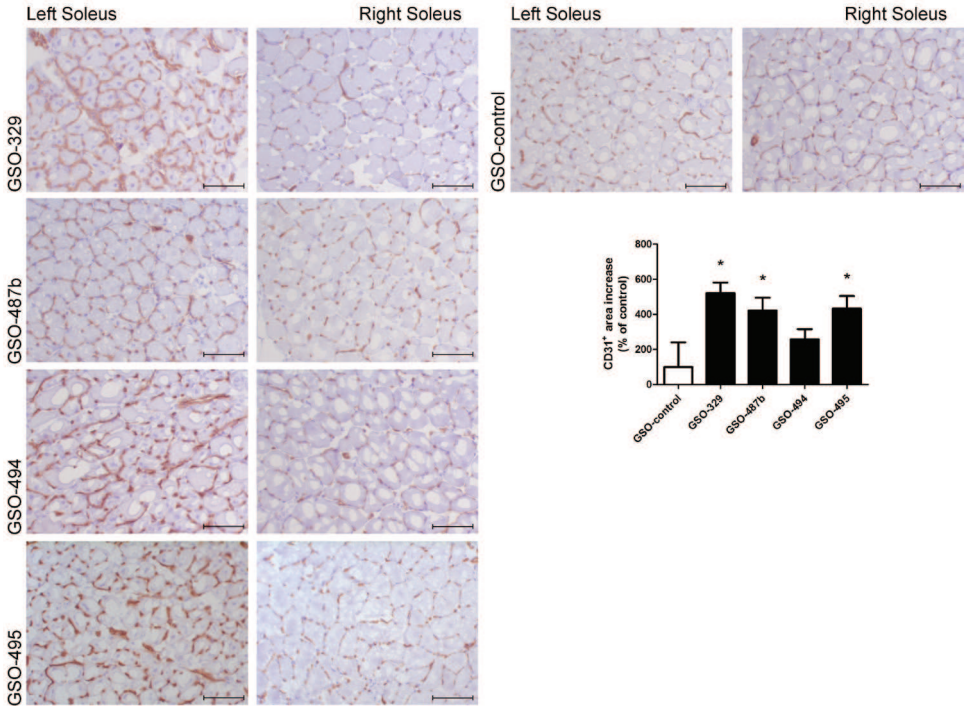

Figure 6. In vivo angiogenesis after 14q32 miR inhibition. Representative images of CD31 staining in right (normoxic) and left (ischemic) soleus muscles of mice treated with GSOs and quantification of the increase in CD31+ area between right and left soleus muscles, relative to the increase in mice treated with GSO-control. Per group, left and right soleus muscles from 9 mice were included. From each muscle, 6 sections were used and from each section, 1 representative photograph was used. The scale bar represents 100 µm. Data are presented as mean ± SEM. *p<0.05.

In Vivo Target Gene Regulation

We selected the 14q32 microRNAs for their potential to target a broad range of pro-arteriogenic and pro-angiogenic target genes. As it would not be feasible to confirm regulation of all putative targets, we made a selection based on the number of target sites, conserved between humans and mice, in the 3'UTRs of potential 14q32 miR targets (Online Table V). As we have previously shown, miR-487b has only 14 conserved putative target genes. We confirmed that miR-487b directly targets the vasoactive Insulin Receptor Substrate 1 (IRS1) in the arterial wall, leading to increased survival of both smooth muscle cells and myofibroblasts[26]. For miR-329, we selected Tlr4[27], Mef2a[20-22], Itgb3[28], Efnb2[29-30], Vegfa and Fgfr2[31]; for miR-494, we selected Arf6[32], Tlr4, Vegfa, Efnb2 and Fgfr2; for miR-495, we selected Tgfb2, Itgav[28], Stat3[33] and Tgfbr[34].

We used rt/qPCR to determine whether these genes were upregulated in the left adductor muscles of mice treated with the relevant GSOs. In the adductor muscles of mice treated with GSO-329, we observed up-regulation of several target genes for miR-329, including Tlr4, Vegfa and Fgfr2 at 3, and Mef2a and Fgfr2 at 7 days after HLI (Figure 7A-B). In mice treated with GSO-494, we observed upregulation of target genes Tlr4 and Vegfa at day 3 and of Tlr4 (p=0.07), Arf6, Efnb2 (p=0.07) and Fgfr2 at day 7 after HLI (Figure 7C-D). As miR-329 was a late-responder, the strongest benefits of miR-329 inhibition were expected to be observed early after HLI, in contrast to miR-494 which as an early-responder was upregulated rapidly after HLI and therefore benefits of inhibition were expected to be observed at later time points. We used both in vitro studies in human primary myofibroblasts and dual luciferase reporter gene assays to determine whether the regulated target genes are also targets for miR-329 and/or miR-494 in humans. We found that human MEF2A is a direct target for hsa-miR-329, while human FGFR2, VEGFA and EFNB2 are direct targets for hsa-miR-494. VEGFA was found to be regulated by hsa-miR-329, but not via direct binding of hsa-miR-329 to the VEGFA 3'UTR (Online Figure VI).

Even though miR-495 was efficiently downregulated and we observed stimulatory effects of GSO-495 on neovascularization and blood flow recovery, we could not confirm upregulation of putative target genes in mice treated with GSO-495 via rt/qPCR (Online Figure VII).

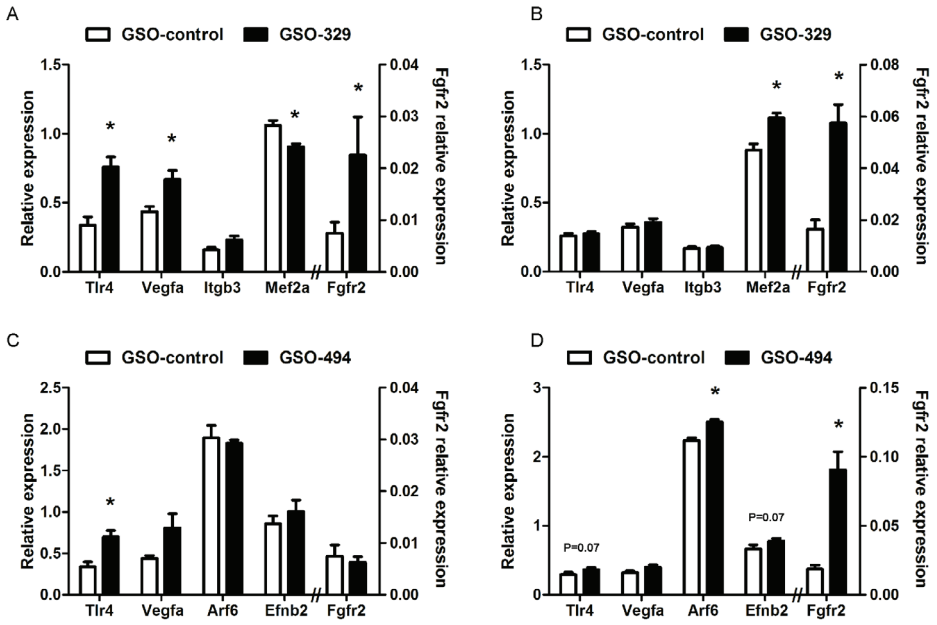

Figure 7. In vivo regulation of putative target genes. Expression levels of putative target genes for miR-329 relative to Hprt1 in adductor muscle tissue of mice treated with GSO-329 at days 3 (A) and 7 (B) after HLI. Expression levels of putative target genes for miR-494 relative to Hprt1 in adductor muscle tissue of mice treated with GSO-494 at days 3 (C) and 7 (D) after HLI. Per group, adductor muscle tissue of 2 (day 3) and 9 (day 7) mice was used. Data are presented as mean ± SEM. *p<0.05.

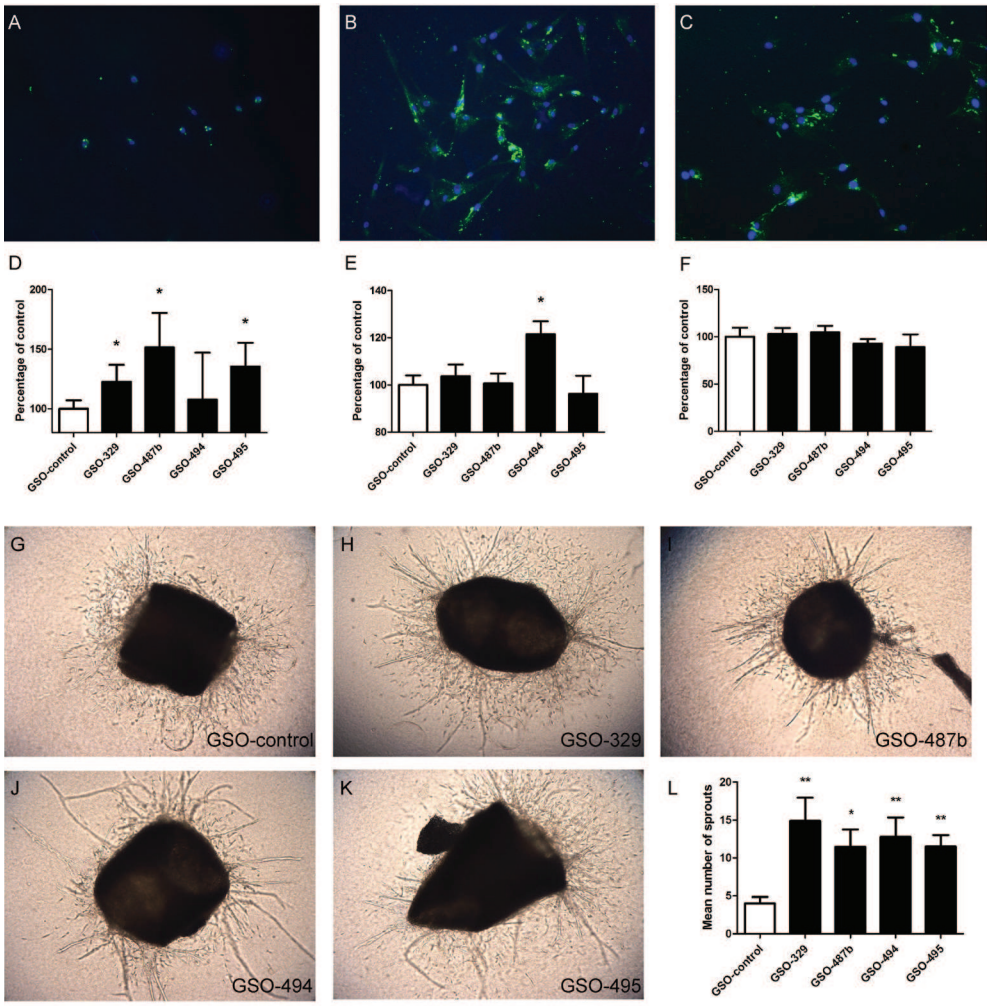

Figure 8. In vitro effects of 14q32 miR inhibition. FITC-labelled GSOs are readily taken up by primary HUVECs (A), primary HUAFs (B) and primary HUASMCs (C). Proliferation of primary HUAECs (D), primary HUAFs (E) and primary HUASMCs (F) after GSO treatment (10ng/µl) measured by 3H-thymidine incorporation relative to GSO-Control. Data are presented as mean ± SEM and represent at least 3 independent experiments. (G-K) Outgrowth of neovessels from 5-day collagen-embedded murine thoracic aortic ring explants treated with GSOs. (L) Quantification of neovessels. Data are presented as mean ± SEM and represent at least 2 independent experiments with 4 rings per condition. *p<0.05 and **p<0,01 compared to GSO control.

In Vitro Effects of 14q32 MiR Inhibition

Whereas angiogenesis depends mainly on activation and proliferation of endothelial cells alone, arteriogenesis requires activation and proliferation of arterial endothelial cells, smooth muscle cells and myofibroblasts. Therefore, we studied the effect of GSO treatment on these three cell types. Using FITC-labeled GSOs, we observed that GSOs are readily taken up into all three cell types within several hours, without the need for any transfection agent (Figures 8A-C). In arterial endothelial cells, inhibition of miR-329, miR-487b and miR-495 all led to increased cell proliferation by approximately 20%, 50% and 35% respectively. Inhibition of miR-494 did not affect endothelial cell proliferation

(Figure 8D). In contrast, in myofibroblasts we observed an increase of 20% in cell proliferation after miR-494 inhibition (Figure 8E), whereas no effects were observed for the other GSOs. None of the GSOs had effects on proliferation of smooth muscle cells (Figure 8F), as we had previously shown for GSO-487b[26].
We performed an aortic ring assay to determine GSO-induced sprout formation ex vivo. We observed that inhibition of all four selected 14q32 microRNAs with GSOs led to increased sprout formation compared to GSO-control (Figures 8G-L).

Discussion

In this study, we show that inhibition of individual 14q32 miRs improves blood flow recovery and stimulates both arteriogenesis in the adductor muscle and angiogenesis in the ischemic calf muscle. We made use of their master switch character to identify miRs that regulate neovascularization via Reverse Target Prediction. In a total set of nearly 200 genes associated with both angiogenesis and arteriogenesis, there was enrichment for binding sites of 27 miRs that all belong to the miR gene cluster on human chromosome 14. 14q32 miRs are upregulated during effective neovascularization in mice. We used Gene Silencing Oligonucleotides to inhibit the expression of four 14q32 miRs in vivo and followed blood flow recovery to the paw after double ligation of the left femoral artery in mice.

Although previous studies have demonstrated beneficial effects of individual miR inhibition on post-ischemic neovascularization, the effect size observed here, particularly for miR-329, is unprecedented. In 2009, Bonauer et al[9] reported on the role of the miR-17/92a cluster in angiogenesis. They showed that inhibition of miR-92a improved post-ischemic blood flow recovery in C57Bl/6 mice. Although the authors do not report the actual percentages of blood flow recovery, their LDPI images clearly show that mice have not recovered at day 14 after double ligation of the femoral artery and vein. In 2011, Grundmann et al[7] showed that inhibition of miR-100 also leads to improved blood flow recovery after ischemia. The authors described an absolute increase in perfusion of 10 to 15% at day 7 after double ligation of the femoral artery in C57BL/6 mice. Finally in 2012, Yin et al[10] took an opposite approach and demonstrated that over-expression of miR-15a attenuates post-ischemic blood flow recovery, resulting in an absolute decrease of perfusion of 10% at day 7 and 25% at day 14 after excision of the femoral artery, compared to control animals.
Using a large-scale RTP to identify miRs that regulate neovascularization, or any physiological process for that matter, is a novel approach. For neovascularization, the RTP proved both a robust and effective method. We recovered most miRs previously reported to be associated with angiogenesis and identified a large set of novel neovascularization miRs, the 14q32 miR gene cluster. The fact that inhibition of 14q32 miRs indeed increases blood flow recovery after ischemia and enhanced both arteriogenesis and angiogenesis in vivo, supports the validity of this novel method.
Interestingly however, we did not only recover miRs previously reported to inhibit neovascularization, but also miRs previously reported to enhance neovascularization, including miR-106b/93/25[8,14] and miR-424[25], although miR-424 has also been reported to have anti-angiogenic effects[35]. Our list of target genes consisted mainly of pro-arteriogenic and pro-angiogenic genes; miRs predicted to target these

genes are therefore likely to inhibit neovascularization. Perhaps, regulation of pro-neovascularization and anti-neovascularization pathways are more tightly intertwined than previously thought. This finding also indicates that the RTP could be used to identify pro-arteriogenic miRs, targeting anti-arteriogenic genes. Neovascularization could potentially be improved by the use of miR-mimics, leading to over-expression of these miRs and down-regulation of their anti-arteriogenic targets. However, miR-overexpression by use of e.g. miR-mimics is likely to lead to more off-target effects than inhibition, as miR over-expression and hence gene-inhibitory activity in organs and tissues not endogenously expressing the targeted miR can likely occur.

Although several miR-target gene prediction algorithms are available online, we chose to restrict our RTPs to www.targetscan.org. In a previous study on polymorphisms in miR-binding sites, we found predictions made by TargetScan to have approximately 60% accuracy[36]; combined with the large number of genes included in the RTP, TargetScan's predictions alone proved robust enough to identify important neovascularization miRs. MicroArray analyses showed upregulation of most 14q32 miR gene cluster members during effective neovascularization, which further validates the findings of both RTPs.

The 14q32 miR gene cluster is highly conserved between humans and mice. Of the four 14q32 miRs selected for in vivo silencing here, only the sequence of hsa-miR-329 varied slightly from its murine variant mmu-miR-329 (Online Tables V-A-E). Yet, many putative binding sites were conserved between humans and mice. Surprisingly, miR-495, which had the most putative pro-arterio- and pro-angiogenic targets in RTP1, had the least conserved target sites of the four selected miRs. As conservation over species often reflects the biological significance of genomic sequences, perhaps this lower degree of conservation explains the more moderate effects of miR-495 inhibition on neovascularization as measured by immunohistochemistry. It may also explain why miR-495 was not regulated during effective vascular remodeling and neovascularization in mice, why it had less putative targets in the evidence-based RTP2 and why we could not confirm upregulation of putative target genes after GSO-495 treatment.

MiR-487b is an exceptional miR as it has only 14 conserved putative target genes in both humans and mice. We previously confirmed the role of miR-487b in outward remodeling of the aorta, via targeting the pro-survival factor Insulin Receptor Substrate 1 in vivo in rats and in vitro in human primary arterial cells[26]. Having only a single conserved neovascularization target gene, IRS1, most likely explains the slightly more moderate effects of miR-487b inhibition on blood flow recovery and neovascularization compared to miR-329 and miR-494 inhibition. A recent study on the role of miR-487b in human lung cancer did confirm SUZ12, BMI1, WNT5A and KRAS as direct targets for miR-487b[37]. However, except for one of two sites in the Wnt5a 3'UTR, the binding sites for miR-487b in these genes were not conserved in mice and can therefore not have contributed to the effects on neovascularization in our murine model.

We set out to identify miRs that act as master switches, having perhaps only moderate effects on expression levels, but of many different target genes, involved in all aspects of neovascularization. Particularly miR-329 and miR-494 proved to regulate most of the selected target genes in vivo. These

target genes, involved in various aspects of vascular remodeling were upregulated in vivo after miR-329 or miR-494 inhibition. Correspondingly, effects on blood flow recovery, arteriogenesis and angiogenesis were robust. Inhibition of miR-329 resulted in an unprecedented rapid recovery of paw perfusion. As miR-329 was late-responder in our microArray analyses, perhaps miR-329 inhibition in the early stages of neovascularization greatly enhances the process as a whole. This hypothesis is supported by the observation that endothelial cell proliferation was enhanced after treatment with GSO-329, as arteriogenesis is initiated after shear stress-induced endothelial activation. MiR-329 was recently reported to inhibit pathological angiogenesis via downregulation of CD146, which can act as a co-receptor of the VEGF Receptor 2[39]. Like miR-329, inhibition of miR-495 also led to increased paw perfusion in the very early stages of post-ischemic neovascularization. Besides the here shown increased proliferation of endothelial cells after miR-495 inhibition, previous studies have also shown a role for miR-495 in both cell survival and migration[39-41]. Inhibition of miR-487b also increases endothelial proliferation.

Our microarray analyses showed that expression of miR-494, after a rapid upregulation, starts to normalize within a week after ischemia. Of the four GSOs used in this study, GSO-494 is the slowest starter with respect to blood flow recovery, but especially between days 7 and 10 after femoral artery ligation, GSO-494 treatment improves paw perfusion compared to the control. MiR-494 was previously reported to impact both proliferation and survival of, amongst other cell types, cardiac myocytes[42, 43]. We observed that miR-494 did not impact arterial endothelial cell proliferation, but enhanced arterial myofibroblast proliferation, which is in agreement with the slow start followed by stronger increases in flow, particularly in the later stages of neovascularization (i.e. myofibroblast recruitment and reinstatement of the extracellular matrix), that we observed in vivo. Potentially, combined administration of GSO-329 and GSO-494 would therefore enhance post-ischemic blood flow recovery and neovascularization even further.

In conclusion, we here demonstrate that inhibition of individual 14q32 miRs leads to increases in post-ischemic blood flow recovery in vivo. We believe that 14q32 miRs function as master switches in vascular remodeling and neovascularization. Inhibition of either individual, or of a combination of, 14q32 miRs, may offer a future alternative to growth factors in therapeutic neovascularization.

Acknowledgements

We thank R. van der Kwast, W. Razawy, W. Zhu and P. Verkerk for their technical support.

Sources of funding

This study was supported by grants from the Netherlands Organisation for Scientific Research (Veni 916.12.041), the Leiden University Fund/Nypels- van der Zee Fund (2219/5-4-12\NZ), BioMedical Materials, Dutch Ministry of Economic Affairs, Agriculture and Innovation (BMM-PENT; P1.03), and by the Netherlands Institute for Regenerative Medicine (NIRM, FES0908).

References

1. van Oostrom MC, van Oostrom O., Quax PH, Verhaar MC, Hoefer IE. Insights into mechanisms behind arteriogenesis: what does the future hold? J Leukoc Biol. 2008;84:1379-1391.
2. Risau W. Mechanisms of angiogenesis. Nature. 1997;386:671-674.
3. Germani A, Di Campli C, Pompilio G, Biglioli P, Capogrossi MC. Regenerative therapy in peripheral artery disease. Cardiovasc Ther. 2009;27:289-304.
4. Gupta R, Tongers J, Losordo DW. Human studies of angiogenic gene therapy. Circ Res. 2009;105:724-736.
5. Bartel DP. MicroRNAs: genomics, biogenesis, mechanism, and function. Cell. 2004;116:281-297.
6. van Solingen C, Seghers L, Bijkerk R, Duijs JM, Roeten MK, van Oeveren-Rietdijk AM, Baelde HJ, Monge M, Vos JB, de Boer HC, Quax PH, Rabelink TJ, van Zonneveld AJ. Antagomir-mediated silencing of endothelial cell specific microRNA-126 impairs ischemia-induced angiogenesis. J Cell Mol Med. 2009;13:1577-1585.
7. Grundmann S, Hans FP, Kinniry S, Heinke J, Helbing T, Bluhm F, Sluijter JP, Hoefer I, Pasterkamp G, Bode C, Moser M. MicroRNA-100 regulates neovascularization by suppression of mammalian target of rapamycin in endothelial and vascular smooth muscle cells. Circulation. 2011;123:999-1009.
8. Hazarika S, Farber CR, Dokun AO, Pitsillides AN, Wang T, Lye RJ, Annex BH. MicroRNA-93 Controls Perfusion Recovery Following Hind-Limb Ischemia by Modulating Expression of Multiple Genes in the Cell Cycle Pathway. Circulation. 2013;127:1818-1828.
9. Bonauer A, Carmona G, Iwasaki M, Mione M, Koyanagi M, Fischer A, Burchfield J, Fox H, Doebele C, Ohtani K, Chavakis E, Potente M, Tjwa M, Urbich C, Zeiher AM, Dimmeler S. MicroRNA-92a controls angiogenesis and functional recovery of ischemic tissues in mice. Science. 2009;324:1710-1713.
10. Yin KJ, Olsen K, Hamblin M, Zhang J, Schwendeman SP, Chen YE. Vascular endothelial cell-specific microRNA-15a inhibits angiogenesis in hindlimb ischemia. J Biol Chem. 2012;287:27055-27064.
11. Spinetti G, Fortunato O, Caporali A, Shantikumar S, Marchetti M, Meloni M, Descamps B, Floris I, Sangalli E, Vono R, Faglia E, Specchia C, Pintus G, Madeddu P, Emanueli C. MicroRNA-15a and microRNA-16 impair human circulating proangiogenic cell functions and are increased in the proangiogenic cells and serum of patients with critical limb ischemia. Circ Res. 2013;112:335-346.
12. Caporali A, Emanueli C. MicroRNAs in Postischemic Vascular Repair. Cardiol Res Pract. 2012; 486702.
13. Caporali A, Emanueli C. MicroRNA-503 and the extended microRNA-16 family in angiogenesis. Trends Cardiovasc Med. 2011;21:162-166.
14. Semo J, Sharir R, Afek A, Avivi C, Barshack I, Maysel-Auslender S, Krelin Y, Kain D, Entin-Meer M, Keren G, George J. The 106b~25 microRNA cluster is essential for neovascularization after hindlimb ischaemia in mice. Eur Heart J. 2013.
15. Seitz H, Royo H, Bortolin ML, Lin SP, Ferguson-Smith AC, Cavaille J. A large imprinted microRNA gene cluster at the mouse Dlk1-Gtl2 domain. Genome Res. 2004;14:1741-1748.
16. Benetatos L, Hatzimichael E, Londin E, Vartholomatos G, Loher P, Rigoutsos I, Briasoulis E. The microRNAs within the DLK1-DIO3 genomic region: involvement in disease pathogenesis. Cell Mol Life Sci. 2013;70:795-814.
17. Zhou Y, Cheunsuchon P, Nakayama Y, Lawlor MW, Zhong Y, Rice KA, Zhang L, Zhang X, Gordon FE, Lidov HG, Bronson RT, Klibanski A. Activation of paternally expressed genes and perinatal death caused by deletion of the Gtl2 gene. Development. 2010;137:2643-2652.
18. Kagami M, O'Sullivan MJ, Green AJ, Watabe Y, Arisaka O, Masawa N, Matsuoka K, Fukami M, Matsubara K, Kato F, Ferguson-Smith AC, Ogata T. The IG-DMR and the MEG3-DMR at human chromosome 14q32.2: hierarchical interaction and distinct functional properties as imprinting control centers. PLoS Genet. 2010;6:e1000992.
19. Gordon FE, Nutt CL, Cheunsuchon P, Nakayama Y, Provencher KA, Rice KA, Zhou Y, Zhang X, Klibanski A. Increased expression of angiogenic genes in the brains of mouse meg3-null embryos. Endocrinology. 2010;151:2443-2452.
20. Snyder CM, Rice AL, Estrella NL, Held A, Kandarian SC, Naya FJ. MEF2A regulates the Gtl2-Dio3 microRNA mega-cluster to modulate WNT signaling in skeletal muscle regeneration. Development. 2013;140:31-42.
21. Zhao W, Zhao SP, Peng DQ. The effects of myocyte enhancer factor 2A gene on the proliferation, migration and phenotype of vascular smooth muscle cells. Cell Biochem Funct. 2012;30:108-113.
22. Firulli AB, Miano JM, Bi W, Johnson AD, Casscells W, Olson EN, Schwarz JJ. Myocyte enhancer binding factor-2 expression and activity in vascular smooth muscle cells. Association with the activated phenotype. Circ Res. 1996;78:196-204.
23. Bhagat L, Putta MR, Wang D, Yu D, Lan T, Jiang W, Sun Z, Wang H, Tang JX, La MN, Kandimalla ER, Agrawal S. Novel oligonucleotides containing two 3'-ends complementary to target mRNA show optimal gene-silencing activity. J Med Chem. 2011;54:3027-3036.
24. Hellingman AA, Bastiaansen AJ, de Vries MR, Seghers L, Lijkwan MA, Lowik CW, Hamming JF, Quax PH. Variations in surgical procedures for hind limb ischaemia mouse models result in differences in collateral formation. Eur J Vasc Endovasc Surg. 2010;40:796-803.
25. Ghosh G, Subramanian IV, Adhikari N, Zhang X, Joshi HP, Basi D, Chandrashekhar YS, Hall JL, Roy S, Zeng Y, Ramakrishnan S. Hypoxia-induced microRNA-424 expression in human endothelial cells regulates HIF-alpha isoforms and promotes angiogenesis. J Clin Invest. 2010;120:4141-4154.
26. Nossent AY, Eskildsen T, Andersen LB, Bie P, Bronnum H, Schneider M, Andersen D, Welten SM, Jeppesen PL,

Hamming JF, Hansen JL, Quax PH, Sheikh SP. The 14q32 MicroRNA-487b Targets the Anti-Apoptotic Insulin Receptor Substrate 1 in Hypertension Induced Remodeling of the Aorta . Ann Surg. 2013; 258:743-751.

27. de Groot D, Hoefer IE, Grundmann S, Schoneveld A, Haverslag RT, van Keulen JK, Bot PT, Timmers L, Piek JJ, Pasterkamp G, de Kleijn DP. Arteriogenesis requires toll-like receptor 2 and 4 expression in bone-marrow derived cells. J Mol Cell Cardiol. 2011;50:25-32.
28. Cai WJ, Li MB, Wu X, Wu S, Zhu W, Chen D, Luo M, Eitenmuller I, Kampmann A, Schaper J, Schaper W. Activation of the integrins alpha 5beta 1 and alpha v beta 3 and focal adhesion kinase (FAK) during arteriogenesis. Mol Cell Biochem. 2009;322:161-169.
29. Katsu M, Koyama H, Maekawa H, Kurihara H, Uchida H, Hamada H. Ex vivo gene delivery of ephrin-B2 induces development of functional collateral vessels in a rabbit model of hind limb ischemia. J Vasc Surg. 2009;49:192-198.
30. Korff T, Braun J, Pfaff D, Augustin HG, Hecker M. Role of ephrinB2 expression in endothelial cells during arteriogenesis: impact on smooth muscle cell migration and monocyte recruitment. Blood. 2008;112:73-81.
31. Tille JC, Wood J, Mandriota SJ, Schnell C, Ferrari S, Mestan J, Zhu Z, Witte L, Pepper MS. Vascular endothelial growth factor (VEGF) receptor-2 antagonists inhibit VEGF- and basic fibroblast growth factor-induced angiogenesis in vivo and in vitro. J Pharmacol Exp Ther. 2001 December;299:1073-1085.
32. Ikeda S, Ushio-Fukai M, Zuo L, Tojo T, Dikalov S, Patrushev NA, Alexander RW. Novel role of ARF6 in vascular endothelial growth factor-induced signaling and angiogenesis. Circ Res 20054;96:467-475.
33. Chen Z, Han ZC. STAT3: a critical transcription activator in angiogenesis. Med Res Rev. 2008;28:185-200.
34. Olieslagers S, Pardali E, Tchaikovski V, ten DP, Waltenberger J. TGF-beta1/ALK5-induced monocyte migration involves PI3K and p38 pathways and is not negatively affected by diabetes mellitus. Cardiovasc Res. 2011;91:510-518.
35. Chamorro-Jorganes A, Araldi E, Penalva LO, Sandhu D, Fernandez-Hernando C, Suarez Y. MicroRNA-16 and microRNA-424 regulate cell-autonomous angiogenic functions in endothelial cells via targeting vascular endothelial growth factor receptor-2 and fibroblast growth factor receptor-1. Arterioscler Thromb Vasc Biol 2011;31:2595-2606.
36. Nossent AY, Hansen JL, Doggen C, Quax PH, Sheikh SP, Rosendaal FR. SNPs in microRNA binding sites in 3'-UTRs of RAAS genes influence arterial blood pressure and risk of myocardial infarction. Am J Hypertens 2011;24:999-1006.
37. Xi S, Xu H, Shan J, Tao Y, Hong JA, Inchauste S, Zhang M, Kunst TF, Mercedes L, Schrump DS. Cigarette smoke mediates epigenetic repression of miR-487b during pulmonary carcinogenesis. J Clin Invest 2013;123:1241-1261.
38. Wang P, Luo Y, Duan H, Xing S, Zhang J, Lu D, Feng J, Yang D, Song L, Yan X. MicroRNA 329 suppresses angiogenesis by targeting CD146. Mol Cell Biol 2013;33:3689-3699.
39. Hwang-Verslues WW, Chang PH, Wei PC, Yang CY, Huang CK, Kuo WH, Shew JY, Chang KJ, Lee EY, Lee WH. miR-495 is upregulated by E12/E47 in breast cancer stem cells, and promotes oncogenesis and hypoxia resistance via downregulation of E-cadherin and REDD1. Oncogene 2011;30:2463-2474.
40. Jiang X, Huang H, Li Z, He C, Li Y, Chen P, Gurbuxani S, Arnovitz S, Hong GM, Price C, Ren H, Kunjamma RB, Neilly MB, Salat J, Wunderlich M, Slany RK, Zhang Y, Larson RA, Le Beau MM, Mulloy JC, Rowley JD, Chen J. MiR-495 is a tumor-suppressor microRNA down-regulated in MLL-rearranged leukemia. Proc Natl Acad Sci U S A. 2012;109:19397-19402.
41. Li Z, Cao Y, Jie Z, Liu Y, Li Y, Li J, Zhu G, Liu Z, Tu Y, Peng G, Lee DW, Park SS. miR-495 and miR-551a inhibit the migration and invasion of human gastric cancer cells by directly interacting with PRL-3. Cancer Lett. 2012;323:41-47.
42. Wang X, Zhang X, Ren XP, Chen J, Liu H, Yang J, Medvedovic M, Hu Z, Fan GC. MicroRNA-494 targeting both proapoptotic and antiapoptotic proteins protects against ischemia/reperfusion-induced cardiac injury. Circulation 2010;122:1308-13018.
43. Ohdaira H, Sekiguchi M, Miyata K, Yoshida K. MicroRNA-494 suppresses cell proliferation and induces senescence in A549 lung cancer cells. Cell Prolif 2012;45:32-38.

Supplemental Material

Materials and Methods

Reverse Target Prediction

To identify miRs that are involved in arterio- and angiogenesis, an in silico reverse target prediction (RTP) was performed. A selection was made of 127 genes known from literature and previous studies within our group to play important roles in arterio- and angiogenesis (Table S1A). To ensure the master switch character of the identified miRs, we selected target genes covering all aspects of vascular remodeling; endothelial activation, smooth muscle cell proliferation, extracellular matrix rearrangement, chemo- and cytokines and their receptors, growth factors and their receptors, the natural killer complex, pro-arteriogenic and pro-angiogenic transcription factors and signaling molecules (Table S1A). We then used www.targetscan.org to, for each individual gene, generate a list of all miRs predicted to target these 127 genes. Each list, no restrictions were applied, was copied into a spreadsheet and for each miR we simply counted the number of times it was present in the file.

To confirm the relevance of our findings, we selected an additional 70 genes that we found upregulated, using microArray analysis, at the site of active arteriogenesis, the adductor muscle group, in C57Bl/6 mice subjected to single ligation of the left femoral artery (Table S2A). We repeated the RTP for these 70 genes and looked for similarities in identified miRs between the two reverse target predictions (for 14q32 miRs, Table S3).

Both RTPs were performed looking for miR binding sites in human target genes to ensure clinical relevance. Conservation between human and murine target sites was checked to confirm the validity of our murine model of hind limb ischemia (for 14q32miRs, Table S4).

The procedure of the RTPs is schematically summarized in Supplemental Figure S1.

MicroRNA Inhibitors

AntagomiRs were designed with perfect reverse complementarity to the mature target miR sequence and purchased from VBC Biotech (Vienna, Austria). AntagomiRs were made up of a single-stranded O-methyl-modified RNA strand with 5'-end and 3'-end phosporothioate linkages and a 3'-end cholesterol tail.

Gene Silencing Oligonucleotides (GSOs) were designed with perfect reverse complementarity to the mature target miR sequence and synthesized at Idera Pharmaceuticals (Cambridge, MA, USA)[1]. As a negative control, a scrambled sequence was used, designed not to target any known murine miR. GSOs were made up of two single-stranded O-methyl-modified DNA strands, linked together at their 5' ends by a phosphorothioate-linker. Shielding the 5'-end of the single-stranded oligonucleotides prevents activation of the innate immune system via Toll-like Receptors; the double DNA strand increases specificity for the target miR.

Sequences of all antagomiRs and GSOs used are given in Table S5.

GSO Biodistribution

Three healthy male adult C57Bl/6 mice were injected intravenously with IRDye-800-labelled GSO-329 (0.4mg/mouse; Idera Pharmaceuticals, Cambridge MA). The first mouse was sacrificed one hour after injection. The second mouse was sacrificed 14 hours after injection. The third mouse was subjected to double ligation of the left femoral artery, as described below, 24 hours after injection and sacrificed 48 hours after injection.

Near-InfraRed (NIR) fluorescence measurements were performed using the FLARE™ NIR imaging system[2]. The Pearl Impulse small animal imaging system (LI-COR) was used as an in vivo preclinical reference system to measure NIR fluorescent signals for bio-distribution analysis and to calculate Signal-to-background ratios. The specific and control images were normalized and using the associated software, regions of interest were selected.

Hind Limb Ischemia Models

Healthy adult male C57Bl/6 mice, aged 8 to 12 weeks (Charles River and Harlan) were housed in groups of 4 or 5 mice with free access to tap water and regular chow. All experiments were approved by the committee on animal welfare of the Leiden University Medical Center (Leiden, The Netherlands).

For miR-inhibition experiments, mice were given a bolus injection of 1 mg (~40mg/kg) GSO in PBS or PBS alone via the tail vein (i.v.), 1 day prior to femoral artery ligation.

Mice were anesthetized by intraperitoneal (i.p.) injection of midazolam (8 mg/kg, Roche Diagnostics), medetomidine (0.4 mg/kg, Orion) and fentanyl (0.08 mg/kg, Janssen Pharmaceuticals). Unilateral hind limb ischemia was induced by electrocoagulation of the left femoral artery proximal to the superficial epigastric arteries alone (single ligation: model for effective arteriogenesis), or combined with electrocoagulation of the distal femoral artery proximal to the bifurcation of the popliteal and saphenous artery3 (double ligation: model for severe Peripheral Arterial Disease). After surgery, anaesthesia was antagonized with flumazenil (0.7 mg/kg, Fresenius Kabi), atipamezole (3.3 mg/kg, Orion) and buprenorphine (0.2 mg/kg, MSD Animal Health).

Blood flow recovery to the paw was measured over time using Laser Doppler Perfusion Imaging (LDPI) (Moore Instruments). Mice were anaesthetized by i.p. injection of midazolam (8 mg/kg) and medetomidine (0.4 mg/kg). Mice were place in a double-glazed pot, perfused with water at 37°C for 5 minutes prior to each measurement. After LDPI, anesthesia was antagonized by subcutaneous injection of flumazenil (0.7 mg/kg) and atipamezole (3.3 mg/kg). LDPI measurements in the treated paw were normalized to measurements of the untreated paw, as internal control.

Analgesic fentanyl (0.08 mg/kg) was administered subcutaneously after the final LDPI measurement and mice were sacrificed. The

adductor, gastrocnemius and soleus muscles were harvested and either snap-frozen on dry ice or fixed in 4% PFA.

MicroArray
Healthy male adult C57Bl/6 mice were subjected to single ligation of the femoral artery, as described below. Four mice were sacrificed at each of the following time points: before ligation; 24 hours after ligation; 72 hours after ligation; 1 week after ligation. The adductor muscles were collected and snap-frozen on dry ice. Total RNA was isolated using the RNeasy fibrous tissue minikit (Qiagen). RNA concentration, purity and integrity were examined by nanodrop (Nanodrop® Technologies) and Bioanalyzer (Agilent 2100) measurements.
For whole-genome expression profiling, amplified biotinylated RNA was generated using the Illumina TotalPrep RNA Amplification Kit. For array analysis, MouseWG-6 v2.0 Expression Beadchips (Illumina), which contain more than 45,200 transcripts, were used. Expression levels were Log2-transformed and after quantile normalization, transcripts showing background intensity, both at baseline and after induction of HLI, were removed from the analysis.
MiR expression profiling was performed as two-color common reference hybridizations on LNA based arrays (miRCURY LNATM miR Array ready-to-spot probe set, Exiqon, Denmark), spotted in-house on CodeLinkTM HD Activated slides (DHD1-0023, SurModics, Eden Prairie, MN) according to manufacturer's protocol. Samples were labeled with Hy3, by use of miRCURY LNA miR Array Power labeling kit (208032-A, Exiqon) and hybridized for 16 hours. A pool of equal volumes of each individual sample was labeled with Hy5 and used as reference. Slides were washed (208021, Exiqon), scanned on an Agilent (G2565CA) Microarray scanner and analyzed by the Genepix 6.0 software. Normalization and background correction was performed in the "statistical language R" using "vsn" package (Bioconductor), and quadruplicate spots were averaged. Differential expression was assayed using the "limma" package (Bioconductor) by fitting the eBayes linear model and contrasting individual treatments with untreated controls. Log2 fold changes were calculated using the toptable function of the limma package.

rt/qPCR
MiR rt/qPCR. Total RNA was isolated using a standard TRIzol-chloroform extraction protocol. RNA concentration, purity and integrity were examined by nanodrop (Nanodrop® Technologies). MiR quantification was performed according to manufacturer's protocol using TaqMan® miR assays (Applied Biosystems). qPCRs were run on a 7900HT Fast Real-Time PCR System (Applied Biosystems), and amplification efficiencies were checked by standard curves. Normalization of data was performed using a stably expressed endogenous control (mmu-let-7c and mmu-miR-122 for in murine samples and hsa-miR-191 for human cell cultures).
mRNA rt/qPCR. Relative quantitative mRNA PCR was performed on reverse transcribed cDNA using Taqman gene expression assays. qPCRs were run on a 7900HT Fast Real-Time PCR System (Applied Biosystems), and amplification efficiencies were checked by standard curves. Normalization of data was performed using stably expressed endogenous controls (GAPDH, HPRT1).

Immunohistochemistry
α-SMA. Five µm thick paraffin-embedded cross-sections of adductor muscle were re-hydrated and endogenous peroxidase activity was blocked. Smooth muscle cells were stained with anti-α-smooth muscle actin (anti-α-SMA) (DAKO, Glostrup, Denmark). Sections were counterstained with hematoxylin. α-SMA positive arterioles were analyzed using image analysis (Image J 1.43, NHI, USA).
MAC3. Five µm thick paraffin-embedded cross-sections of adductor muscle were re-hydrated and endogenous peroxidase activity was blocked. Macrophages were stained with anti-Mac3 (BD Pharmingen). Sections were counterstained with hematoxylin. Mac3 positive cells were analyzed using image analysis (Image J 1.43).
CD31. In 6 µm thick fresh-frozen cross-sections of soleus muscle, endothelial cells were fixed in ice-cold acetone and stained with anti-CD31 (BD Pharmingen). Sections were counterstained with hematoxylin. Quantification of CD31 positive area was performed on sections photographed randomly (six representative images per muscle per mouse, three animals per group) using image analysis (Qwin, Leica, Wetzlar, Germany).

Aortic Ring Assay
Mouse aortic ring assays were performed as described previously[4]. In brief, the thoracic aorta was removed from 8 to 10-week old mice and transferred to a petri dish containing Opti-MEM (Gibco). The surrounding fat and branching vessels were carefully removed and the aorta was flushed with Opti-MEM (Gibco). Aortic rings of 0.5 to 1 mm were transferred to fresh Opti-MEM and serum-starved overnight in addition with GSOs (10ng/ul). Collagen (Type I, Millipore) was diluted to a concentration of 1mg/ml with 1xDMEM (Gibco) and pH was adjusted with 5N NaOH. 96-well plates were coated with 75 µl collagen matrix. Rings were transferred into the wells and after 1 hour, 150 µl Opti-MEM supplemented with 2.5% FBS (PAA, Austria), penicillin-streptomycin (PAA, Austria) and 30ng/ml VEGF (in-house production and purification) and GSOs was added to each well. Medium was changed first on day 3, then every other day. Microvessel outgrowth was quantified after 5 days by live phase-contrast microscopy (Axiovert 40C, Carl Zeiss). Starting from a specific point on the ring, each microvessel emerging from the ring was counted as a sprout and individual branches arising from each microvessel counted as a separate sprout, working around the ring clockwise.

Isolation of Human umbilical arterial endothelial cells, smooth muscle cells and myofibroblasts (HUAECs, HUASMCs & HUAFs)
Umbilical cords were collected from full-term pregnancies and stored in sterile PBS at 4°C and subsequently used for cell isolation within 7 days. For HUAEC isolation, a cannula was inserted in one of the umbilical arteries and flushed with sterile PBS. The artery was infused with 0.075% collagenase type II (Worthington, Lakewood, NJ, USA) and incubated at 37°C for 20 minutes. The collagenase solution was collected and the artery was flushed with PBS in order to collect all detached endothelial cells. The cell suspension was centrifuged at 400 g for 5 minutes and the pellet was resuspended in HUAEC culture medium (M199 (PAA, Pasching, Austria), 10% heat inactivated human serum (PAA), 10% heat inactivated newborn calf serum (PAA), 1% penicillin/streptomycin

(MP Biomedicals, Solon, OH, USA), 150µg/ml endothelial cell growth factor (kindly provided by Dr. Koolwijk, VU Medical Center, Amsterdam, the Netherlands) and 0.1% heparin (LEO Pharma, Ballerup Danmark)). HUAECs were cultured in plates coated with 1% gelatin.
The second artery was removed and cleaned from remaining connective tissue. Endothelial cells were removed by gently rolling the artery over a blunted needle. The tunica adventitia and tunica media were separated using surgical forceps. After overnight incubation in HUASMC/HUAF culture medium, (DMEM GlutaMAX™ (Invitrogen, GIBCO, Auckland, New Zealand), 10% heat inactivated fetal bovine serum (PAA), 10% heat inactivated human serum, 1% penicillin/streptomycin and 1% nonessential amino acids (PAA)), both tunicae were incubated separately in a 2mg/ml collagenase type II solution (Worthington) at 37 °C. Cell suspensions were filtered over a 70µm cell strainer and centrifuged at 400g for 10 minutes. Cell pellets were resuspended and plated in culture medium. Cells isolated from the tunica adventitia were washed with culture medium after 90 minutes to remove slow-adhering non-fibroblast cells.

Primary cell culture
Cells were cultured at 37°C in a humidified 5% CO2 environment. Culture medium was refreshed every 2-3 days. Cells were passed using trypsin-EDTA (Sigma, Steinheim, Germany) at 90-100% (HUAECs and HUASMCs) or 70-80% confluency (HUAFs). HUASMCs and HUAFs were used up to passage six and HUAECs up to passage three. Stock solutions of isolated HUASMCs and HUAFs up to passage four and HUAECs up to passage two were stored at -180°C in DMEM GlutaMAX™ containing 20% FBS and 10% DMSO (Sigma).

GSO uptake in primary cells
Cells were grown on 15 mm Ø cover glasses (Thermo Scientific, Braunschweig Germany) until 50% confluent. FITC-labelled GSO-329 was added to HUVECs, HUASMCs and HUAFs at a concentration of 10ng/µl. After 4 to 6 hours, cells were washed with PBS, fixed for 10 minutes in 4% paraformaldehyde (PFA, Klinipath, Duiven Netherlands), washed with PBS, permeated for 5 minutes with 0.1% Triton-X100 (Sigma Steinheim Germany) and washed again with PBS. Cover glassed were then put on slides with vectashield (Vectorlaboratories, Burlingame CA), stored overnight at 4°C and analyzed the next day by fluorescence microscopy.

Proliferation assay in primary human arterial cells
Isolation and culture of primary human umbilical cord arterial endothelial cells (HUAECs), smooth muscle cells (HUASMCs) and myofibroblasts (HUAFs) are described in the Supplemental Data.
Cells were seeded in 48-wells plates at 2500 (HUAFs) or 5000 (HUASMCs and HUAECs) cells per well. The next day, cells were incubated with GSOs (10 ng/µl) in culture medium. After 24 hours, medium was replaced by medium containing 0.5% FCS for HUAFs and HUASMCs or 10% NBCS for HUAECs with GSOs. Again after 24 hours, cells were stimulated for 24 hours for HUAFs and HUASMCs or 40 hours for HUAECs and consecutively, cell proliferation was determined by adding 3H-thymidine (PerkinElmer, Zaventum, Belgium) at a final concentration of 0.5 µCi/ml. After 5 hours, cells were washed with ice-cold PBS, fixed with 100% methanol, permeated with 5% tri-chloric acid and lysed with 0.3N NaCl. Disintegrations per minute (DPM) were counted for 5 minutes per sample in Ultima Gold™ scintillation cocktail (Canberra-Packard, Frankfurt, Germany).

Immunocytochemistry
HUAFs were grown on 15 mm Ø cover glasses (Thermo Scientific, Braunschweig Germany) until 50% confluent. Subsequently, cells were fixed for 10 minutes in 4% PFA (Klinipath), washed with PBS, permeated for 5 minutes with 0.1% Triton-X100 (Sigma), washed again with PBS and blocked at least 15 minutes with 2% BSA (Roche Diagnostics, Mannheim Germany). Cells were stained in 1% BSA with 2ng/µl polyclonal antibody (pAb) vimentin goat IgG (Abcam, Uithoorn NL), 0.35 ng/µl mAb α-sma mouse IgG2a (DAKO, Glostrup Denmark), 2 ng/µl Goat IgG (Invitrogen, Camarillo CA) or 0.35 ng/µl Mouse IgG2a (BD, San Jose CA) for one hour at 4°C. After washing three times with PBS, cells were incubated with the second antibody, 1µg/ml Alexa Fluor®488 donkey anti-goat IgG (Invitrogen Molecular Probes, Eugene Oregon) or 1µg/ml Alexa Fluor®568 goat anti-mouse IgG2a (Invitrogen Molecular Probes) for one hour at 4°C. Cover glasses were washed three times and put on slides with vectashield containing DAPI to stain nuclei (Vectorlaboratories, Burlingame CA), stored overnight at 4°C and analyzed by fluorescence microscopy the next day.

HeLa cell culture
HeLa cells were cultured at 37°C under 5% CO2. Cells were grown in DMEM (PAA) with high glucose and stable L-glutamine, supplemented with 10% fetal calf serum and Penicillin/Streptomycin.

Dual Luciferase Reporter Gene Assays
Constructs. For the human putative target genes, fragments of approximately 750 bp of the 3'UTRs, containing the predicted miR-329 and miR-494 binding sites, weres amplified from human genomic DNA using primers with a short extension, containing cleavage sites for XhoI (5'-end) and NotI (3'-end). Amplicons were cleaved with XhoI and NotI and cloned in between the XhoI and NotI cleavage sites of the PsiCHECK™-2 vector (Promega) at the 3'-end of the coding region of the Renilla luciferase reporter gene. The cloned sequences were confirmed using direct sequencing. Sequences of the primers used are available in Supplemental Table S7.
Luciferase Assays. HeLa cells were grown to 85-90% confluence in white 96 well plates in their normal growth medium, at 37°C under 5% CO2. Cells were transfected, with 20 ng of the PsiCHECK2 vector with the human target-3'UTR cloned behind the coding sequence for Renilla Luciferase, during four hours in serum- and antibiotics-free Opti-MEM (Gibco) with Lipofectamine 2000 (Invitrogen). Cells were co-transfected with hsa-premiR-329, -494 or a negative control (Applied Biosystems) in concentrations of 10 or 20 nM. After transfection, the medium was replaced by culture medium and cells were incubated for 24 hours. Firefly and

Renilla luciferase were measured in cell lysates according to manufacturer's protocol using a Dual-Luciferase Reporter Assay System (Promega) on a FusionTM plate reader (PerkinElmer). Firefly luciferase activity was used as an internal control for cellular density and transfection efficiency.

Statistical Analysis

With the exception of the microArray data (Supplemental Figure S2; see section above MicroArray), results are expressed as mean ± SEM. All in vitro experiments were performed in triplicate and represent at least three independent experiments. Differences between groups were tested using student's t-tests.

References

1. Bhagat L, Putta MR, Wang D, Yu D, Lan T, Jiang W, Sun Z, Wang H, Tang JX, La MN, Kandimalla ER, Agrawal S. Novel oligonucleotides containing two 3'-ends complementary to target mRNA show optimal gene-silencing activity. J Med Chem 2011 April 28;54(8):3027-36.
2. Troyan SL, Kianzad V, Gibbs-Strauss SL, Gioux S, Matsui A, Oketokoun R, Ngo L, Khamene A, Azar F, Frangioni JV. The FLARE intraoperative near-infrared fluorescence imaging system: a first-in-human clinical trial in breast cancer sentinel ymph node mapping. Ann Surg Oncol 2009 October;16(10):2943-52.
3. Hellingman AA, Bastiaansen AJ, de Vries MR, Seghers L, Lijkwan MA, Lowik CW, Hamming JF, Quax PH. Variations in surgical procedures for hind limb ischaemia mouse models result in differences in collateral formation. Eur J Vasc Endovasc Surg 2010 December;40(6):796-803.
4. Baker M, Robinson SD, Lechertier T, Barber PR, Tavora B, D'Amico G, Jones DT, Vojnovic B, Hodivala-Dilke K. Use of the mouse aortic ring assay to study angiogenesis. Nat Protoc 2012 January;7(1):89-104.

Supplemental Figures and Tables

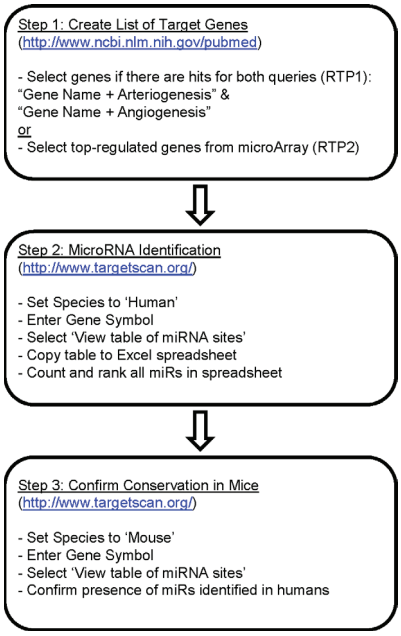

Supplemental Figure S1. Reverse Target Prediction. A schematic overview of miR-identification via Reverse Target Prediction, using public databases PubMed and TargetScan.

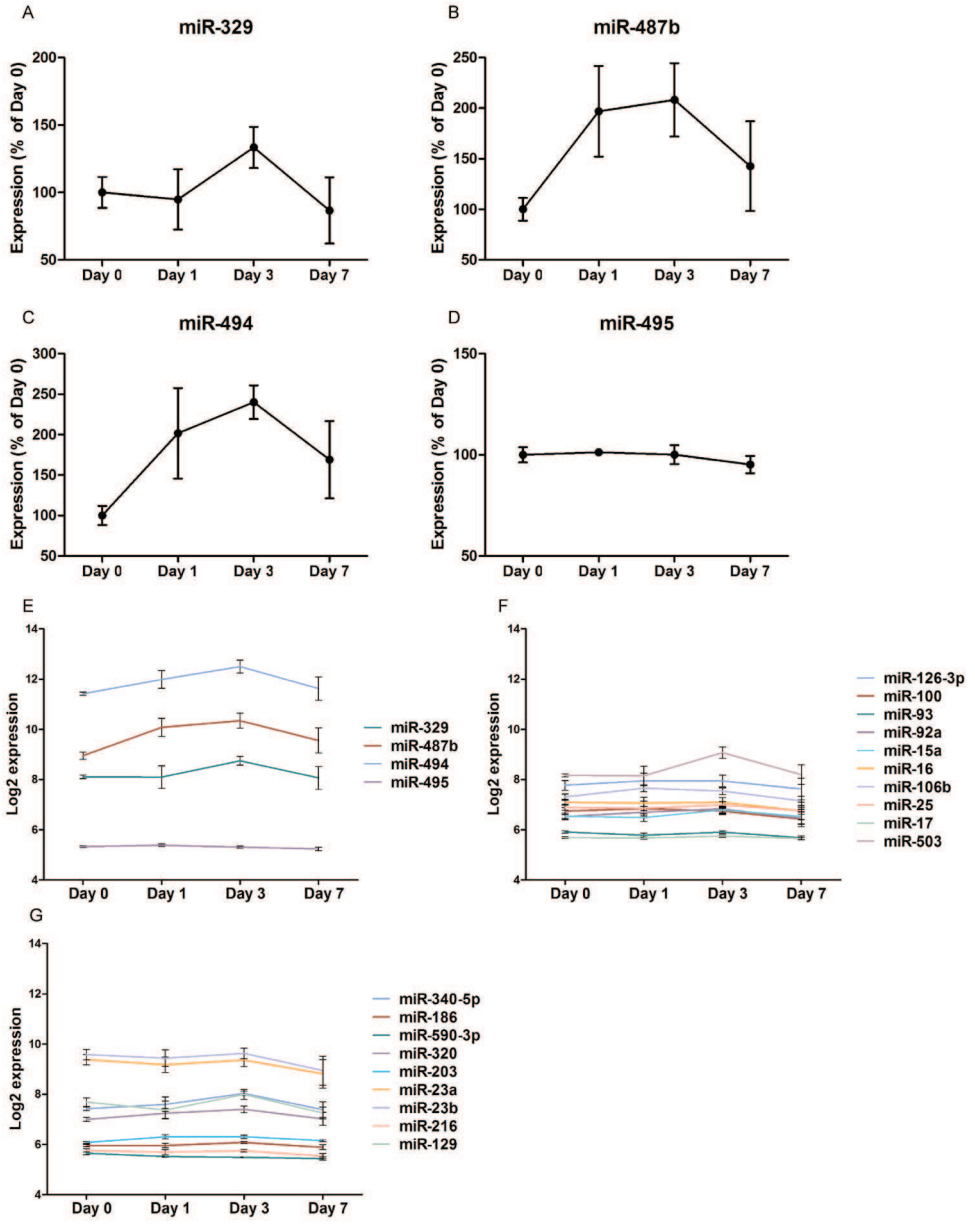

Supplemental Figure S2. MiR expression during effective neovascularization. MicroArray analyses of total RNA isolated from left adductor muscles of mice (4 mice per time point) before and at 1, 3 and 7 days after single ligation of the left femoral artery. Expression levels of late-responder miR-329 (A), early-responders miR-487b (B) and miR-494 (C) and non-responder miR-495 (D) are expressed as percentages of their individual expression levels before femoral artery ligation. (E) Log2 expression of 14q32 miRs miR-329, miR-487b, miR-494 and miR-495. (F) Log2 expression of ten miRs previously reported to influence neovascularization. (G) Log2 expression of the top nine non-14q32 miRs identified via RTP.

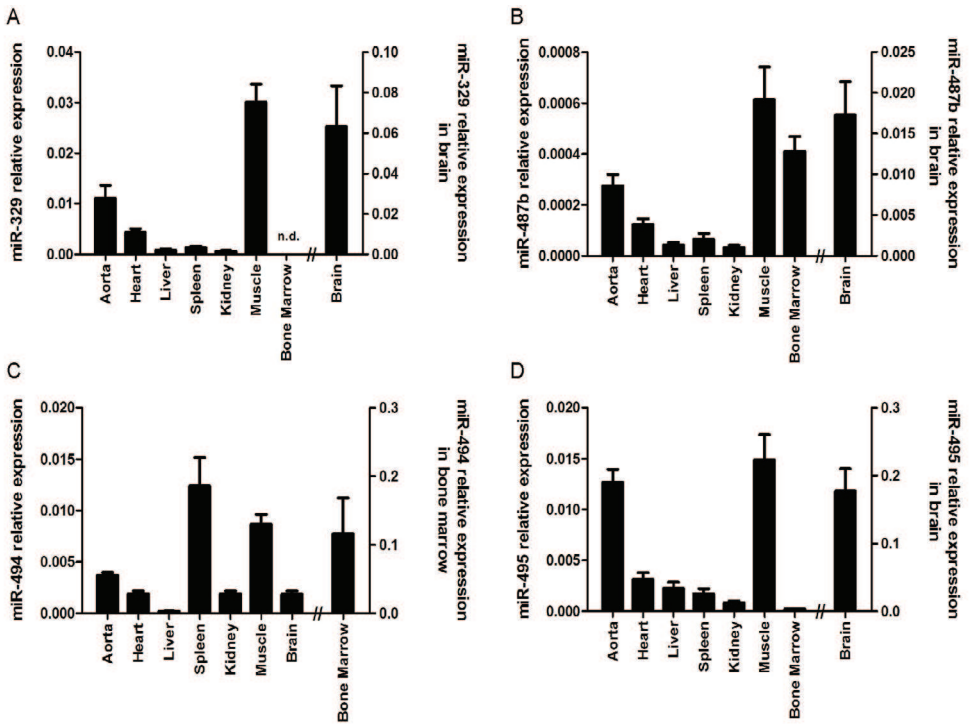

Supplemental Figure S3. Expression of 14q32/12F1 miRs. Expression levels of miR-329 (A), miR-487b (B), miR-494 (C) and miR-495 (D), relative to Let-7c in aorta, heart, spleen, kidney, skeletal muscle, bone marrow and brain and relative to Let-7c and miR-122 in the liver in healthy, male, adult C57Bl/6 mice. Tissues/organs from 9 mice were included and pooled per 3 animals. Data are presented as mean ± SEM.

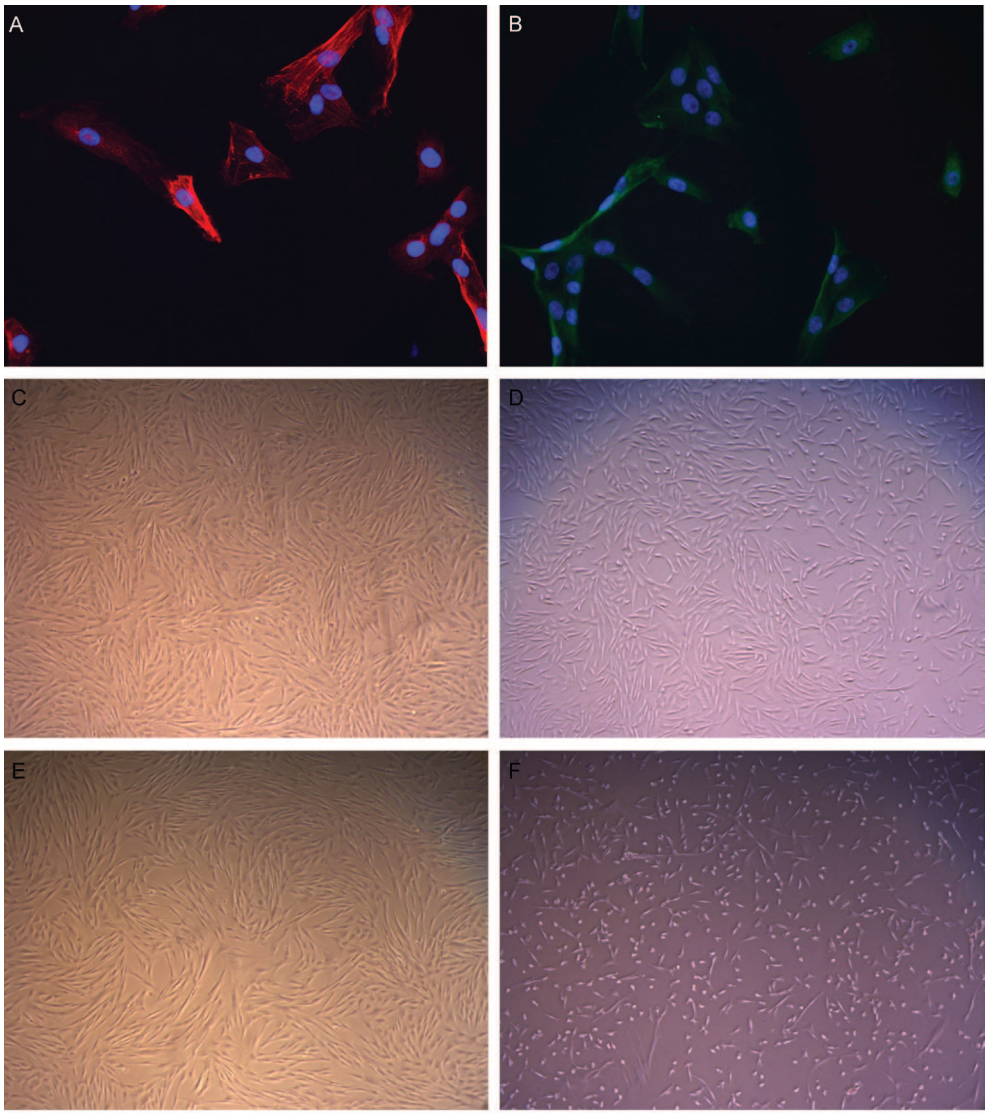

Supplemental Figure S4. Primary human arterial myofibroblasts. HUAFs stain positive for both the smooth muscle cell marker α-smooth muscle actin (A) and the mesenchymal marker Vimentin (B). HUAFS treated with GSOs at a concentration of 10ng/µl (C) and 15ng/µl (D). Cells have a typical phenotype (spindle shape) at 10ng/µl, whereas at 15ng/µl, some signs of cytotoxicity are observed (small round cells). HUAFs treated with antagomiRs at a concentration of 10ng/µl (E) and 15ng/µl (F). Cells have a typical phenotype (spindle shape) at 10ng/µl, whereas at 15ng/µl, clear signs of cytotoxicity are observed (small round cells).

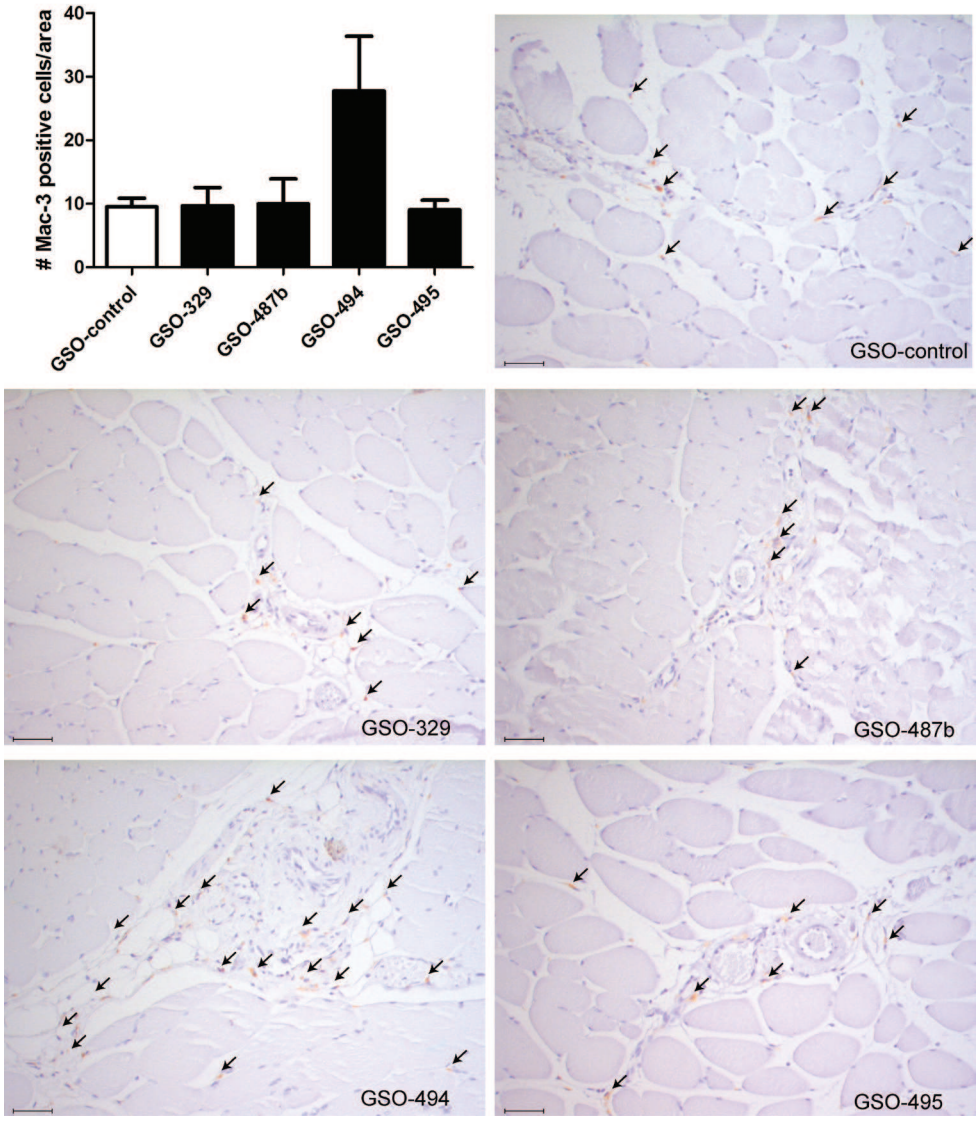

Supplemental Figure S5. Macrophage accumulation around remodelling collateral arterioles. Quantification of the number of Mac3-positive cells (arrows) around remodelling collateral arterioles in the adductor muscle of GSO-treated mice, 7 days after induction of HLI. From each muscle, 3 sections were used and from each section, 1 representative photograph was included. Data are presented as mean ± SEM. The scale bar represents 100 µm.

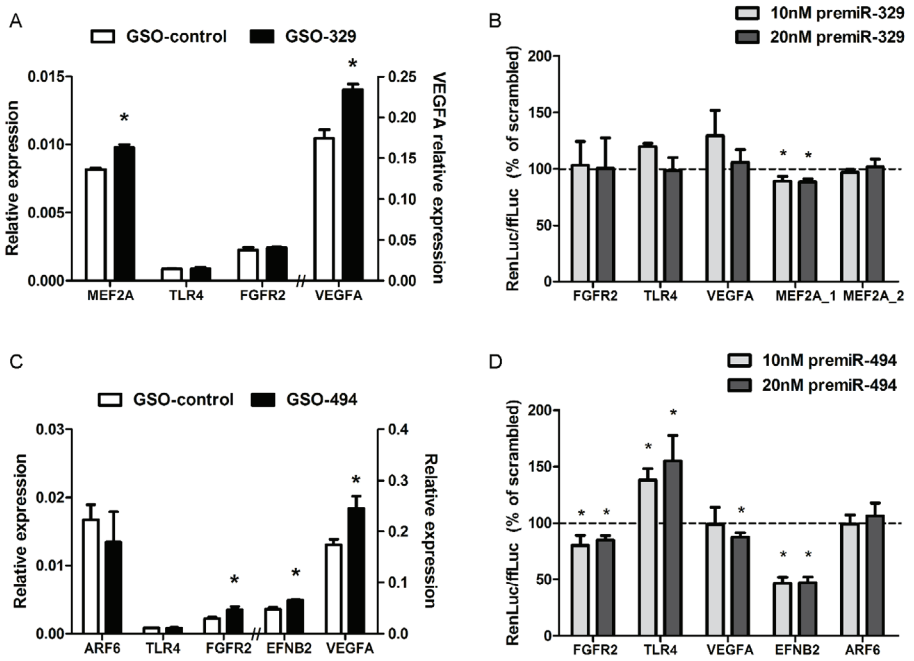

Supplemental Figure S6. Regulation of human target genes for hsa-miR-329 and hsa-miR-494. Expression levels of putative human target genes, relative to GAPDH, in HUAFs after treatment with 10ng/µl GSO-329 (A) or GSO-494 (C).
Luciferase expression in HeLa cells co-transfected with 20 ng human target gene 3'-UTR, cloned into the PsiCHECK2 vector, and 10 or 20 nM of hsa-pre-miR-329 (B) or pre-miR-494 (D). The Renilla Luciferase signal (renLuc) was normalized by dividing it over the Firefly Luciferase signal (ffLuc), to adjust for transfection efficiency. The renLuc/ffLuc ratio measured for the negative controls (20nM pre-miR-Scrambled) was set at 100% (dashed line). *p < 0.05

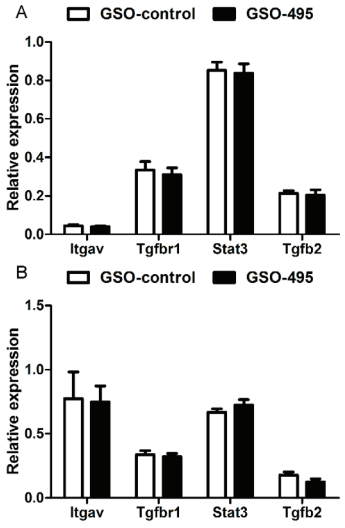

Supplemental Figure S7. In vivo regulation of putative target genes of miR-495. Expression levels of putative target genes for miR-495 relative to HPRT1 in adductor muscle tissue of mice treated with GSO-495 at days 3 (A) and 7 (B) after HLI. Per group, adductor muscle tissue of 3 mice was used. Data are presented as mean ± SEM.

Supplemental Table S1A. Reverse Target Prediction 1; Target genes selected from literature.

Process	Target Gene	PubMed Hits (N) on Search Term "gene name/protein name/alias + arteriogenesis"	PubMed Hits (N) on Search Term "gene name/protein name/alias + angiogenesis"
Endothelial Activation	NOS3	30	649
	NOS2	8	288
	EDN1	2	373
	VEGFA	16	3130
	BMP4	0	46
	KLF2	1	20
Smooth Muscle Cell Proliferation	PTK2	2	282
	ITGA5	2	7
	ITGAV	1	13
	ITGB1	1	6
	ITGB2	1	6
	ITGB3	3	2
	ITGAM	2	7
	ITGAL	0	3
	GJA4	3	24
	GJA5	5	15
	GJA1	5	37
	GJC1	0	2
Adhesion Molecules	ICAM1	7	274
	VECAM1	10	9
	PECAM1	20	1193
	CCL2	45	439
	CDH5	5	366
	SELE	2	190
	SELP	2	96
	CCR2	6	54
Extracellular Matrix	MMP2	3	207
	MMP9	1	183
	SERPINE1	3	399
	PLAT	0	48
	PLAU	3	552
	PLG	8	1598
	TIMP1	2	43
	TIMP2	0	38
	VTN	0	485
	FN1	6	931
	FBN1	0	14
	PRTN3	0	3
	CTSK	0	6
	CTSL1	0	38
	CTSL2	0	1
	CTSS	0	18
Cytokines	IL5	4	29
	IL6	3	980
	IL8	3	1181
	IL17	2	111
	IL18	2	72
	IL20	1	9
	IL27	1	16
	IL33	1	8
	TNFA	10	2143
	INFA1	1	626
	INFB1	2	168
	INFG	4	455
	CHGA	1	2
	CCL4	0	34
	LEP	3	278

Supplemental Table S1A (continued). Reverse Target Prediction 1; Target genes selected from literature.

Process	Target Gene	PubMed Hits (N) on Search Term "gene name/protein name/alias + arteriogenesis"	PubMed Hits (N) on Search Term "gene name/protein name/alias + angiogenesis"
Immune Receptors	TLR1	3	68
	TLR2	2	21
	TLR4	3	36
	TLR6	2	1
	IL6R	1	137
	CXCR1	1	56
	CXCR2	2	131
	IL18R1	1	7
	IL20RA	1	3
	IL20RB	1	1
	IL27RA	0	4
	IL1RL1	0	2
Natural Killer Complex	KLRG1	2	0
	A2M		
	CD69		
	CLEC1B		
	CLEC7A		
	KLRD1		
	NKG2D		
	NKG2C		
	NKG2A		
	LY49L		
Growth Factors	PDGFA	0	9
	PDGFB	19	314
	FGF1	6	257
	FGF2	61	2918
	FGF4	4	44
	FGF5	1	12
	FGF6	1	5
	FGF11	2	131
	TGFB1	12	740
	TGFB2	1	93
	EFNB2	8	114
	ANGPT2	5	808
Growth Factor Receptors	FLT1	20	1555
	FGFR1	2	214
	FGFR2	0	90
	FGFR3	0	32
	FGFR4	0	17
	PDGFRA	3	196
	PDGFRB	5	323
	PPHB4	3	103
	TIE2	6	772
	TGFBR1	6	7
	TGFBR2	4	11
	TGFBR3	3	14
Signaling Molecules	MAPK1	11	944
	MAPK3	7	444
	MAPK7	0	1
	MAPK8	3	38
	MAPK9	0	4
	MAPK10	0	1
	MAPK14	0	11
	PTPN6	0	32
	PTPN11	0	20
	ABRA	3	0
	TMSB4X	5	89
	DLL1	5	53

Supplemental Table S1A (continued). Reverse Target Prediction 1; Target genes selected from literature.

Process	Target Gene	PubMed Hits (N) on Search Term "gene name/protein name/alias + arteriogenesis"	PubMed Hits (N) on Search Term "gene name/protein name/alias + angiogenesis"
Transcription Factors	JUN	4	244
	FOS	1	143
	MYC	2	356
	EGR1	6	102
	NFKB1	4	535
	NFKB2	2	467
	KAT2B	1	2
	NR4A1	0	7
	HDAC5	0	7
	ANKRD1	3	6
Inhibitors	CD180	1	1
	CDKN1A	1	1

Supplemental Table S1B. Reverse Target Prediction 1; Conserved MiRs Identified

MiR	Number of Putative Target Genes	% of Genes Included
miR-495/1192	**44**	**34,6**
miR-590/590-3p	42	33,1
miR-23ab	36	28,3
miR-340/340-5p	34	26,8
miR-186	33	26,0
miR-185/882	**33**	**26,0**
miR-203	33	26,0
miR-128	32	25,2
miR-216/216b	32	25,2
miR-494	**31**	**24,4**
miR-485/485-5p	**31**	**24,4**
miR-299/299-3p	**30**	**23,6**
miR-214/761	30	23,6
miR-129/129-5p	30	23,6
miR-300	**29**	**22,8**
miR-544	**29**	**22,8**
miR-17-5p/20/93.mr/106/519.d	29	22,8
miR-873	28	22,0
miR-143	28	22,0
miR-543	**27**	**21,3**
miR-149	27	21,3
miR-491/491-5p	27	21,3
miR-124/506	27	21,3
miR-150	27	21,3
miR-19	27	21,3
miR-125a-3p	26	20,5
miR-320/320abcd	26	20,5
miR-15/16/195/424/497	26	20,5
miR-130/301	26	20,5
miR-24	26	20,5
miR-27ab	26	20,5
miR-141/200a	26	20,5
miR-204/211	26	20,5
miR-370	**25**	**19,7**
miR-290-5p/292-5p/371-5p	25	19,7
miR-374/374ab	25	19,7
miR-125/351	25	19,7
miR-144	25	19,7
miR-539	**24**	**18,9**
miR-328	24	18,9
miR-34a/34b-5p/34c/34c-5p/449/449abc/699	24	18,9
miR-205	24	18,9
miR-197	23	18,1
miR-421	23	18,1
miR-7/7ab	23	18,1
miR-326/330/330-5p	22	17,3
miR-101	22	17,3
miR-135	22	17,3
miR-9	22	17,3
miR-377	**21**	**16,5**
miR-342/342-3p	21	16,5

Supplemental Table S1B (continued). Reverse Target Prediction 1; Conserved MiRs Identified

MiR	Number of Putative Target Genes	% of Genes Included
miR-592/599	21	16,5
miR-33/33ab	21	16,5
miR-103/107	21	16,5
miR-25/32/92/92ab/363/367	21	16,5
miR-145	21	16,5
miR-138	21	16,5
miR-153	21	16,5
miR-22	21	16,5
miR-338/338-3p	21	16,5
miR-181	21	16,5
miR-136	**20**	**15,7**
miR-410	**20**	**15,7**
miR-329/362-3p	**20**	**15,7**
miR-335/335-5p	20	15,7
miR-542/542-3p	20	15,7
miR-200bc/429	20	15,7
miR-139-5p	20	15,7
miR-183	20	15,7
miR-217	20	15,7
miR-122	20	15,7
miR-431	**19**	**15,0**
miR-448	19	15,0
miR-384/384-3p	19	15,0
miR-106/302	19	15,0
miR-433	**18**	**14,2**
miR-874	**18**	**14,2**
miR-224	18	14,2
miR-378/422a	18	14,2
miR-876-5p	18	14,2
miR-31	18	14,2
miR-499/499-5p	18	14,2
miR-29abc	18	14,2
miR-1/206	18	14,2
miR-148/152	18	14,2
miR-30a/30a-5p/30b/30b-5p/30cde/384-5p	18	14,2
miR-134	**17**	**13,4**
miR-376c	**17**	**13,4**
miR-488	17	13,4
miR-339-5p	17	13,4
miR-361/361-5p	17	13,4
miR-221/222	17	13,4
miR-146	17	13,4
miR-411	**16**	**12,6**
miR-199/199-5p	16	12,6
miR-let7/98	16	12,6
miR-194	16	12,6
miR-223	16	12,6
miR-376/376ab/376b-3p	**15**	**11,8**
miR-653	15	11,8
miR-202/202-3p	15	11,8
miR-296/296-3p	15	11,8
miR-132/212	15	11,8

Supplemental Table S1B (continued). Reverse Target Prediction 1; Conserved MiRs Identified

MiR	Number of Putative Target Genes	% of Genes Included
miR-137	15	11,8
miR-133	15	11,8
miR-96/1271	15	11,8
miR-490/490-3p	15	11,8
miR-486/486-5p	14	11,0
miR-505.hm	14	11,0
miR-26ab/1297	14	11,0
miR-455/455-5p	14	11,0
miR-365	14	11,0
miR-425/489	14	11,0
miR-10	14	11,0
miR-218	14	11,0
miR-208/208ab	14	11,0
miR-182	14	11,0
miR-382	**13**	**10,2**
miR-324-5p	13	10,2
miR-140/140-5p/876-3p	13	10,2
miR-196ab	13	10,2
miR-379	**12**	**9,4**
miR-758	**12**	**9,4**
miR-155	12	9,4
miR-383	12	9,4
miR-496	**11**	**8,7**
miR-346	11	8,7
miR-504	11	8,7
miR-503	11	8,7
miR-193ab	11	8,7
miR-28/28-5p/708	10	7,9
miR-192/215	10	7,9
miR-21/590-5p	10	7,9
miR-154	**9**	**7,1**
miR-375	9	7,1
miR-142-3p	7	5,5
miR-219/219-5p	7	5,5
miR-18ab	7	5,5
miR-190	6	4,7
miR-187	6	4,7
miR-875-5p	5	3,9
miR-127	**2**	**1,6**
miR-615-3p	2	1,6
miR-191	2	1,6
miR-451	2	1,6
miR-184	2	1,6
miR-99ab/100	2	1,6
miR-551ab	1	0,8
miR-210	1	0,8

14q32 miRs are indicated in bold type

Supplemental Table S1C. Reverse Target Prediction 1; Unconserved miRs Identified*

MiR	Number of Putative Target Genes	% of Genes Included
miR-548c-3p	47	37,0
miR-607	34	26,8
miR-548d-3p	29	22,8
miR-520d-5p/524-5p	24	18,9
miR-664.hr	24	18,9
miR-579	23	18,1
miR-548a-3p/548ef	23	18,1
miR-513a-3p	23	18,1
miR-1305	22	17,3
miR-576-5p	22	17,3
miR-655	22	17,3
miR-520gh	22	17,3
miR-105.h	22	17,3
miR-656	21	16,5
miR-338-5p	21	16,5
miR-486-3p	21	16,5
miR-561	21	16,5
miR-548a-5p/548b-5p/548c-5p/548d-5p/548hij/559	20	15,7
miR-330-3p	20	15,7
miR-142-5p	20	15,7
miR-548n	20	15,7

*: Unconserved miRs predicted to target more than 15% of the included target genes only

Supplemental Table S2A. Reverse Target Prediction 2; Target genes selected from microArray data.

Target Gene	
CCL19	ARPC5
CCL21	IGFBP4
CCR7	MSN
FCER1G	LCN2
MEF2A	DNAJB1
MEF2B	DBP
MEF2C	LRG1
MEF2D	CHI3L3
USP18	HSPA1B
IRF9	S100A8
IRF1	HSPA1A
IFIT2	C1QB
PML	RRAD
CCL5	S100A9
VCAN	RNF213
MMP3	MT2
SELL	SOCS3
CD44	PRG4
LGALS3	OASL2
CXCL13	SLPI
CXCL10	PHF11
PLCG2	MPEG1
VAV1	CFB
ARF6	KBTBD5
TGFBR2	FPR2
STAT3	SAP30
RORC	CEBPB
LBP	GADD45A
MYD88	BST2
FCGR3A	SLC6A9
ARPC1A	C1QC
ARPC1B	CXCL1
ARPC2	TUBA6
ARPC3	HSP105
ARPC4	IL1B

Supplemental Table S2B. Reverse Target Prediction 2; All MiRs Identified.

MiR	Number of Putative Target Genes	% of Genes Included
miR-340/340-5p	17	18,9
miR-186	13	14,4
miR-590/590-3p	12	13,3
miR-485/485-5p	**11**	**12,2**
miR-320/320abcd	11	12,2
miR-329/362-3p	**10**	**11,1**
miR-204/211	10	11,1
miR-106/302	10	11,1
miR-124/506	10	11,1
miR-326/330/330-5p	10	11,1
miR-491/491-5p	10	11,1
miR-544	**9**	**10,0**
miR-218	9	10,0
miR-34a/34b-5p/34c/34c-5p/449/449abc/699	9	10,0
miR-144	9	10,0
miR-203	9	10,0
miR-27ab	9	10,0
miR-217	9	10,0
miR-410	**8**	**8,9**
miR-539	**8**	**8,9**
miR-494	**8**	**8,9**
miR-7/7ab	8	8,9
miR-338/338-3p	8	8,9
miR-182	8	8,9
miR-129/129-5p	8	8,9
miR-23ab	8	8,9
miR-24	8	8,9
miR-17-5p/20/93.mr/106/519.d	8	8,9
miR-133	8	8,9
miR-150	8	8,9
miR-181	8	8,9
miR-197	8	8,9
miR-377	**7**	**7,8**
miR-370	**7**	**7,8**
miR-495/1192	**7**	**7,8**
miR-185/882	**7**	**7,8**
miR-136	**7**	**7,8**
miR-30a/30a-5p/30b/30b-5p/30cde/384-5p	7	7,8
miR-138	7	7,8
miR-125/351	7	7,8
miR-31	7	7,8
miR-425/489	7	7,8
miR-143	7	7,8
miR-135	7	7,8
miR-383	7	7,8
miR-216/216a	7	7,8
miR-365	7	7,8
miR-122	7	7,8
miR-26ab/1297	7	7,8

Supplemental Table S2B (continued). Reverse Target Prediction 2; All MiRs Identified.

MiR	Number of Putative Target Genes	% of Genes Included
miR-378/422a	7	7,8
miR-335/335-5p	7	7,8
miR-542/542-3p	7	7,8
miR-384/384-3p	7	7,8
miR-873	7	7,8
miR-290-5p/292-5p/371-5p	7	7,8
miR-149	7	7,8
miR-300	**6**	**6,7**
miR-758	**6**	**6,7**
miR-433	**6**	**6,7**
miR-21/590-5p	6	6,7
miR-199/199-5p	6	6,7
miR-214/761	6	6,7
miR-101	6	6,7
miR-216/216b	6	6,7
miR-33/33ab	6	6,7
miR-103/107	6	6,7
miR-140/140-5p/876-3p	6	6,7
miR-200bc/429	6	6,7
miR-130/301	6	6,7
miR-9	6	6,7
miR-10	6	6,7
miR-1/206	6	6,7
miR-28/28-5p/708	6	6,7
miR-339-5p	6	6,7
miR-421	6	6,7
miR-488	6	6,7
miR-592/599	6	6,7
miR-376c	**5**	**5,6**
miR-543	**5**	**5,6**
let-7/98	5	5,6
miR-96/1271	5	5,6
miR-155	5	5,6
miR-19	5	5,6
miR-190	5	5,6
miR-219/219-5p	5	5,6
miR-132/212	5	5,6
miR-503	5	5,6
miR-375	5	5,6
miR-202/202-3p	5	5,6
miR-361/361-5p	5	5,6
miR-125a-3p	5	5,6
miR-431	**4**	**4,4**
miR-411	**4**	**4,4**
miR-379	**4**	**4,4**
miR-134	**4**	**4,4**
miR-205	4	4,4
miR-22	4	4,4
miR-139-5p	4	4,4
miR-194	4	4,4
miR-183	4	4,4

Supplemental Table S2B (continued). Reverse Target Prediction 2; All MiRs Identified.

MiR	Number of Putative Target Genes	% of Genes Included
miR-18ab	4	4,4
miR-29abc	4	4,4
miR-153	4	4,4
miR-455/455-5p	4	4,4
miR-25/32/92/92ab/363/367	4	4,4
miR-221/222	4	4,4
miR-193ab	4	4,4
miR-141/200a	4	4,4
miR-196ab	4	4,4
miR-192/215	4	4,4
miR-146	4	4,4
miR-342/342-3p	4	4,4
miR-328	4	4,4
miR-346	4	4,4
miR-448	4	4,4
miR-224	4	4,4
miR-376/376ab/376b-3p	**3**	**3,3**
miR-154	**3**	**3,3**
miR-299/299-3p	**2**	**2,2**
miR-137	3	3,3
miR-223	3	3,3
miR-128	3	3,3
miR-145	3	3,3
miR-499/499-5p	3	3,3
miR-504	3	3,3
miR-876-5p	3	3,3
miR-374/374ab	3	3,3
miR-296/296-3p	3	3,3
miR-15/16/195/424/497	3	3,3
miR-874	3	3,3
miR-486/486-5p	3	3,3
miR-496	**2**	**2,2**
miR-382	**2**	**2,2**
miR-148/152	2	2,2
miR-208/208ab	2	2,2
miR-505.hm	2	2,2
miR-324-5p	2	2,2
miR-653	2	2,2
miR-875-5p	2	2,2
miR-551ab	1	1,1
miR-451	1	1,1
miR-210	1	1,1
miR-490/490-3p	1	1,1
miR-191	1	1,1
miR-99ab/100	1	1,1
miR-187	1	1,1

14q32 miRs are indicated in bold type

Supplemental Table S3. 14q32 miRs in RTPs 1 and 2.

14q32 MicroRNA	Putative targets in RTP1 (out of 127)	Putative targets in RTP2 (out of 70)
495	**44**	**7**
494	**31**	**8**
485	31	11
299	30	2
300	29	6
544	29	9
543	27	5
370	25	7
539	24	8
377	21	7
136	20	7
410	20	8
329	**20**	**10**
431	19	4
433	18	6
874	18	3
134	17	4
376c	17	5
411	16	4
376a	15	3
376b	15	3
382	13	2
379	12	4
758	12	6
496	11	2
154	9	3
127	2	0

Supplemental Table S4. Conservation of binding sites for miR-329, miR-494 and miR-495 between mice and men.

MiR-329			MiR-494			MiR-495		
Target Gene	Sites in Humans	Sites in Mice	Target Gene	Sites in Humans	Sites in Mice	Target Gene	Sites in Humans	Sites in Mice
MEF2D	4	1	**ARF6**	3	2	**TGFBR1**	3	2
CXCR2	2	1	TLR6	2	0	**STAT3**	3	1
TLR4	2	2	**EFNB2**	2	1	FAK	2	1
MEF2A	2	2	MYC	2	0	**ITGAV**	2	3
ITGB3	2	3	ARPC5	2	1	ITGB3	2	1
FOS	1	0	MEF2D	2	1	CX43	2	1
PTPN11	1	2	RNF213	2	0	CX45	2	1
MAPK1	1	1	EDN1	1	0	ICAM1	2	0
PDGFRA	1	0	**VEGFA**	1	0	CTSS	2	0
TGFBR1	1	0	ITGB1	1	0	TLR4	2	0
FGF4	1	0	ITGAL	1	0	IL8RB	2	1
PDGFB	1	0	VCAM1	1	0	IL1RL1	2	0
FGF5	1	0	PECAM1	1	0	KLRD1	2	0
KLRG1	1	0	SELP	1	2	PDGFA	2	1
CLEC7A	1	2	CCR2	1	1	FGF5	2	0
LEP	1	0	SERPIN1	1	0	PTPN11	2	0
PLAU	1	1	CTSS	1	0	JUN	2	1
PLAT	1	0	IL6	1	0	HDAC4	2	0
CTSS	1	0	IL33	1	1	MEF2C	2	3
ITGAM	1	1	TNFA	1	0	EDN1	1	0
CX45	1	1	**TLR4**	1	1	VEGFA	1	1
VEGFA	1	1	IL18R1	1	0	VCAM1	1	0
CCL19	1	0	CLEC7A	1	0	CCL2	1	1
IGFBP4	1	0	KLRD1	1	0	CDH5	1	0
IRF1	1	0	PDGFA	1	0	SERPINE1	1	1
MEF2B	1	0	FGF2	1	1	PLAT	1	1
MEF2C	1	2	FGF5	1	0	PLG	1	1
MYD88	1	0	**FGFR2**	1	3	TIMP2	1	1
PLCG2	1	0	PDGFRA	1	0	IL5	1	0
CEBPB	1	0	PPHB4	1	0	IL33	1	0
DNAJB1	0	1	MAPK1	1	2	INFG	1	0
SOCS3	0	0	MAPK9	1	0	LEP	1	0
EFNB2	1	2	MAPK14	1	0	IL6R	1	0
FGFR2	0	1	PTPN11	1	0	IL20RB	1	0
			JUN	1	0	KLRG1	1	0
			KAT2B	1	0	CD69	1	0
			ARPC1B	1	1	CLEC7A	1	0
			CD44	1	1	FGF2	1	2
			STAT3	1	1	**TGFB2**	1	3
			DNAJB1	1	1	VEGFR	1	0
			MPEG1	0	1	FGFR3	1	2
			SLC6A9	0	1	MAPK10	1	1
						DLL1	1	1
						KAT2B	1	1
						HDAC5	1	0
						ARF6	1	0
						ARPC1A	1	1
						CD44	1	1
						IFIT2	1	0
						MPEG1	1	0
						SOCS3	1	0
						RRAD	0	1

Supplemental Table S5A. Sequences of miRs, antagomiRs and GSOs.

MiR	Sequence
hsa/mmu-miR-487b	5'-AAUCGUACAGGGUCAUCCACUU-3'
hsa/mmu-miR-494	5'-UGAAACAUACACGGGAAACCUC-3'
hsa/mmu-miR-495	5'-AAACAAACAUGGUGCACUUCUU-3'
mmu-miR-329	5'-AACACACCCAGCUAACCUUUUU-3'
hsa -miR-329	5'-AACACACCUGGUUAACCUCUUU-3'
GSO	**Sequence**
hsa/mmu-GSO-487b	3'-TTAGCATGTCCCAGTAGGTGAA-X-AAGTGGATGACCCTGTACGATT-3'
hsa/mmu-GSO-494	3'-ACTTTGTATGTGCCCTTTGGAG-X-GAGGTTTCCCGTGTATGTTTCA-3'
hsa/mmu-GSO-495	3'-TTTGTTTGTACCACGTGAAGAA-X-AAGAAGTGCACCATGTTTGTTT-3'
mmu-GSO-329	3'-TTGTGTGGGTCGATTGGAAAAA-X-AAAAAGGTTAGCTGGGTGTGTT-3'
hsa-GSO-329	3'-TTGTGTGGACCAATTGGAGAAA-X-AAAGAGGTTAACCAGGTGTGTT-3'
negative control GSO	3'-TGTACGACTCCATAACGGT-X-TGGCAATACCTCAGCATGT-3'
AntagomiR	**Sequence**
hsa/mmu-antagomiR-487b	5'-AsAsGUGGAUGACCCUGUACGsAsUsUs-Chol-3'
hsa/mmu-antagomiR-494	5'-GsAsGGUUUCCCGUGUAUGUUsUsCsAs-Chol-3'
hsa/mmu-antagomiR-495	5'-AsAsGAAGUGCACCAUGUUUGsUsUsUs-Chol-3'
mmu-antagomiR-329	5'-AsAsAAAGGUUAGCUGGGUGUsGsUsUs-Chol-3'
hsa-antagomiR-329	5'-AsAsAGAGGUUAACCAGGUGUsGsUsUs-Chol-3'
negative control antagomiR	5'-AsUsGACUAUCGCUAUUCGCsAsUsGs-Chol-3'

'X': Phosphorothioate linker
'-NNN-': 2'-O-methyl-modified nucleotides
's': Phosphorothioate linkage
'Chol': cholesterol group linked through a hydroxyprolinol-linkage

Supplemental Table S5B. Conservation of (Seed-)Sequences of miR-329

Species	MiR	Sequence
Human	hsa-miR-329-1-3p	A**ACACACC**UGGUUAACCUCUUU
	hsa-miR-329-2-3p	A**ACACACC**UGGUUAACCUCUUU
Mouse	mmu-miR-329	A**ACACACC***CA*G*C*UAACCU*U*UUU
Rat	rno-miR-329	A**ACACACC***CA*G*C*UAACCU*U*UUU
Chimpanzee	ptr-miR-329-1	A**ACACACC**UGGUUAACCUCUUU
	ptr-miR-329-2	A**ACACACC**UGGUUAACCUCUUU
Orangutan	ppy-miR-329-1	A**ACACACC**UGGUUAACCUCUUU
	ppy-miR-329-2	A**ACACACC**UGGUUAACCUCUUU
Gorilla	ggo-miR-329b	A**ACACACC**UGGUUAACCUCU- -
Rhesus Monkey	mml-miR-329-1-3p	A**ACACACC**UGGUUAACCUCUUU
	mml-miR-329-2-3p	A**ACACACC**UGGUUAACCUCUUU
Dog	cfa-miR-329a	*AGAGGUUUUCUGGGUUUCUGUUU**
	cfa-miR-329b	A**ACACACC**UGGUUAACCUCUUU
Cow	bta-miR-329a	A**ACACACC**UGGUUAACCU*U*UUU
	bta-miR-329b	*AGAGGUUUUCUGGGUUUCUGUUU**
Sheep	oar-miR-329a-3p	A**ACACACC**UGGUUAACCU*U*UUU
	oar-miR-329b-3p	A**ACACACC**UGGUUAACCUCUUU

Supplemental Table S5C. Conservation of (Seed-)Sequences of miR-487b

Species	MiR	Sequence
Human	hsa-miR-487b-3p	A**AUCGUAC**AGGGUCAUCCACUU
Mouse	mmu-miR-487b-3p	A**AUCGUAC**AGGGUCAUCCACUU
Rat	rno-miR-487b	A**AUCGUAC**AGGGUCAUCCACUU
Chimpanzee	ptr-miR-487b	A**AUCGUAC**AGGGUCAUCCACUU
Gorilla	ggo-miR-487b	A**AUCGUAC**AGGGUCAUCCACU-
Orangutan	ppy-miR-487b	A**AUCGUAC**AGGGUCAUCCACUU
Rhesus Monkey	mml-miR-487b-3p	A**AUCGUAC**AGGGUCAUCCACUU
Dog	cfa-miR-487b	A**AUCGUAC**AGGGUCAUCCACUU
Cow	bta-miR-487b	A**AUCGUAC**AGGGUCAUCCACUU
Sheep	oar-miR-487b-3p	A**AUCGUAC**AGGGUCAUCCACUU
Horse	eca-miR-487b	A**AUCGUAC**AGGGUCAUCCACUU
Pig	ssc-miR-487b	*GUGGUUAUCCCUGUCCUGUUCG**

Supplemental Table S5D. Conservation of (Seed-)Sequences of miR-494

Species	MiR	Sequence
Human	hsa-miR-494-3p	U**GAAACAU**ACACGGGAAACCUC
Mouse	mmu-miR-494-3p	U**GAAACAU**ACACGGGAAACCUC
Rat	rno-miR-494	U**GAAACAU**ACACGGGAAACCUC*U*
Chimpanzee	ptr-miR-494	U**GAAACAU**ACACGGGAAACCUC
Gorilla	ggo-miR-494	U**GAAACAU**ACACGGGAAACCUC
Orangutan	ppy-miR-494	U**GAAACAU**ACACGGGAAACCUC
Rhesus Monkey	mml-miR-494-3p	U**GAAACAU**ACACGGGAAACCUC
Dog	cfa-miR-494	U**GAAACAU**ACACGGGAAACCUC
Cow	bta-miR-494	U**GAAACAU**ACACGGGAAACCUC
Sheep	oar-miR-494-3p	U**GAAACAU**ACACGGGAAACCUC*U*
Horse	eca-miR-494	U**GAAACAU**ACACGGGAAACCUC
Pig	ssc-miR-494	*AGGUUGUCGUGUUGUCUUCUCU**

Supplemental Table S5E. Conservation of (Seed-)Sequences of miR-495

Species	MiR	Sequence
Human	hsa-miR-495-3p	A**AACAAAC**AUGGUGCACUUCUU
Mouse	mmu-miR-495-3p	A**AACAAAC**AUGGUGCACUUCUU
Rat	rno-miR-495	A**AACAAAC**AUGGUGCACUUCUU
Chimpanzee	ptr-miR-495	A**AACAAAC**AUGGUGCACUUCUU
Gorilla	ggo-miR-495	A**AACAAAC**AUGGUGCACUUCU-
Orangutan	ppy-miR-495	A**AACAAAC**AUGGUGCACUUCUU
Rhesus Monkey	mml-miR-495	A**AACAAAC**AUGGUGCACUUCUU
Dog	cfa-miR-495	A**AACAAAC**AUGGUGCACUUCUU
Cow	bta-miR-495	A**AACAAAC**AUGGUGCACUUCUU
Sheep	oar-miR-495-3p	A**AACAAAC**AUGGUGCACUUCUU
Horse	eca-miR-495	A**AACAAAC**AUGGUGCACUUCUU

Sequences and nomenclature according to miRbase 20 (www.mirbase.org)
'NNN': Seed Sequence
'NNN': Conserved with human
'NNN': Different from human
'*': Sequence corresponds to '*' or '-5p' sequences in other species

Chapter 3-II

Letter Regarding Article “MicroRNA-155 exerts cell specific antiangiogenic but proarteriogenic effects during adaptive neovascularization”

Circulation. 2015 Dec 8;132(23):e375

SMJ Welten[1,2]

PHA Quax[1,2]

AY Nossent[1,2]

[1]Department of Surgery, Leiden University Medical Center, Leiden, the Netherlands

[2]Einthoven Laboratory for Experimental Vascular Medicine,

Leiden University Medical Center, Leiden, the Netherlands

To the Editor:

We read with interest the article by Pankratz and colleagues[1] in *Circulation* in which the authors identified miR-155 as a dual player in postischemic neovascularization following hindlimb ischemia in mice. Although this study elegantly describes an antiangiogenic but proarteriogenic role for miR-155 in postischemic neovascularization, it remains unclear on several other aspects.[1]

Using microRNA expression profiling, miR-155 was identified as one of the strongest downregulated miRs at 7 days after induction of hindlimb ischemia.1 However, in a previous study from 2010 by the same research group, Grundmann et al already used microarrays to explore microRNA expression patterns during adaptive neovascularization in the same mouse model.[2] MicroRNA analyses in both studies were performed on RNA isolated from the distal adductor muscle at overlapping time points after ischemia.[1,2] Whereas Grundmann et al focused on the expression of microRNAs at 3 days after ischemia, Pankratz et al mainly looked at differentially regulated microRNAs at 7 days after ischemia.[1,2] Interestingly, in the paper by Grundmann et al, miR-155 was not identified as one of the top 15 downregulated microRNAs; in fact, miR-155 was not identified within the total of 42 downregulated microRNAs.[2] It remains unclear how the authors expanded their previously published microRNA profiling during neovascularization in this current study.[1,2] Our group has also investigated microRNA expression profiles after hind limb ischemia.[3] In agreement with the findings of Grundmann et al, we observed only marginal regulation of miR-155 after hind limb ischemia.[2,3] In our analyses, miR-155 was upregulated slightly at 1, 3, and 7 days after ischemia, rather than downregulated. The question remains what could explain the discrepancies in microRNA regulation between the arrays performed.

In addition to their findings on miR-155, the authors revealed miR-329 among their top 15 downregulated microRNAs during ischemia. In their discussion, authors state that miR-329 was identified as a novel promising candidate for future studies on neovascularization. However, the authors have overlooked 2 articles that already described the function of miR-329 in both angiogenesis and arteriogenesis.

In 2013, Wang and colleagues[4] described miR-329 as a novel member of the 'angiomiR' family, which negatively regulates angiogenesis by targeting of CD146. Inhibition of miR-329 promoted migration and tube formation in HUVECs. Using a murine model of oxygen-induced retinopathy, these authors showed that miR-329 treatment inhibited pathological angiogenesis.[4]

In 2014, we demonstrated an essential role for miR-329, as part of the 14q32 microRNA cluster, in postischemic neovascularization.[3] We observed upregulation of miR-329 at 3 days after induction of ischemia. In vivo inhibition of miR-329 drastically improved blood flow recovery after hindlimb ischemia, shown by increased capillary densities in the ischemic soleus muscle and a trend toward increased collateral artery diameters in the adductor muscle.[3] Moreover, inhibition of miR-329 also leads to cell-specific effects like miR-155. GSO-329 treatment in vitro increased proliferation of en-

dothelial cells, but not myofibroblasts.

In their article, Pankratz et al have convincingly shown that miR-155 plays an important, yet complex, role in postischemic neovascularization. However, we feel that the aforementioned points should be considered.

Sabine M.J. Welten, Msc
Paul H.A. Quax, PhD
A. Yaël Nossent, PhD
Department of Vascular Surgery and Einthoven Laboratory for Experimental Vascular Medicine
Leiden University Medical Center
Leiden, the Netherlands

Reference List

1. Pankratz F, Bemtgen X, Zeiser R, Leonhardt F, Kreuzaler S, Hilgendorf I, Smolka C, Helbing T, Hoefer I, Esser JS, Kuster mann M, Moser M, Bode C, Grundmann S. MicroRNA-155 Exerts Cell-Specific Antiangiogenic but Proarteriogenic Effects During Adaptive Neovascularization. Circulation 2015; 131:1575-89.
2. Grundmann S, Hans FP, Kinniry S, Heinke J, Helbing T, Bluhm F, Sluijter JP, Hoefer I, Pasterkamp G, Bode C, Moser M. MicroRNA-100 regulates neovascularization by suppression of mammalian target of rapamycin in endothelial and vascular smooth muscle cells. Circulation 2011; 123:999-1009.
3. Welten SM, Bastiaansen AJ, de Jong RC, de Vries MR, Peters EA, Boonstra MC, Sheikh SP, La Monica N, Kandimalla ER, Quax PH, Nossent AY. Inhibition of 14q32 MicroRNAs miR-329, miR-487b, miR-494, and miR-495 increases neovascu larization and blood flow recovery after ischemia. Circ Res 2014; 115:696-708.
4. Wang P, Luo Y, Duan H, Xing S, Zhang J, Lu D, Feng J, Yang D, Song L, Yan X. MicroRNA 329 suppresses angiogenesis by targeting CD146. Mol Cell Biol 2013; 33:3689-99.

Chapter 4

Inhibition of MicroRNA-494 Reduces Carotid Artery Atherosclerotic Lesion Development and Increases Plaque Stability

Ann Surg 2015 Nov;262:841-848

A Wezel[1,2]
SMJ Welten[1,3]
W Razawy[1,2]
HM Lagraauw[2]
MR de Vries[1,3]
EAC Goossens[1,3]
MC Boonstra[1]
JF Hamming[1]
ER Kandimalla[4]
J Kuiper[2]
PHA Quax[1,3]
I Bot[1,2*]
AY Nossent[1,3*]

[*]Authors contributed equally to this work

[1]Department of Surgery, Leiden University Medical Center, Leiden, the Netherlands
[2]Division of Biopharmaceutics, LACDR, Leiden University, Leiden, the Netherlands
[3]Einthoven Laboratory for Experimental Vascular Medicine,
Leiden University Medical Center, Leiden, the Netherlands
[4]Idera Pharmaceuticals, Cambridge, MA, United States of America

Abstract

Objectives: Unstable atherosclerotic lesions in carotid arteries require surgical endarterectomy to reduce the risk of ischemic stroke. We aimed to identify microRNAs that exert a broad effect on atherosclerotic plaque formation and stability in the carotid artery.

Background: We made a selection of 164 genes involved in atherosclerosis. Using www.targetscan.org, we determined which microRNAs potentially regulate expression of these genes. We identified multiple microRNAs from the 14q32 microRNA cluster, which is highly involved in vascular remodeling. In human plaques, collected during carotid endarterectomy surgery, we found that 14q32 microRNA miR-494 was abundantly expressed in unstable lesions.

Methods: We induced atherosclerotic plaque formation in hypercholesterolemic ApoE$^{-/-}$ mice by placing semi-constrictive collars around both carotid arteries. We injected 'Gene Silencing Oligonucleotides' against miR-494 (GSO-494) or negative control (GSO-control). Using fluorescently labeled GSOs, we confirmed uptake of GSOs in affected areas of the carotids, but not elsewhere in the vasculature.

Results: After injection of GSO-494, we observed significant downregulation of miR-494 expression in the carotid arteries, while miR-494 target genes were upregulated. Further analyses revealed a 65% decrease in plaque size after GSO-494 treatment. Plaque stability was increased in GSO-494-treated mice, determined by an 80% decrease in necrotic core size and a 50% increase in plaque collagen content. Inhibition of miR-494 also resulted in decreased cholesterol levels and decreased VLDL fractions.

Conclusions: Treatment with GSO-494 results in smaller atherosclerotic lesions with increased plaque stability. Inhibition of miR-494 may decrease the risk of surgical complications or even avert endarterectomy surgery in some cases.

Introduction

Atherosclerosis in the carotid arteries is an important contributor to ischemic stroke. Carotid endarterectomy has proven to be effective in reducing the risk of ischemic stroke above carotid artery stenosis of 70%. Although patients with lower degrees of stenosis, between 50 and 69%, may also benefit from endarterectomy, the risk of surgical complications and per-operative Transient Ischemic Attack (TIA) or stroke currently appear to outweigh the benefits[1]. Besides atherosclerotic plaque size, plaque vulnerability is a major determinant of stroke risk[2,3]. Ideally, therapeutic strategies to decrease atherosclerotic disease would therefore not only address plaque size, but also plaque stability. Atherosclerosis is a complex, multifactorial disease in which various processes in immune modulation and cholesterol homeostasis are involved[4,5]. Taking into account this multifactorial nature of atherosclerosis, improvement of treatment strategies may be accomplished by targeting the process of atherogenesis as a whole rather than focusing on single factors.

MicroRNAs (miRs) are a class of short, non-coding RNAs, approximately 20 nucleotides long, capable of downregulating target gene expression at post-transcriptional level[6]. A single miR has, on average, 200 predicted target genes[7]. MiRs are excellent drug targets for complex diseases such as atherosclerosis, based on their ability to fine-tune expression of multiple genes[8,9]. Inhibition of miRs in atherosclerosis has been investigated in several studies and Rayner et al. showed that inhibiting miR-33 results in a lowering of plasma VLDL while increasing plasma HDL[10]. Besides regulation of cholesterol homeostasis, miRs have also been implicated in cellular mechanisms affecting atherosclerosis. MiR-126 for instance regulates post-transcriptional VCAM-1 expression in response to triglyceride-rich lipoproteins[11]. Also, inhibition of miR-92a has been demonstrated to up-regulate the expression of the atheroprotective Krüppel-like Factors KLF-2 and KLF-4 in endothelial cells[12,13]. Furthermore, smooth muscle cell proliferation and migration can be repressed by miR-195; consequently, neointima formation can be reduced by miR-195 gene therapy[14]. MiR-155 has been shown to repress the transcription factor Bcl6, thereby increasing NF-κB activation and CCL2 expression in macrophages[15]. However, it is apparent that most of these studies focus on the effect of miRs on a single cell type or process, thereby failing to do justice to the ability of miRs to exert a broad range of effects.

A commonly used tool to identify miRs involved in atherosclerosis is microarray profiling[16,17]. However, in order to utilize the specific characteristic of miRs to regulate many genes, we used a Reverse Target Prediction (RTP) strategy. Instead of investigating the miR with the highest regulation during atherosclerosis, we made use of a 'reversed' approach by taking multiple target genes as a starting point and subsequently selecting miRs that are predicted to regulate these genes. MiRs obtained by this method potentially target a larger subset of atherosclerosis-related genes and may thus function as a so-called 'master switch' in the development of atherosclerosis.

Using our unique RTP strategy, we identified miRs that are predicted to exert a broad effect on atherosclerosis. We singled out one miR from the large 14q32 miR-gene cluster, miR-494, which had thus far not been linked to atherosclerosis. Subsequently, we inhibited this miR using Gene Silencing Oligonucleotides (GSOs) in order to investigate its in vivo effect on atherosclerotic plaque formation and stability in the carotid artery.

Methods

A detailed description of the Materials and Methods is given in the Online Data Supplement.

Results

Identification of miRs From the 14q32 miR Gene Cluster by Reverse Target Prediction

We performed a RTP based on a list we compiled of atherosclerosis-related genes known from literature. As expected, we identified multiple miRs that have previously been described in atherosclerosis, including miR-155, miR-23/24,18 and miR-33. Interestingly, we found enrichment of binding sites for multiple miRs from a singe miR-gene cluster, located in an imprinted region on the long arm of human chromosome 14 (14q32; chromosome 12F1 in mice) (Supplemental Table 1A). We identified 11 miRs within this gene cluster, including miR-495 (45 putative targets), miR-494 (38 putative targets), and miR-329 (30 putative targets). We also performed our RTP by analyzing for murine target genes (Supplemental Table 1B), in which we again identified multiple targets for miR-495 (37 putative targets), miR-494 (34 putative targets), and miR-329 (26 putative targets). Recently, our group has shown an important role for miR-494, miR-495, and miR-329 in vascular remodeling[19] and we selected these miRs for further investigations.

Expression of miR-494, miR-495, and miR-329 in Human Atherosclerotic Plaques

To investigate whether miR-494, miR-495, and miR-329 are expressed in human atherosclerotic plaques, we isolated RNA from both stable and unstable lesions obtained from patients undergoing endarterectomy of the carotid artery. We detected abundant expression of miR-494 in all five unstable lesions and in one of three stable lesions. MiR-495 was expressed in all lesions, but at lower levels than miR-494, while the expression of miR-329 was not detectable in any of the lesions (Figure 1A).

Expression of miR-494, miR-495, and miR-329 in Murine Organs

In mouse carotid arteries, miR-494 and miR-495 are expressed approximately twice as high as miR-329 (Figure 1B). Analysis of the aorta revealed that the expression of miR-495 and miR-329 is higher as compared with miR-494. However, measurement of miR expression in the liver, spleen, bone marrow, and white blood cells demonstrated that the expression of miR-494 is higher as compared with miR-495 and miR-329 (Figure 1B). Taken into account the expression levels of miR-494 in murine organs and the higher expression of miR-494 in human atherosclerotic plaques, we selected miR-494 for further investigation regarding its effect on atherosclerotic lesion development.

In Vitro Target Gene Upregulation After Inhibition of miR-494

Inhibition of miR-494 led to a significant upregulation of the chemokine receptor CXCR4 in both endothelial cells and smooth muscle cells. Also, its ligand CXCL12 (SDF-1) was significantly increased in macrophages and mast cells. It has previously been shown that CXCR4/CXCL12 plays a protective role in atherosclerosis.[20,21] Inhibition of miR-494 also led to an upregulation of ACVR1 (a member of the TGF-beta superfamily) in macrophages and of TIMP3 (TIMP metallopeptidase inhibitor 3,

Supplemental Figure 1) in macrophages and mast cells.

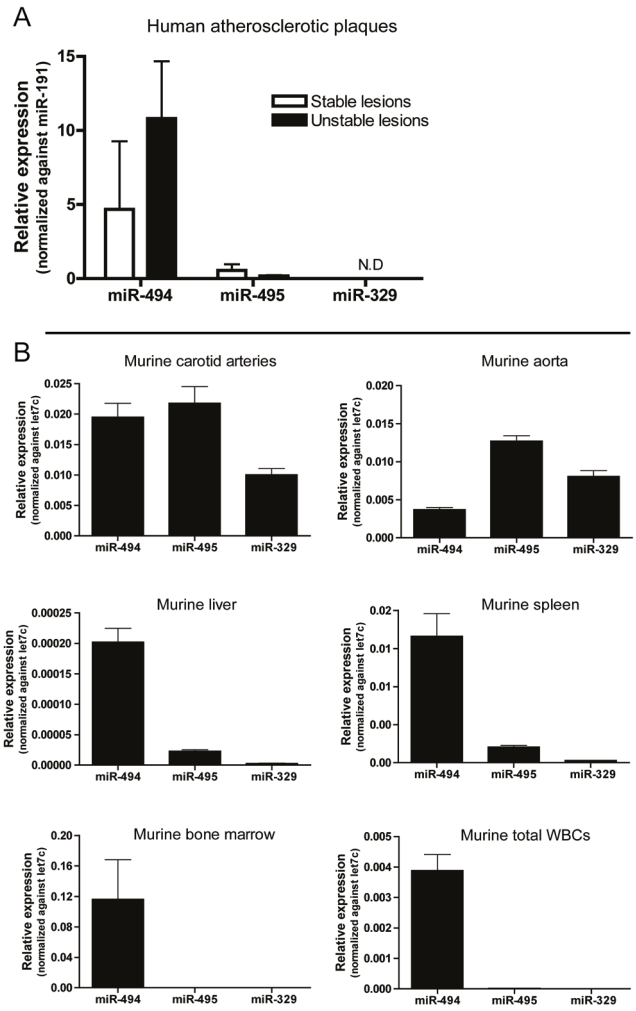

Figure 1. (A) Expression of miR-494, miR-495, and miR-329 in stable and unstable human carotid artery atherosclerotic plaques, relative to miR-191. (B) Expression of miR-494, miR-495, and miR-329, relative to miR-let-7c in the carotid artery, aorta, liver, spleen, bone marrow, and peripheral total white blood cells (WBCs) of ApoE$^{-/-}$ mice fed a western-type diet for three weeks.

Uptake of GSO-494 at Site of Collar Placement

At day 4 and 28, uptake of labeled GSO-494 (Figure 2) was clearly visible in the carotid artery in which the collar was placed, whereas no uptake was detected in the control carotid artery. Uptake of labeled GSO-494 was not observed in the aortic arch of mice fed a western-type diet for 2 weeks. However, a clear uptake of labeled GSO-494 was detected in the aortic arch of mice fed a western type diet for 6 weeks, which are known to contain early lesions. The descending aorta did not show any uptake of GSO-494. Also, no uptake was detected in the carotid arteries and aorta of control IRDye 800CW treated mouse.

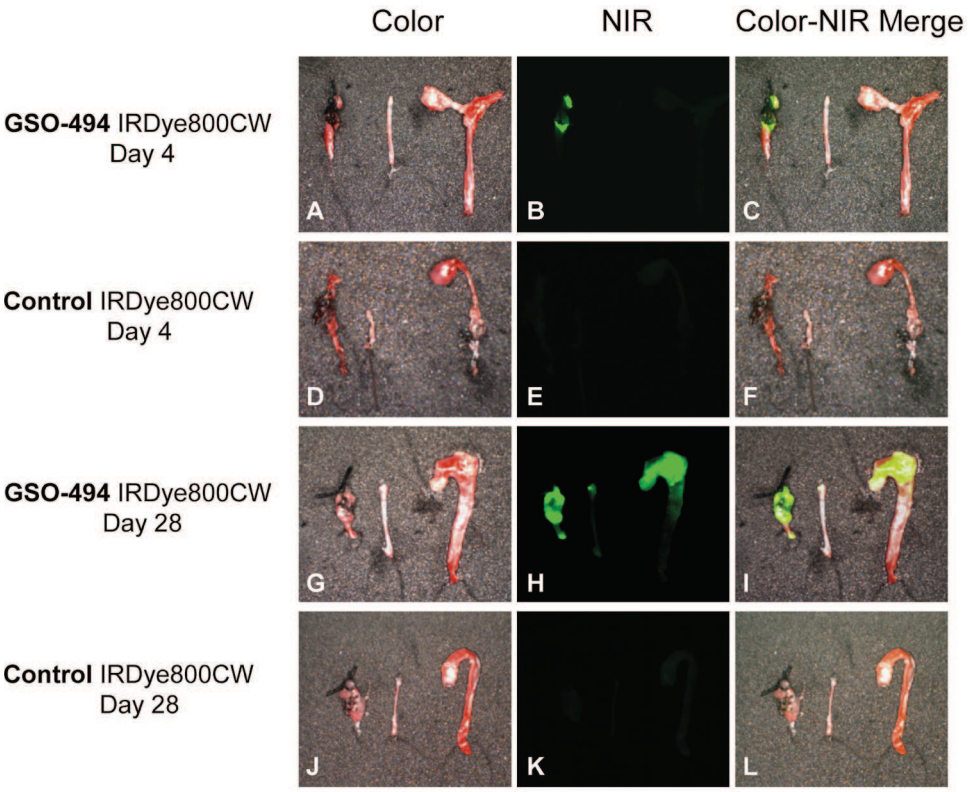

Figure 2. Uptake of IRDye 800CW-labeled GSO-494 or IRDye 800CW in the arterial wall. Each micrograph displays a carotid artery with collar induced atherosclerosis (left), contra-lateral control carotid artery from the same mouse without collar (middle), and aortic arch with descending aorta from the same mouse (left). Of note: all collars were removed before visualization. A-F: Arteries from mice receiving a high-cholesterol diet, 4 days after collar placement. (A) Arteries from mice 24 hours after intravenous injection of IRDye 800CW-labeled GSO-494. (B) Near-infrared (NR) image showing uptake of GSO-494 by the carotid artery in which a collar has been placed, which is absent in the control carotid artery. (C) Merged picture showing uptake of labeled GSO-494.
(D, E, F): Uptake of control unlabeled IRDye 800CW 24 hours after intravenous injection, 4 days after collar placement. G-L: Arteries from mice receiving a high-cholesterol diet, 28 days after collar placement, 24 hours after labeled GSO or control injection.
(G, H, I) Near-infrared (NR) image showing uptake of GSO-494 by the carotid artery in which a collar has been placed and in the aortic arch. No uptake is observed in the control carotid artery or in the descending aorta. (J, K, L) Uptake of control unlabeled IRDye 800CW 24 hours after intravenous injection, 4 weeks after collar placement.

In Vivo Repression of miR-494 and Target Gene Upregulation After GSO-494 Treatment

Three days after GSO-494 treatment, miR-494 was significantly downregulated by 46% in the carotid arteries compared with GSO-control (Figure 3A). Moreover, we observed upregulation of the selected target genes TIMP3, IL33, and TGFB2 in the carotid arteries of mice treated with GSO-494 (Figure 3B; $P < 0.05$).

Inhibition of miR-494 Affects Plasma Cholesterol Levels

Treatment with GSO-494 did not significantly affect either body weight (Supplemental Figure 2), or total white blood cell and cytokine levels (Supplemental Figure 3A and B). Also, body weight or plasma cholesterol levels did not differ between the PBS and GSO-control treated groups (Supplemental Figure 4A and B). Plasma cholesterol levels however showed a reduction of 13% after treatment with

GSO-494 (GSO-control: 30.4 ± 1.1 mM; GSO-494: 26.4 ± 0.7 mM; P < 0.01; Figure 4A). Lipid profiling using FPLC revealed that the reduced cholesterol level after inhibition of miR-494 was mainly owing to a decrease in the VLDL fraction (Figure 4B).

We aimed to elucidate the mechanism behind these changes in cholesterol levels by measurement of various target genes in liver and small intestine, which did not show any upregulation in gene expression after GSO-494 treatment (Supplemental Figure 5A and B). However, treatment of macrophages with GSO-494 in vitro resulted in a significant increase of cholesterol efflux towards HDL, compared with GSO-control treated cells (GSO-control: 8.1 ± 0.6% efflux; GSO-494: 10.4 ± 0.8%; P < 0.05; Figure 4C).

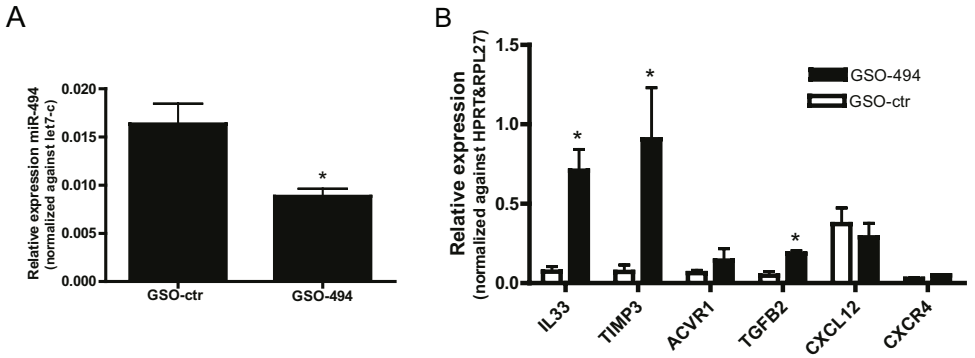

Figure 3. (A) Expression of miR-494 in carotid arteries of ApoE-/- mice, 4 days after injection of either GSO-494 or GSO-control (GSO-ctr), relative to expression of miR-let-7c. (B) Expression of selected target genes IL-33, TIMP3, ACVR1, TGFB2, CXCL12, and CXCR4 in carotid arteries of ApoE-/- mice, 4 days after injection of either GSO-494 or GSO-ctr, relative to expression of HPRT & RPL27.
*P < 0.05 compared with GSO-ctr.

Inhibition of miR-494 Reduces Atherosclerotic Lesion Formation

Atherosclerotic plaques were analyzed for size and composition and interestingly, revealed a marked reduction of 65% in atherosclerotic plaque size in the group treated with GSO-494 (GSO-control: 47 ± 11×103 μm^2; GSO-494: 16 ± 3×103 μm^2; P < 0.05; Figure 4D). We did not observe differences in lesion size between PBS and GSO-control treated groups (Supplemental Figure 4C), illustrating that GSOs did not exert nonspecific effects.

Treatment With GSO-494 Leads to an Enhanced Stable Phenotype of Atherosclerotic Lesions

Atherosclerotic plaques were not only reduced in size after treatment with GSO-494; the plaques also showed an increase in plaque stability. So-called “stable lesions” are characterized by a small necrotic core and a thick fibrous cap rich in collagen and smooth muscle cells. Indeed, necrotic core size was significantly reduced by 80% in mice treated with GSO-494 (GSO-control: 33 ± 6%; GSO-494: 6 ± 3%; P < 0.001; Figure 5A). Furthermore, collagen content was significantly increased after inhibition of miR-494 (GSO-control: 6.6 ± 1.6%; GSO-494: 12.7 ± 2.1%; P < 0.05; Figure 5B).

Plaque morphology was further examined by visualizing smooth muscle cells using an alpha smooth muscle actin staining. The percentage of positively stained lesion area was similar in both treatment groups (GSO-control: 4.6 ± 1.0%; GSO-494: 6.4 ± 1.8%; Figure 5C); moreover, lesional macrophage content remained unaltered after GSO-494 treatment (GSO-control: 20.0 ± 2.2%; GSO-494: 23.6 ± 2.7%; Figure 5D). We also stained for mast cells, as these have previously been described as important

players in atherosclerotic plaque development and destabilization.[22,23] However, no differences were found in either mast cell numbers (Figure 5E) or in their activation status (data not shown).

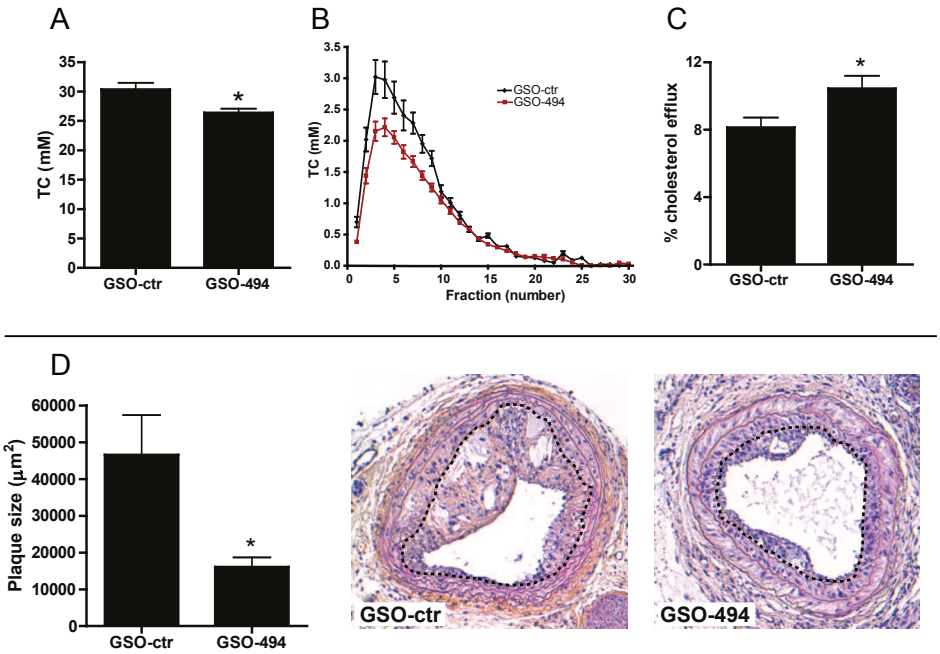

Figure 4. (A) Total plasma cholesterol levels of ApoE$^{-/-}$ mice treated with GSO-494 compared with GSO-control (GSO-ctr), 6 weeks after start of the western-type diet. (B) AKTA-FPLC analysis revealed a decrease in VLDL/LDL levels in mice treated with GSO-494 compared with GSO-ctr. (C) Cholesterol efflux towards HDL in macrophages treated with GSO-494 or GSO-ctr in vitro. (D) Maximal plaque size (µm2) in carotid arteries of ApoE$^{-/-}$ mice treated with GSO-494 compared with GSO-ctr. Micrographs show representative images of both treatment groups (100x enlarged). *P < 0.05, compared with GSO-ctr.

Inhibition of miR-494 Results in Altered Collagen Homeostasis

To elucidate the mechanism behind the increased amount of collagen present in the plaque, we studied both collagen synthesis and collagen degradation in an in vitro setup. Inhibition of miR-494 in smooth muscle cells did not result in increased collagen synthesis rate (Supplemental Figure 6A). Regarding collagen degradation, we determined TIMP expression after treatment of cultured cells with GSO-494, as TIMPs inhibit matrix degradation by MMPs. TIMP3 is a predicted target of miR-494 and indeed, the expression levels of TIMP3 were increased in mast cells (1.5-fold; P < 0.05) and macrophages (21-fold; P < 0.05) after inhibition of miR-494. The expression levels of MMP9 remained unchanged after treatment with GSO-494, resulting in a net increase in TIMP/MMP ratio (Supplemental Figure 6B).

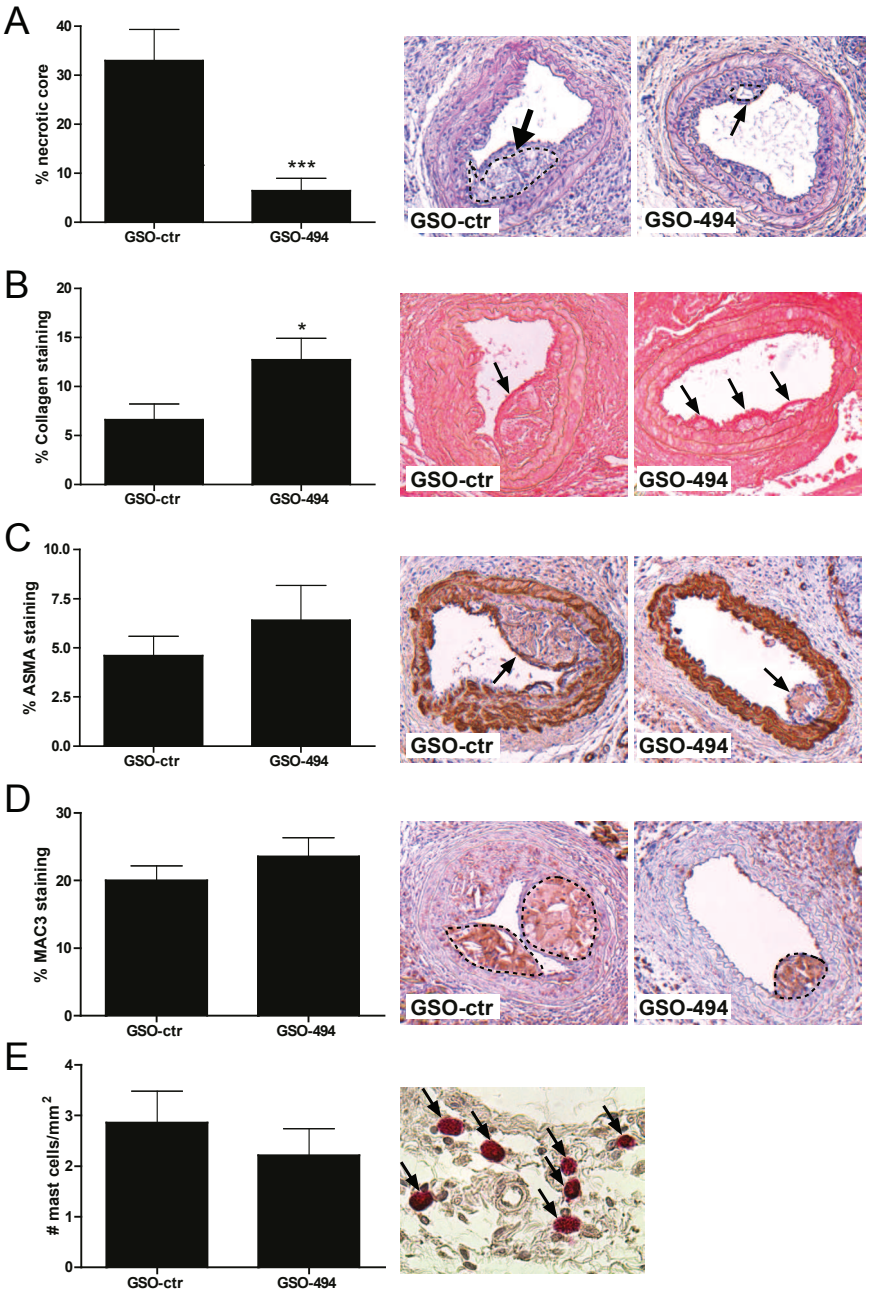

Figure 5. Effect of miR-494 inhibition on plaque morphology and lesion stability. (A) Necrotic core size was defined as an acellular area rich of debris and was measured as a percentage of total plaque area. Necrotic cores are indicated by dashed lines and arrows. (B) Collagen content in the lesions of mice treated with either GSO-494 or GSO-control (GSO-ctr). Collagen-positive areas are indicated by arrows. (C) Smooth muscle cells in the plaque were stained with an antibody against [alpha]-SMA (indicated by arrows), whereas (D) macrophages were visualized with a MAC-3 antibody (dashed lines). (E) Resting mast cells in the perivascular tissue of mice treated with either GSO-494 or GSO-ctr are indicated by arrows. The micrographs show representative images of both groups (A-D: 100x; E: 400x). *P < 0.05, ***P < 0.001, compared with GSO-ctr.

Discussion

The current study is the first to report a role for miR-494 from the 14q32 miR-gene cluster in the development of atherosclerosis. We used a unique RTP strategy to identify miR-494, by combining knowledge from our own previous experiments and literature in an in silico approach. Besides recovering miRs known to be important in atherosclerosis, we identified miRs that had not yet been investigated in this disease, in particular miRs from the 14q32 cluster. The 14q32 miR gene cluster is highly conserved in mammals and consists of 61 miR genes in mice and 54 in human[24]. Previously, it has been shown that many of the 14q32 miRs are implicated in human disease[25]. A recent study by Aavik et al[26] showed that hypomethylation of the 14q32 locus is associated with atherosclerosis. We showed that 14q32 miR-494 is abundantly expressed in human atherosclerotic plaques, in particular in unstable lesions. Also, miR-494 was found to be expressed in the murine carotid artery wall, and in other organs involved in the development of atherosclerosis, such as the liver and the spleen. In vivo, inhibition of miR-494 resulted in a decrease in atherosclerotic plaque formation with a marked increase in plaque stability.

Even though miR-494 was predicted to target more pro- than anti-inflammatory target genes in our RTP, the in vivo effects of inhibiting miR-494 revealed a positive effect on atherosclerosis. This may be explained by the fact that several atheroprotective genes, including TGFB2[27] or IL33[28] were upregulated in vivo after GSO-494 treatment. Numerous studies have targeted proatherogenic genes to reduce atherosclerosis, but our data suggest that upregulation of antiatherogenic genes may be just as, or even more, promising when treating this complex disease.

In our study, we inhibited miR-494 by means of GSOs, as described previously[19]. We were able to detect fluorescently labeled GSO-494 in the affected area of the carotid artery in which collars were placed, but not in control carotids. Moreover, uptake of labeled GSO-494 was observed in the aortic arch, which is known to contain lesions in $ApoE^{-/-}$ mice fed a western-type diet for 6 weeks. These data show that GSOs are targeted to atherosclerotic lesions. This is highly relevant for therapeutic applicability of GSOs, as patients at risk of atherosclerotic complications, such as TIA and/or stroke, already have advanced atherosclerotic lesions.

Inhibition of miR-494 reduced plasma cholesterol levels by 13%. Surprisingly, we did not detect any regulation of miR-494 target genes related to lipid or cholesterol metabolism in the liver. Also, target gene expression in the intestine of GSO treated mice was unaltered. We did however observe a significant increase in HDL-mediated efflux in vitro in macrophages treated with GSO-494 compared with GSO-control. This suggests that inhibition of miR-494 increases the removal of excess cholesterol from the vessel wall to the liver via HDL, resulting in reduced atherogenesis and a reduced necrotic core size in the lesions.

Besides the reduction in necrotic core size, plaque stability under miR-494 inhibition was further increased by an increase in collagen content. We initially hypothesized that this may have been caused by increased collagen homeostasis. However, no changes in collagen synthesis rate were detected after treating smooth muscle cells in vitro with GSO-494. The TIMP/MMP ratio was significantly increased however, indicative of decreased collagen degradation. In vivo, decreased collagen degradation results in an increased thickness of the fibrous cap, thereby reducing the risk of plaque rupture with concomitant cardiovascular events, including TIA and/or stroke.

Involvement of miR-494 in atherosclerosis had not previously been shown. However, our group has recently described a role of miR-494 in therapeutic neovascularization. For patients suffering from ischemia, restoring blood flow to the downstream tissues is crucial. Stimulating arterio- and angiogenesis, however, is always accompanied by an inflammatory reaction, which often leads to an aggravation of the underlying cause of the ischemia: atherosclerosis. This so-called Janus phenomenon[29] is a major drawback in this field of research, especially when translating controlled, univariate animal models towards a clinical setting. Intriguingly, our group showed that inhibition of miR-494 leads to a profound increase in blood flow after hindlimb ischemia[19]. Therapeutic inhibition of miR-494 may therefore be unique in inducing neovascularization, whereas simultaneously reducing atherosclerosis formation and increasing plaque stability in patients with occlusive arterial disease.

In conclusion, we discovered a role for miR-494 from the 14q32 miR gene cluster in atherosclerosis by utilizing the specific characteristic of miRs to regulate multiple genes and cellular processes. Inhibition of miR-494 led to a reduction in lesion size and an increase in plaque stability in mice. As miR-494 expression was also elevated in unstable human atherosclerotic plaques, future studies will have to determine whether our findings in this murine model also apply in a clinical setting. As both carotid artery plaque size and stability are major determinants of risk of TIA and/or stroke, this would make miR-494 a promising new therapeutic target for patients suffering from carotid artery atherosclerosis as well as for other occlusive arterial diseases.

Acknowledgments
The authors would like to thank Dr. JFP Berbée and Dr. GHM van Puijvelde for their technical support, the Netherlands Organization for Scientific Research (NWO; Veni 916.12.041), the Leiden University Fund/Nypels-van der Zee Fund (2219/5-4-12\NZ), and the Netherlands Institute for Regenerative Medicine (NIRM; FES0908).

References

1. Rothwell PM, Eliasziw M, Gutnikov SA, et al.; Carotid Endarterectomy Trialists' Collaboration. Analysis of pooled data from the randomised controlled trials of endarterectomy for symptomatic carotid stenosis. *Lancet*. 2003;361:107-116.
2. Shah PK. Mechanisms of plaque vulnerability and rupture. *J Am Coll Cardiol*. 2003;41:15S-22S.
3. Saba L, Potters F, van der Lugt A, et al. Imaging of the fibrous cap in atherosclerotic carotid plaque. *Cardiovasc Intervent Radiol*. 2010;33:681-689.
4. Galkina E, Ley K. Immune and inflammatory mechanisms of atherosclerosis. *Annu Rev Immunol*. 2009;27:165-197.
5. Libby P. Inflammation in atherosclerosis. *Arterioscler Thromb Vasc Biol*. 2012;32:2045-2051.
6. Chen K, Rajewsky N. The evolution of gene regulation by transcription factors and microRNAs. *Nat Rev Genet*. 2007;8:93-103.
7. Rajewsky N. MicroRNA target predictions in animals. *Nat Genet*. 2006;38:S8-S13.
8. van Rooij E, Olson EN. MicroRNA therapeutics for cardiovascular disease: opportunities and obstacles. *Nat Rev Drug Discov*. 2012;11:860-872.
9. Nossent AY, Eskildsen TV, Andersen LB, et al. The 14q32 MicroRNA-487b Targets the Antiapoptotic Insulin Receptor Substrate 1 in Hypertension-Induced Remodeling of the Aorta. *Ann Surg*. 2013;258:743-753.
10. Rayner KJ, Esau CC, Hussain FN, et al. Inhibition of miR-33a/b in non-human primates raises plasma HDL and lowers VLDL triglycerides. *Nature*. 2011;478:404-407.
11. Sun C, Alkhoury K, Wang YI, et al. IRF-1 and miRNA126 modulate VCAM-1 expression in response to a high-fat meal. *Circ Res*. 2012;111:1054-1064.
12. Fang Y, Davies PF. Site-specific microRNA-92a regulation of Kruppel-like factors 4 and 2 in atherosusceptible endothelium. *Arterioscler Thromb Vasc Biol*. 2012;32:979-987.
13. Alaiti MA, Orasanu G, Tugal D, et al. Kruppel-like factors and vascular inflammation: implications for atherosclerosis. *Curr Atheroscler Rep*. 2012;14:438-449.
14. Wang YS, Wang HY, Liao YC, et al. MicroRNA-195 regulates vascular smooth muscle cell phenotype and prevents neointimal formation. *Cardiovasc Res*. 2012:95:517-526.
15. Nazari-Jahantigh M, Wei Y, Noels H, et al. MicroRNA-155 promotes atherosclerosis by repressing Bcl6 in macrophages. *J Clin Invest*. 2012;122:4190-4202.
16. Zhu J, Chen T, Yang L, et al. Regulation of microRNA-155 in atherosclerotic inflammatory responses by targeting MAP3K10. *PLoS One*. 2012;7:e46551.
17. J i R, Cheng Y, Yue J, et al. MicroRNA expression signature and antisense-mediated depletion reveal an essential role of MicroRNA in vascular neointimal lesion formation. *Circ Res*. 2007;100:1579-1588.
18. Boon RA, Hergenreider E, Dimmeler S. Atheroprotective mechanisms of shear stress-regulated microRNAs. *Thromb Haemost*. 2012;108:616-620.
19. Welten SM, Bastiaansen AJ, de Jong R, et al. Inhibition of 14q32 MicroRNAs miR-329, miR-487b, miR-494 and miR-495 Increases Neovascularization and Blood Flow Recovery after Ischemia. *Circ Res*. 2014;115:696-708.
20. Zernecke A, Bot I, Djalali-Talab Y, et al. Protective role of CXC receptor 4/CXC ligand 12 unveils the importance of neutrophils in atherosclerosis. *Circ Res*. 2008;102:209-217.
21. Bot I, Daissormont IT, Zernecke A, et al. CXCR4 blockade induces atherosclerosis by affecting neutrophil function. *J Mol Cell Cardiol*. 2014;74C:44-52.
22. Bot I, de Jager SC, Zernecke A, et al. Perivascular mast cells promote atherogenesis and induce plaque destabilization in apolipoprotein E-deficient mice. *Circulation*. 2007;115:2516-2525.
23. Willems S, Vink A, Bot I, et al. Mast cells in human carotid atherosclerotic plaques are associated with intraplaque microvessel density and the occurrence of future cardiovascular events. *Eur Heart J*. 2013;34:3699-3706.
24. Seitz H, Royo H, Bortolin ML, et al. A large imprinted microRNA gene cluster at the mouse Dlk1-Gtl2 domain. *Genome Res*. 2004;14:1741-1748.
25. Benetatos L, Hatzimichael E, Londin E, et al. The microRNAs within the DLK1-DIO3 genomic region: involvement in disease pathogenesis. *Cell Mol Life Sci*. 2013;70:795-814.
26. Aavik E, Lumivuori H, Leppänen O, et al. Global DNA methylation analysis of human atherosclerotic plaques reveals extensive genomic hypomethylation and reactivation at imprinted locus 14q32 involving induction of a miRNA cluster. *Eur Heart J*. 2015;36(16):993-1000.
27. Mallat Z, Gojova A, Marchiol-Fournigault C, et al. Inhibition of transforming growth factor-beta signaling accelerates atherosclerosis and induces an unstable plaque phenotype in mice. *Circ Res*. 2001 ;89:930-934.
28. Pei C, Barbour M, Fairlie-Clarke KJ, et al. Emerging role of interleukin-33 in autoimmune diseases. *Immunology*. 2014;141:9-17.
29. Epstein SE, Stabile E, Kinnaird T, et al. Janus phenomenon: the interrelated tradeoffs inherent in therapies designed to enhance collateral formation and those designed to inhibit atherogenesis. *Circulation*. 2004;109:2826-2831.

Supplemental Material

Materials and Methods

Reverse Target Prediction
Based on existing knowledge from both literature[1-5] and previous studies within our group, we compiled a list of 164 genes involved in atherosclerosis. Using the online algorithm Targetscan (www.targetscan.org), a list was generated of all miRs predicted to target our selected genes. We ranked the miRs according to the number of putative target genes with a predicted 3'UTR binding site. The RTP was performed by analyzing binding sites in human target genes to ensure clinical relevance (Supplemental table 1A). We then performed the RTP by analyzing binding sites in murine target genes, to confirm the validity of the use of our mouse model for atherosclerosis (Supplemental table 1B).

Human carotid artery plaques
Human were collected anonymously during endarterectomy surgery at the Leiden University Medical Center. Plaques were fixed in 4% formaldehyde and embedded in paraffin. From a biobank of approximately 50 human carotid artery plaques, 6 highly unstable and 6 relatively stable plaques were selected based on three parameters for plaque instability (i.e. necrotic core size, macrophage content and intra-plaque hemorrhage). Total RNA was isolated using the RNeasy FFPE Kit according to manufacturer's protocol (Qiagen). Sufficient RNA was isolated from 3 stable and 5 unstable plaques for miR quantification as described below.
According to Dutch law, no informed consent is required for the collection human tissue samples, as long as only fully anonymized 'leftover' material is collected and stored.

Mice
All animal work was performed in compliance with the Dutch government guidelines and the Directive 2010/63/EU of the European Parliament. Male ApoE$^{-/-}$ mice, obtained from the local animal breeding facility (Gorlaeus Laboratories, Leiden University, Leiden, the Netherlands), were fed a Western type diet, containing 0.25% cholesterol and 15% cacao butter (SDS, Sussex, UK) for six weeks. Before surgical intervention mice were age-, cholesterol-, and weight-matched. Details of cholesterol measurement are described below. White blood cell (WBC) numbers and cellular differentiation were determined on a Sysmex cell differentiation apparatus (Goffin Meyvis, Etten-Leur, The Netherlands).

Carotid collar placement
Two weeks after start of the Western type diet, carotid artery plaque formation was induced by perivascular collar placement as described previously[6]. Before surgery and sacrifice, mice were anaesthetized by an intra-peritoneal injection with midazolam (5 mg/kg; Roche, Woerden, The Netherlands), domitor (0.5 mg/kg; AST Farma, Oudewater, The Netherlands) and fentanyl (0.05 mg/kg; Janssen, Beerse, Belgium). After surgery, mice were antagonized with a subcutaneous injection of flumazenil (0.5 mg/kg; Fresenius Kabi, Schelle, Belgium), antesedan (2.5 mg/kg; AST Farma) and buprenorphine (0.1 mg/kg; MSD Animal Health, Boxmeer, The Netherlands). In brief, a semi-constrictive collar was placed around both left and right carotid arteries of the mice. Low shear stress and disturbed flow at the proximal site of the collar result in increased expression of endothelial adhesion molecules and atherosclerotic lesion formation. At either one week or four weeks after collar placement, mice were anaesthetized and in situ perfused, after which carotid artery lesions were harvested for further analysis.

Treatment with IRDye labelled GSOs
Four male adult ApoE$^{-/-}$ mice received one perivascular collar around the right carotid artery, while the contra-lateral carotid artery was left unaffected. At day 4 and day 28 after surgery, mice were injected intravenously with IRDye-800CW-labelled GSO-494 (0.4mg/mouse; Idera Pharmaceuticals, Cambridge MA) or control unlabelled IRDye. Mice were sacrificed by orbital exsanguination one day after injection. Near-InfraRed (NIR) fluorescence measurements were performed using the FLARE™ NIR imaging system7.

Treatment with GSOs
At day 4 after surgery, mice received an intravenous injection of either 1 mg Gene Silencing Oligonucleotide dissolved in 200 µl PBS (GSO, kindly provided by Idera Pharmaceuticals, Cambridge, MA, USA) or 200 µl PBS control at day 4 after surgery. A subset of mice (n=6 per group) was sacrificed 3 days later (1 week after surgery) in order to establish downregulation of miR-494 in vivo. For effects on atherosclerosis, the remaining mice received a second injection of 0.5 mg GSO dissolved in 200 µl PBS per mouse at day 18 (n=15 per group). GSO-494 was designed with perfect reverse complementarity to the mature target miR sequence and synthesized by Idera Pharmaceuticals. As a negative control, a scrambled sequence was used, designed not to target any known murine miR. GSOs consist of two single-stranded O-methyl-modified DNA strands, linked together at their 5'ends by a phosphorothioate-linker to avoid TLR-activation[8,9]. Sequences of GSOs used are given in Supplemental table 2.

Plasma analysis
Blood was collected from the mice by tail bleeding. The concentration of cholesterol in plasma was determined by incubation with 0.025 U/ml cholesterol oxidase (Sigma, Zwijndrecht, The Netherlands) and 0.065 U/ml peroxidase and 15 µg/mL cholesterol esterase (Roche Diagnostics, Mannheim, Germany) in polyoxyethylene-9-laurylether, and 7.5% methanol). Precipath (standardized serum; Boehringer Mannheim, Germany) was used as an internal standard. Absorbance was measured at 490 nm.

For lipid profiling, plasma was pooled (n=3 mice per sample) and diluted 6 times, after which fractionation of plasma lipoproteins was performed using an AKTA-FPLC. Triglyceride levels and total cholesterol levels were determined in each fraction and in the original pooled sample by incubation with cholesterol CHOD-PAP Reagent (Roche, Woerden, The Netherlands). Absorbance was measured at 492 nm.
Plasma cytokines and chemokines were measured using ProcartaPlex™ Multiplex Immunoassays Mouse Cytokine and Chemokine Panel 1 (26 plex), according to manufacturer's protocol (eBioscience, San Diego, CA, USA) and read on a Luminex Magpix (Luminex Corporation, Austin, Tx, USA).

Histology and morphometry
Paraffin sections (5 µm thick) were routinely stained with HPS (hematoxylin-phloxine-saffron), which were used to determine plaque size. Picrosirius red staining was used to visualize collagen and for measurement of necrotic core size. Plaque composition was further examined by staining for smooth muscle cells (alpha smooth muscle actin, Sigma) and macrophages (MAC 3, BD-Pharmingen, San Diego, CA, USA). The amount of mast cells and their activation status was visualized using an enzymatic staining kit (Naphtol-CAE, Sigma).
Morphometric analysis (Leica Qwin image analysis software) was performed on HPS-stained atherosclerotic lesions at site of maximal stenosis. (Immuno) histochemical stainings were quantified by computer assisted analysis (Leica, Qwin, Cambridge, UK) and expressed as the percentage of positive stained area of the total lesion area. Mast cells were counted manually. A mast cell was considered resting when all granula were maintained inside the cell, while mast cells were assessed as activated when granula were deposited in the tissue surrounding the mast cell. The necrotic core was defined as the a-cellular, debris-rich plaque area as percentage of total plaque area.

Cell culture
Bone marrow (BM) cells isolated from C57Bl/6 mice were cultured in petridishes (Greiner Bio-one, Alphen aan den Rijn, Netherlands) for 7 days in RPMI medium supplemented with 20% fetal calf serum (FCS), 2 mmol/L l-glutamine, 100 U/mL penicillin and 100 µg/mL streptomycin and 30% L929 cell-conditioned medium, as the source of macrophage colony-stimulating factor (M-CSF), to generate BM-derived macrophages (BMDMs)[10]. For generation of primary mast cells, BM cells were cultured in RPMI medium supplemented with 10% IL-3 supernatant (supernatant of WEHI-cells overexpressing and secreting murine Interleukin 3 (mIL3)), 1 mM sodium pyruvate, MEM non-essential amino acids, 10% FCS, 2 mmol/L l-glutamine, 100 U/mL penicillin and 100 µg/mL streptomycin for 4 weeks[11]. Mast cell purity and maturation was determined microscopically by staining of cytospins with 0.5% aqueous toluidin blue. Primary cultured murine smooth muscle cells (vSMC) and cell lines for fibroblasts (3T3) and endothelial cells (H5V) were cultured in complete DMEM medium supplemented with 10% FCS, 2 mmol/L l-glutamine, 100 U/mL penicillin and 100 µg/mL streptomycin in T75 tissue culture flasks (Greiner Bio-one).
Mast cells, fibroblasts, smooth muscle cells and endothelial cells were plated in triplicate at a density of 10^6 cells/mL. GSOs were added overnight at a concentration of 5 µg/mL, after which the cells were lysed for RNA isolation.
For BMDMs, GSOs were added immediately after isolation from BM in a concentration of 5 µg/mL. After three days medium was refreshed with a similar addition of GSOs in a concentration of 5 µg/mL. Four days later, medium was removed and cells were lysed for RNA isolation.

RNA isolation, cDNA synthesis and qPCR
Three carotid artery segments from 7 days after collar placement were pooled and homogenized by grounding using a Pellet Pestle Cordless Motor (Kimble Chase Life Science, USA). Spleen, liver and intestines from these mice were isolated and homogenized by grounding with the use of liquid nitrogen. Also, BM was isolated, after which total RNA was extracted using a standard TRIzol-chloroform protocol. RNA concentration, purity and integrity were examined by nanodrop (Nanodrop® Technologies). MiR quantification was performed according to manufacturer's protocol using TaqMan® miR assays (Applied Biosystems, Foster City, CA, USA). qPCRs were run on a 7900HT Fast Real-Time PCR System (Applied Biosystems). Normalization of data was performed using a stably expressed endogenous control (mmu-let-7c; for the liver miR-122 was used).
For the in vitro experiments, total RNA was extracted from the cells using the guanidine thiocyanate (GTC) method[12]. RNA was reverse transcribed by M-MuLV reverse transcriptase (RevertAid, MBI Fermentas, Leon-Roth, Germany) and used for quantitative analysis of mouse genes (Supplemental Table 3) with an ABI PRISM 7700 Taqman apparatus (Applied Biosystems). Murine HPRT and RPL27 were used as standard housekeeping genes.

Cholesterol efflux assay
BMDMs, cultured and treated with GSOs as described above, were seeded at a density of $0.5*10^6$ per well. The next day, medium was aspirated and cells were loaded with 20 mg/mL cholesterol for 24 hours with 1 µCi/mL 3H-cholesterol in DMEM with 10% BSA, with the addition of either GSO-control or GSO-494 (5 µg/mL) (n=6). The following day, loading medium was removed and the cells were washed with PBS, after which DMEM/10%BSA was added to the cells for one hour. Subsequently, the medium was removed and cells were incubated overnight with control DMEM/10%BSA medium or DMEM/10%BSA medium supplemented with HDL (50 µg/mL). After a 24-hour efflux period, radioactivity in the cells and medium was determined by liquid scintillation counting (Packard 1500 Tricarb, Downers Grove, IL, USA). Cholesterol efflux is defined as ($dpm_{medium}/dpm_{cells}+dpm_{medium}$) x100%, and is depicted as the percentage HDL specific efflux, which was corrected for non-specific efflux to control medium.

Collagen synthesis assay
To measure collagen production by vSMC, cells were seeded at a density of 0.2*106 cells per well. After attachment of the cells,

control medium or medium containing GSO-control or GSO-494 (5 µg/mL), was added. Subsequently, 1 µCi [^{3}H]proline (Perkin Elmer, Groningen, The Netherlands) in the presence of 50 µg/mL ascorbic acid was added and incubated overnight at 37°C. Cells were detached from the wells in 20 mM Tris*HCl/0.36 mM CaCl2 (pH=7.6) and sonicated for 2 minutes. Collagen was degraded by incubation with 100 U/mL collagenase for 2 hours at 37°C, after which samples were centrifuged for 15 minutes at 13.2 g. Proteins were precipitated for 30 minutes on ice using 50% trichloroacetic acid, after which [^{3}H]proline content in the supernatant as a measure for collagen production was quantified in a liquid scintillation analyzer as described above. Protein content was measured using a standard BCA protein assay.

Statistical analysis

Data are expressed as mean ± SEM. Two-tailed Student's t-tests were used to compare individual groups in the in vivo studies. Non-parametric data were analyzed using a Mann-Whitney U test. A level of $P<0.05$ was considered significant.

References

1. Seo D, Wang T, Dressman H, et al. Gene expression phenotypes of atherosclerosis. *Arterioscler Thromb Vasc Biol*. 2004;24:1922-1927.
2. Tabibiazar R, Wagner RA, Ashley EA, et al. Signature patterns of gene expression in mouse atherosclerosis and their correlation to human coronary disease. *Physiol Genomics*. 2005;22:213-226.
3. Fu S, Zhao H, Shi J, et al. Peripheral arterial occlusive disease: global gene expression analyses suggest a major role for immune and inflammatory responses. *BMC Genomics*. 2008;9:369.
4. Laukkanen J, Ylä-Herttuala S. Genes involved in atherosclerosis. *Exp Nephrol.* 2002;10:150-163.
5. Lusis AJ. Genetics of atherosclerosis. *Trends Genet*. 2012;28:267-275.
6. Von der Thüsen JH, van Berkel TJC, Biessen EAL. Induction of rapid atherogenesis by perivascular carotid collar placement in apolipoprotein E-deficient and low-density lipoprotein receptor-deficient mice. *Circulation*. 2001;103:1164-1170.
7. Welten SM, Bastiaansen AJ, de Jong R, et al. Inhibition of 14q32 MicroRNAs miR-329, miR-487b, miR-494 and miR-495 Increases Neovascularization and Blood Flow Recovery after Ischemia. *Circ Res*. 2014;115:696-708.
8. Nossent AY, Eskildsen TV, Andersen LB, et al. The 14q32 MicroRNA-487b Targets the Antiapoptotic Insulin Receptor Substrate 1 in Hypertension-Induced Remodeling of the Aorta. *Ann Surg*. 2013;258:743-753.
9. Bhagat L, Putta MR, Wang D, et al. Novel oligonucleotides containing two 3'-ends complementary to target mRNA show optimal gene-silencing activity. *J Med Chem*. 2011;54:3027-3036.
10. Zhao Y, Pennings M, Hildebrand RB, et al. Enhanced foam cell formation, atherosclerotic lesion development, and inflammation by combined deletion of ABCA1 and SR-BI in Bone marrow-derived cells in LDL receptor knockout mice on western-type diet. *Circ Res*. 2010;107:e20-e31.
11. Razin E, Marx G. Thrombin-induced degranulation of cultured bone marrow-derived mast cells. *J Immunol*. 1984;133:3282-3285.
12. McGookin R. RNA extraction by the guanidine thiocyanate procedure. *Methods Mol Biol*. 1985;2:113-116.

Supplemental Figures and Tables

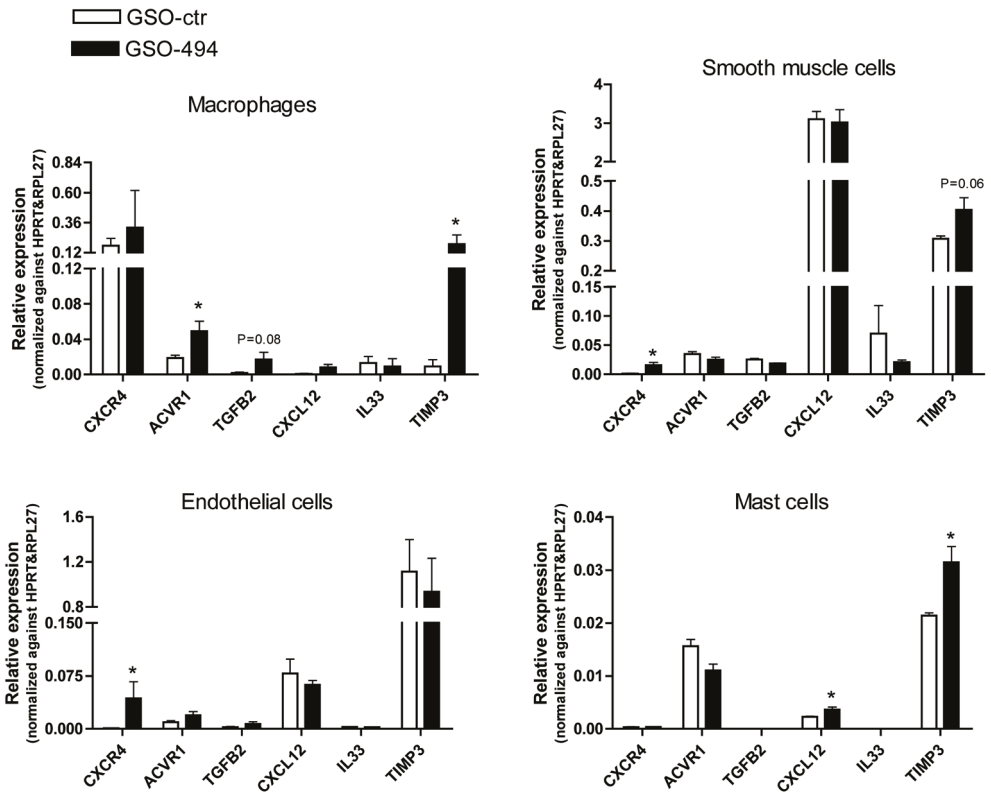

Supplemental Figure 1. In vitro expression of selected target genes CXCR4, ACVR1, TGFB2, CXCL12, IL33 and TIMP3 in macrophages, smooth muscle cells, endothelial cells, and mast cells after treatment with either GSO-494 or GSO-ctr, relative to expression of HPRT & RPL27. *P<0.05, compared to GSO-ctr.

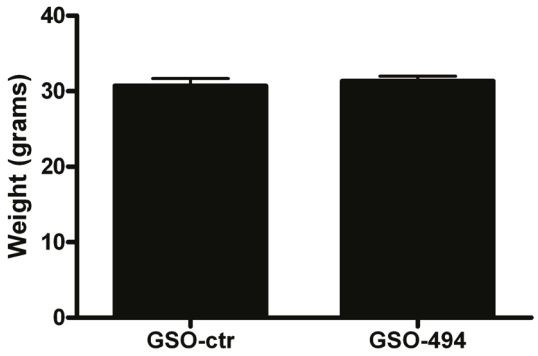

Supplemental Figure 2. Body weight (in grams) of mice after treatment with GSO-494 or GSO-ctr.

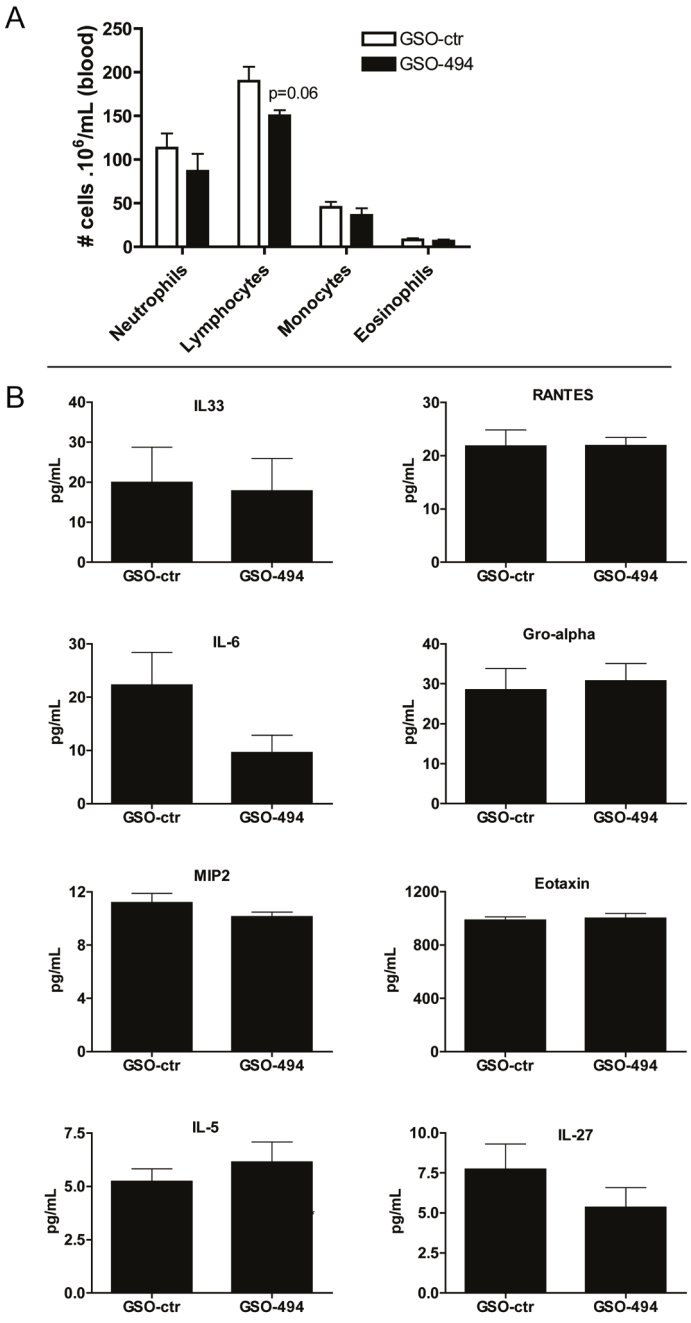

Supplemental Figure 3. A trend towards a decrease in absolute amount of lymphocytes 4 days after treatment with GSO-494 was observed, while the absolute numbers of neutrophils, monocyte or eosinophils remained unaltered compared to GSO-ctr. (A) Multiplex immunoassay analysis showed no major changes in systemic cytokine and chemokine levels after GSO-494 treatment (B).

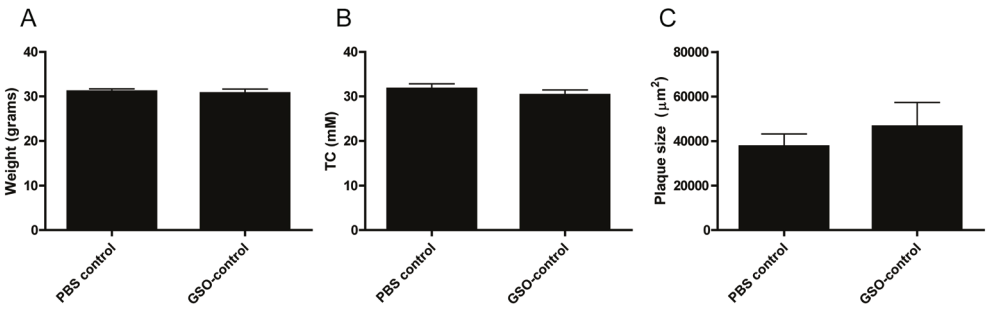

Supplemental Figure 4. (A) Body weight (in grams), (B) plasma cholesterol and (C) plaque size of mice treated with PBS or GSO-ctr.

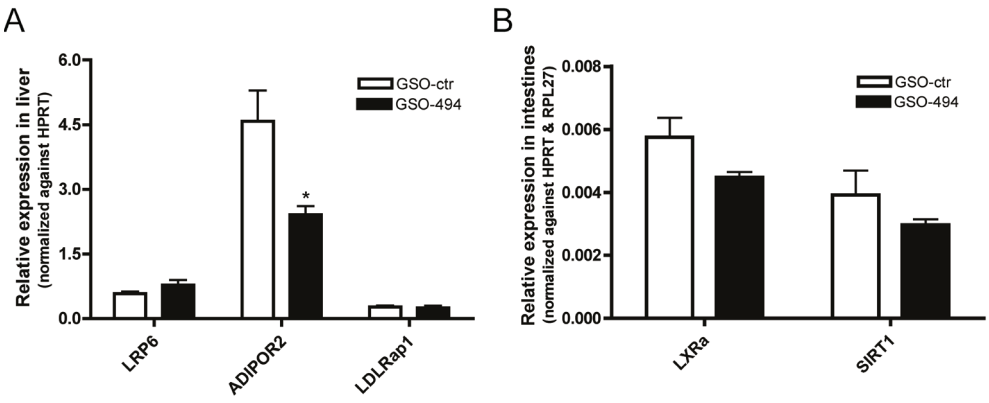

Supplemental Figure 5. (A) Expression of selected target genes LRP6, ADIPOR2 and LDLRap1 in the liver and (B) LXRa and SIRT1 in the intestines at 3 days after GSO injection, normalized against HPRT and RPL27. *P<0.05, compared to GSO-ctr.

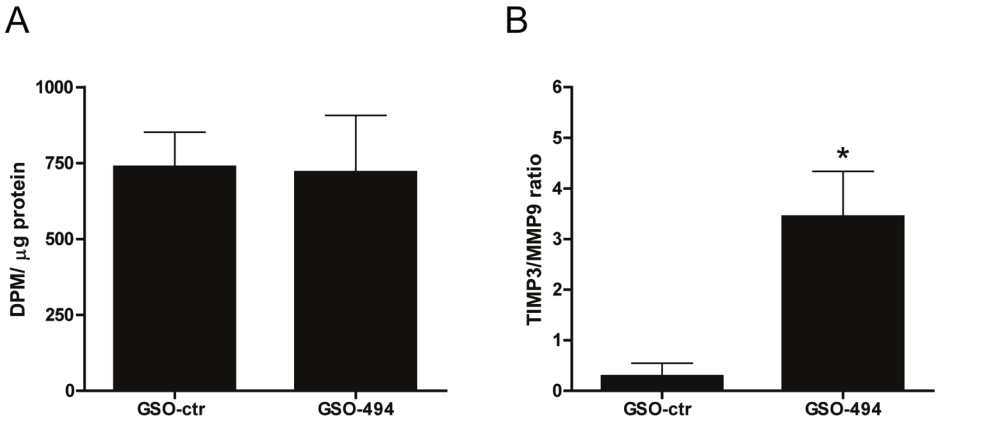

Supplemental Figure 6. (A) Collagen synthesis of smooth muscle cells treated with GSO-494 and (B) TIMP3/MMP9 ratio in macrophages was increased after GSO-494 treatment as TIMP3 expression significantly increased, whereas MMP9 expression remained unaltered. *P<0.05, compared to GSO-ctr.

MiR	# of putative target genes
miR-590-3p	65
miR-129-5p/129ab-5p	46
miR-186	46
***miR-495/1192**	45
*miR-543	45
miR-24/24ab/24-3p	45
miR-150/5127	44
miR-340-5p	43
miR-203	42
*miR-410/344de/344b-1-3p	42
miR-326/330/330-5p	41
*miR-300/381/539-3p	41
miR-128/128ab	41
miR-149	40
miR-33ab/33-5p	40
miR-181abcd/4262	39
*miR-539/539-5p	39
***miR-494**	38
*miR-485-5p/1698/1703/1962	38
*miR-376c/741-5p	37
miR-204/204b/211	37
miR-290-5p/292-5p/371-5p/293	37
miR-384/384-3p	37
miR-93/93a/105/106a/291a3p/294/295/302abcde /372/373/428 /519a/520be/520acd-3p/1378/1420ac	36
miR-197	36
*miR-544/544ab/544-3p	36
miR-23abc/23b-3p	35
miR-124/124ab/506	35
miR-185/882/3473/4306/4644	35
miR-874	34
miR-374ab	34
miR-17/17-5p/20ab/20b-5p/93/106ab/427/518a-3p/519d	33
miR-320abcd/4429	33
miR-214/761/3619-5p	33
*miR-134/3118	32
miR-488	32
miR-339b/339-5p/3586-5p	31
miR-15abc/16/16abc/195/322/424/497/1907	31
***miR-329/329ab/362-3p**	30
miR-873	30
miR-155	30
miR-125a-5p/125b-5p/351/670/4319	30
miR-9/9ab	29
miR-199ab-5p	29
miR-27abc/27a-3p	29
miR-342-3p	29
miR-34ac/34bc-5p/449abc/449c-5p	29
miR-141/200a	28
miR-103a/107/107ab	28
miR-7/7ab	28

Supplemental table 1A. Reversed target prediction performed by analyzing binding sites in human target genes. MiRs of the 14q32 miR gene cluster are identified with an asterisk (*).

MiR	# of putative target genes
miR-466l-3p	63
miR-694	44
miR-325-3p	43
miR-340-5p	42
miR-875-3p.m	42
*miR-410/344de/344b-1-3p	41
miR-1958	40
miR-335-3p	40
miR-5101	40
miR-677/4276	40
miR-590-3p	39
miR-692/4753-3p	39
***miR-495/1192**	37
miR-326/330/330-5p	37
miR-466k/466di-5p	37
miR-181abcd/4262	37
miR-186	36
miR-669f-3p	35
***miR-494**	34
*miR-300/381/539-3p	34
miR-450b-3p/3100-5p	34
miR-141/200a	34
miR-452-3p	34
miR-5110	34
miR-5113	34
miR-669m-3p	34
miR-1587/3083/4505	33
miR-1756b/1896	33
miR-33ab/33-5p	33
miR-545/3065/3065-5p	33
miR-125b-2-3p	32
miR-1941-5p	32
miR-207	32
miR-290-5p/292-5p/371-5p/293	32
miR-3057-3p	32
miR-3474	32
miR-466d/466l-5p	32
miR-488	32
miR-5112	32
*miR-543	32
miR-683	32
miR-712	32
miR-1968	31
miR-214/761/3619-5p	31
miR-297b-3p/466ade-3p/467g	31
miR-3090/4726-3p	31
miR-873	31
*miR-377	30
miR-204/204b/211	30
*miR-1906	30

Supplemental table 1B. Reversed target prediction performed by analyzing binding sites in murine target genes. MiRs of the 14q32 miR gene cluster are identified with an asterisk (*).

MiR	Sequence
mmu-miR-494	5’-UGAAACAUACACGGGAAACCUC-3’
mmu-miR-495	5’-AAACAAACAUGGUGCACUUCUU-3’
mmu-miR-329	5’-AACACACCCAGCUAACCUUUUU-3’
mmu-miR-122	5’-UGGAGUGUGACAAUGGUGUUUG-3’
mmu/hsa-miR-let7c-5p	5’-UGAGGUAGUAGGUUGUAUGGUU-3’
GSO	**Sequence**
mmu-GSO-494	3’-ACTTTGTATGTGCCCTTTGGAG-X-GAGGTTTCCCGTGTATGTTTCA-3’
negative control GSO	3’-TGTACGACTCCATAACGGT-X-TGGCAATACCTCAGCATGT-3’

Supplemental table 2. The sequences of miRs and GSOs used for in vitro and in vivo experiments are listed.

Gene	Forward primer	Reversed primer
CXCR4	GGTGATCCTGGTCATGGGTT	TGACAGGTGCAGCCGGTA
TIMP3	ACTGTGCAACTTTGTGGAGAGGT	GAGACACTCATTCTTGGAGGTCA
CXCL12	TGCATCAGTGACGGTAAACCA	GGCTCTCGAAGAACCGGC
ADIPOR2	CATGTTTGCCACCCCTCAGTATC	AGCCAGCCTATCTGCCCTATG
TGFB2	AGACCCCACATCTCCTGCTAATC	AATCAATGTAAAGAGGGCGAAGGC
LRP6	TTTGAACCCACCACCATCGCCTGCC	GCGGTGCAAAGTGCCGGTAGCTGTA
LDLrap1	CAGCCTCACTAGCCAGCTCATC	CGAACACCTTGTCGTGCATCTTG
LXRa	TCAGCATCTTCTCTGCAGACC	TCATTAGCATCCGTGGGAACA
SIRT1	ACCTTGGAGCAGGTTGCAGGAATCCAA	GCACCTAGGGCACCGAGGAACTACC
ACVR1	GGAAGTCCGCCATTGCCCATC	GGTTGTTTCCCACATCAAGCTGGT
IL33	CCAGGTGCTACTACGCTACTATGAG	AGATGTCTGTGTCTTTGATGGGACT
HPRT	TTGCTCGAGATGTCATGAAGGA	AGCAGGTCAGCAAAGAACTTATAG
RPL27	TGAAAGGTTAGCGGAAGTGC	TTTCATGAACTTGCCCATCTC

Supplemental table 3. List of all primers used for in vitro and in vivo experiments.

Chapter 5

The role of 14q32 microRNAs in restenosis: inhibition of the 14q32 microRNA miR-495 reduces lesion formation, intimal hyperplasia and plasma cholesterol levels in experimental restenosis

Submitted to Atherosclerosis

SMJ Welten[1,2*]

RCM de Jong[1,2*]

A Wezel[3]

MR de Vries[1,2]

MC Boonsta[1]

HAB Peters[1,2]

JW Jukema[4]

TC van der Sluis[5]

R Arens[5]

I Bot[3]

S Agrawal[6]

PHA Quax[1,2 †]

AY Nossent[1,2 †]

[*]Authors contributed equally to this work

[†]Authors contributed equally to this work

[1]Department of Surgery and [2]Einthoven Laboratory for Experimental Vascular Medicine, Leiden University Medical Center, Leiden, the Netherlands

[3]Division of Biopharmaceutic, LACDR, Leiden University, Leiden, the Netherlands

[4]Department of Cardiology and [5]Department of Immunohematology and Blood Transfusion, Leiden University Medical Center, Leiden, the Netherlands

[6]Idera Pharmaceuticals, Cambridge, MA, United States of America

Abstract

Aims: To investigate the role of 14q32 microRNAs in intimal hyperplasia and accelerated atherosclerosis; two major contributors to restenosis. Restenosis occurs regularly in patients treated for coronary artery disease and peripheral arterial disease. We have previously shown that inhibition of 14q32 microRNAs leads to increased post-ischemic neovascularization. Inhibition of 14q32 microRNA miR-494 also decreased atherosclerosis, while increasing plaque stability. We hypothesized that 14q32 microRNA inhibition has beneficial effects on intimal hyperplasia, as well as accelerated atherosclerosis.

Methods and Results: Non-constrictive cuffs were placed around both femoral arteries of normocholesterolemic C57BL/6J mice to induce intimal hyperplasia. Accelerated atherosclerotic plaque formation was induced in hypercholesterolemic ApoE$^{-/-}$ mice by placing semi-constrictive collars around both carotid arteries. 14q32 microRNAs miR-329, miR-494 and miR-495 were inhibited *in vivo* using Gene Silencing Oligonucleotides (GSOs). Effects of microRNA inhibition on intimal hyperplasia, accelerated atherosclerosis and vessel wall remodelling were investigated after 21 days in the cuff model and after 28 days in the collar model. Inhibition of miR-495 led to a 32% reduction of intimal hyperplasia. Moreover, the number of macrophages in the arterial wall of mice treated with GSO-495 was reduced by 55%. Inhibition of miR-329 and miR-494 had less profound effects on intimal hyperplasia. Inhibition of miR-495 also decreased atherosclerotic plaque formation by 52% and plaques of GSO-495 treated animals showed a more stable phenotype. Finally, cholesterol levels were also decreased in GSO-495 treated animals, via reduction of the VLDL-fraction.

Conclusions: Inhibition of miR-495 decreased our primary outcomes, namely intimal hyperplasia and accelerated atherosclerosis, both major contributors to restenosis. Inhibition of miR-495 also favourably affected multiple secondary outcomes, including macrophage influx, plaque stability and total plasma cholesterol levels. We conclude that 14q32 microRNA miR-495 is a promising target for prevention of restenosis.

Introduction

Severe atherosclerosis can cause narrowing and occlusions of affected arteries, that require endovascular intervention (such as balloon angioplasty with or without stenting) to restore and maintain blood flow. Unfortunately, vascular damage inflicted by these interventions can lead to rapid restenosis of the artery[1]. Intimal hyperplasia is an important contributor to restenosis, which is characterized by extracellular matrix rearrangements, smooth muscle cell (SMC) proliferation and inflammation. On top of that, accelerated atherosclerosis is observed, especially under hypercholesterolemic conditions. Intimal hyperplasia is initiated by damage to the endothelium caused by vascular interventions and results in the activation of endothelial cells (ECs). Subsequently, leukocytes adhere to and infiltrate the vessel wall. These leukocytes secrete inflammatory cytokines and chemokines promoting inflammation and release matrix metalloproteinases and growth factors leading to extracellular matrix remodeling as well as smooth muscle cell (SMC) proliferation and migration. Accelerated atherosclerosis is initiated by severe flow disturbance combined with the uptake of lipids by macrophages in the vessel wall and subsequent formation of foam cells under hypercholesterolemic conditions.

MicroRNAs are short endogenous RNA molecules which, through binding to the 3'UTR of their target mRNA, regulate gene expression by inhibiting translation of the mRNA into protein. A single microRNA is able to regulate numerous, up to several hundred, target genes[2]. The fact that a single microRNA can fine-tune the expression of large sets of target genes and thus genetic programs for specific physiological processes makes microRNAs an interesting therapeutic tool for complex diseases[3].

We have previously shown that several members of a large microRNA gene cluster on human chromosome 14 (14q32) are highly involved in vascular remodeling, targeting multiple processes important for neovascularization and atherosclerosis[4]. The 14q32 cluster encodes over 54 microRNA genes and is highly conserved between mammals. Inhibition of 14q32 microRNAs miR-329, miR-487b, miR-494 and miR-495 improved post-ischemic neovascularization in an hind limb ischemia model[4]. Inhibition of 14q32 microRNA miR-494 also reduced collar-induced plaque size (accelerated atherosclerosis), increased plaque stability and decreased plasma cholesterol levels[5]. Han et. al. also observed upregulation of other 14q32 microRNAs (namely miR-431, miR-668 and miR-758) in atherosclerotic aortas of $ApoE^{-/-}$ mice compared to healthy aortas of C57BL/6 mice[6]. Moreover, hypomethylation of 14q32 microRNAs was observed in human atherosclerotic plaques, resulting in the upregulation of several 14q32 cluster members[7]. The role of 14q32 microRNAs in restenosis however, is unknown.

The involvement of microRNAs in restenosis has been demonstrated in several studies and was recently reviewed[8]. For example, inhibition of miR-21 decreased neointima formation in rat carotid arteries after angioplasty, whereas overexpression of miR-29b inhibited the formation of neointima in balloon-injured rat carotid arteries[9,10]. Based on our previous findings, we hypothesized that 14q32 microRNA inhibition would reduce lesion formation in experimental models for restenosis. In this study, we inhibited 14q32 microRNAs miR-329, miR-494 and miR-495 in a model for intimal hyperplasia and subsequently, we inhibited miR-329 and miR-495 in an accelerated atherosclerosis

model and examined the effects on primary outcomes of vascular remodeling or arterial stenosis. In addition, we studied the effects of 14q32 microRNA inhibition on secondary outcomes such as target gene regulation, vascular cell proliferation, plaque stability and cholesterol homeostasis.

Methods

Mice

This study was performed in compliance with Dutch government guidelines and the Directive 2010/63/EU of the European Parliament. All animal experiments were approved by the Institutional Committee for Animal Welfare of the Leiden University Medical Center (approval reference numbers 13119 and 12165). Male C57BL/6J (10 weeks old) animals were purchased from the Jackson Laboratory. Male ApoE$^{-/-}$ (7-14 weeks old at start of diet) were bred in the local animal breeding facility (Gorlaeus Laboratories, Leiden University, Leiden, the Netherlands). C57BL/6J mice received chow diet during the whole experiment. ApoE$^{-/-}$ mice were fed a Western-type diet, containing 0.25% cholesterol and 15% cacao butter (Special Diet Services) for six weeks, two weeks prior to surgery. All animals received food and water ad libitum during the entire experiment. During surgery, mice were anesthetized by intraperitoneal (i.p) injection of midazolam (8mg/kg, Roche Diagnostics), medetomidine (0.4 mg/kg, Orion) and fentanyl (0.08 mg/kg, Janssen Pharmaceutica). The adequacy of the anaesthesia was monitored by keeping track of the breathing frequency and the response to toe pinching of the mice. After surgery, mice were antagonized with a subcutaneous injection of flumenazenil (0.5 mg/kg; Fresenius Kabi), antesedan (2.5 mg/kg; AST Pharma) and buprenorphine (0.1 mg/kg; MSD Animal Health).

Femoral artery cuff mouse model

Intimal hyperplasia was induced by placement of a non-constrictive cuff around the femoral artery of C57BL/6J mice (n=10 per group). The left and right femoral arteries were isolated and a rigid, non-constrictive polyethylene cuff was placed around the artery. Thereafter, the wound was closed by a continuous suture. After 21 days, mice were anesthetized and sacrificed via perfusion. Venous blood was drawn in EDTA collection tubes and centrifuged (6000 rpm for 10 min at 4°C) to obtain plasma. The thorax was opened and mild pressure-perfusion (100mm Hg) with PBS was performed for 4 minutes by cardiac puncture in the left ventricle. Lymph nodes and spleen were isolated for FACS analysis. After perfusion with 3.7% formaldehyde, cuffed femoral arteries were harvested, fixed 5 hours in formaldehyde and paraffin-embedded.

Carotid collar mouse model

Carotid artery plaque formation was induced by perivascular collar placement as described earlier[11]. In brief, a semi-constrictive cuff collar was placed around both left and right carotid arteries to induce accelerated atherosclerosis. Four weeks (28 days) after collar placement, mice (n=15 per group) were anesthetized and sacrificed via perfusion, after which carotid arteries were harvested, fixed overnight in formaldehyde and paraffin-embedded.

Gene Silencing Oligonucleotides (GSOs)

Gene Silencing Oligonucleotides (GSOs) were designed with perfect reverse complementarity to the mature target microRNA sequences and synthesized by Idera Pharmaceuticals (GSOs kindly provided by Idera pharmaceuticals). As a negative control, a scrambled sequence was used, designed not to target any known murine microRNA. GSOs consist of two single-stranded 2'O-methylated DNA strands, linked together at their 5'ends by a phosphothioate-linker to avoid TLR-activation[12]. Sequences of microRNAs and GSOs used are given in Supplemental table 1.

Uptake of IRDye-800CW labelled GSOs

Two adult male C57BL/6J mice received one non-constrictive cuff around the left femoral artery, while the contra-lateral femoral artery was left unaffected. One day prior to cuff placement, mice were injected intravenously with IRDye-800CW-labelled GSO-329 (0.4 mg/mouse; Idera Pharmaceuticals) or with IRDye-800CW-unlabelled control. Mice were sacrificed by cervical dislocation, 24 hours after cuff placement. Near-InfraRed (NIR) fluorescence measurements were performed using the FLARE™ NIR imaging system[13].

Treatment with GSOs in *in vivo* models

In case of the femoral artery cuff model, mice received a single intravenous injection of 1 mg GSO dissolved in 200 µl PBS, one day before cuff placement. In case of the carotid collar model, mice received a first intravenous injection of 1 mg GSO dissolved in 200

µl PBS, 4 days after collar placement. At day 18 after collar placement, mice received a second injection of 0.5 mg GSO dissolved in 200 µl PBS.
A subset of mice (n=3 per group for cuff model and n=6 per group for collar model) was sacrificed 3 days after the first GSO injection in order to establish downregulation of microRNAs *in vivo*.

Plasma analysis

Blood was collected from mice prior to surgery, at sacrifice and at indicated timepoints (day 2, day 7, day 21 in cuff model for FACS analysis), by tail bleeding. The concentration of cholesterol in plasma was determined by incubation with 0.025 U/ml cholesterol oxidase (Sigma) and 0.065 U/ml peroxidase and 15 µg/mL cholesterol esterase (Roche Diagnostics) in polyoxyethylene-9-laurylether, and 7.5% methanol. Precipath (standardized serum; Roche Diagnostics) was used as an internal standard. Absorbance was measured at 490 nm.
For lipid profiling, plasma was pooled (n=3 mice per sample) and diluted 6 times, after which fractionation of plasma lipoproteins was performed using an AKTA-FPLC. Total cholesterol levels were determined in each fraction and in the original pooled sample using a colorimetric assay (Roche Diagnostics, kit 11489232). Absorbance was measured at 490 nm.

Histology and morphometry

Formaldehyde fixed carotid and femoral arteries were paraffin-embedded and 5 µm thick cross sections of arteries were stained to visualize vessel morphology. Paraffin sections of femoral arteries were stained with Weigert's Elastin to visualize the elastic laminae to determine intimal hyperplasia. Paraffin sections of carotid arteries were stained with hematoxylin-phloxine-saffron (HPS) to determine plaque size. Sirius red staining was used to visualize collagen content.
To visualize macrophages and smooth muscle cells, cross sections of arteries were re-hydrated and endogenous peroxidase activity was blocked. Macrophages and smooth muscle cells were stained using anti-Mac3 (BD Pharmingen, clone M3/84) and anti-smooth muscle actin (SMA; DAKO, clone 1A4) respectively and counterstained using haematoxylin.
To assess proliferation of smooth muscle cells, cross sections of femoral arteries were stained using anti-Ki-67 (proliferation marker) (Abcam, clone SP6) and anti-SMA (DAKO, clone 1A4). Ki-67 was visualized using Alexa 647 conjugated secondary antibody (Invitrogen) and SMA was visualized using Alexa 555 conjugated secondary antibody (Invitrogen). Nuclei were stained using Fluoroshield with DAPI (Sigma).
All quantifications of femoral arteries were performed on six equally spaced cross sections through the cuffed femoral artery by a single blinded observer. Vessel wall parameters, collagen content and smooth muscle cell area were quantified using Qwin (Leica). Macrophage content and the number of Ki-67/SMA positive cells in the cuffed femoral artery of C57Bl6/J mice were counted manually.

Morphometric analysis of carotid arteries was performed on atherosclerotic lesions at the site of maximal stenosis by a single blinded observer. Plaque size, necrotic core, collagen content, smooth muscle cell area and macrophage content were quantified using image analysis software for morphometric analysis (Qwin, Leica).

Cell culture

Bone marrow (BM) cells isolated from C57BL/6J mice were cultured for 7 days in RPMI medium supplemented with 20% inactivated fetal calf serum (FCSi, PAA), 2 mmol/L l-glutamine (PAA), 100 U/mL penicillin and 100 µg/mL streptomycin and 30% L929 cell-conditioned medium, as the source of macrophage colony-stimulating factor (M-CSF), to generate BM-derived macrophages (BMDMs)[14].
Primary cultured murine vascular smooth muscle cells (vSMC) and cell lines for fibroblasts (3T3) and endothelial cells (H5V) were cultured in complete DMEM GlutaMAX™ medium (Gibco) supplemented with 10% FCSi, 1% penicillin/streptomycin.
VSMCs, H5V and 3T3 cells were plated in triplicate at a density of 10^6 cells/mL. GSOs were added overnight at a concentration of 5 µg/mL, after which the cells were lysed for RNA isolation. For BMDMs, GSOs were added immediately after isolation from BM in a concentration of 5 µg/mL. After three days medium was refreshed with a similar addition of GSOs in a concentration of 5 µg/mL. Four days later, medium was removed and cells were lysed for RNA isolation.

RNA isolation, cDNA synthesis and quantitative PCR (qPCR)

Two femoral artery segments from 3 days after cuff placement were pooled and homogenized by grounding using a Pellet Pestle Cordless Motor (Kimble Chase Life Science). Three carotid artery segments from 7 days after collar placement (3 days after GSO injections) were pooled and homogenized using the same Pellet Pestle Cordless Motor. Liver was isolated and homogenized by grounding with pestle and mortar in liquid nitrogen. Total RNA was extracted using a standard TRIzol-chloroform extraction method. RNA concentration and purity were examined by nanodrop (Nanodrop Technologies). MiR quantification was performed using Taqman® miR assays (Thermo Fisher) following manufacturer's protocol. qPCR was performed on the Viia7 system (Thermo Fisher). Normalization of data was performed using a stably expressed endogenous control (snRNA U6 and mmu-let-7c).

For *in vitro* and *in vivo* experiments, total RNA was extracted from cells and tissues using the standard TRIzol-choloform extraction method. RNA was reverse transcribed using high-capacity RNA to cDNA RT kits (Life technologies) and used for quantitative analysis of mouse genes with the Viia7 system (Applied Biosystems). The relative expression of putative miR-495 target genes was quantified using the QuantiTect SYBR® Green technology (Qiagen). Normalization of the data was performed by using stably expressed endogenous controls (Hprt and Rpl27). Primer sequences can be found in Supplemental Table 2.

Cholesterol efflux assay

BMDMs, cultured and treated with GSOs as described above, were plated at a density of $0.5x10^6$ cells per well. The following day, medium was changed with DMEM containing 10% BSA and 1 µCi/mL ^{3}H-cholesterol (loading medium) to which either GSO-control of GSO-495 was added and cells were treated with 20 mg/mL cholesterol. After 24 hours, loading medium was replaced with DMEM with 10% BSA for 1 hour. Next, medium was changed for control DMEM with 10% BSA or DMEM with 10% BSA supplemented with HDL (50 µg/mL). After 24 hours, radioactivity in the cells and medium was determined by liquid scintillation counting (Packard 1500 Tricard). Cholesterol efflux was defined as $(dpm_{medium}/dpm_{cells}+dpm_{medium})x100\%$ and shown as the percentage of HDL specific efflux, corrected for non-specific efflux to control medium.

Statistical analysis

Data are expressed as mean ± SEM. Comparisons of absolute miR expression were performed using one-way ANOVA< followed by a Tukey's multiple comparison test. Comparisons of multiple treatment groups with the control group were performed using one-way ANOVA, followed by multiple comparisons without correction for multiple t-tests. Two-tailed Student's t-tests were used to compare a single treatment group with the control group. A level of $p<0.05$ was considered significant.

Results

***In vivo* inhibition of miR-329, miR-494 and miR-495 after GSO treatment in the cuff model**

Expression levels of 14q32 microRNAs miR-329, miR-494 and miR-495 were measured in the femoral arteries of wildtype C57BL/6J mice and the carotid arteries of ApoE$^{-/-}$ mice, representing the two models used to study post-interventional intimal hyperplasia and accelerated atherosclerosis. Expression of miR-329, miR-494 and miR-495 was also measured in the aorta of ApoE$^{-/-}$ mice. In the femoral arteries of wildtype mice, expression of miR-329 and miR-495 was highest, followed by miR-494 expression (Figure 1A (absolute expression) and Figure 1B, left panel (relative expression)). As we have previously established, the expression of miR-495 was highest in the aorta of ApoE$^{-/-}$ mice (Figure 1A (absolute expression) and Figure 1B, middle panel (relative expression)), whereas in the carotid arteries of these animals, both miR-495 and miR-494 were highly expressed (Figure 1A (absolute expression) and Figure 1B, right panel (relative expression))[5].

Next, we measured expression of these microRNAs after GSO treatment in the femoral cuff model. Expression of miR-329, miR-494 and miR-495 was measured at a single timepoint in the femoral artery of in C57BL/6J mice, 3 days after cuff placement, 4 days after GSO injection. MiR-329 was significantly downregulated by 52% in the femoral arteries of C57BL/6J mice compared to GSO-control treated animals. Although not statistically significant at this specific timepoint, microRNA inhibition is a time-dependent process[4] and miR-495 was downregulated by 34% in the femoral arteries of C57BL/6J mice (p=0.22). For miR-494, we could not observe downregulation at this specific timepoint (Figure 1C (absolute expression) and 1D (relative expression)).

Uptake of GSOs at site of cuff placement

To visualize uptake of GSOs in the femoral artery, C57BL/6J mice were injected with either IRDye-800CW-labelled GSO-329, or IRDye-800CW-unlabelled control, one day prior to cuff placement. As expression of miR-329 was highest in the femoral artery, we injected mice with IRDye 800CW-labelled GSO-329. Since the GSO chemistry is comparable for GSO-329, GSO-494 and GSO-495, we assume similar uptake of the other GSOs. Uptake of labelled GSO-329 was observed in both cuffed (left) and non-cuffed (right) femoral arteries, whereas minimal uptake was detected in the femoral arteries of mice treated with IRDye-800CW control (Figure 1C). These data demonstrate effective uptake of GSOs in the femoral arteries. Previously, we have shown that GSOs are also taken up specifically in the carotid arteries of ApoE$^{-/-}$ mice, 4 days and 28 days after collar placement[5].

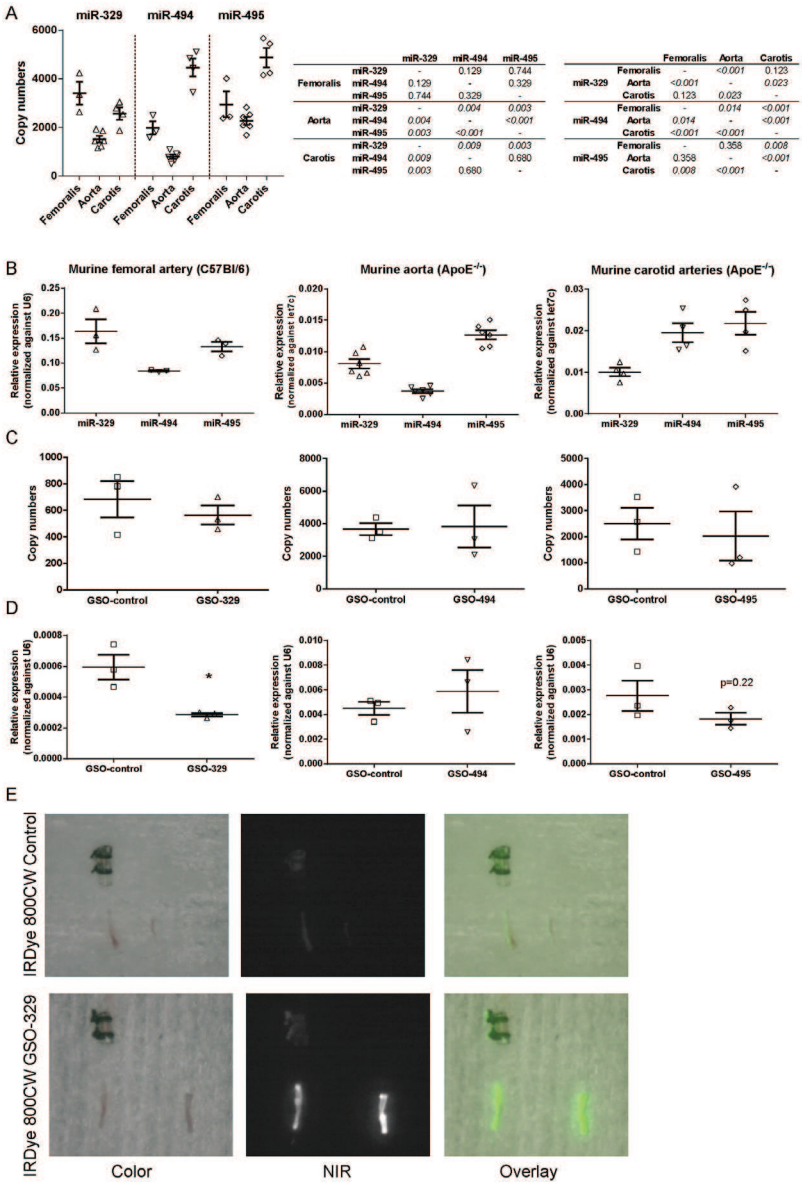

		miR-329	miR-494	miR-495
Femoralis	miR-329	-	0.129	0.744
	miR-494	0.129	-	0.329
	miR-495	0.744	0.329	-
Aorta	miR-329	-	*0.004*	*0.003*
	miR-494	*0.004*	-	*<0.001*
	miR-495	*0.003*	*<0.001*	-
Carotis	miR-329	-	*0.009*	*0.003*
	miR-494	*0.009*	-	0.680
	miR-495	*0.003*	0.680	-

		Femoralis	Aorta	Carotis
miR-329	Femoralis	-	*<0.001*	0.123
	Aorta	*<0.001*	-	*0.023*
	Carotis	0.123	*0.023*	-
miR-494	Femoralis	-	*0.014*	*<0.001*
	Aorta	*0.014*	-	*<0.001*
	Carotis	*<0.001*	*<0.001*	-
miR-495	Femoralis	-	0.358	*0.008*
	Aorta	0.358	-	*<0.001*
	Carotis	*0.008*	*<0.001*	-

Figure 1. Expression and inhibition of 14q32 microRNAs miR-329, miR-494 and miR-495. (A) An estimation of absolute expression (±SEM) of miR-329, miR-494 and miR-495 in the femoral artery of C57BL/6J mice (n=3 pooled samples, 3 femoral arteries were pooled for 1 sample), and in the aorta (n=6) and carotid artery (n=4 pooled samples, 3 carotids were pooled for 1 sample) of ApoE$^{-/-}$ mice. (B) Relative expression levels (±SEM) of miR-329, miR-494 and miR-495 in the femoral artery of C57BL/6J mice and the aorta and carotid artery of ApoE$^{-/-}$ mice (data on microRNA expression in ApoE$^{-/-}$ mice was adapted with permission from Wezel *et.al*[5].).. (C) Absolute expression (±SEM) of miR-329, miR-494 and miR-495 in cuffed femoral arteries, 4 days after GSO treatment (n=3 pooled samples, 3 femoral arteries were pooled for 1 sample). (D) Mean expression levels, relative to U6, of miR-329, miR-494 and miR-495 in cuffed femoral arteries are shown here 4 days after GSO treatment (±SEM). *p<0.05. (E) Uptake of IRDye-800CW-labelled GSO-329 in the cuffed femoral artery. In each micrograph the cuffed femoral artery (cuff removed; left) and contra-lateral non-cuffed femoral artery (right) are displayed. Upper panels show femoral arteries of IDRye-800CW-unlabelled control treated animals and lower panels femoral arteries of IRDye-800CW-labelled GSO-329 treated animals, 24 hours after cuff placement and 48 hours after GSO-injection. Colour images are shown on the left, near-infrared (NIR) images in the middle and an overlay of colour and NIR images is shown on the right.

Effects of miR-329, miR-494 and miR-495 inhibition on vascular remodelling in C57BL/6J mice

At 21 days after cuff placement, intimal hyperplasia was significantly reduced by 33% following treatment with GSO-495 compared to GSO-control. Although not statistically significant, treatment with GSO-329 also decreased intimal hyperplasia by 24% (p=0.09), whereas GSO-494 treatment had no effect on intimal hyperplasia (Figure 2A and representative images in Figure 2B). In addition, a decreased intima/media ratio was observed following GSO-495 treatment (35% reduction). This ratio was not decreased in GSO-329 and GSO-494 treated animals (Supplemental Figure 1A). No differences were found regarding luminal area and lumenstenosis following GSO-494 or GSO-495 treatment (Supplemental Figure 1B and 1C). GSO-329 treatment significantly increased luminal area and decreased lumenstenosis in these animals (Supplemental Figure 1B and 1C). These data show a beneficial effect of GSO-495 treatment on intimal hyperplasia in C57BL/6J mice.

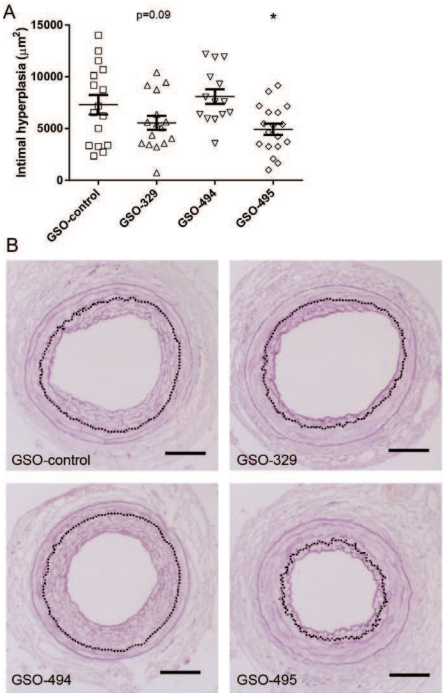

Figure 2. Inhibition of 14q32 microRNA miR-495 reduces intimal hyperplasia. (A) Quantification of intimal hyperplasia 21 days after cuff placement in C57BL/6J mice (n=10 per group) treated with GSOs (±SEM). *p<0.05 compared to GSO-control. (B) Representative images of elastin staining of cuffed femoral arteries, dashed line represents lamina elastic interna (scale bar = 50 μm).

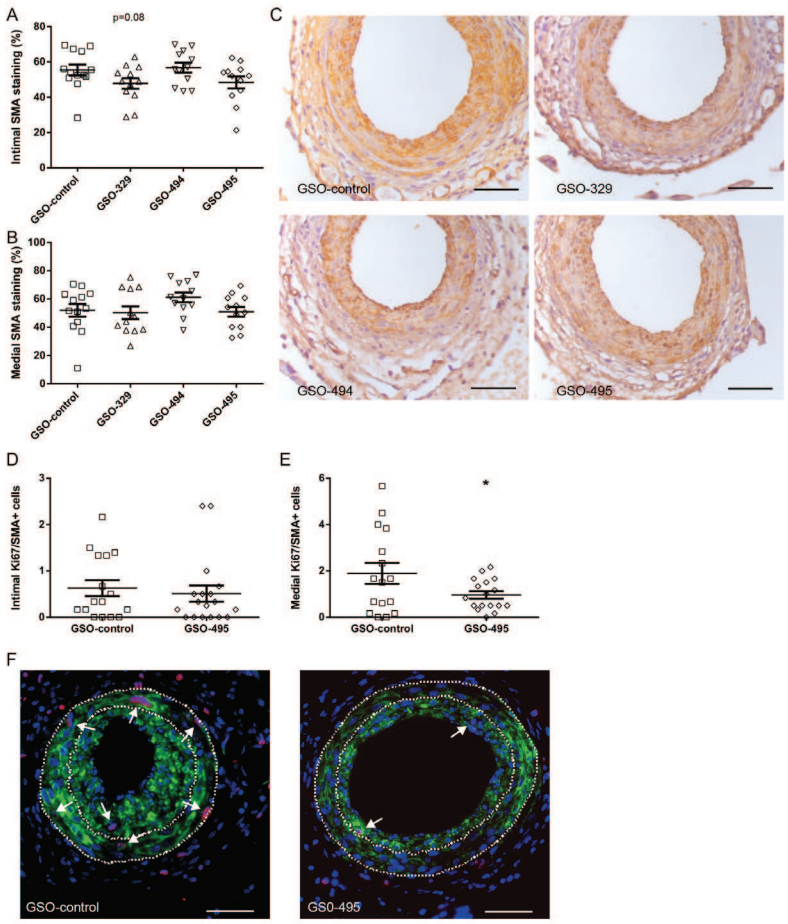

Figure 3. Inhibition of 14q32 microRNA miR-495 reduces vascular smooth muscle cell proliferation. Quantification of intimal (A) and medial (B) smooth muscle cell area (%) 21 days after cuff placement in C57BL/6J mice (n=10 per group) treated with GSOs (±SEM). (C) Representative images of SMA staining of cuffed femoral arteries (scale bar = 50 µm). Quantification of intimal (D) and medial (E) smooth muscle cell proliferation 21 days after cuff placement in C57BL/6J mice (n=10 per group) treated with GSO-495 (±SEM). *p<0.05. (F) Representative images of Ki67/SMA staining of cuffed femoral arteries, arrows indicate Ki67/SMA positive cells, dashed lines indicate the elastic laminae (scale bar = 50 µm). Nuclei are shown in blue, SMA staining in green and Ki67 in red.

Effects of miR-329, miR-494 and miR-495 inhibition on vessel wall composition in C57BL/6J mice

To assess the effect of microRNA inhibition on vessel wall composition following cuff placement, we (immuno-)stained serial sections with SMA, Mac-3 or Sirius red. No differences were observed regarding SMC content in the intima and media of GSO treated groups (Figure 3A and 3B, representative images in Figure 3C). Since GSO-495 treatment reduced intimal hyperplasia, we examined the number of proliferating SMCs in this group by staining for Ki67 and SMA and compared the number of double positive cells ($Ki67^+/SMA^+$ cells) in GSO-495 treated animals with GSO-control treated animals (Figure 3D and 3E). Inhibition of miR-495 reduced the number of proliferating SMCs by 47% in the media of these animals, but not in the intima (Figure 3D and 3E, representative images in Figure 3F)

Following GSO- 494 and GSO-495 treatment, macrophage influx was significantly reduced by 35% and 78% respectively in the intimal area compared to GSO-control (Figure 4A). Macrophage influx in the medial area was reduced, although not statistically significant, by 35% following GSO-494 (p=0.13) treatment and by 27% following GSO-495 (p=0.23) treatment (Figure 4B, representative images in Figure 4C). MicroRNA inhibition did not alter collagen content in either the intima or the media of GSO treated animals (Supplemental Figure 2A and 2B, representative images in Supplemental Figure 2C).

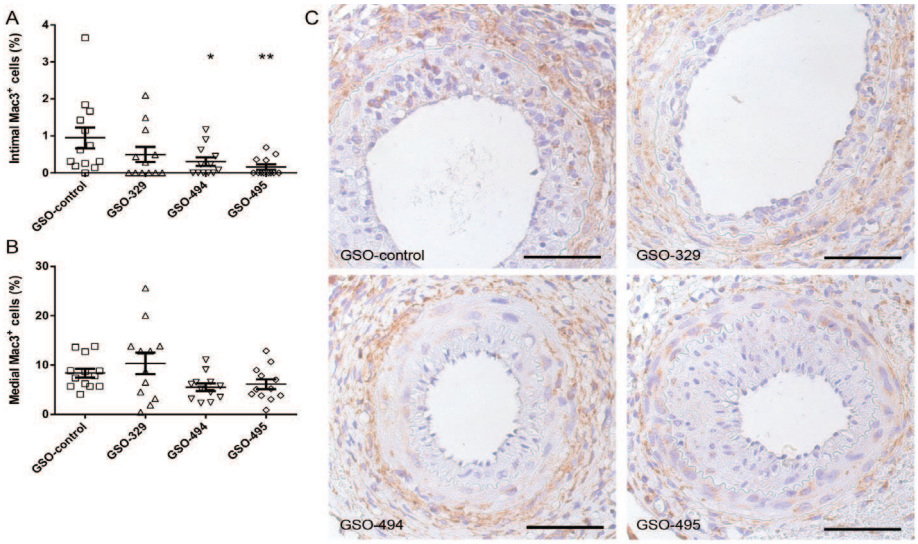

Figure 4. Inhibition of 14q32 microRNA miR-495 reduces macrophage influx. Quantification of intimal (A) and medial (B) macrophage influx (%) 21 days after cuff placement in C57BL/6J mice (n=10 per group) treated with GSOs (±SEM). *p<0.05, **p<0.01 compared to GSO-control. (C) Representative images of Mac3 staining of cuffed femoral arteries (scale bar = 50 μm).

Effects of miR-495 and miR-329 inhibition in the carotid collar mouse model in ApoE$^{-/-}$ mice

Next, we assessed the effects of 14q32 microRNA miR-329 and miR-495 inhibition on accelerated atherosclerotic plaque formation. Atherosclerotic plaque sizes were significantly decreased with 53% in GSO-495 treated animals (Figure 5A and representative images in Figure 5B). In GSO-329 treated animals, a trend towards a 43% decrease in atherosclerotic plaque size compared to GSO-control animals (p=0.09, Figure 5A, representative images Figure 5B) was observed. In addition to the decreased plaque size, composition of the lesions was also affected by GSO-495 treatment. Inhibition of miR-495 resulted in smaller necrotic core sizes (60% reduction), whereas inhibition of miR-329 had no significant effects on necrotic core size (Figure 6A). In addition, the percentage of macrophage content in the lesions was decreased by 30% in GSO-495 treated animals (Figure 6B), but not in GSO-329 treated animals. No difference was observed in the percentage of SMA positive lesion area between groups (Figure 6C). Inhibition of miR-495, but not miR-329, increased collagen content by 139% (Figure 6D), further increasing plaque stability.

Plasma cholesterol levels in GSO-495 treated animals were significantly decreased with 13% (Figure 5C). Lipid profiling using AKTA-FPLC revealed a reduction in the VLDL fraction after treatment with miR-495 inhibition (Figure 5D). This reduction in plasma cholesterol and VLDL levels was not observed in

animals treated with GSO-329 (Figure 5C and 5D). In order to elucidate the mechanism behind the VLDL reduction in GSO-495 treated animals, we investigated the *in vitro* cholesterol efflux in macrophages. We found that treatment of macrophages with GSO-495 significantly increased cholesterol efflux *in vitro* by 96% (Figure 5E).

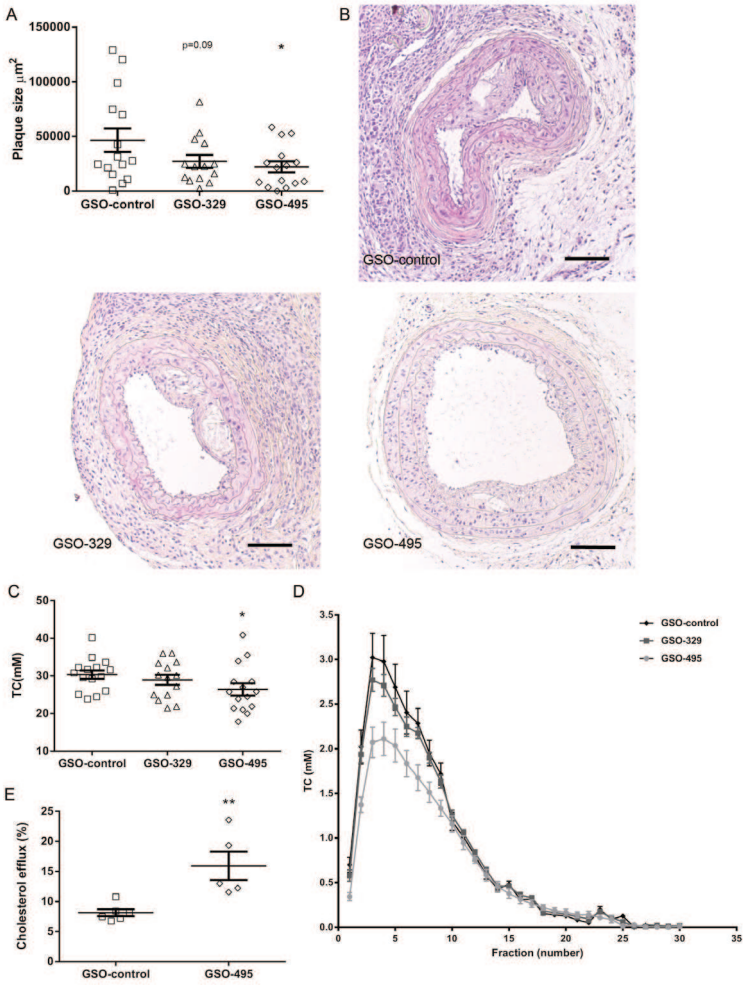

Figure 5. Inhibition of 14q32 microRNA miR-495 reduces plaque size and cholesterol levels. (A) Quantification of plaque size 28 days after collar placement in ApoE$^{-/-}$ mice (n=15 per group) treated with GSO-control, GSO-329 or GSO-495. *p<0.05 compared to GSO-control. (B) Representative images of HPS staining of carotid arteries (scale bar = 100 µm). (C) Total cholesterol levels of ApoE$^{-/-}$ mice treated with GSO-control, GSO-329 or GSO-495, 6 weeks after start of the western type diet. *p<0.05 compared to GSO-control. (D) Cholesterol profile of GSO treated ApoE$^{-/-}$ mice (n=5 pooled samples per group, plasma samples of 3 animals were pooled per sample) analysed using AKTA-FPLC. (E) Quantification of cholesterol efflux (%) from macrophages treated with GSO-control or GSO-495. **p<0.01.

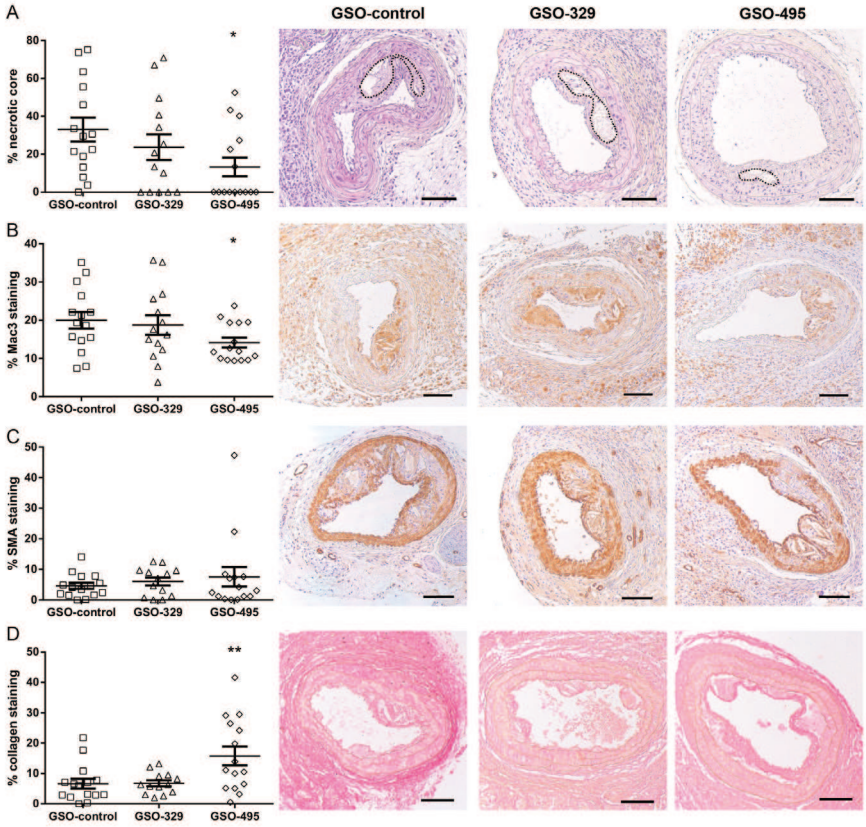

Figure 6. Inhibition of 14q32 microRNA miR-495 increases plaque stability 28 days after collar placement in ApoE$^{-/-}$ mice.
(A) Quantification of necrotic core size. (B) Percentage (%) of macrophage influx. (C) Percentage (%) of smooth muscle cell area. (D) Percentage (%) of collagen content. *p<0.05, **p<0.01 compared to GSO-control. Representative images of (A) HPS staining, (B) Mac3 staining, (C) SMA staining and (D) Sirius red staining are shown (n=15 mice per group, scale bar = 100 µm).

Target gene regulation after miR-495 inhibition

We investigated the effects of miR-495 inhibition on target gene regulation. We made a selection of putative target genes, that have predicted binding sites for miR-495 in their 3'UTR. Treatment with GSO-495 in the collar model resulted in decreased expression of miR-495 in the carotids, 3 days after GSO injection (23% decreased, p=0.25, Figure 7). Although *in vivo* inhibition of miR-495 was not statistically significant at this specific timepoint, we could observe upregulation of miR-495 target genes Tgfβ2 and Il13ra1 in the carotid arteries (Figure 7B). Furthermore, expression of target genes Acvr1 (p=0.07) in the carotids and Il10 (p=0.05) in the spleen were upregulated in GSO-495 treated animals (Figure 7B). In addition, we determined the expression of multiple cholesterol metabolism related target genes of miR-495 in the liver but no differences were observed in the expression of Lrp6, Mttp, Ldlr and Abca1 (Supplemental Figure 3).

To investigate the effects of miR-495 inhibition on various individual cell types in vascular remodelling, H5V endothelial cells, vSMCs, 3T3 fibroblasts and BMDMs were treated with GSOs against miR-495. Multiple target genes with predicted binding sites for miR-495 were examined, including cytokines,

complement components, lipid-related target genes and tissue inhibitors of metalloproteinases (TIMPs). Inhibition of miR-495 led to upregulation of Tlr7 in H5V cells and vSMCs (p=0.05), whereas the anti-inflammatory Il10 was upregulated in 3T3 cells (p=0.06) and H5V cells (p=0.11) (Supplemental Figure 4). Other genes that were upregulated after miR-495 inhibition included Cdknb1 (p=0.09) in 3T3 cells, Cd59 (p=0.08) and Ccr2 (p=0.06) in BMDMs.

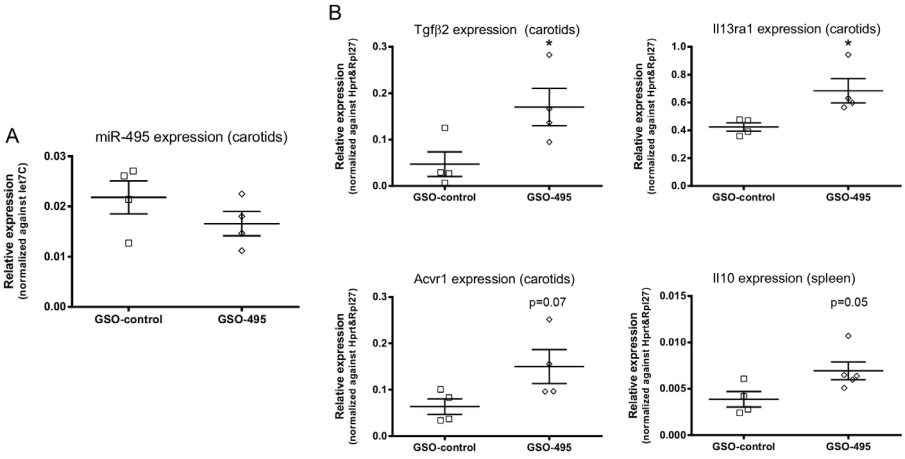

Figure 7. ***In vivo*** **inhibition of miR-495 increases putative target gene expression.** (A) Mean expression levels of miR-495 in carotid arteries, relative to let7c, are shown here 3 days after GSO treatment in ApoE$^{-/-}$ mice (n=4 pooled samples per group, 3 carotids were pooled per sample). (B) Mean expression levels of putative miR-495 target genes Tgfβ2, Il13ra1 and Acvr1 in carotids (n=5 samples per group; 3 carotids were pooled per sample), and Il10 in spleen (n=5 per group), relative to Hprt and Rpl27, are shown here 3 days after GSO treatment in ApoE$^{-/-}$ mice. *p<0.05.

Discussion

Here, we hypothesized that inhibition of 14q32 microRNAs would reduce restenosis through decreased intimal hyperplasia and decreased accelerated atherosclerosis. We show that inhibition of miR-495 leads to less intimal hyperplasia following vascular injury and decreased plaque formation in atherosclerosis prone mice, whilst increasing plaque stability in these animals. In addition, we investigated the effects of 14q32 microRNA miR-495 inhibition on secondary outcomes such as target gene regulation, smooth muscle cell proliferation, plaque stability and cholesterol homeostasis. The 14q32 microRNA gene cluster is the largest known mammalian microRNA gene cluster to date and many 14q32 microRNAs have been implicated within human disease[15]. Recently, we have reported the role of multiple microRNAs from this cluster in several aspects of vascular remodelling, including angiogenesis, arteriogenesis and atherosclerosis[5, 16].

MicroRNAs are known for their ability to regulate the expression of numerous genes[17]. Especially miR-495 may have the ability to target a large number of genes; bioinformatics analysis using www.targetscan.org (TargetScan 7.0, consulted January 2016) revealed over 5103 transcripts with in total 7998 putative binding sites for human miR-495 (of which 1015 conserved sites and 6983 poorly conserved sites) and 4879 transcripts with putative binding sites for murine miR-495 (and a total of 7886 sites). It is therefore unlikely that the observed effects are attributable to strong regulation of one target gene in particular, but are rather the sum of modest regulation of multiple target genes involved in all aspects of the processes of vascular remodelling studied here, namely intimal hyperplasia and accelerated atherosclerosis. Moreover, binding of a certain microRNA to its target gene does not completely silence its expression, but rather downtunes its expression[2]. This corresponds to the modest effects that we observed on miR-495 target gene regulation.

In vivo, treatment with GSO-495 led to upregulation of target genes Tgfβ2 and Il13ra1 and more modest upregulation of Acvr1 and Il10 targets. IL-13, one of the cytokines secreted by $CD4^+$ Th2-cells, inhibits macrophage activation and decreases the production of pro-inflammatory cytokines by activated macrophages.[18] More specifically, the IL-13 receptor alpha 1 chain (Il13ra1) is implicated within the signal transduction route of IL-13 and inhibits interferon-γ induced gene expression in macrophages[19]. Likewise, IL-10, which is also a Th2 cytokine has anti-inflammatory properties and protects against atherosclerosis and neointima formation by inhibiting macrophage activation and inhibition of matrix metalloproteinases[20-23]. These findings are in line with our results that GSO-495 treatment decreases macrophage numbers within the arterial lesions investigated. Tgfβ2 is known to be an important regulator of collagen synthesis[24]. This is in line with the observed increase in collagen content and upregulation of Tgfβ2 in the carotid artery. Furthermore, it has been shown that inhibition of Tgfβ1, -β2 and -β3 activity induces atherosclerosis and favours development of an unstable plaque phenotype, which suggests Tgfβ2 has atheroprotective properties and could therefore contribute to the reduced plaque formation seen in this study[25].

Inhibition of miR-495 reduced proliferation of SMCs in neointimal lesions of GSO-495 treated animals. Proliferation and migration of vascular SMCs is one of the most important events in intimal hyperplasia[26]. In agreement with the reduced proliferation of SMCs after miR-495 inhibition, overexpression of miR-495 has previously been shown to increase proliferation of neonatal rat cardiomyocytes[27]. On the other hand, it has also been shown that miR-495 promotes proliferation of HUVECs[28]. These and our findings demonstrate different actions of microRNAs in different cell types, which comes with both benefits and limitations for possible therapeutic uses.

Following GSO-495 treatment we found a reduction of total cholesterol levels of 13%, which could mainly be attributed to a reduction of VLDL. One of the most frequently used therapy against atherosclerosis is the use of statins, which aims for reduction of (V)LDL cholesterol levels in the blood. Statins reduce (V)LDL cholesterol levels in a range of 40 to 60% depending on the dose administered, which subsequently reduces the risk of ischemic heart disease by 61% and of stroke by 17%[29]. Although we cannot explain the reduced plaque size and increased stability of the plaques completely by the modest reduction of VLDL plasma cholesterol levels, it is plausible that this reduction contributes, at least partly, to the reduced plaque size and increased plaque stability. This hypothesis is supported by the observed increase in cholesterol efflux from macrophages *in vitro* following GSO-495 treatment. This suggests GSO-495 can inhibit atherogenesis by facilitating removal of cholesterol from the vessel wall to the liver in an HDL dependent manner.

Inhibition of miR-495 also led to a decrease in necrotic core size and macrophage content, while it increased collagen content in atherosclerotic lesions. A decrease in necrotic core size and macrophage content together with an increase in collagen content are characteristics of increased plaque stability[30]. MiR-495 was thus shown to not only contribute to atherosclerotic lesion formation, but also plaque stability in $ApoE^{-/-}$ mice. To our knowledge, we are the first to report that inhibition of miR-495 leads to therapeutic benefits in two models of vascular remodelling, namely the femoral artery cuff model for intimal hyperplasia and the carotid collar model for accelerated atherosclerosis. Not only were the lesions in these models reduced in size, but the lesions also contained fewer macrophages and in case of the carotid collar model, plaque stability was increased. Atherosclerosis is the most common underlying cause of cardiovascular disease and can lead to, amongst others, myocardial infarction, ischemic stroke and peripheral arterial disease. Restenosis occurs upon endovascular interventions performed to target these atherosclerotic lesions and involves the re-narrowing of arteries. Reducing both intimal hyperplasia and accelerated atherosclerosis is of crucial importance for the prevention of restenosis.

Taken together, we conclude that miR-495 inhibition improves both primary and secondary parameters of restenosis. Inhibition of miR-495 reduces both intimal hyperplasia and accelerated atherosclerosis, which makes it a highly attractive therapeutic target for patients treated for occlusive arterial disease who are at risk of developing restenosis.

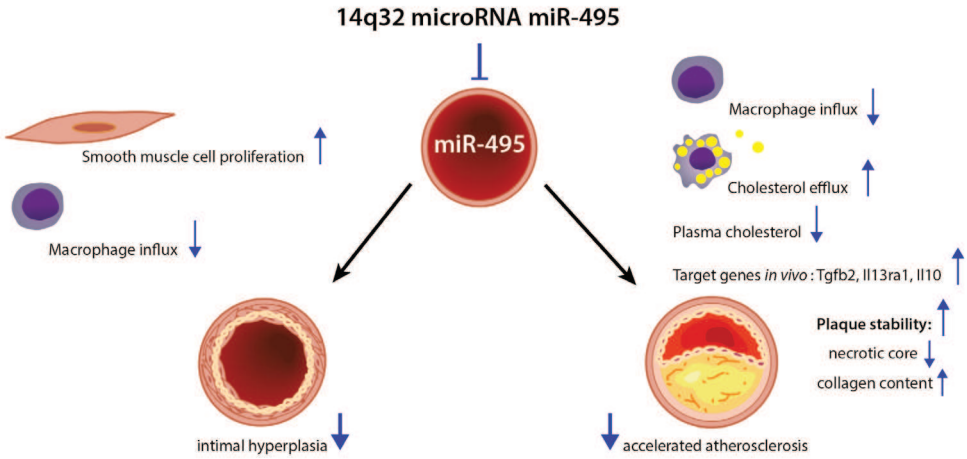

Summary of major findings of this study. Inhibition of miR-495 increases SMC proliferation and decreases macrophage influx in the femoral artery cuff model, resulting in decreased intimal hyperplasia (shown by the blue arrows). In the carotid collar model, inhibition of miR-495 affects plasma cholesterol levels, increases cholesterol efflux by macrophages, decreases macrophage influx and results in decreased lesion sizes. Several miR-495 target genes are upregulated *in vivo* after miR-495 inhibition. In addition, plaque stability is increased via reduced necrotic core sizes and increased collagen content in these lesions. Taken together, inhibition of miR-495 decreases lesion formation in intimal hyperplasia and accelerated atherosclerosis, the two major contributors of restenosis.

Funding

This work was supported by the Netherlands Institute for Regenerative Medicine (NIRM, FES0908), the Netherlands Organization for Scientific Research (NWO, Veni-916.12.041) and the Dutch Heart Foundation (2010B029 and Dr. E. Dekker Senior Postdoc, 2014T102). We acknowledge the support from the Netherlands CardioVascular Research Initiative: “the Dutch Heart Foundation, Dutch Federation of University Medical Centres, the Netherlands Organisation for Health Research and Development and the Royal Netherlands Academy of Sciences” for the GENIUS project “Generating the best evidence-based pharmaceutical targets for atherosclerosis” (CVON2011-19).

Acknowledgements

We thank A. Uijl for her technical support.

References

1. Clowes AW, Reidy MA, Clowes MM. Mechanisms of stenosis after arterial injury. *Lab Invest* 1983;**49**:208-215.
2. van Rooij E., Olson EN. MicroRNA therapeutics for cardiovascular disease: opportunities and obstacles. *Nat Rev Drug Discov* 2012;**11**:860-872.
3. Welten SM, Goossens EA, Quax PH, Nossent AY. The multifactorial nature of microRNAs in vascular remodelling. *Cardiovasc Res* 2016.
4. Welten SM, Bastiaansen AJ, de Jong RC, de Vries MR, Peters EA, Boonstra MC, Sheikh SP, Monica NL, Kandimalla ER, Quax PH, Nossent AY. Inhibition of 14q32 MicroRNAs miR-329, miR-487b, miR-494, and miR-495 increases neovascu larization and blood flow recovery after ischemia. *Circ Res* 2014;**115**:696-708.
5. Wezel A, Welten SM, Razaway W, Lagraauw, de Vries MR, Goossens E.A.C., Boonstra MC, Kandimalla ER, Kuiper J, Quax PH, Bot I, Nossent AY. Inhibition of microRNA-494 reduces atherosclerotic lesion development and increases plaque stability. *Ann Surg* 2015;**262**:841-847.
6. Han H, Wang YH, Qu GJ, Sun TT, Li FQ, Jiang W, Luo SS. Differentiated miRNA expression and validation of signaling pathways in apoE gene knockout mice by cross-verification microarray platform. *Exp Mol Med* 2013;**45**:e13.
7. Aavik E, Lumivuori H, Leppanen O, Wirth T, Hakkinen SK, Brasen JH, Beschorner U, Zeller T, Braspenning M, van CW, Makinen K, Yla-Herttuala S. Global DNA methylation analysis of human atherosclerotic plaques reveals extensive genomic hypomethylation and reactivation at imprinted locus 14q32 involving induction of a miRNA cluster. *Eur Heart J* 2014.
8. Gareri C, De Rosa S., Indolfi C. MicroRNAs for Restenosis and Thrombosis After Vascular Injury. *Circ Res* 2016;**118**:1170-1184.
9. Ji R, Cheng Y, Yue J, Yang J, Liu X, Chen H, Dean DB, Zhang C. MicroRNA expression signature and antisense-mediated depletion reveal an essential role of MicroRNA in vascular neointimal lesion formation. *Circ Res* 2007;**100**:1579-1588.
10. Lee J, Lim S, Song BW, Cha MJ, Ham O, Lee SY, Lee C, Park JH, Bae Y, Seo HH, Seung M, Choi E, Hwang KC. MicroRNA-29b Inhibits Migration and Proliferation of Vascular Smooth Muscle Cells in Neointimal Formation. *J Cell Biochem* 2014.
11. von der Thusen JH, van Berkel TJ, Biessen EA. Induction of rapid atherogenesis by perivascular carotid collar place ment in apolipoprotein E-deficient and low-density lipoprotein receptor-deficient mice. *Circulation* 2001;**103**:1164-1170.
12. Bhagat L, Putta MR, Wang D, Yu D, Lan T, Jiang W, Sun Z, Wang H, Tang JX, La Monica N., Kandimalla ER, Agrawal S. Novel oligonucleotides containing two 3'-ends complementary to target mRNA show optimal gene-silencing activity. *J Med Chem* 2011;**54**:3027-3036.
13. Troyan SL, Kianzad V, Gibbs-Strauss SL, Gioux S, Matsui A, Oketokoun R, Ngo L, Khamene A, Azar F, Frangioni JV. The FLARE intraoperative near-infrared fluorescence imaging system: a first-in-human clinical trial in breast cancer senti nel lymph node mapping. *Ann Surg Oncol* 2009;**16**:2943-2952.
14. Zhao Y, Pennings M, Hildebrand RB, Ye D, Calpe-Berdiel L, Out R, Kjerrulf M, Hurt-Camejo E, Groen AK, Hoekstra M, Jessup W, Chimini G, van Berkel TJ, Van Eck M. Enhanced foam cell formation, atherosclerotic lesion development, and inflammation by combined deletion of ABCA1 and SR-BI in Bone marrow-derived cells in LDL receptor knockout mice on western-type diet. *Circ Res* 2010;**107**:e20-e31.
15. Benetatos L, Hatzimichael E, Londin E, Vartholomatos G, Loher P, Rigoutsos I, Briasoulis E. The microRNAs within the DLK1-DIO3 genomic region: involvement in disease pathogenesis. *Cell Mol Life Sci* 2013;**70**:795-814.
16. Welten SM, Bastiaansen AJ, de Jong RC, de Vries MR, Peters EA, Boonstra MC, Sheikh SP, Monica NL, Kandimalla ER, Quax PH, Nossent AY. Inhibition of 14q32 MicroRNAs miR-329, miR-487b, miR-494, and miR-495 increases neovascu larization and blood flow recovery after ischemia. *Circ Res* 2014;**115**:696-708.
17. Rajewsky N. microRNA target predictions in animals. *Nat Genet* 2006;**38 Suppl**:S8-13.
18. Doherty TM, Kastelein R, Menon S, Andrade S, Coffman RL. Modulation of murine macrophage function by IL-13. *J Immunol* 1993;**151**:7151-7160.
19. Sheikh F, Dickensheets H, Pedras-Vasconcelos J, Ramalingam T, Helming L, Gordon S, Donnelly RP. The Interleukin-13 Receptor-alpha1 Chain Is Essential for Induction of the Alternative Macrophage Activation Pathway by IL-13 but Not IL-4. *J Innate Immun* 2015;**7**:494-505.
20. Mallat Z, Besnard S, Duriez M, Deleuze V, Emmanuel F, Bureau MF, Soubrier F, Esposito B, Duez H, Fievet C, Staels B, Duverger N, Scherman D, Tedgui A. Protective role of interleukin-10 in atherosclerosis. *Circ Res* 1999;**85**:e17-e24.
21. Holven KB, Halvorsen B, Bjerkeli V, Damas JK, Retterstol K, Morkrid L, Ose L, Aukrust P, Nenseter MS. Impaired inhibitory effect of interleukin-10 on the balance between matrix metalloproteinase-9 and its inhibitor in mononuclear cells from hyperhomocysteinemic subjects. *Stroke* 2006;**37**:1731-1736.
22. Wang P, Wu P, Siegel MI, Egan RW, Billah MM. Interleukin (IL)-10 inhibits nuclear factor kappa B (NF kappa B) activa tion in human monocytes. IL-10 and IL-4 suppress cytokine synthesis by different mechanisms. *J Biol Chem* 1995;**270**:9558-9563.
23. Eefting D, Schepers A, de Vries MR, Pires NM, Grimbergen JM, Lagerweij T, Nagelkerken LM, Monraats PS, Jukema JW, van Bockel JH, Quax PH. The effect of interleukin-10 knock-out and overexpression on neointima forma tion in hypercholesterolemic APOE*3-Leiden mice. *Atherosclerosis* 2007;**193**:335-342.
24. Wang X, Smith P, Pu LL, Kim YJ, Ko F, Robson MC. Exogenous transforming growth factor beta(2) modulates collagen I

and collagen III synthesis in proliferative scar xenografts in nude rats. *J Surg Res* 1999;**87**:194-200.
25. Mallat Z, Gojova A, Marchiol-Fournigault C, Esposito B, Kamate C, Merval R, Fradelizi D, Tedgui A. Inhibition of transforming growth factor-beta signaling accelerates atherosclerosis and induces an unstable plaque phenotype in mice. *Circ Res* 2001;**89**:930-934.
26. Newby AC, Zaltsman AB. Molecular mechanisms in intimal hyperplasia. *J Pathol* 2000;**190**:300-309.
27. Clark AL, Naya FJ. MicroRNAs in the Myocyte Enhancer Factor 2 (MEF2)-regulated Gtl2-Dio3 Noncoding RNA Locus Promote Cardiomyocyte Proliferation by Targeting the Transcriptional Coactivator Cited2. *J Biol Chem* 2015;**290**:23162-23172.
28. Liu D, Zhang XL, Yan CH, Li Y, Tian XX, Zhu N, Rong JJ, Peng CF, Han YL. MicroRNA-495 regulates the proliferation and apoptosis of human umbilical vein endothelial cells by targeting chemokine CCL2. *Thromb Res* 2015;**135**:146-154.
29. Law MR, Wald NJ, Rudnicka AR. Quantifying effect of statins on low density lipoprotein cholesterol, ischaemic heart disease, and stroke: systematic review and meta-analysis. *BMJ* 2003;**326**:1423.
30. Hansson GK, Libby P, Tabas I. Inflammation and plaque vulnerability. *J Intern Med* 2015;**278**:483-493.

Supplemental Material

Supplemental Tables

MiR	Sequence
hsa/mmu-miR-494	5'-UGAAACAUACACGGGAAACCUC-3'
hsa/mmu-miR-495	5'-AAACAAACAUGGUGCACUUCUU-3'
mmu-miR-329	5'-AACACACCCAGCUAACCUUUUU-3'
GSO	**Sequence**
hsa/mmu-GSO-494	3'-ACTTTGTATGTGCCCTTTGGAG-X-GAGGTTTCCCGTGTATGTTTCA-3'
hsa/mmu-GSO-495	3'-TTTGTTTGTACCACGTGAAGAA-X-AAGAAGTGCACCATGTTTGTTT-3'
mmu-GSO-329	3'-TTGTGTGGGTCGATTGGAAAAA-X-AAAAAGGTTAGCTGGGTGTGTT-3'
negative control GSO	3'-TGTACGACTCCATAACGGT-X-TGGCAATACCTCAGCATGT-3'

Supplemental table S1. Sequences of miRs and GSOs.
'X': Phosphorothioate linker
'-NNN-': 2'-O-methyl-modified nucleotides
's': Phosphorothioate linkage
'Chol': cholesterol group linked through a hydroxyprolinol-linkage

Gene	Forward primer	Reversed primer
Abca1	GGTTTGGAGATGGTTATACAATAGTTGT	TTCCCGGAAACGCAAGTC
Acvr1	GGAAGTCCGCCATTGCCCATC	GGTTGTTTCCCACATCAAGCTGGT
Ccr2	GCTGCCTGCAAAGACCAGAAGAG	TGCCGTGGATGAACTGAGGTAACA
Cd36	ATGGTAGAGATGGCCTTACTTGGG	AGATGTAGCCAGTGTATATGTAGGCTC
Cd59a	TCACTGGCGATCTGAAAAGTGTCTA	GCAGCACTATCTTGAGCCACATC
Cdkn1b	CGGCTGGGTTAGCGGAGCAGTGT	CCAGCGTTCGGGGAACCGTCTGAA
Hprt	TTGCTCGAGATGTCATGAAGGA	AGCAGGTCAGCAAAGAACTTATAG
Il10	GGGTGAGAAGCTGAAGACCCTC	TGGCCTTGTAGACACCTTGGTC
Il13ra1	TTCCAGTCTTTGTCGCAGTGGC	TTGCCAGGATCAGGAATTGGAGGA
Ldlr	TGAGGTTCCTGTCCATCTTCTTCCC	TTGATGTTCTTCAGCCGCCAGTTC
Lrp6	TTTGAACCCACCACCATCGCCTGCC	GCGGTGCAAAGTGCCGGTAGCTGTA
Mttp	TCTCACAGTACCCGTTCTTGGT	GAGAGACATATCCCCTGCCTGT
Rpl27	TGAAAGGTTAGCGGAAGTGC	TTTCATGAACTTGCCCATCTC
Tgfβ2	AGACCCCACATCTCCTGCTAATC	AATCAATGTAAAGAGGGCGAAGGC
Timp2	GTTTATCTACACGGCCCCCTCTT	ATCTTGCCATCTCCTTCTGCCTT
Tlr7	TGCAGGAGCTGGTGGCAAAATTGGA	TGCTGAGCTGTATGCTCTGGGAAAGGT

Supplemental table S2. List of primers used for *in vivo* and *in vitro* mRNA quantification.

Supplemental Figures

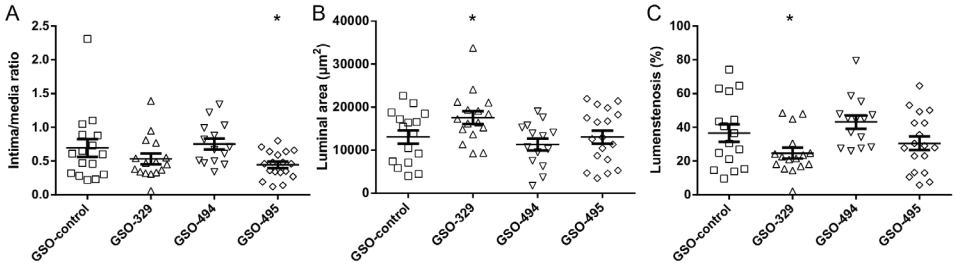

Supplemental figure 1. 14q32 microRNA inhibition in the femoral artery cuff model. (A) Quantification of intima/media ratio, (B) luminal area and (C) lumenstenosis, 21 days after cuff placement in C57Bl/6J mice treated with GSOs (±SEM). *p<0.05 compared to GSO-control.

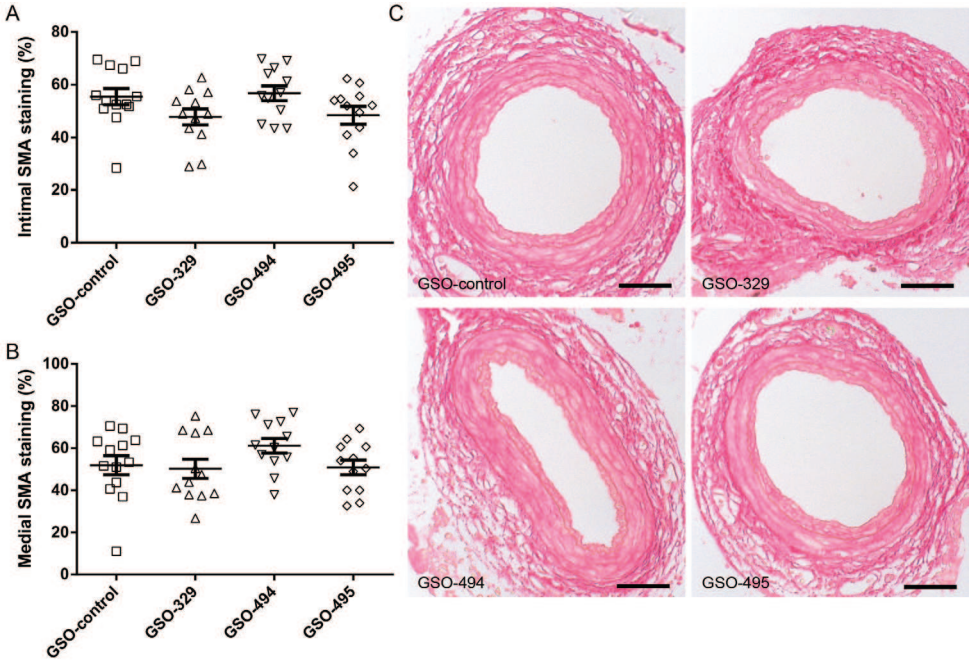

Supplemental figure 2. Effect of 14q32 microRNA inhibition on collagen content. Quantification of intimal (A) and medial (B) collagen content (%) 21 days after cuff placement in C57BL/6J mice (n=10 per group) treated with GSOs (±SEM). (C) Representative images of Mac3 staining of cuffed femoral arteries (scale bar = 50 µm).

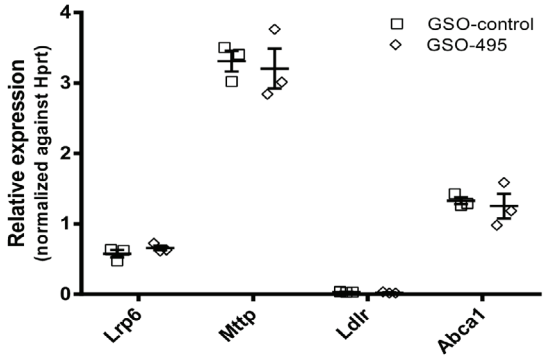

Supplemental figure 3. *In vivo* expression of putative miR-495 target genes in the liver of ApoE$^{-/-}$ mice. Mean expression levels of cholesterol metabolism related target genes Lrp6, Mttp, Ldlr and Abca1 in liver, relative to Hprt, are shown here 3 days after GSO-495 treatment (±SEM).

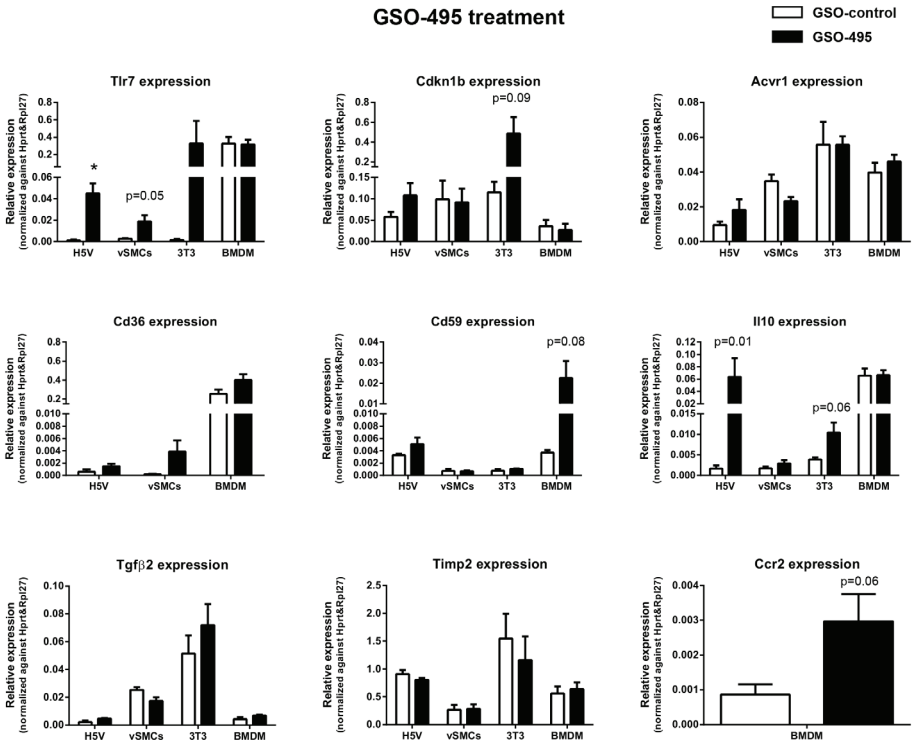

Supplemental figure 4. *In vitro* expression of putative miR-495 target genes in different cell types. Mean expression levels of at least 3 independent experiments, relative to Hprt and Rpl27, are shown here (±SEM). Expression of selected genes were measured in H5Vs, vSMCs, 3T3s and BMDMs.*p<0.05.

Part II

(post)transcriptional regulation of 14q32 microRNAs

Chapter 6

Inhibition of Mef2a enhances post-ischemic neovascularization via 14q32 microRNAs miR-329 and miR-494

Submitted to Molecular Therapy

SMJ Welten[1,2]

MR de Vries[1,2]

HAB Peters[1,2]

S Agrawal[3]

PHA Quax[1,2*]

AY Nossent[1,2*]

[*]Authors contributed equally to this work

[1]Department of Surgery and [2]Einthoven Laboratory for Experimental Vascular Medicine,

Leiden University Medical Center, Leiden, the Netherlands

[3]Idera Pharmaceuticals, Cambridge, MA, United States of America

Abstract

Improving the efficacy of neovascularization is a promising strategy to restore perfusion of ischemic tissues in patients with peripheral arterial disease. The 14q32 microRNA cluster is highly involved in neovascularization. The Mef2a transcription factor has been shown to induce transcription of the microRNAs within this cluster. In the present study, we examined the role of Mef2a inhibition on post-ischemic neovascularization, potentially via regulation of the 14q32 microRNA cluster.

We inhibited expression of Mef2a using gene silencing oligonucleotides (GSOs) in an *in vivo* hind limb ischemia model. Treatment with GSO-Mef2a clearly improved blood flow recovery within 3 days (44% recovery versus 25% recovery in control) and persisted until 14 days after ischemia induction (80% recovery versus 60% recovery in control). Animals treated with GSO-Mef2a showed increased arteriogenesis and angiogenesis in the relevant muscle tissues. Inhibition of Mef2a decreased expression of 14q32 microRNAs miR-329 ($p=0.026$) and miR-494 (trend, $p=0.06$), but not of other 14q32 microRNAs, nor of 14q32 pri-miR or pre-miR transcripts.

Our study demonstrates a novel function for Mef2a in post-ischemic neovascularization via indirect regulation of 14q32 microRNAs miR-329 and miR-494. Inhibition of Mef2a could be a promising therapeutic strategy to increase blood flow recovery in patients with peripheral arterial disease.

Introduction

Patients with peripheral arterial disease (PAD) suffer from reduced blood supply towards the extremities, caused by the build-up of obstructive atherosclerotic plaques in the arterial wall. Restoration of blood flow in these patients is imperative for the prevention of critical limb ischemia and limb loss. This can be accomplished by stimulating post-ischemic neovascularization, i.e. arteriogenesis and angiogenesis. Arteriogenesis, the outward remodelling of pre-existent collateral arterioles, is initiated upon increases in shear stress through the arterioles[1]. Angiogenesis is driven by ischemia and leads to sprouting of new capillaries from existing blood vessels into the ischemic tissue[2]. Both arteriogenesis and angiogenesis are multifactorial processes that involve for example the activation of endothelial cells (ECs), proliferation of vascular cell types (especially smooth muscle cells (SMCs)) and recruitment of immune cells.

MicroRNAs are short, non-coding RNA molecules that regulate the expression of their target genes at the post-transcriptional level[3]. Each microRNA has multiple target genes and microRNA-binding to a target messenger RNA downregulates the expression of that gene. The ability of microRNAs to target numerous genes makes them attractive targets for the regulation of multifactorial physiological processes. In the past decade, microRNAs have emerged as key regulators in the development and progression of cardiovascular disease[4-9]. Recently, we have shown the involvement of multiple microRNAs from a single microRNA cluster located on human chromosome 14q32 in post-ischemic neovascularization[10]. The 14q32 locus contains the largest known mammalian microRNA gene cluster and contains 54 microRNAs in humans (12F1 locus in mice, containing 61 microRNAs)[11]. In our previous study, we showed that inhibition of microRNAs miR-329, miR-487b, miR-494 and miR-495 from the 14q32 microRNA cluster led to improved blood flow recovery after induction of hind limb ischemia in mice[10]. Arteriogenesis and angiogenesis were both increased in respectively the adductor and soleus muscles of these mice. Myocyte Enhancer Factor 2a (Mef2a) was confirmed as a target gene of miR-329 and Mef2a expression was upregulated in the ligated hind limb after miR-329 inhibition. Interestingly, MEF2A itself was reported to target miR-329 and the other 14q32 microRNAs[12]. Several studies reported transcriptional regulation of the 14q32 microRNA cluster by the MEF2 family of transcription factors and in particular by MEF2A[12-14].

The MEF2 family of transcription factors consists of four members, namely MEF2A, -B, -C and –D. Although mainly studied for their role in muscle development and differentiation, MEF2 family members are also expressed in ECs and vascular SMCs[15, 16]. MEF2A and MEF2C are the predominant isoforms expressed in vascular cells. In ECs, MEF2 proteins have been shown to control vascular integrity by promoting EC survival whereas in SMCs, MEF2 proteins are expressed in cells with an activated phenotype and control differentiation of SMCs[17, 18]. Moreover, inhibition of MEF2A induced phenotypic switching of vascular SMCs, leading to proliferation and migration of these cells[19].

The aim of this study was to evaluate the effect of Mef2a inhibition on post-ischemic blood flow recovery. We hypothesized that Mef2a could act as a novel switch in neovascularization via regulation of 14q32 microRNAs. We show here that inhibition of Mef2a, via subsequent inhibition of 14q32 microRNAs miR-329 and miR-494, but not other 14q32 microRNAs, indeed improves post-ischemic

blood flow recovery *in vivo*.

Methods

Mef2a inhibitors

Gene silencing oligonucleotides (GSOs) were designed with reverse complementarity to the murine Mef2a target mRNA sequence and synthesized at Idera Pharmaceuticals (Cambridge, MA, USA)[23]. As a negative control, a scrambled sequence was used, designed not to target any known murine mRNA. GSOs were made up of two single-stranded DNA strands, which were 2'O-methylated. The two DNA strands were linked together at their 5'ends by a phosphothioate-linker in order to prevent Toll-like receptor mediated immune activation. Sequences of Mef2a GSOs are given in Figure 1.

Hind limb ischemia model

This study was performed in accordance with Dutch government guidelines and the Directive 2010/63/EU of the European Parliament. All experiments were approved by the committee on animal welfare of the Leiden University Medical Center (Leiden, the Netherlands. Approval reference number 12029). C57Bl/6 male mice, aged 8 to 12 weeks (Harlan) were housed in groups of 4 or 5 mice with free access to water and regular chow. For Mef2a-inhibition experiments, mice were given intraperitoneal (i.p) injections of 1 mg (~40 mg/kg) GSO in PBS or PBS alone at 10, 7, 4 days and directly before surgery and at 3, 7 and 10 days after surgery. Mice were anesthetized by i.p. injection of midazolam (8 mg/kg, Roche Diagnostics), medetomidine (0.4 mg/kg, Orion) and fentanyl (0.08 mg/kg, Janssen Pharmaceuticals). Unilateral hind limb ischemia was induced by electrocoagulation of the left femoral artery proximal to the superficial epigastric artery and proximal to the bifurcation of the popliteal and saphenous artery (double ligation model)[24]. After surgery, anaesthesia was antagonized with flumazenil (0.7 mg/kg, Fresenius Kabi), atipamezole (3.3 mg/kg, Orion) and buprenorphine (0.2 mg/kg, MSD Animal Health).

Laser Doppler perfusion measurements

Blood flow recovery to the ligated hind limb was measured over time using Laser Doppler Perfusion Imaging (LDPI) (Moor Instruments) before and directly after surgery and at at 3, 7, 10 and 14 days after surgery. For LDPI measurements, mice were anesthetized by i.p. injection of midazolam (8 mg/kg, Roche Diagnostics) and medetomidine (0.4 mg/kg, Orion). Before each measurement, mice were placed in a double glazed pot, perfused with water at 37°C for 5 minutes. After LDPI, anaesthesia was antagonized by subcutaneous injection of flumazenil (0.7 mg/kg, Fresenius Kabi) and atipamezole (3.3 mg/kg, Orion). LDPI measurements in the ligated paw were normalized to measurements of the unligated paw, as internal control. After the last LDPI measurement at day 14, analgesic fentanyl (0.08 mg/kg, Janssen Pharmaceuticals) was administered subcutaneously and mice were sacrificed via cervical dislocation. The adductor, gastrocnemius and soleus muscles were harvested and either snap-frozen or fixed in 4% PFA.

Cell culture

Primary murine smooth muscle cells. Primary murine smooth muscle cells were isolated from mouse aortae of C57Bl/6 mice. Aortae were cut into small pieces and embedded on gelatin coated 6-well plates. Culture medium was added to the wells with aortic fragments (DMEM (Invitrogen, GIBCO), 10% heat inactivated fetal bovine serum (PAA), 1% penicillin/streptomycin). Outgrowth of smooth muscle cells occurred within one week, after which cells were passed using Trypsin-EDTA (Sigma) and transferred to fresh 6-well plates. Smooth muscle cells were characterized by positive α-smooth muscle actin staining as described previously[10]. Cells were cultured at 37°C in a humidified 5% CO_2 environment.

3T3 cells. 3T3 cells were cultured at 37ºC in a humidified 5% CO_2 environment. Culture medium consisted of DMEM GlutaMAX (Gibco) supplemented with 10% heat inactivated fetal bovine serum (PAA) and 1% penicillin/streptomycin (PAA). Culture medium was refreshed every 2-3 days. Cells were passed using trypsin-EDTA (Sigma) at 90% confluency.

In vitro GSO mediated inhibition of Mef2a expression

For GSO experiments, murine smooth muscle cells were plated at 50.000 cells per well of a 12-well plate. After 24 hrs, GSOs against

Mef2a were added to the culture media at a concentration of 10ng/µl for 48 hrs. After 48 hrs, cells were washed with PBS and TRIzol (Invitrogen) was added to the cells for RNA isolation.

rt/qPCR

mRNA rt/qPCR. Adductor and gastrocnemius muscles from 14 days after surgery were homogenized by grounding with a pestle and mortar in liquid nitrogen. Total RNA was isolated using a standard TRIzol-chloroform extraction protocol. RNA concentration and purity were determined by nanodrop (Nanodrop Technologies). RNA was reverse transcribed using high-capacity RNA to cDNA RT kits (Life Technologies, Foster City, CA, USA). Relative quantitative mRNA PCR was performed on reverse transcribed cDNA using Mef2a Taqman gene expression assays. For quantification of pri-miR and pre-miR levels of microRNAs, SYBR green dye (Qiagen) was used and primers were designed using Primer3. Sequences of primers are listed in Supplementary Table 1. qPCRs were run on a 7900HT Fast Real-Time PCR system (Applied Biosystems), and amplification efficiencies were checked by standard curves. Data were normalized using a stably expressed endogenous control (HPRT for Mef2a quantification, snRNA-U6 for pri-miR and pre-miR quantification).

microRNA rt/qPCR. microRNA quantification was performed using Taqman microRNA assays (Applied Biosystems) according to manufacturer's protocol. Relative quantitative PCR was performed on the Viia7 system (Applied Biosystems) and amplification efficiencies were checked by standard curves. Data were normalized using a stably expressed endogenous control (mmu-let-7c), as previously described[25].

Immunohistochemistry

CD31. Six µm thick fresh-frozen cross-sections of soleus muscle were fixed in ice-cold acetone and stained with anti-CD31 (BD Pharmingen). Sections were counterstained with hematoxylin. Quantification of CD31 positive area was performed on sections photographed randomly (six representative images per muscle per mouse, ten animals per group) using image analysis (Image J 1.48v, NHI, USA), as described previously[26].

α-SMA, CD31 and CD45 triple staining. Five µm thick paraffin-embedded cross-sections of adductor muscle were re-hydrated and antigen retrieval was performed using citrate buffer. Smooth muscle cells were stained using primary antibodies against α-smooth muscle actin (α-SMA, DAKO), endothelial cells were stained with CD31 antibodies (BD Pharmingen) and leukocytes were stained using CD45 antibodies (Abcam). Alexa Fluor 647, Alexa Fluor 488 and Alexa Fluor 594 antibodies (Life Technologies and Invitrogen (Alexa Fluor 594)) were used to visualize smooth muscle cells, endothelial cells and leukocytes respectively. Finally, sections were mounted in Fluoroshield with DAPI (Sigma-Aldrich). The Pannoramic MIDI digital slide scanner (3DHistech) was used to create high resolution images of the adductor muscles. Snapshots were taken using the Pannoramic viewer software (3DHistech) with 20x magnification. The amount and size of α-SMA positive collaterals was measured using Image J (Image J 1.48v, NHI, USA).

MEF2A. Five µm thick paraffin-embedded cross-sections of adductor muscle were re-hydrated and endogenous peroxidase activity was blocked. Antigen retrieval was performed with Tris-EDTA (pH 9.0) at 100°C for 10 minutes. Adductor muscles were stained with Anti-MEF2A antibodies (Abcam, ab86755) to visualize MEF2A expression and counterstained with haematoxylin.

Western Blot analysis

Immunoblotting was performed to quantify MEF2A expression *in vivo*. Homogenized adductor muscle tissue of GSO-control (n=2) and GSO-Mef2a (n=2) treated animals were lysed on ice for 30 minutes with lysis buffer. Lysates were briefly centrifuged to remove debris. Equal amounts of protein (20 µg per sample) were loaded onto a PAGE minigel (Mini-PROTEAN TGX precast gel, Biorad) and run at 70V for 10 min and subsequently at 120V for 90 min. Fractionated tissue extracts were transferred to a nitrocellulose membrane using a transfer apparatus according to the manufacturer's protocol (Bio-Rad). Incubation with primary rabbit anti-MEF2A antibody (Abcam, ab86755 1:100) was followed by incubation with HRP-conjugated secondary antibody goat anti-rabbit IgG (CST7074, Cell Signalling Technology). Signals were visualized using the SuperSignal ELISA Pico chemiluminescent substrate (ThermoScientific). Blots were stripped for 15 min using Restore Stripping Buffer (ThermoScientific) and incubated with anti-Actin (C-11) (SC1615, Santa-Cruz) for normalization. The proportional expression of MEF2A per lane was normalized against the proportional expression of Actin per lane (Biorad Image Lab Software 5.2.1).

Aortic Ring assay

Mouse aortic ring assays were performed as described previously[27]. In brief, the thoracic aorta was removed from 8 to 10-week old mice and transferred to a 15 mL tube containing Opti-MEM (Gibco). Surrounding fat and branching vessels were carefully removed and aortas were flushed with Opti-MEM (Gibco). Collagen Type I (Millipore) was diluted to a final concentration of 1mg/ml with DMEM (Gibco) and pH was adjusted with 5N NaOH. 96-well plates were coated with 75 µl collagen matrix. After serum starvation overnight in Opti-MEM, aortic rings (0.5 to 1 mm) were transferred to the 96-well plate and after 1 hour, 150 µl Opti-MEM supplemented with 2.5% FBS (PAA, Austria), penicillin-streptomycin (PAA, Austria), 30ng/ml VEGF (Millipore) and GSOs (15ng/ul) was added to each well. Microvessel outgrowth was quantified after 5 days by live phase-contrast microscopy (Axiovert 40C, Carl Zeiss). Starting from a specific point on the ring, each microvessel emerging from the ring was counted as a sprout and individual branches arising from each microvessel counted as a separate sprout, working around the ring clockwise.

RNA Binding Protein Immunoprecipitation

RNA binding protein immunoprecipitation (RIP) was performed using the EZMagna RIP kit (Millipore), according to manufacturer's instructions. 3T3 cells were grown to 90% confluency and lysed in complete RIP lysis buffer. Cell lysates were incubated with RIP buffer containing magnetic beads conjugated with antibodies against MEF2A (Abcam ab86755) and rabbit control IgG (Millipore PP64B). Before immunoprecipitation, 10% of cell lysate was taken and served as 10% input control. Next, samples were treated with proteinase K to digest protein and RNA was isolated using a standard TRIzol-chloroform extraction protocol.

Statistical analysis

Results are expressed as mean ± SEM. *In vitro* experiments were performed in triplicate and represent at least three independent experiments. Differences between groups were tested using student's t-tests. P values of <0.05 were considered statistically significant.

Results

Gene Silencing Oligonucleotide mediated inhibition of Mef2a expression

We tested several Gene Silencing Oligonucleotides (GSOs) *in vitro* for their capacity to inhibit Mef2a mRNA expression in murine primary smooth muscle cells (GSO-1, GSO-2, GSO-3 and GSO-4, Fig. 1A). Expression of Mef2a was significantly inhibited by GSO-2 (35% expression of control, p=0.0005) and GSO-3 (30% expression of control, p=0.0094), but not by treatment with GSO-1 or GSO-4 (Fig. 1B). For *in vivo* experiments, we selected GSO-3 for inhibition of Mef2a (GSO-Mef2a from here on) which gave the strongest downregulation of Mef2a expression.

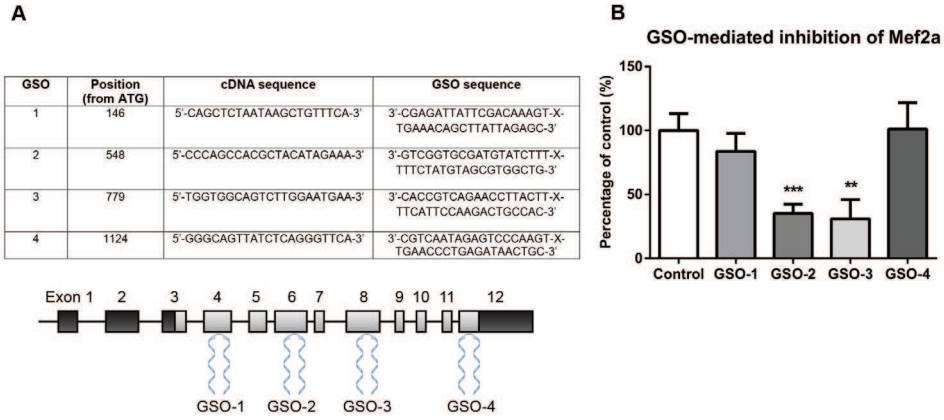

GSO	Position (from ATG)	cDNA sequence	GSO sequence
1	146	5'-CAGCTCTAATAAGCTGTTTCA-3'	3'-CGAGATTATTCGACAAAGT-X-TGAAACAGCTTATTAGAGC-3'
2	548	5'-CCCAGCCACGCTACATAGAAA-3'	3'-GTCGGTGCGATGTATCTTT-X-TTTCTATGTAGCGTGGCTG-3'
3	779	5'-TGGTGGCAGTCTTGGAATGAA-3'	3'-CACCGTCAGAACCTTACTT-X-TTCATTCCAAGACTGCCAC-3'
4	1124	5'-GGGCAGTTATCTCAGGGTTCA-3'	3'-CGTCAATAGAGTCCCAAGT-X-TGAACCCTGAGATAACTGC-3'

Figure 1. **Inhibition of Mef2a by Gene Silencing Oligonucleotides (GSOs). (A)** Four different GSOs were developed and tested for their capacity to inhibit Mef2a expression *in vitro*. GSOs were designed to target different exons on the murine Mef2a mRNA sequence. **(B)** Inhibition of Mef2a in primary murine vascular smooth muscle cells for 48 hrs by GSOs (10ng/µl). Mean expression levels, from at least 3 independent experiments, relative to HPRT and as percentage of GSO-Control are shown here (±SEM). **p<0.01, ***p<0,001.

In vivo inhibition of Mef2a using GSOs

Immunohistochemical staining of murine adductor muscle tissue demonstrated that MEF2A is expressed in this tissue, particularly in the nuclei of cells (Fig. 2A). Expression of Mef2a was measured in the adductor and gastrocnemius muscles of animals, 14 days after induction of ischemia, 4 days after the final GSO injection. Expression of Mef2a was downregulated in both adductor and gastrocnemius muscle tissue of GSO-Mef2a treated mice compared to control treated animals (Fig. 2B and 2C, respectively). Although inhibition of Mef2a was less strong than *in vitro* cell cultures, inhibition was highly significant (72% expression of control, p=0.00052 in the adductor and 78% expression of control, p<0.0001 in the gastrocnemius muscle). GSO-Mef2a treatment furthermore reduced MEF2A protein levels in the adductor muscle by 30% (Fig. 2D).

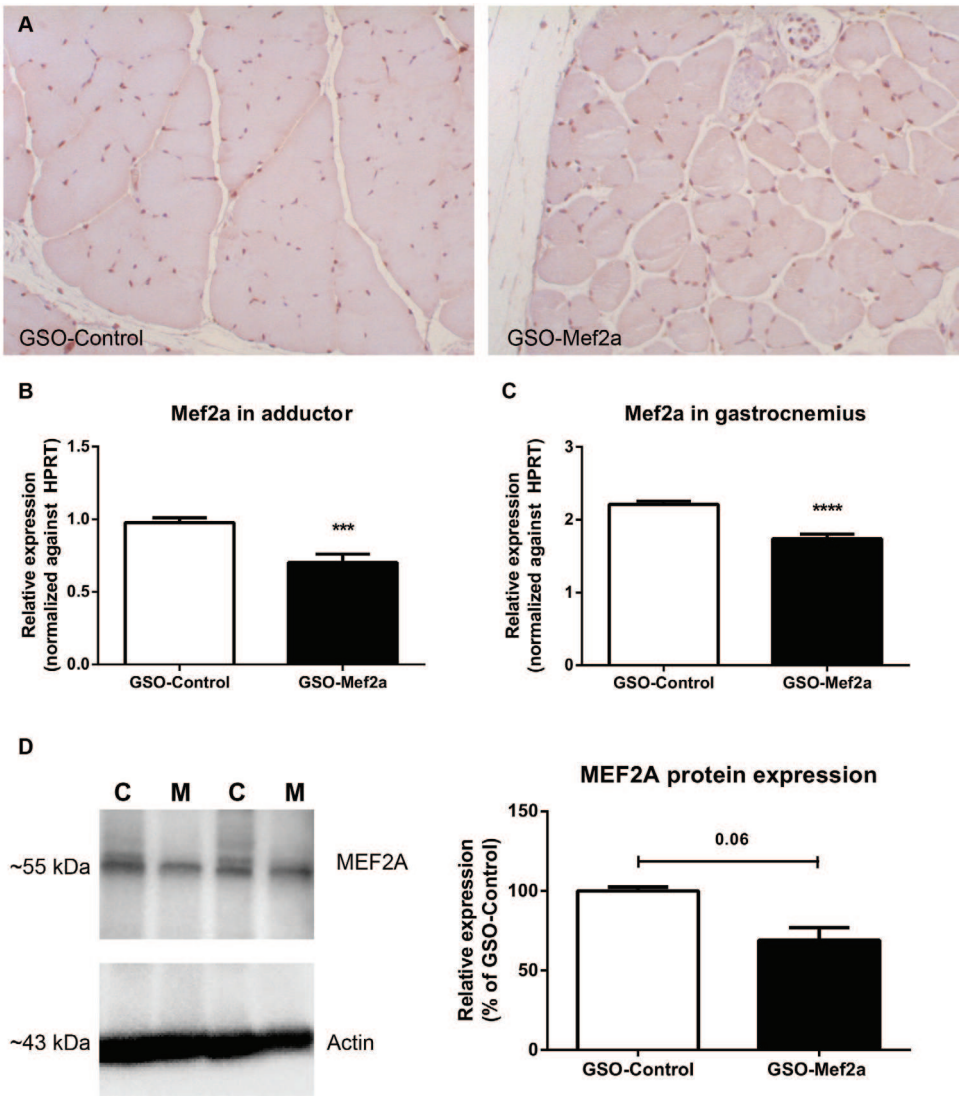

Figure 2. ***In vivo*** **inhibition of Mef2a by GSO-Mef2a**. **(A)** Immunohistochemical staining of MEF2A in the adductor muscle of GSO-Mef2a and GSO-Control treated mice. **(B)** Expression of Mef2a in the adductor muscle of C57Bl/6 mice treated with GSO-Mef2a or GSO-control, 14 days after double ligation of the left femoral artery. Per group, adductor muscle tissue of 10 animals was used. **(C)** Expression of Mef2a in the gastrocnemius muscle of C57Bl/6 mice treated with GSO-Mef2a or GSO-Control, 14 days after ischemia induction. Per group, gastrocnemius muscle tissue of 10 animals was used. Mean expression levels relative to HPRT are shown here (±SEM). **(D)** MEF2A and Actin protein expression and quantification in adductor muscle lysates of GSO-Mef2a (M) and GSO-Control (C) treated mice (n=2 animals per group). Mean expression as percentage of control is shown here (±SEM). ***p<0,001, ****p<0,0001.

Improved blood flow recovery upon Mef2a inhibition

The effect of Mef2a inhibition on blood flow recovery was evaluated at different time points after ligation of the femoral artery (pre-operative, post-operative, day 3, day 7, day 10 and day 14 after ischemia induction, Fig. 3). Already within 3 days after hind limb ischemia, animals injected with GSOs against Mef2a showed improved blood flow recovery (44% recovery in GSO-Mef2a animals versus

25% recovery in GSO-control animals, Fig. 3). This increase in perfusion persisted over time. At time of sacrifice, GSO-Mef2a treated animals showed 80% recovery in blood flow compared to 60% recovery of perfusion in GSO-Control treated animals.

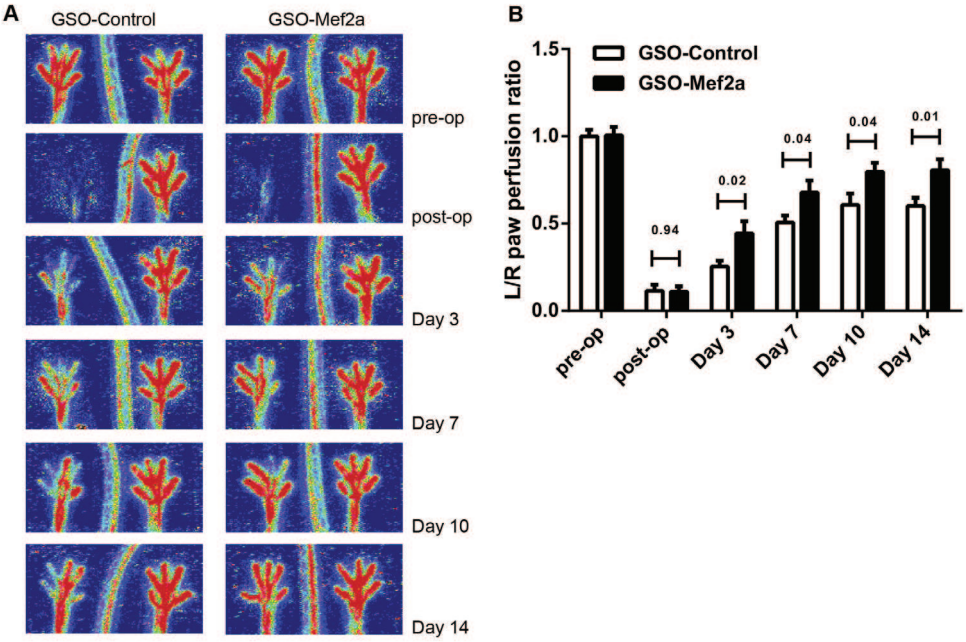

Figure 3. Blood flow recovery after *in vivo* Mef2a inhibition. (A) Laser Doppler perfusion images (LDPI) from paws of mice subjected to unilateral hind limb ischemia, showing blood flow recovery in these animals over time. **(B)** Quantification of LDPI measurements over time in mice (11 per group) treated with GSO-Mef2a or GSO-Control (1 mg per mouse injected i.p. at different time points as described in materials and methods). Data are calculated as the ratio of the left (ischemic) over the right (non-ischemic) paw and presented as mean ± SEM. P-values are shown for each time point.

In vivo inhibition of Mef2a increases arteriogenesis

Alpha smooth muscle actin (α-SMA$^+$) staining was used to visualize collateral vessels in the adductor muscle. Significant increases in arteriole diameters were observed between the left and right adductor muscles for GSO-Mef2a treated mice compared to GSO-control treated mice (increase in arteriole diameter in left over right adductor (LA/RA ratio) was 2.057 compared to LA/RA ratio of 1.16 in controls, p=0.0060, Fig. 4A). Both total α-SMA$^+$ area per section (LA GSO-Mef2a 846±99μm^2 vs RA GSO-Mef2a 404±37μm^2, p=0.00043 and LA GSO-Control 654±68μm^2 vs RA GSO-Control 480±27μm^2, p=0.05) as well as mean lumen area per α-SMA$^+$ collateral (LA GSO-Mef2a 342±25μm^2 vs RA GSO-Mef2a 170±9μm^2, p=0.0002 and LA GSO-Control 237±47μm^2 vs RA GSO-Control 217±18μm^2, p=0.54) were increased in the left adductor muscles of GSO-Mef2a treated animals compared to the right adductor muscles which was not the case for GSO-Control treated animals (Fig. 4B and 4C, respectively). Moreover, α-SMA$^+$ area per collateral was increased in the left adductor of GSO-Mef2a treated animals compared to controls (GSO-Mef2a 342±25μm^2 vs GSO-Control 237±47μm^2, p=0.03, Fig. 4C and representative images in Fig. 4D). The number of α-SMA$^+$ vessels between the left and right paw were similar in the GSO-Mef2a group (LA/RA ratio 1.04), whereas GSO-Control treated animals had more α-SMA$^+$ vessels

in the left compared to the right paw (LA/RA ratio 1.27, Fig. 4E). Arteriogenesis is the enlargement of pre-existing arterioles to form collateral arteries. Therefore, not the increase in number of collateral arteries but rather the increase in arteriole diameters demonstrate increased arteriogenesis in GSO-Mef2a treated mice. Furthermore, as an inflammatory environment facilitates extracellular matrix rearrangement and outward remodelling of collateral arterioles, we also looked at the number of inflammatory cells surrounding the collaterals. There was a trend towards an increase in the number of perivascular CD45$^+$ leukocytes around the remodelling collaterals of GSO-Mef2a treated animals compared to controls (64% increase compared to GSO-Control animals, p=0.09, Fig. 4F).

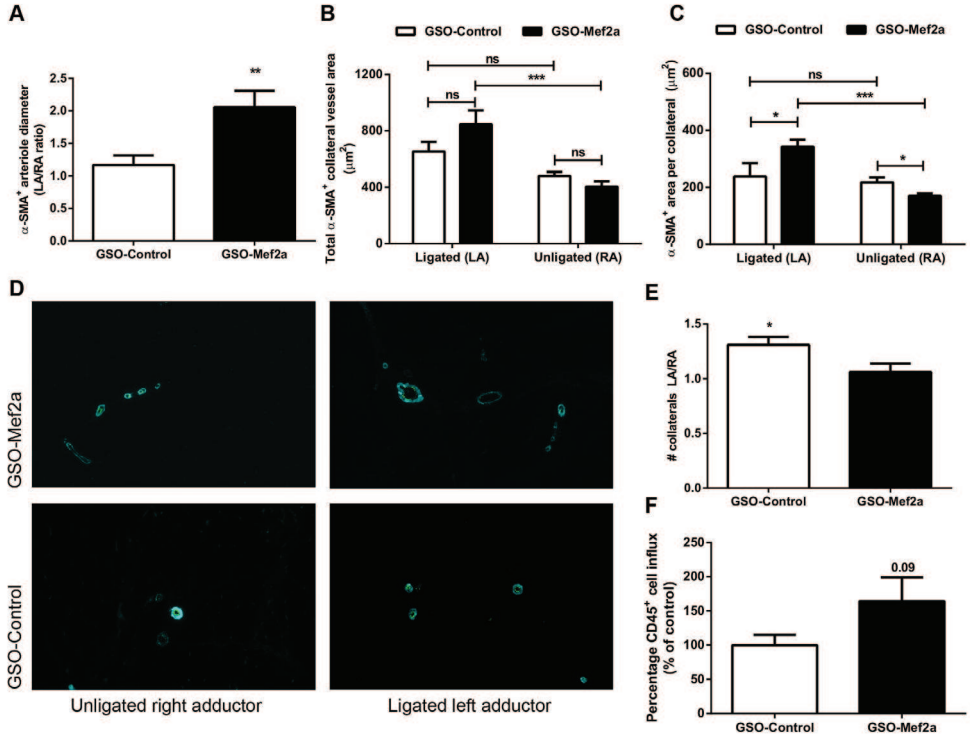

Figure 4. ***In vivo*** **arteriogenesis after Mef2a inhibition.** Immunofluorescence staining of paraffin-embedded adductor muscle group of C57Bl/6 mice treated with either GSO-control (n=11 animals) and GSO-Mef2a (n=10 animals), 14 days after ischemia induction, using anti-αSMA (turquoise) antibodies. **(A)** Quantification of the increase in diameter of α-SMA$^+$ arterioles between the left and the right adductor muscles of mice. **(B)** Total α-SMA$^+$ area per section as well as **(C)** mean lumen area per α-SMA$^+$ collateral are shown. **(D)** Representative images of α-SMA staining in unligated and ligated adductor muscle tissues of mice treated with GSO-Mef2a or GSO-Control. **(E)** Number of total collateral arterioles in left (ligated) over right (unligated) adductor muscles of mice. **(F)** Quantification of the number of CD45$^+$ cells around remodelling collateral arterioles in the adductor muscle of GSO-Control or GSO-Mef2a treated mice, 14 days after induction of ischemia. From each muscle, 8 representative images were used for quantification. Data are presented as mean ± SEM. *p<0.05, *p<0.001, ***p<0.0005.

In vivo angiogenesis upon Mef2a inhibition

Capillary formation was evaluated in the left (ischemic) and right (normoxic) soleus muscles of GSO-treated mice, 14 days after induction of ischemia. Muscle tissues were stained with anti-CD31 to visualize capillaries. Inhibition of Mef2a increased capillary formation in the soleus muscles of these mice (1.4 fold, p=0.04) compared to the soleus muscles of GSO-control treated mice (Fig. 5). We also

investigated the effect of Mef2a inhibition on *ex vivo* angiogenesis using aortic explants. GSO mediated inhibition of Mef2a led to a mild increase in the number of sprouts from aortic explants, compared to GSO-Control (Supplemental Fig. 1).

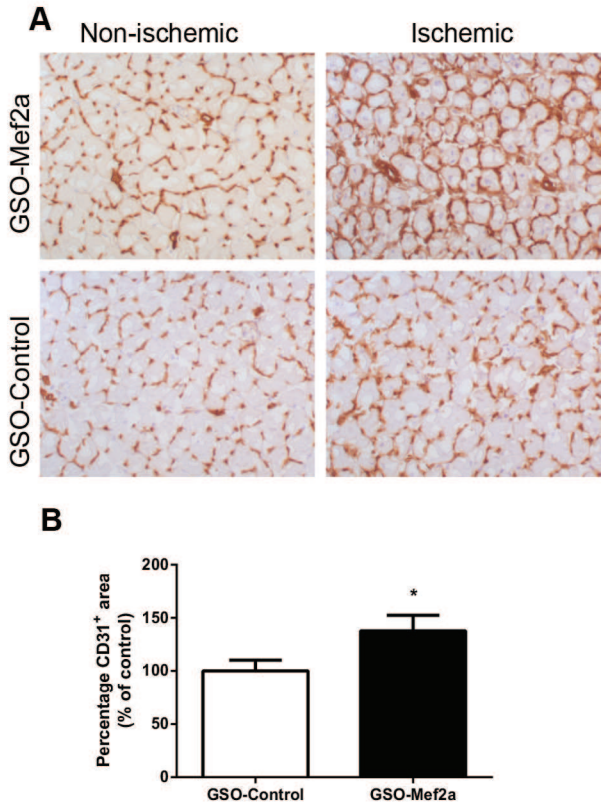

Figure 5. *In vivo* angiogenesis after Mef2a inhibition. (A) Representative images of CD31 staining in the right (non-ischemic) and left (ischemic) soleus muscles of C57Bl/6 mice treated with GSO-Mef2a (n=10 animals) or GSO-Control (n=11 animals). **(B)** Quantification of the capillary density in the soleus muscle, defined as the increase in $CD31^+$ area between left and right soleus muscles, shown as percentage relative to the increase in mice treated with GSO-Control. From each soleus muscle, 6 representative photographs were used for quantification. Data are presented as mean ± SEM. *p<0.05.

Mef2a targets miR-329 of the 14q32 microRNA cluster

We determined expression of 14q32 microRNAs miR-329, miR-487b, miR-494, miR-495 and miR-410 in the adductor muscles of GSO-Mef2a and GSO-Control treated mice. Inhibition of Mef2a led to significant downregulation of 14q32 microRNA miR-329 (Fig. 6A, p=0.0026) and a borderline significant downregulation of miR-494 (Fig. 6B, p=0.06). However, expression of 14q32 microRNAs miR-487b, miR-410 and miR-495 was not inhibited in animals treated with GSO-Mef2a (Fig. 6C-E). MicroRNAs are transcribed as primary microRNAs (pri-miRs) before being processed into pre-microRNAs (pre-miRs) and subsequently into mature microRNAs. To determine whether Mef2a does influence transcription of multiple 14q32 microRNAs, we also measured expression of the pri-miR transcripts and the intermediate pre-miRs in adductor muscle tissue of GSO-treated animals. No differences were

observed in pri-miR and pre-miR levels of any of the microRNAs between GSO-Mef2a and GSO-control treated animals, indicating that the regulation of mature miR-329 and miR-494 levels was indirect (Fig. 7).

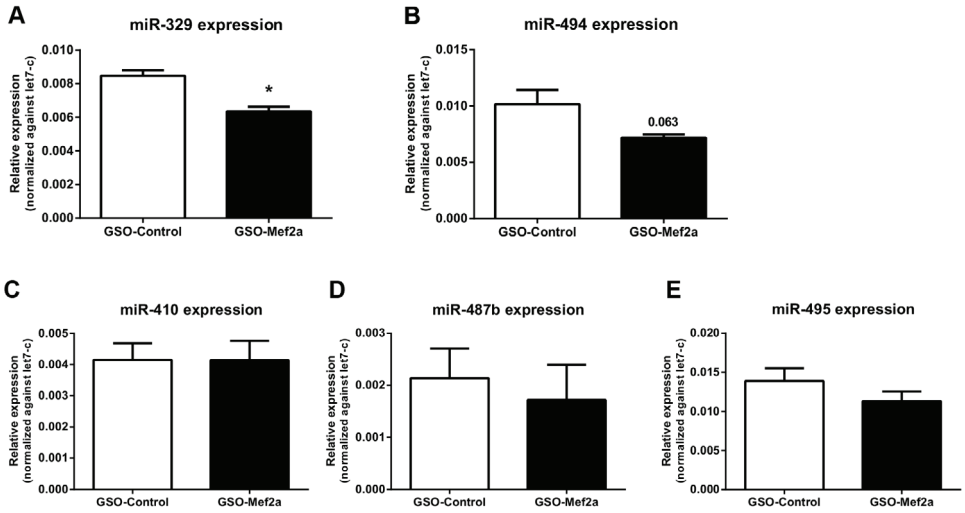

Figure 6. Regulation of 14q32 microRNA expression *in vivo*. Expression of 14q32 microRNAs miR-329 **(A)**, miR-494 **(B)**, miR-487b **(C)**, miR-410 **(D)** and miR-495 **(E)** in adductor muscle tissue of GSO-Mef2a or GSO-Control treated animals at 14 days after hind limb ischemia. Per group, adductor muscle tissue of 4 mice was used. Mean expression levels are shown here relative to expression of let-7c (±SEM). *p<0.05

Mef2a binds to the pri-miR transcript of 14q32 microRNA miR-494, but not miR-487b

To investigate whether Mef2a could regulate post-transcriptional processing of 14q32 microRNAs, we performed RNA binding protein immunoprecipitation (RIP) assays. RIP experiments on 3T3 cell lysates performed with anti-MEF2A antibodies demonstrated specific binding of MEF2A to the pri-miR-494 transcript, but not to the pri-miR-487b transcript (Supplemental Fig. 2). Expression of pri-miR-329 was too low to confirm or exclude MEF2A binding in these cells.

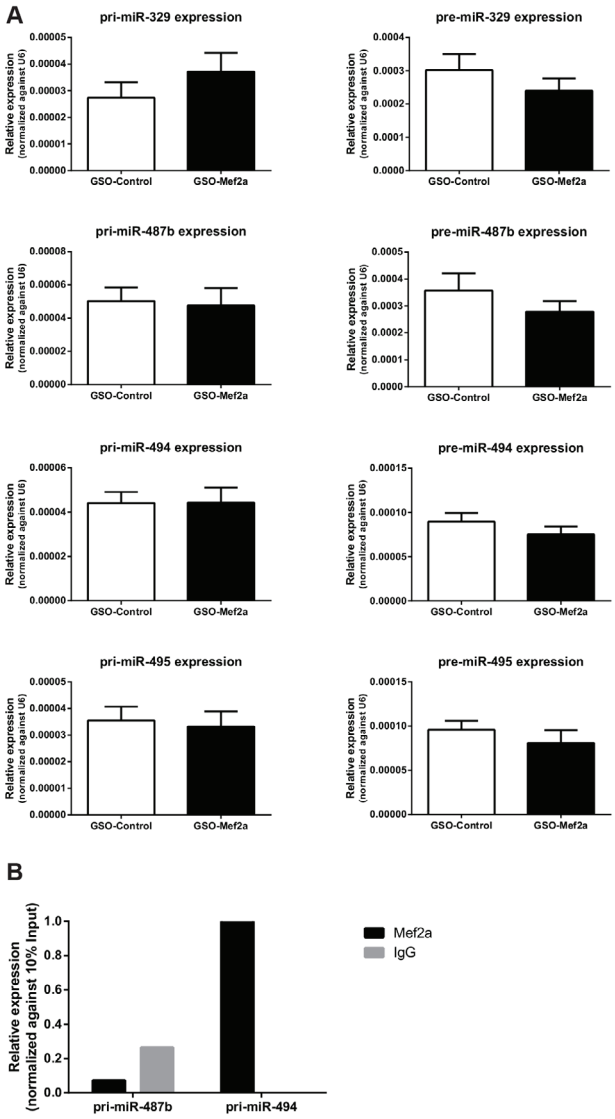

Figure 7. Regulation of 14q32 pri-miR and pre-miR expression *in vivo*. (A) Expression of pri-miR and pre-miR transcripts of 14q32 microRNAs miR-329, miR-487b, miR-494 and miR-495 in adductor muscle tissue of GSO-Mef2a or GSO-Control treated animals at 14 days after hind limb ischemia. Per group, adductor muscle tissue of 11 mice was used. Mean expression levels are shown here relative to expression of snRNA-U6 (±SEM). **(B)** RNA binding protein immunoprecipitation with either MEF2A antibodies or negative control rabbit IgG followed by rt/qPCR on pri-miR transcripts of 14q32 microRNAs miR-494 and miR-487b. Data are normalized against 10% input.

Discussion

We demonstrate here that the Mef2a transcription factor plays a role in post-ischemic neovascularization. Inhibition of MEF2A improved blood flow recovery in animals after unilateral ligation of the femoral artery. Previous reports have demonstrated the role of Mef2a in other forms of vascular remodelling as well. One study showed that the expression of MEF2 members Mef2a, Mef2b and Mef2d was increased in the neointima of rat carotid arteries after balloon injury[18]. In another study, overexpression of a dominant-negative mutant form of Mef2a reduced neointima formation, inhibited macrophage infiltration and decreased MCP1 expression upon wire injury in rats[20]. However, to our knowledge, a role of Mef2a in post-ischemic neovascularization is a completely novel finding.
We hypothesized that inhibition of Mef2a expression would improve post-ischemic neovascularization via subsequent downregulation of 14q32 microRNAs, as Mef2a was reported to control 14q32 microRNA expression and because we have previously shown that 14q32 microRNAs have anti-angiogenic and anti-arteriogenic functions[10, 12]. Inhibition of Mef2a in our study revealed decreased expression of 14q32 microRNA miR-329 and a trend towards decreased expression of miR-494, but not of several other 14q32 microRNAs studied here. Indeed, animals treated with GSO-Mef2a showed ~80% recovery of blood flow, 14 days after ischemia induction. However, this effect was not greater than inhibition of single 14q32 microRNAs miR-329 and miR-494, as inhibition of these microRNAs led to (nearly) complete restoration of blood flow within 7 and 10 days respectively.

In addition to the mature miR levels, we also determined expression levels of pri-miR transcripts and pre-miR intermediates of several 14q32 microRNAs. Pri-miR levels directly indicate the level of transcription of the 14q32 microRNA genes, which were expected to be influenced by the transcription factor Mef2a. Pre-miRs are an intermediate form of the microRNA transcript and changes in expression of the pri-miR to the pre-miR or from pre-miR to the mature microRNA indicate changes in post-transcriptional processing of the microRNA. Pri-miR and pre-miR levels for miR-329, miR-487b, miR-494 and miR-495 showed no difference in expression levels between the GSO-treated groups. These data indicate that there is no direct transcriptional regulation by MEF2a of the 14q32 microRNAs studied here in this model and that the effects on mature miR-329 and miR-494 levels were achieved through other mechanism than transcription. Using RIP experiments, we demonstrated specific binding of MEF2A to the pri-miR-494 transcript, but not to pri-miR-487b, a microRNA that was not regulated by Mef2a inhibition in our study. As pri-miR-329 levels were too low in 3T3 cells, we could not confirm or exclude MEF2A binding. Nonetheless, we show here for the first time that MEF2A may not only function as transcription factor, but potentially also as RNA Binding Protein. Future experiments will have to determine whether MEF2A can regulate post-transcriptional processing of other 14q32 microRNAs as well as non-14q32 microRNAs. For example, a recent study demonstrated that MEF2A, via miR-143, regulates proliferation, migration and H_2O_2 induced senescence of vascular smooth muscle cells[21]. This work by Zhao et. al. indeed shows that MEF2A can also regulate expression of microRNAs outside the 14q32 gene cluster.

In the study by Snyder *et al.,* microarray analysis of injured muscle tissue from Mef2a knockout mice revealed downregulation of multiple microRNAs located on mouse chromosome 12F1 (14q32 in humans), indicating regulation of the 12F1/14q32 region by Mef2a, at least in response to injury[12]. To evaluate the role of Mef2a in skeletal muscle regeneration, the authors induced muscle injury in mice[12]. In our study, we made use of the hind limb ischemia model to investigate the role of Mef2a in post-ischemic neovascularization in which no direct damage to the muscle itself was introduced. Furthermore, Snyder *et al.* determined the expression of 14q32 microRNAs in (injured) muscle tissue of Mef2a knockout mice, whereas we measured expression of 14q32 microRNAs in C57Bl/6 muscle tissue wherein Mef2a expression was reduced by ~25% only using GSOs[12]. These differences in the chosen models may explain the observed discrepancies in the regulation of 14q32 microRNAs by Mef2a.

Following the improved blood flow recovery in GSO-Mef2a treated mice, we observed increased arteriogenesis in the adductor muscle of these mice. Phenotypic switching of SMCs, from a contractile to proliferative state, is an important processes in arteriogenesis and other forms of vascular remodelling[22]. Our results would imply that inhibition of Mef2a stimulates proliferation of SMCs, as GSO-Mef2a treated animals showed increased αSMA$^+$ collateral areas compared to GSO-Control treated mice. These findings are in line with the study of Zhao *et al.*, who reported increased proliferation and migration of human SMCs and downregulation of SMC markers upon MEF2A siRNA treatment[19]. Firulli *et al.* reported that the high levels of MEF2A expression in the neointima of rats upon balloon injury correlated with an activated SMC phenotype rather than a mere differentiated phenotype[18]. In addition, we observed increased angiogenesis in the ischemic soleus muscle of GSO-Mef2a treated animals. Collectively, our data suggest that Mef2a plays a role in SMC differentiation and proliferation as well as EC proliferation.

In conclusion, our study demonstrates a novel function for MEF2A in post-ischemic neovascularization and provides a link between MEF2A, 14q32 microRNAs miR-329 and miR-494 and arteriogenesis and angiogenesis. MEF2A acts a novel switch in vascular remodelling and neovascularization. Inhibition of MEF2A expression may be a promising therapeutic strategy to increase neovascularization and blood flow towards the extremities in patients with PAD.

Acknowledgements
We thank W. Razawy, W. Wong, T. Bezhaeva and C.M. Janssen for their technical support. We thank R.A. Boon for sharing the protocol on RNA binding protein immunoprecipitation. This work was supported by the Netherlands Institute for Regenerative Medicine (NIRM, FES0908), the Netherlands Organization for Scientific Research (NWO, Veni-916.12.041) and the Dutch Heart Foundation (Dr. E. Dekker Senior Postdoc, 2014T102).

References

1. van Oostrom MC, van Oostrom O., Quax PH, Verhaar MC, Hoefer IE. Insights into mechanisms behind arteriogenesis: what does the future hold? J Leukoc Biol. 2008;84:1379-1391.
2. Risau W. Mechanisms of angiogenesis. Nature. 1997;386:671-674.
3. Bartel,D.P. MicroRNAs: genomics, biogenesis, mechanism, and function. *Cell* **116**, 281-297 (2004).
4. van Rooij E. & Olson,E.N. MicroRNA therapeutics for cardiovascular disease: opportunities and obstacles. *Nat. Rev. Drug Discov.* **11**, 860-872 (2012).
5. Ono,K., Kuwabara,Y., & Han,J. MicroRNAs and cardiovascular diseases. *FEBS J.* **278**, 1619-1633 (2011).
6. Thum,T. & Condorelli,G. Long noncoding RNAs and microRNAs in cardiovascular pathophysiology. *Circ. Res.* **116**, 751-762 (2015).
7. Boon,R.A. & Dimmeler,S. MicroRNAs in myocardial infarction. *Nat. Rev. Cardiol.* **12**, 135-142 (2015).
8. Feinberg,M.W. & Moore,K.J. MicroRNA Regulation of Atherosclerosis. *Circ. Res.* **118**, 703-720 (2016).
9. Welten,S.M., Goossens,E.A., Quax,P.H., & Nossent,A.Y. The multifactorial nature of microRNAs in vascular remodel ling. *Cardiovasc. Res.*(2016).
10. Welten,S.M. *et al.* Inhibition of 14q32 MicroRNAs miR-329, miR-487b, miR-494, and miR-495 increases neovascular ization and blood flow recovery after ischemia. *Circ. Res.* **115**, 696-708 (2014).
11. Seitz,H. *et al.* A large imprinted microRNA gene cluster at the mouse Dlk1-Gtl2 domain. *Genome Res.* **14**, 1741-1748 (2004).
12. Snyder,C.M. *et al.* MEF2A regulates the Gtl2-Dio3 microRNA mega-cluster to modulate WNT signaling in skeletal muscle regeneration. *Development* **140**, 31-42 (2013).
13. Clark,A.L. & Naya,F.J. MicroRNAs in the Myocyte Enhancer Factor 2 (MEF2)-regulated Gtl2-Dio3 Noncoding RNA Locus Promote Cardiomyocyte Proliferation by Targeting the Transcriptional Coactivator Cited2. *J. Biol. Chem.* **290**, 23162-23172 (2015).
14. Fiore,R. *et al.* Mef2-mediated transcription of the miR379-410 cluster regulates activity-dependent dendritogenesis by fine-tuning Pumilio2 protein levels. *EMBO J.* **28**, 697-710 (2009).
15. Edmondson,D.G., Lyons,G.E., Martin,J.F., & Olson,E.N. Mef2 gene expression marks the cardiac and skeletal muscle lineages during mouse embryogenesis. *Development* **120**, 1251-1263 (1994).
16. Potthoff,M.J. & Olson,E.N. MEF2: a central regulator of diverse developmental programs. *Development* **134**, 4131-4140 (2007).
17. Hayashi,M. *et al.* Targeted deletion of BMK1/ERK5 in adult mice perturbs vascular integrity and leads to endothelial failure. *J. Clin. Invest* **113**, 1138-1148 (2004).
18. Firulli,A.B. *et al.* Myocyte enhancer binding factor-2 expression and activity in vascular smooth muscle cells. Associa tion with the activated phenotype. *Circ. Res.* **78**, 196-204 (1996).
19. Zhao,W., Zhao,S.P., & Peng,D.Q. The effects of myocyte enhancer factor 2A gene on the proliferation, migration and phenotype of vascular smooth muscle cells. *Cell Biochem. Funct.* **30**, 108-113 (2012).
20. Suzuki,E. *et al.* Myocyte enhancer factor 2 mediates vascular inflammation via the p38-dependent pathway. *Circ. Res.* **95**, 42-49 (2004).
21. Zhao,W., Zheng,X.L., Peng,D.Q., & Zhao,S.P. Myocyte Enhancer Factor 2A Regulates Hydrogen Peroxide-Induced Senescence of Vascular Smooth Muscle Cells Via microRNA-143. *J. Cell Physiol* **230**, 2202-2211 (2015).
22. Schirmer,S.H., van Nooijen,F.C., Piek,J.J., & van,R.N. Stimulation of collateral artery growth: travelling further down the road to clinical application. *Heart* **95**, 191-197 (2009).
23. Bhagat,L. *et al.* Novel oligonucleotides containing two 3'-ends complementary to target mRNA show optimal gene-silencing activity. *J. Med. Chem.* **54**, 3027-3036 (2011).
24. Hellingman,A.A. *et al.* Variations in surgical procedures for hind limb ischaemia mouse models result in differences in collateral formation. *Eur. J. Vasc. Endovasc. Surg.* **40**, 796-803 (2010).
25. Nossent,A.Y. *et al.* The 14q32 microRNA-487b targets the antiapoptotic insulin receptor substrate 1 in hypertension-induced remodeling of the aorta. *Ann. Surg.* **258**, 743-751 (2013).
26. Bastiaansen,A.J. *et al.* TLR4 accessory molecule RP105 (CD180) regulates monocyte-driven arteriogenesis in a murine hind limb ischemia model. *PLoS. One.* **9**, e99882 (2014).
27. Baker,M. *et al.* Use of the mouse aortic ring assay to study angiogenesis. *Nat. Protoc.* **7**, 89-104 (2012).

Supplemental Material

Gene	Forward Primer	Reverse Primer
primiR-329	AAGGTCACGTTGGGGAATTA	ACCACGAAGCCTCCAAGAT
premiR-329	TGGTACCGGAAGAGAGGTTTT	AGGTTAGCTGGGTGTGTTTCA
primiR-487b	CTGAGGCGGTGGCTTTG	GAAGCCAGGCTGCAGAGTC
premiR-487b	TGTCCTCTTCGCTTCACTCA	TGAAAAAGTGGATGACCCTGT
primiR-494	TGCCTTTGTTTGCTTTCTGA	GTCATCAGGGACAGGGAGTG
premiR-494	GGAGAGGTTGTCCGTGTTGT	AGGTTTCCCGTGTATGTTTCA
primiR-495	AGCATCCCTTCACACTCAGG	GAGCTCTCCAAGGTGAGATTTG
premiR-495	GTTGCCCATGTTATTTTTCG	AGTGCACCATGTTTGTTTCG

Supplementary Table 1. List of primers used for primiR and premiR quantification.

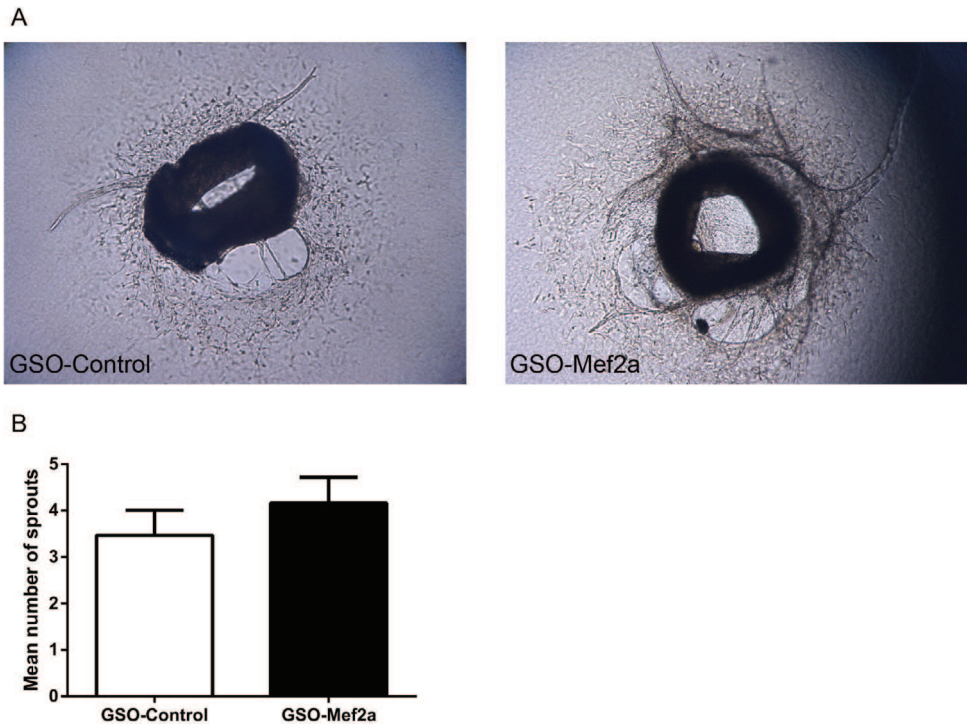

Supplemental Figure 1. Ex vivo sprouting angiogenesis. (A) Outgrowth of neovessels from 5-day collagen-embedded aortic rings treated with GSO-Control or GSO-Mef2a. **(B)** Quantification of neovessels. Data are presented as mean ± SEM and represent 3 independent experiments with 10 rings per condition.

Chapter 7

Posttranscriptional regulation of 14q32 microRNA miR-329 during vascular regeneration after ischemia

Manuscript in preparation

SMJ Welten[1,2]

A Downie Ruiz Velasco[3]

PHA Quax[1,2]

G Michlewski[3]

AY Nossent[1,2]

[1]Department of Surgery, Leiden University Medical Center, Leiden, the Netherlands

[2]Einthoven Laboratory for Experimental Vascular Medicine,

Leiden University Medical Center, Leiden, the Netherlands

[3]The Wellcome Trust Centre for Cell Biology,

University of Edinburgh, United Kingdom

Abstract

The human imprinted 14q32 locus holds the largest known microRNA gene cluster, encoding 54 individual microRNAs. We have previously shown that the 14q32 microRNA cluster plays a role in neovascularization. After induction of ischemia in mice, 14q32 microRNAs are regulated in three distinct temporal patterns. These expression patterns, as well as basal expression levels, were independent of the microRNA genes' order in the 14q32 locus. These findings indicate that posttranscriptional processing of 14q32 microRNA precursors is a major determinant of 14q32 microRNA expression.

Using rt/qPCR primers specific for each stage of microRNA processing, i.e. pri-microRNA, pre-microRNA and mature microRNA, we found that increased expression of 14q32 microRNAs after hindlimb ischemia is determined by increased processing from pre- to mature microRNA, rather than increased transcription. We used Stable Isotope Labelling of Amino Acids (SILAC), followed by pre-microRNA pull-down and Mass Spectrometry to identify proteins that are responsible for posttranscriptional regulation of 14q32 microRNA precursors.
We observed differential binding of proteins CIRBP and HADHB to the precursors of late-responder miR-329-3p and non-responder miR-495-3p. Immunohistochemical staining confirmed expression of both CIRBP and HADHB in the adductor muscle of mice and expression of both CIRBP and HADHB was upregulated after hind limb ischemia. Using RNA Binding Protein immunoprecipitation (RIP) experiments, we showed specific binding of CIRBP to pre-miR-329, but not to pri-miR-329. Finally, inhibition of CIRBP, using RNAi, reduced miR-329-3p and miR-495-3p levels in 3T3 cells.

These data demonstrate a novel role for CIRBP and HADHB in posttranscriptional regulation of 14q32 microRNAs under ischemia.

Introduction

MicroRNAs are short endogenous RNA molecules (~22 nucleotides) that decrease expression of their target genes via translational repression[1]. MicroRNA genes are transcribed by RNA polymerase II as primary microRNA (pri-miR) transcripts. Subsequently, these pri-miRs are processed by the microprocessor complex, consisting of the RNase III Drosha and co-factor DGCR8, to form precursor microRNAs (pre-miRs) of about 70 nucleotides long. Pre-miRs are exported to the cytoplasm where the enzyme Dicer cleaves the pre-miR into a microRNA duplex. Generally, one strand of the microRNA duplex (guide strand) is preferred for association with an Argonaute (AGO) protein and loading into the RNA induced silencing complex (RISC). However, accumulating evidence suggests that the other strand (passenger strand) can also be loaded into the RISC[2, 3]. MicroRNAs guide the RISC to specific mRNA targets, in order to control mRNA translation[1]. A single microRNA is able to target numerous genes and by doing so, that microRNA can regulate complex, physiological processes. Over the past decade, microRNAs have been shown to play an important role in human disease, including cardiovascular disease. Although microRNAs regulate physiological and pathological processes via modulation of target gene expression, microRNA expression itself is subject to regulation too.

MicroRNA expression can be regulated at transcriptional as well as posttranscriptional level. Processing of microRNA precursors can be controlled at the conversion of pri-miR to pre-miR through modulation of Drosha/DGCR8 activity and at the conversion of pre-miR to mature microRNA through modulation of Dicer activity. RNA binding proteins (RBPs) have been found to bind sequences in the terminal loop and stem of pri-miRs, thereby enhancing or inhibiting pri- to pre-miR cleavage[4-7]. For example, processing of pri-miRs with conserved terminal loop regions, such as pri-miR-18a or pri-let-7a have been shown to be affected by hnRNP A1 protein[7-9]. Furthermore, a subset of murine microRNAs was affected by depletion of p68 and p72 helicases, resulting in reduced levels of pre-miRs, but not pri-miRs[10]. In addition, p53 and SMADs have been reported to (in)directly interact with Drosha and modulate pri- to pre-miR cleavage[6, 11]. The RNA binding protein LIN-28 was reported to block accumulation of let-7 levels by repression of both Drosha and Dicer[12]. Another RBP, AUF1, was shown to interact with Dicer and lowered Dicer mRNA stability, leading to a decrease in mature microRNA levels, but not pre-miR levels[13]. Recently, Rbfox proteins were found to bind pre-miRs of miR-20b and miR-107 through specific Rbfox RNA recognition motifs in their terminal loops and Rbfox2 was shown to decrease mature miR-20b and miR-107 levels[14].

Many microRNAs are encoded within clusters and can be transcribed as long polycistronic transcripts. With 54 microRNA precursors, the 14q32 cluster is the largest known polycistronic microRNA gene cluster in humans. In mice, this cluster is located on chromosome 12F1 and contains 61 microRNAs. We have previously described the differential regulation of 14q32 microRNAs in a mouse model for ischemia in the hind limb[15]. MicroRNAs from the 14q32 cluster followed three different expression patterns after induction of ischemia. These patterns are independent of the chromosomal location of the 14q32 microRNA genes. Furthermore, even baseline expression levels of these 14q32 microRNAs vary greatly. These findings indicate that individual 14q32 microRNA expression is regulated predominantly at posttranscriptional level.

In this study, we show that 14q32 microRNAs are indeed regulated at posttranscriptional level. We identified RBPs that bind and process specific 14q32 microRNA precursors. This helps to explain the differential expression of 14q32 microRNAs under ischemia and expands our knowledge of regulation of microRNA biogenesis under pathological conditions.

Methods

Hind limb ischemia model

All experiments were approved by the committee on animal welfare of the Leiden University Medical Center (Leiden, the Netherlands. Approval reference numbers 09163 and 10243). This study was conducted in accordance with the Dutch government guidelines and the Directive 2010/63/EU of the European Parliament. Unilateral hind limb ischemia was induced in healthy adult male C57BL6 mice by single ligation of the left femoral artery, as previously described[15]. Briefly, electrocoagulation of the femoral artery was performed proximal to the superficial epigastric artery (single ligation model) or combined with electrocoagulation of the distal femoral artery, proximal to the bifurcation of the popliteal and saphenous artery (double ligation model)[16]. C57Bl/6 mice (n=4 per timepoint) were sacrificed at several timepoints (day 0 (before ligation of the femoral artery), day 1, 3, 7, 10, 14 and 28) after hind limb ischemia induction. Upon sacrifice, the adductor and gastrocnemius muscles were harvested and either snap-frozen on dry ice or fixed in 4% paraformaldehyde.

Microarray

For microarray analysis, total RNA was isolated from adductor muscles using the RNeasy fibrous tissue minikit (Qiagen). RNA concentration, purity and integrity were analysed by nanodrop (Nanodrop® Technologies) and Bioanalyzer (Agilent 2000) measurements. Animals

For microRNA expression profiling, adductor muscle tissue of day 0, 1, 3 and 7 after induction of hind limb ischemia was used. MicroRNA expression profiling was performed as previously described, using LNA based arrays (miRCURY LNA™ miR Array ready-to-spot probe set, Exiqon)[15]. Normalization and background correction was performed in the “statistical language R” using “vsn” package (Bioconductor). Differential expression was assayed using the “limma” package (Bioconductor) by fitting the eBayes linear model and contrasting individual treatments with untreated controls. Log2 fold changes were calculated using the toptable function of the limma package.

For whole genome expression profiling, adductor muscle tissue of day 0, 1, 3, 7, 14 and 28 after induction of hind limb ischemia was used. Whole genome expression profiling was performed using MouseWG-6 v2.0 Expression Beadchips (Illumina) and expression levels were Log2-transformed, as previously described[15].

Cell culture

3T3 cells were cultured at 37ºC in a humidified 5% CO_2 environment. Culture medium consisted of DMEM GlutaMAX™ (Gibco) supplemented with 10% heat inactivated fetal calf serum (PAA) and 1% penicillin/streptomycin (PAA). Culture medium was refreshed every 2-3 days. Cells were passed using trypsin-EDTA (Sigma) at 90% confluency.

In vitro regulation of microRNA expression

To mimic the differential microRNA expression after *in vivo* ischemia, 3T3 cells were cultured under serum starvation conditions (DMEM glutaMAX™ supplemented with 0.5% heat inactivated fetal calf serum and 1% penicillin/streptomycin). Cells were starved overnight under serum starve conditions (~16 hours) and the next morning cells were either placed on starve medium (0.5% FCSi) or stimulation medium (10% FCSi) for 24 or 48 hours.

RNA pull-down and SILAC Mass Spectrometry

RNA pull-down and mass spectrometry were performed as described previously, with slight modifications[17]. In brief, total protein extracts from normal serum and serum starved 3T3 cells grown in ‘light’ [^{12}C]Arg/[12C]Lys and ‘heavy’ [^{13}C]Arg/[^{13}C]Lys isotopes, respectively, were incubated with in vitro transcribed RNAs chemically coupled to agarose beads. The incubation was followed by a series of washes with buffer G (20 mM Tris pH 7.5, 135 mM NaCl, 1.5 mM MgCl2, 10% (v/v) glycerol, 1 mM EDTA, 1 mM DTT and 0.2 mM PMSF). After the final wash, the proteins associated with the RNA on the beads were analyzed by SDS–PAGE followed by in-gel digestion and mass spectrometry or western blotting.

Western Blot Analysis

Total protein samples from 3T3 cells (100 µg per lane), isolated by sonication, were resolved by standard NuPAGE SDS–PAGE electrophoresis with MOPS running buffer (Life Technologies) and transferred onto a nitrocellulose membrane.

Total protein samples (5 µg per lane) from murine adductor muscle tissue were isolated using a standard TRIzol protocol (Thermo Fisher) at day 0, 1, 3 and 10 after induction of ischemia (double ligation model). The membrane was blocked overnight at 4°C with 1:10 western blocking reagent (Roche) in TBS buffer with 0.1% Tween-20 (TBST). The following day, the membrane was incubated for 1 h at room temperature with primary antibody solution in 1:20 western blocking reagent diluted in TBST in the following concentrations; rabbit polyclonal CIRBP (Protein Tech 10209-2-AP) 1:1000, rabbit polyclonal HADHB (LSBio-LS-C334236) 1:500. After washing in TBST, the blots were incubated with the appropriate secondary antibody conjugated to horseradish peroxidase and detected with SuperSignal West Pico detection reagent (Thermo Scientific). The membranes were stripped using ReBlot Plus Strong Antibody Stripping Solution (Chemicon) equilibrated in water, blocked in 1:10 western blocking solution in TBST and re-probed as described above.

Western Blots were quantified using ImageJ analysis software (1.48v, NIH) and normalized to the input.

RNA Binding Protein Immunoprecipitation

RNA Binding Protein immunoprecipitation (RIP) was performed using the EZMagna RIP kit (Millipore), according to manufacturer's instructions. 3T3 cells were grown to 90% confluency and lysed in complete RIP lysis buffer. Cell lysates were incubated with RIP buffer containing magnetic beads conjugated with antibodies against Cold Induced RNA binding protein (CIRBP, Abcam ab106230), hydroxyacyl-CoA dehydrogenase/3-ketoacyl-CoA thiolase/enoyl-CoA hydratase (trifunctional protein), beta subunit (HADHB, Novus Biologicals NBP1-82609), SND1 (Abcam ab71186) and rabbit control IgG (Millipore PP64B). Before immunoprecipition, 10% of cell lysate was taken and served as input control. Next, samples were treated with proteinase K to digest protein and RNA was isolated using a standard TRIzol-chloroform extraction protocol.

RNA interference

The following sense siRNA sequences (Sigma-Aldrich) were used to target CIRBP in 3T3 cells;

CIRBP1: GAGACAGCUAUGACAGUUAUU and *CIRBP2: GUGGUAAAGGACAGGGAGA.*

SiRNAs were transfected using Lipofectamine 2000 (Life Technologies) in either a single event or two events separated by 48h, as indicated. A concentration of RNA in Opti-MEM medium of 400nM was ensured, following manufacturer's instructions.

RT/qPCR

Adductor and gastrocnemius muscles from day 0 and day 1, 3 and 7 after surgery were homogenized by grounding with a pestle and mortar in liquid nitrogen. Total RNA was isolated using a standard TRIzol-chloroform extraction protocol. RNA concentration and purity were determined by nanodrop (Nanodrop® Technologies). RNA was reverse transcribed using high-capacity RNA to cDNA RT kits (Life Technologies, USA). Relative quantitative mRNA PCR was performed on reverse transcribed cDNA using, SYBR® green dye (Qiagen). Primers for pri-miRs, pre-miRs, HADHB and CIRBP were designed using Primer3. Sequences of primers are listed in Supplementary Table 1. MicroRNA quantification was performed using Taqman® microRNA assays (Applied Biosystems) according to manufacturer's protocol. Relative quantitative PCR was performed on the Viia7 system (Applied Biosystems) and amplification efficiencies were checked by standard curves. Data were normalized using a stably expressed endogenous control (snRNA-U6).

Levels of mature microRNAs in serum-starvation experiments on 3T3 cells were measured using miRScript RT (Qiagen) and SYBR® green (Qiagen). MicroRNA levels were normalized to microRNA-16.

Immunohistochemical staining

Formaldehyde fixed adductor muscles were paraffin-embedded and 5 µm thick cross-sections of muscles were stained to visualize expression of RNA binding proteins. Cross sections of adductor muscles were re-hydrated and endogenous peroxidase activity was blocked. Antigen retrieval was performed with Citrate buffer (pH 6.0) at 100ºC for 10 minutes. Muscles were stained with rabbit polyclonal anti-HADHB (Novus Biologicals, NBP1-82609, 1:1000) or goat polyclonal anti-CIRBP (Abcam, ab106230, 1:400) to visualize HADHB and CIRBP respectively, and counterstained using haematoxylin.

Results

In vivo microRNA regulation

MicroRNA microarray was performed in order to determine differential expression of microRNAs after induction of ischemia in vivo. MicroRNAs from the 14q32 cluster showed three different temporal expression patterns after single ligation of the femoral artery. One third of the 14q32 microRNAs were upregulated within 24 hours after ischemia induction (early responders, Figure 1A, average expression Figure 1B). Another third of 14q32 microRNAs were upregulated 72 hours after induction of ischemia (late responders, Figure 1C, average expression Figure 1D), whereas the other 14q32 microRNAs were not differentially expressed after ischemia (non-responders, Figure 1E, average expression Figure 1F). When looking at the distribution of early, late and non-responders on the 14q32 locus, there was no association between the expression profiles of microRNAs and their corresponding gene's chromosomal location (Figure 1G). In addition, baseline expression levels of 14q32 microRNAs were variable and also independent of their corresponding gene's chromosomal location. Because of their proven efficacy in post-ischemic neovascularization[15], we focused on early responder miR-494-3p, late responder miR-329-3p and non-responder miR-495-3p for further experiments.

Pri-miR, pre-miR and mature miR levels of 14q32 microRNAs

Using specific primers for each of the microRNA processing steps of 14q32 microRNAs miR-329-3p, miR-494 and miR-495-3p, we determined the expression levels of the pri-miR, pre-miR and mature microRNA of these microRNAs in the adductor muscle tissue after induction of ischemia in mice. Expression of pri-miR-329 decreased slightly after ischemia induction, but increased in expression by day 7 after induction of ischemia. Pre-miR-329 followed expression of pri-miR-329 at 24 hours after ischemia but continued to decrease until 72 hours after ischemia induction. Expression of mature miR-329-3p mirrored expression of pre-miR-329 (Figure 2A). For early responder miR-494, expression of the pri-miR transcript was also decreased at 24 and 72 hours after ischemia induction. The abundance of pre-miR-494 however was slightly reduced 24 hours after ischemia, whereas mature miR-494 levels were upregulated (Figure 2B). Expression of microRNA-495 pri-miR and pre-miR followed the same pattern after ischemia, showing decreased expression within 24 hours (Figure 2C). However, mature miR-495-3p levels remained unchanged after ischemia induction. Where pre-miR expression levels were exhausted, we observed increased expression of mature miR levels, which was especially true for early responder miR-494 and late responder miR-329-3p. These data suggest that regulation of 14q32 microRNA processing takes places at the conversion from pre-miR to mature microRNA.

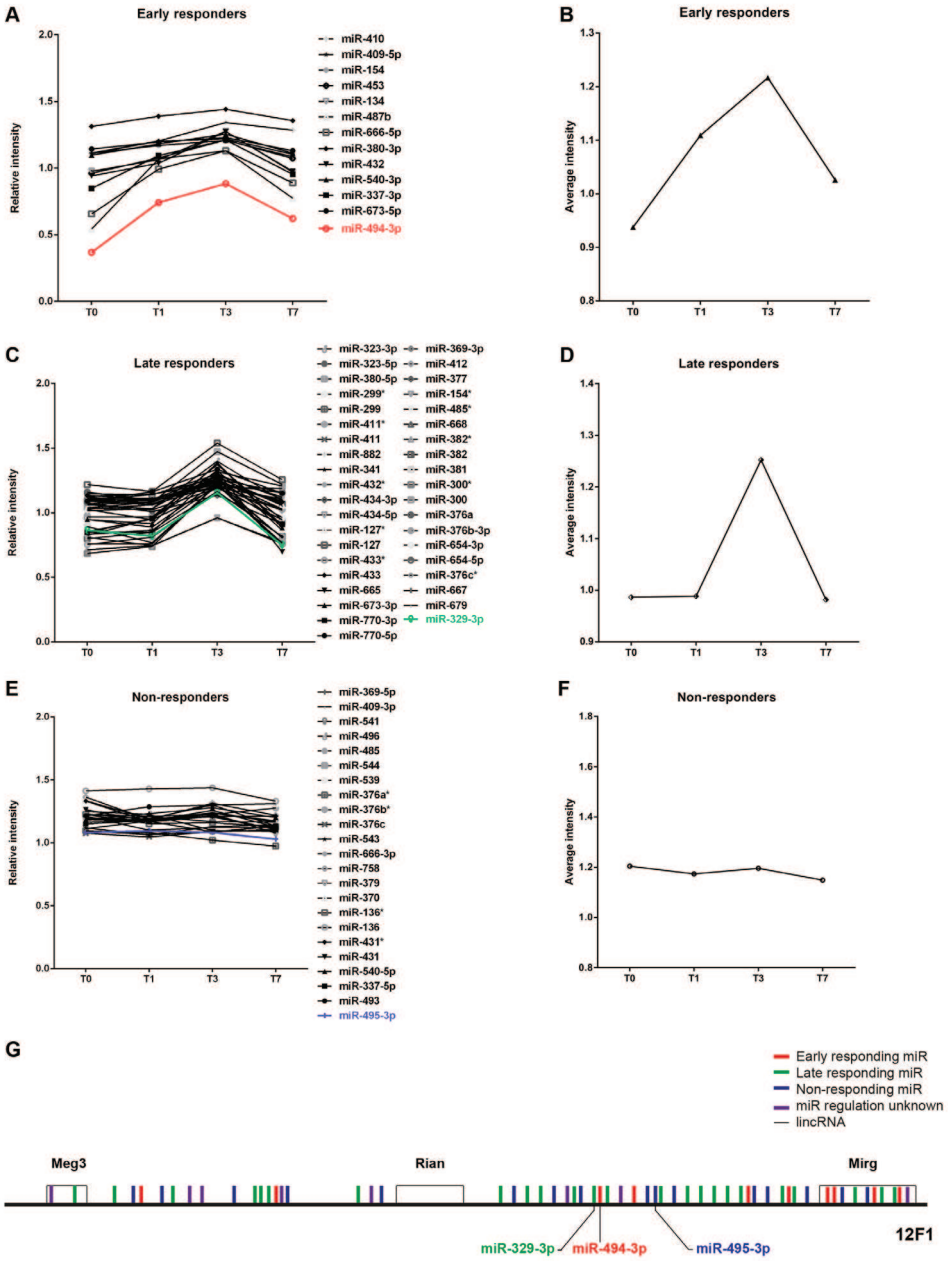

Figure 1. Differential expression patterns of 14q32 microRNAs after induction of ischemia. MicroRNA expression was evaluated before induction of ischemia (T0), day 1 (T1), day 3 (T3) and day 7 (T7) after induction of ischemia. Early responder 14q32 microRNAs were upregulated within 24 hours after ischemia (A). Average intensity of all early responders (B). Late responder 14q32 microRNAs were not upregulated until 72 hours after ischemia induction (C). Average intensity of all late responders (D). Non-responder 14q32 microRNAs were not regulated after ischemia (E). Average intensity of all non-responders (F). Chromosomal location of early (red), late (green) and non-responders (blue) on the murine 12F1 locus (G).

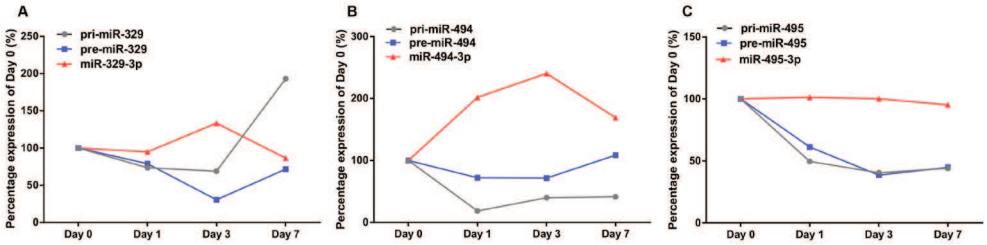

Figure 2. Pri-miR, pre-miR and mature miR expression levels of 14q32 microRNAs. Percentage of expression (relative to day 0) of pri-miR-329, pre-miR-329 and mature miR-329-3p at day 0 (no ischemia), day 1, day 3 and day 7 after ischemia induction (A). Percentage expression of day 0 of pri-, pre- and mature miR-494-3p after ischemia (B). Percentage expression of day 0 of pri-, pre- and mature miR-495 after ischemia (C).

Pre-microRNA pull down followed by SILAC Mass Spectrometry reveals putative 14q32 microRNA biogenesis factors

Using serum-starvation of 3T3 cells, we were able to mimic the *in vivo* regulation of 14q32 microRNAs miR-329-3p and miR-495-3p, but not miR-494-3p *in vitro* (Figure 3). We therefore focussed on miR-329-3p and miR-495-3p. To identify the RBPs that are responsible for differential expression of these two microRNAs via posttranscriptional regulation, we performed Stable Isotope Labelling of Amino Acids, followed by RNA pull down and Mass Spectrometry (Figure 4A-B). We identified several proteins, which were specifically bound to pre-miR-329 and pre-miR-495, namely RBM28 and TBL3 (pre-miR-329 specific), RBM15 (pre-miR-495 specific) as well as proteins CKAP4, P4HB, CIRBP and HADHB, which were bound to both pre-miR-329 and pre-miR-495, showing an increase in binding after serum starvation. Using Western Blot analysis, we validated binding of HADHB and CIRBP to miR-329 and miR-495 precursors (Figure 4C-F). While both proteins seemed to bind pre-miR-495 in both serum starvation and non-starvation conditions, binding to pre-miR-329 was greatly increased following serum starvation.

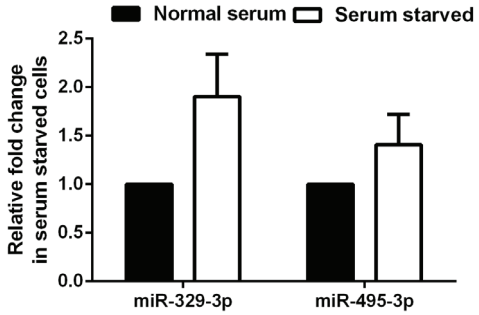

Figure 3. Levels of mature miR-329 and miR-495 in serum starved 3T3 cells. The levels of mature miR-329-3p and miR-495-3p were determined by rt/qPCR. 3T3 cells were serum-starved for 24h and expression levels were compared to non-starved cells.

CIRBP and HADHB expression in vivo

We next determined expression of RNA binding proteins CIRBP and HADHB *in vivo* in the adductor muscle at different timepoints after induction of ischemia. Using immunohistochemistry, we confirmed expression of both CIRBP and HADHB in the adductor muscle of mice after ischemia (Figure 5A and 5B,

respectively). Expression of CIRBP mRNA was increased within 24 hours after induction of ischemia, whereas HADHB mRNA was increased at 3 days after induction of ischemia (Figures 5C and 5D). Finally, using western blot analysis of CIRBP and HADHB in adductor muscle at different time points, we observed an acute but transient increase in CIRBP protein levels at day 1 after ischemia induction. HADHB protein levels were also upregulated within 1 day, but they remained elevated until 10 days after induction of ischemia (Figure 5E and 5F).

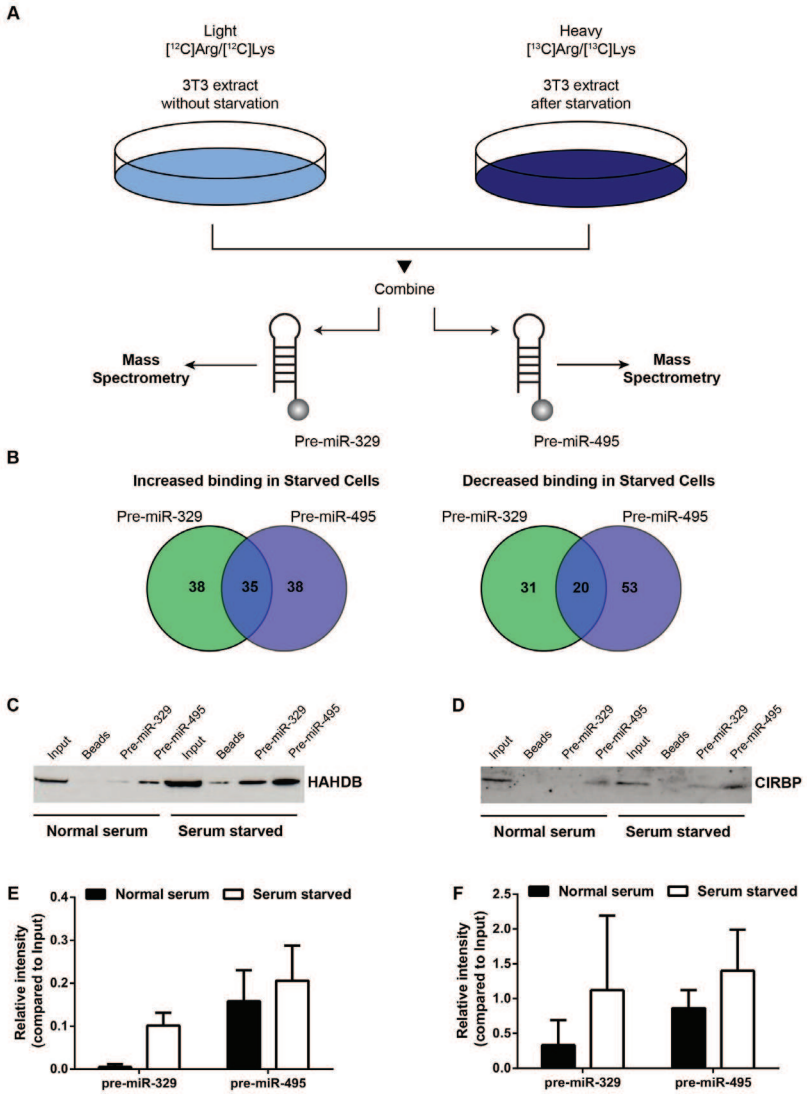

Figure 4. Identification of proteins binding pre-miR-329 and pre-miR-495 (A) Schematic representation of RNA pull down combined with SILAC mass spectrometry (B) Number of proteins showing increased and decreased binding to pre-miR-329, pre-miR-495 or both. Western Blot validation of HADHB (C) and CIRBP (D) binding to pre-miR-329 and pre-miR-495 under conditions of normal serum and serum starvation. (E-F) Western Blot quantification of HADHB (E) and CIRBP (F) binding to pre-miR-329 and pre-miR-495 under conditions of normal serum and serum starve conditions (relative to input (n=3)).

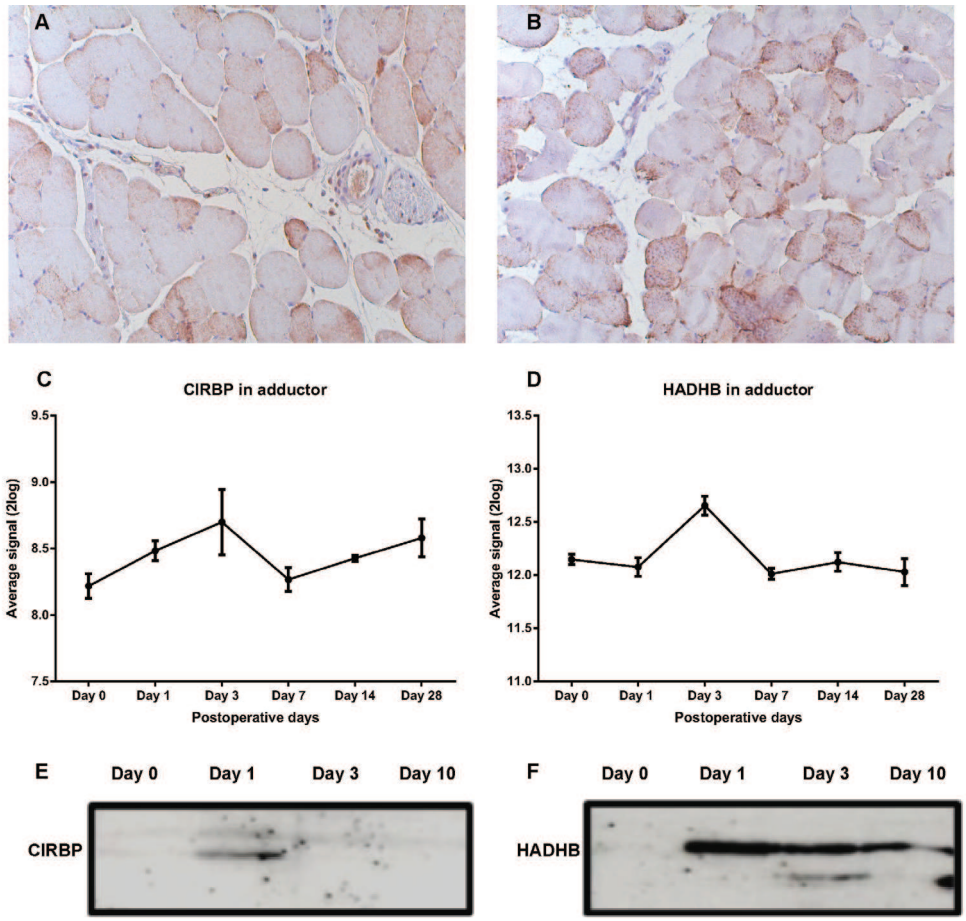

Figure 5. Expression of CIRBP and HADHB *in vivo*. Immunohistochemical staining of the murine adductor muscle after ischemia induction revealed expression of both CIRBP (A) and HADHB (B) in these tissues, predominantly in the cytoplasm of cells. Microarray analysis of mRNA expression of CIRBP (C) and HADHB (D) mRNA in the adductor muscle of mice at several time points after induction of ischemia. (E, F) Western Blot analysis of CIRBP and HADHB protein levels in the adductor muscle at several time points after ischemia.

HADHB and CIRBP binding to miR-329 pri-miR, pre-miR and mature miR transcripts

RIP experiments using antibodies against HADHB and CIRBP or a negative control IgG was performed to determine interaction between RBPs HADHB and CIRBP and 14q32 miR-329 and miR-495 precursors in 3T3 cell cultures. Whereas HADHB binds both pri-miR-329 and pre-miR-329, CIRBP showed specific binding to pre-miR-329, not to pri-miR-329 (Figure 6). CIRBP and HADHB both bind the mature miR-329-3p. Expression of pri-miR-495 and pre-miR-495 was too low to either confirm or exclude binding of CIRBP or HADHB. RIP experiments using an unrelated RBP that has been shown to regulate processing of polycistronic microRNAs, namely SND1[18], showed no specific binding to either pri-miRs or pre-miRs of miR-329 and miR-495 (Supplemental Figure 1).

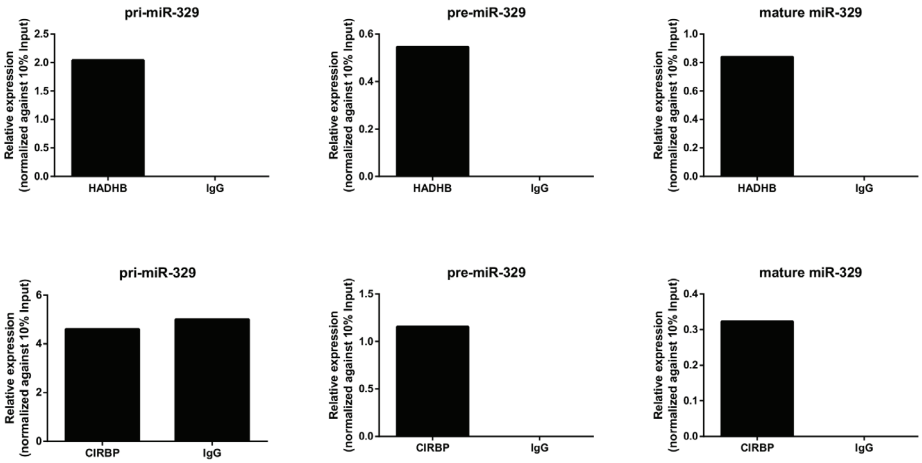

Figure 6. RNA binding protein immunoprecipitation with HADHB and CIRBP antibodies. Pri-miR-329, pre-miR-329 and mature miR-329 expression levels were measured in 3T3 cell lysates after immunoprecipitation with HADHB (top) and CIRBP (bottom) antibodies and non-specific IgG antibody.

Expression of miR-329-3p and miR-495-3p after CIRBP silencing

Next, we used two different siRNAs (CIRBP-1 and CIRBP-2) to knock-down the levels of CIRBP in 3T3 cells. Silencing of CIRBP was performed using either a single or double transfection with CIRBP targeting siRNAs. Both single and double transfections reduced CIRBP protein levels, which was confirmed using Western Blot analysis (Figure 7A). Next, we measured the levels of mature microRNAs miR-329-3p and miR-495-3p in 3T3 cells following 24 hours serum-starvation (Figure 7B). Following serum-starvation, expression of both miR-329-3p and miR-495-3p was downregulated in CIRBP knock-down cells, which was not observed in cells that were either mock transfected or transfected with control siRNA.

Figure 7. siRNA mediated knockdown of CIRBP. Western Blot showing protein levels of CIRBP (A). The first 4 lanes show decreased

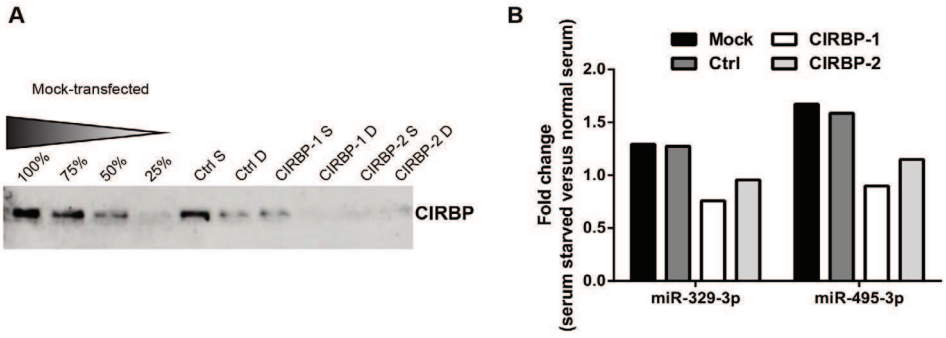

concentrations of mock-transfected 3T3 extract, reflecting decreased CIRBP concentrations. The next lanes show CIRBP protein levels in 3T3 cells following either a single (S) or double (D) transfection with siRNAs targeting CIRBP (CIRBP-1 and CIRBP-2) or control siRNA (A). Fold change of mature miR-329-3p or miR-495-3p levels in starved cells after double transfection with siRNAs against CIRBP (B).

Discussion

In this study, we investigated posttranscriptional regulation of 14q32 microRNAs during ischemia. Using specific primers for each of the microRNA processing steps, we found that increased expression of 14q32 microRNAs after hind limb ischemia is not determined by increased transcription, but that it is the result of increased processing of pre-microRNA to mature microRNA. The observed expression pattern of 14q32 microRNAs *in vivo* after ischemia was mimicked *in vitro* using serum starvation of 3T3 cells. This allowed us to investigate which RBPs can bind to pre-miR transcripts of 14q32 microRNAs, using Stable Isotope Labelling of Amino Acids (SILAC), followed by RNA pull-down and Mass Spectrometry. The RNA binding proteins CIRBP and HADHB were shown to specifically bind miR-329 and miR-495 precursors. We confirmed expression and upregulation of these RBPs in murine muscle tissues during ischemia, at mRNA level as well as protein level.

Posttranscriptional regulation of polycistronic microRNAs has been described previously. In fact, differential expression after induction of hindlimb ischemia, similar to that of the 14q32 microRNAs, has also been shown for microRNAs of the polycistronic miR-17-92a cluster. The miR-17-92a cluster encodes for seven mature microRNAs and is transcribed as one single primary transcript[19]. However, individual members of the miR-17-92a cluster were differentially expressed during endothelial differentiation of murine embryonic stem cells[20]. The SND1 protein, which is a component of the RISC, was found to bind to pri-miRs, pre-miRs and mature microRNAs of the miR-17-92a cluster. Silencing of SND1 reduced processing of miR-17-92a cluster members, especially under hypoxic conditions[18]. Here, we could not demonstrate binding of SND1 to either pri-miRs or pre-miRs of 14q32 microRNAs miR-329 and miR-495 using RIP experiments. Our data demonstrate that processing of 14q32 microRNAs miR-329 and miR-495 is independent of SND1 binding, but instead relies on CIRBP and HADHB.

CIRBP is an evolutionary conserved RBP that is transcriptionally upregulated in low temperature conditions or other conditions of stress, including ischemia[21, 22]. CIRBP protein is predominantly expressed in the nucleus, but can also be transported to the cytoplasm under physiological or stressful conditions[23]. MicroRNA processing from pre-miR to mature microRNA also occurs in the cytoplasm. CIRBP is involved in posttranscriptional regulation of mRNAs. Here however, we show for the first time that CIRBP is also involved in posttranscriptional regulation of microRNAs. Future experiments will have to determine whether CIRBP can also regulate other microRNAs during ischemia.

HADHB forms the beta subunit of the mitochondrial trifunctional protein, which catalyzes the last steps of mitochondrial beta-oxidation of long chain fatty acids. In addition, HADHB was found to act as an RBP and bind renin mRNA, leading to destabilization of renin mRNA[24]. Localization of HADHB was found to be predominantly in mitochondria, but also in the cytoplasm and nucleoli of Calu-6 cells[25]. In this study, we observed both cytoplasmic as well as nuclear expression of both HADHB and CIRBP in murine adductor muscle tissue after ischemia. In addition, we have now shown that HADHB can also bind pri-miRs, pre-miRs and mature microRNAs of the 14q32 microRNA cluster, indicating its role in posttranscriptional regulation of microRNA expression under ischemia.

Regulation of microRNA processing under stress conditions such as hypoxia has been previously reported by several studies[26-28]. In endothelial cells, hypoxia was shown to both increase expression of certain microRNAs (such as miR-210)[27] as well as to reduce microRNA processing[28]. Further examination revealed that chronic hypoxia down-regulated expression of Dicer, reducing subsequent microRNA processing[28]. More recently, the involvement of the Epidermal Growth Factor Receptor (EGFR) in microRNA processing under hypoxic conditions was reported. EGFR was shown to increase phosphorylation of AGO2 under hypoxic conditions, which reduced AGO2 binding to Dicer and subsequent microRNA processing from pre-microRNA to mature microRNA by Dicer[29]. Although we did not study regulation of 14q32 microRNA processing under true hypoxic conditions *in vitro*, we were able to demonstrate increased processing under conditions of serum starvation.

In this study, we identified RBPs that bind and regulate specific 14q32 microRNA precursors. These results provide insights into the complex regulation of the 14q32 microRNAs. We showed for the first time that CIRBP and HADHB, which have been shown to control posttranscriptional regulation of mRNAs, are also involved in posttranscriptional processing of microRNAs. Through manipulation of CIRBP and HADHB, that control expression of 14q32 microRNAs, we may be able to influence 14q32 microRNA expression higher up the regulatory cascade, possibly having more profound therapeutic effects on post-ischemic neovascularization.

References

1. Bartel DP. MicroRNAs: genomics, biogenesis, mechanism, and function. Cell 2004 Jan 23;116(2):281-97.
2. Yang X, Du WW, Li H, Liu F, Khorshidi A, Rutnam ZJ, et al. Both mature miR-17-5p and passenger strand miR-17-3p target TIMP3 and induce prostate tumor growth and invasion. Nucleic Acids Res 2013 Nov;41(21):9688-704.
3. Schober A, Nazari-Jahantigh M, Wei Y, Bidzhekov K, Gremse F, Grommes J, et al. MicroRNA-126-5p promotes endothelial proliferation and limits atherosclerosis by suppressing Dlk1. Nat Med 2014 Apr;20(4):368-76.
4. Viswanathan SR, Daley GQ, Gregory RI. Selective blockade of microRNA processing by Lin28. Science 2008 Apr 4;320(5872):97-100.
5. Trabucchi M, Briata P, Garcia-Mayoral M, Haase AD, Filipowicz W, Ramos A, et al. The RNA-binding protein KSRP promotes the biogenesis of a subset of microRNAs. Nature 2009 Jun 18;459(7249):1010-4.
6. Suzuki HI, Yamagata K, Sugimoto K, Iwamoto T, Kato S, Miyazono K. Modulation of microRNA processing by p53. Nature 2009 Jul 23;460(7254):529-33.
7. Michlewski G, Guil S, Semple CA, Caceres JF. Posttranscriptional regulation of miRNAs harboring conserved terminal loops. Mol Cell 2008 Nov 7;32(3):383-93.
8. Guil S, Caceres JF. The multifunctional RNA-binding protein hnRNP A1 is required for processing of miR-18a. Nat Struct Mol Biol 2007 Jul;14(7):591-6.
9. Michlewski G, Caceres JF. Antagonistic role of hnRNP A1 and KSRP in the regulation of let-7a biogenesis. Nat Struct Mol Biol 2010 Aug;17(8):1011-8.
10. Fukuda T, Yamagata K, Fujiyama S, Matsumoto T, Koshida I, Yoshimura K, et al. DEAD-box RNA helicase subunits of the Drosha complex are required for processing of rRNA and a subset of microRNAs. Nat Cell Biol 2007 May;9(5):604-11.
11. Davis BN, Hilyard AC, Lagna G, Hata A. SMAD proteins control DROSHA-mediated microRNA maturation. Nature 2008 Jul 3;454(7200):56-61.
12. Heo I, Joo C, Kim YK, Ha M, Yoon MJ, Cho J, et al. TUT4 in concert with Lin28 suppresses microRNA biogenesis through pre-microRNA uridylation. Cell 2009 Aug 21;138(4):696-708.
13. Abdelmohsen K, Tominaga-Yamanaka K, Srikantan S, Yoon JH, Kang MJ, Gorospe M. RNA-binding protein AUF1 represses Dicer expression. Nucleic Acids Res 2012 Dec;40(22):11531-44.
14. Chen Y, Zubovic L, Yang F, Godin K, Pavelitz T, Castellanos J, et al. Rbfox proteins regulate microRNA biogenesis by sequence-specific binding to their precursors and target downstream Dicer. Nucleic Acids Res 2016 Mar 21.
15. Welten SM, Bastiaansen AJ, de Jong RC, de Vries MR, Peters EA, Boonstra MC, et al. Inhibition of 14q32 MicroRNAs miR-329, miR-487b, miR-494, and miR-495 increases neovascularization and blood flow recovery after ischemia. Circ Res 2014 Sep 26;115(8):696-708.
16. Hellingman AA, Bastiaansen AJ, de Vries MR, Seghers L, Lijkwan MA, Lowik CW, et al. Variations in surgical procedures for hind limb ischaemia mouse models result in differences in collateral formation. Eur J Vasc Endovasc Surg 2010 Dec;40(6):796-803.
17. Choudhury NR, de Lima AF, de Andres-Aguayo L, Graf T, Caceres JF, Rappsilber J, et al. Tissue-specific control of brain-enriched miR-7 biogenesis. Genes Dev 2013 Jan 1;27(1):24-38.
18. Heinrich EM, Wagner J, Kruger M, John D, Uchida S, Weigand JE, et al. Regulation of miR-17-92a cluster processing by the microRNA binding protein SND1. FEBS Lett 2013 Aug 2;587(15):2405-11.
19. He L, Thomson JM, Hemann MT, Hernando-Monge E, Mu D, Goodson S, et al. A microRNA polycistron as a potential human oncogene. Nature 2005 Jun 9;435(7043):828-33.
20. Treguer K, Heinrich EM, Ohtani K, Bonauer A, Dimmeler S. Role of the microRNA-17-92 cluster in the endothelial differentiation of stem cells. J Vasc Res 2012;49(5):447-60.
21. Wellmann S, Buhrer C, Moderegger E, Zelmer A, Kirschner R, Koehne P, et al. Oxygen-regulated expression of the RNA-binding proteins RBM3 and CIRP by a HIF-1-independent mechanism. J Cell Sci 2004 Apr 1;117(Pt 9):1785-94.
22. Jackson TC, Manole MD, Kotermanski SE, Jackson EK, Clark RS, Kochanek PM. Cold stress protein RBM3 responds to temperature change in an ultra-sensitive manner in young neurons. Neuroscience 2015 Oct 1;305:268-78.
23. Zhu X, Buhrer C, Wellmann S. Cold-inducible proteins CIRP and RBM3, a unique couple with activities far beyond the cold. Cell Mol Life Sci 2016 May 4.
24. Adams DJ, Beveridge DJ, van der Weyden L, Mangs H, Leedman PJ, Morris BJ. HADHB, HuR, and CP1 bind to the distal 3'-untranslated region of human renin mRNA and differentially modulate renin expression. J Biol Chem 2003 Nov 7;278(45):44894-903.
25. Morris BJ, Adams DJ, Beveridge DJ, van der Weyden L, Mangs H, Leedman PJ. cAMP controls human renin mRNA stability via specific RNA-binding proteins. Acta Physiol Scand 2004 Aug;181(4):369-73.
26. Leung AK, Sharp PA. MicroRNA functions in stress responses. Mol Cell 2010 Oct 22;40(2):205-15.
27. Fasanaro P, D'Alessandra Y, Di S, V, Melchionna R, Romani S, Pompilio G, et al. MicroRNA-210 modulates endothelial cell response to hypoxia and inhibits the receptor tyrosine kinase ligand Ephrin-A3. J Biol Chem 2008 Jun 6;283(23):15878-83.
28. Ho JJ, Metcalf JL, Yan MS, Turgeon PJ, Wang JJ, Chalsev M, et al. Functional importance of Dicer protein in the adaptive cellular response to hypoxia. J Biol Chem 2012 Aug 17;287(34):29003-20.
29. Shen J, Xia W, Khotskaya YB, Huo L, Nakanishi K, Lim SO, et al. EGFR modulates microRNA maturation in response to hypoxia through phosphorylation of AGO2. Nature 2013 May 16;497(7449):383-7.

Supplemental Material

Gene	Forward Primer	Reverse Primer
primiR-329	AAGGTCACGTTGGGGAATTA	ACCACGAAGCCTCCAAGAT
premiR-329	TGGTACCGGAAGAGAGGTTTT	AGGTTAGCTGGGTGTGTTTCA
primiR-495	AGCATCCCTTCACACTCAGG	GAGCTCTCCAAGGTGAGATTTG
premiR-495	GTTGCCCATGTTATTTTTCG	AGTGCACCATGTTTGTTTCG
CIRBP	TTTTCGTGGGAGGACTCAGC	CCCTGTCCTTTACCACCACC
HADHB	CAGCGCCTGTCCTTACTCAG	CAGAGTGGCCCATGGTCTC

Supplementary Table 1. List of primers used.

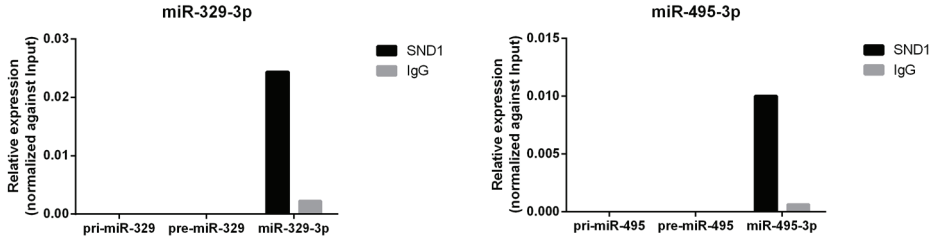

Supplemental Figure 1. RNA binding protein immunoprecipitation with SND1 antibody. Pri-miR, pre-miR and mature microRNA expression levels of miR-329-3p and miR-495-3p were measured in 3T3 cell lysates after immunoprecipitation with SND1 antibody and a non-specific IgG antibody.

Part III

14q32 microRNAs in adipose tissue

Chapter 8

Upregulation of 14q32 microRNAs in human subcutaneous adipose tissue samples of patients with critical limb ischemia undergoing major amputation

Submitted to PLoS One

SMJ Welten[1,2]

A Longchamp[3]

M Tao[3]

SM Kielbasa[4]

PHA Quax[1,2]

CK Ozaki[3*]

AY Nossent[1,2*]

[*]Authors contributed equally to this work

[1]Department of Surgery, Leiden University Medical Center, Leiden, the Netherlands

[2]Einthoven Laboratory for Experimental Vascular Medicine,
Leiden University Medical Center, Leiden, the Netherlands

[3]Division of Vascular and Endovascular Surgery,
Brigham and Women's Hospital/Harvard Medical School, Boston, USA

[4]Department of Medical Statistics and Bioinformatics,
Leiden University Medical Center, Leiden, The Netherlands

Abstract

Objective: In recent years, it has become clear that adipose tissue, both subcutaneous adipose tissue (SAT) as well as perivascular adipose tissue (PVAT), is a major contributor to the development and progression of peripheral arterial disease. We aimed to identify suitable microRNAs biomarkers to identify severe critical limb ischemia (CLI) patients at risk of major amputation.

Methods: SAT and PVAT samples were collected from patients undergoing major amputation because of severe CLI. As controls, SAT was collected from patients that underwent elective knee-replacement. Multiplex qPCRs, followed by individual qPCRs, were performed to determine differential microRNA expression between CLI and control samples. Receiver operating characteristic (ROC) curve analyses were performed to determine sensitivity and specificity for differentially expressed microRNAs.

Results: Multiplex qPCR analyses demonstrated global downregulation of microRNA expression in SAT of CLI patients compared to controls. Eight microRNAs however, of which six belong to a single microRNA gene cluster (14q32), were upregulated in CLI patients. Using individual qPCRs, we confirmed significant upregulation of 14q32 microRNAs miR-127, miR-134, miR-370, miR-376c, miR-411 and miR-539 in SAT of CLI patients compared to controls. ROC curve analyses showed an area under the curve of greater than 0.96 for all microRNAs in the studied population, which was highly significant ($P<0.01$ for all microRNAs). Finally, upregulation of 14q32 microRNAs in SAT and in PVAT of CLI patients was validated in a second independent study population.

Conclusions: Six 14q32 microRNAs are significantly upregulated in SAT and PVAT of patients with CLI. We show that 14q32 microRNAs miR-127, miR-134, miR-370, miR-376c, miR-411 and miR-539 in SAT are promising biomarkers to identify CLI patients who are at risk of major amputation.

Introduction

Peripheral arterial disease (PAD) due to atherosclerosis limits blood flow towards the lower extremities[1]. In a small portion of the patient population, PAD evolves to critical limb ischemia (CLI). CLI is characterized by rest pain, ischemic ulceration and/or gangrene of the lower limb. One year survival for CLI patients is only 75% and 30 to 40% will have undergone amputation within three years[2-4]. Aggressive medical management reduces the risk of progression to CLI, but there is to date no reliable biomarker to predict PAD development, progression and outcome, which could be useful in treatment choices for this group of patients.

Because of their important regulatory role, microRNAs are suitable biomarkers for the diagnosis and prognosis of cardiovascular diseases, including acute myocardial infarction, heart failure, diabetes mellitus and PAD[5-12]. MicroRNAs are a class of non-coding RNA molecules (~22 nucleotides long) that regulate the expression of their target genes at the messenger RNA (mRNA) level. In addition, each microRNA has up to several hundred target genes, potentially regulating as many biological processes. Important for biomarkers, the stability of microRNAs has been shown to be exceptionally high, as their small size protects them from endogenous RNase activity[13].

Cardiovascular morbidity and mortality has been linked to obesity[14]. Generally, obesity increases the risk for the development cardiovascular disease. However, the 'obesity paradox' has also been described, where obesity is associated with a more favourable prognosis compared to non-obese patients in for example heart failure patients and patients with coronary heart disease[15-17]. In addition to the classical roles in energy storage and thermoregulation, adipose tissue is nowadays considered an endocrine organ that secretes inflammatory mediators and adipokines[18]. Variations in body fat distribution, but also the inflammatory status and metabolic profile of these adipose tissue depots, can contribute to the risk of cardiovascular disease [19-21]. For example, subcutaneous adipose tissue of patients with CLI and patients with metabolic syndrome has been described to display a more pro-inflammatory phenotype, with increased expression of pro-inflammatory cytokines IL-6 and IL-8 but also of PAI-1, leptin and resistin, compared to controls[22, 23]. Thus, the composition of the adipose tissue may be as important as the quantity in patients with cardiovascular disease.

Perivascular adipose tissue, which lines the blood vessels, has both endocrine and paracrine effects on the vasculature through secretion of cytokines and adipokines. Perivascular adipose tissue has received increasing attention in vascular biology as it has been shown to play a role in type 2 diabetes and cardiovascular disease[24].

In this study, we examined the expression of microRNAs in subcutaneous adipose tissue (SAT) of CLI patients that underwent major amputation versus "healthy" control patients that underwent elective orthopaedic surgery. In addition, we looked at microRNA expression in perivascular adipose tissue (PVAT) of CLI patients. The aim of this study was to identify microRNAs that can be used as suitable biomarkers to identify patients with severe CLI who are at risk of major amputation. On the long term, the identified microRNAs may also provide insights into the complex interplay between adipose and vascular organs in health and disease.

Chapter 8

Methods

Patient Population

Boston study population. This study was conducted in accordance with the Declaration of Helsinki. The institutional review board (IRB) of the Brigham and Women's Hospital (Boston) approved the study protocol. All subjects were recruited at the department of surgery of the Brigham and Women's Hospital in Boston (MA, USA) and provided written informed consent (when applicable) before participating in the study.

SAT was collected from patients as described previously[22]. In brief, patients undergoing lower extremity major amputation (below knee or above knee) due to unreconstructable CLI (n=18) or elective orthopaedic total knee replacement (n=18) were prospectively identified via procedures approved by the local IRB. Patients in the amputation group were enrolled under an IRB approval that allowed us to collect de-identified medical information and tissue from the amputated limb without informed consent. Patients in the control group all underwent elective knee replacement for osteoarthritis. Informed consent was obtained from the control elective orthopaedic group.

Leiden study population. This study was conducted in accordance with the Declaration of Helsinki. The institutional medical ethics committee of the Leiden University Medical Center approved the study protocol (P12.265). Patients (n=6) undergoing lower extremity major amputation (below or above the knee) were recruited at the department of surgery of the Leiden University Medical Center and provided written informed consent before participating in the study. SAT and PVAT was collected from patients undergoing amputation due to untreatable critical limb. SAT and PVAT samples of these patients were de-identified and only age and gender of these patients were documented.

Subcutaneous adipose tissue collection, storage and RNA isolation

All samples were collected in the operation room by trained surgeons. SAT (~2 g) and PVAT (~50 to 100 mg; only in the Leiden study population) were collected from the amputated limb or from the operated knee of patients and immediately flash frozen in liquid nitrogen. Adipose tissue samples were stored at -80°C in RNAse free vials until the time of analysis. For RNA isolation, adipose tissue samples were homogenized by grounding using a Pellet Pestle Cordless Motor (Kimble Chase Life Science). RNA was isolated from homogenized adipose tissue using a standard TRIzol-chloroform extraction protocol. RNA concentration and purity were examined by nanodrop (Nanodrop® Technologies).

Multiplex rt/qPCR

Expression profiling of 384 different microRNAs was conducted by rt/qPCR multiplex assays. From the Boston study population, SAT samples used for multiplex rt/qPCR analyses were randomly selected from 6 out of the 18 patients that underwent amputation due to CLI (amputation samples) and 6 out of the 18 patients undergoing knee replacement (controls). Isolated RNA was reverse transcribed using Megaplex RT primers (Pool A, Life Technologies). Taqman® Universal PCR Mastermix (Life Technologies) was used to prepare the PCR reaction mix with diluted RT product. 384-well microfluidic cards (Taqman® MicroRNA Human Array A, Life technologies) were loaded with the PCR master mix. Each microRNA was assayed once by qPCR on the human panel A array cards. Amplification was performed on the Viia7 system (Applied Biosystems), using the array card block. Amplification curves were analysed using the AB software. All data were normalized against snRNA-U6 (RNU-6B). The heatmap was generated using heatmap.3 function of GMD library of R language.

Individual microRNA rt/qPCR

MicroRNA quantification was performed on all SAT samples of the Boston study population (n=18 per group) and all SAT and PVAT samples (n=6) of the Leiden study population. MicroRNA rt/qPCRs were performed according to manufacturer's protocol using individual Taqman® miR assays for miR-127-3p, miR-134-5p, miR-370-3p, miR-376c-3p, miR-411-5p and miR-539-5p (Life Technologies). Rt/qPCRs were run on the Viia7 system (Applied Biosystems). Normalization of data was performed using stably expressed endogenous control snRNA-U6 (RNU-6B).

Statistical analyses

Values are expressed as mean ± standard deviation (SD) for multiplex rt/qPCR data and for individual microRNA rt/qPCR data. Statistically significant outliers in individual microRNA rt/qPCR data were identified using a Grubb's test and subsequently excluded. Unpaired student's t-tests were used to compare groups with normal distribution and the Mann-Whitney U test was performed for data with a non-normal distribution. Receiver Operator Characteristic (ROC) Curves were analysed to determine sensitivity and specificity for each microRNA. For the patient characteristics, Student t-Test or Mann-Whitney Rank Sum Test was performed on continuous variables and Chi-square or Fisher Exact Test on categorical variables. A P-value <0.05 was considered statistically significant.

Results

Patient characteristics

Adipose samples were collected from 24 patients who underwent lower limb amputation due to severe CLI and 18 control patients who underwent knee replacement surgery. The mean age of the patients included in the Boston study population was 67.8 years for the CLI group and 60.2 years for the control group. The percentage of females was 16.7% in the CLI group compared to 50% in the control group (P=0.075). CLI patients in the Boston cohort had a greater prevalence of diabetes mellitus, coronary artery disease, chronic heart failure, renal disease and pulmonary disease and had an overall lower BMI compared to control patients. In addition, statin and insulin use was higher in these patients. Further patient characteristics can be found in Table I. For the Leiden study population, only age and gender were documented. In these patients, the mean age was 70 years and 16.7% were female (Table I).

Boston study population	**Amputation (%) (n=18)**	**Control (%) (n=18)**	***P* value**
Age (years), mean ± SD	67.8 ± 15.7	60.2 ± 13.9	0.133
Race			
White:	10 (55.56)	12 (66.67)	
Black:	5 (27.78)	4 (22.2)	0.782
Hispanic:	3(16.67)	2 (11.1)	
Female	3 (16.67)	9 (50)	0.075
BMI (kg/m^2)	25.0 ± 5.3	34.0 ± 8.0	**<0.001**
Diabetes Mellitus	14 (77.78)	2 (11.1)	**<0.001**
Hypertension	16 (88.89)	12 (66.67)	0.228
Hyperlipidemia	13 (72.22)	7 (38.89)	0.094
CAD	12 (66.67)	1 (5.56)	**<0.001**
CHF	6 (33.33)	0 (0.00)	**0.019**
CVA	4 (22.22)	0 (0.00)	0.104
Renal disease	9 (50)	0 (0.00)	**0.001**
Pulmonary disease	5 (27.78)	0 (0.00)	**0.045**
Smoking history	11 (61.11)	6 (33.33)	0.182
Antiplatelet therapy	14 (77.78)	11 (61.11)	0.469
Warfarin	4 (22.22)	10 (55.56)	0.087
Calcium channel blocker	7 (38.89)	1 (5.56)	**0.041**
Beta blocker	13 (72.22)	1 (5.56)	**<0.001**
ACE inhibitor/ARB	6 (33.33)	6 (33.33)	0.724
Statin	14 (77.78)	6 (33.33)	**0.019**
Insulin	13 (72.22)	1 (5.56)	**<0.001**
NSAID	13 (72.22)	16	0.402
Steroid	2 (11.11)	1 (5.56)	1.000

Leiden study population (n=6)	**Amputation (%)**
Age	70 ± 11.6
Female	1 (16.67)

Table I. Patient characteristics for the Boston and Leiden study populations

MicroRNA expression profiles in subcutaneous adipose tissues

The expression profiles of ~384 microRNAs were assessed in SAT samples of six CLI patients and in SAT samples of six control patients of the Boston study population. Figure 1 shows a heat map of the 40 microRNAs with the highest differential expression between CLI and control samples. Interestingly,

most microRNAs were downregulated in SAT samples of CLI patients, whereas only a subset of microRNAs was upregulated in these patients compared to the control samples (Figure 2). Increased expression of miR-127, miR-134, miR-370, miR-376c, miR-411, miR-539, miR-886-3p and miR-146b was observed in CLI samples compared to samples of the control group. Notably, six out of eight upregulated microRNAs, miR-127, miR-134, miR-370, miR-376c, miR-411 and miR-539, belong to a single microRNA gene cluster, the 14q32 microRNA cluster.

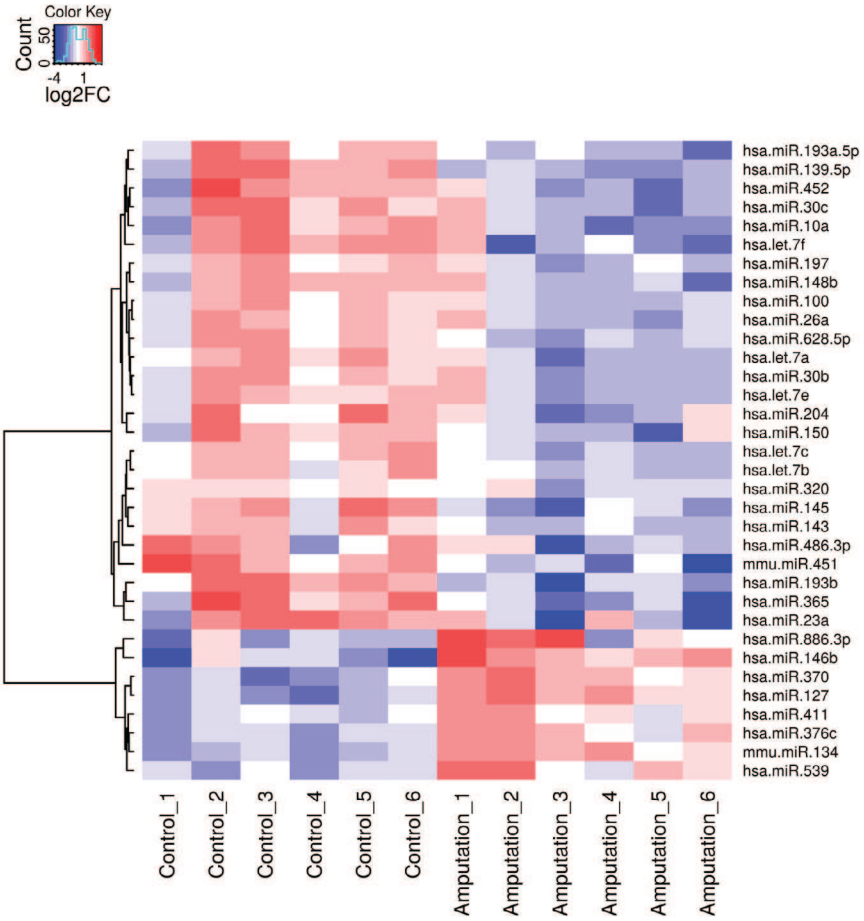

Figure 1. Heat map of differentially expressed microRNAs. MicroRNA expression of control (control_1 to control_6) and CLI (amputation_1 to amputation_6) samples are shown. Each row represents one microRNA and each column represents one sample. The colour scale shows the microRNA expression fold change relative to the average expression of the microRNA across all samples. Red colour indicates an expression level above the mean and blue colour represents expression below the mean.

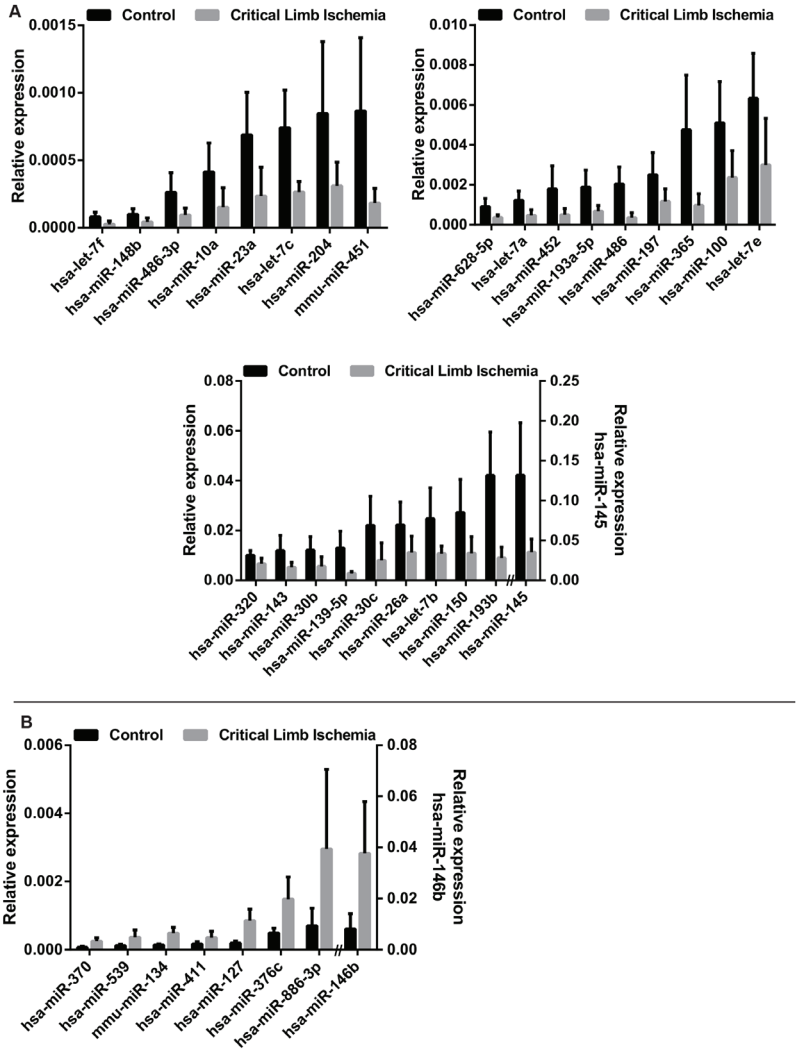

Figure 2. Differential microRNA expression between control and amputation patients. MicroRNA expression was determined by multiplex rt/qPCR in subcutaneous adipose tissue samples of control and CLI patients that underwent major amputation (n=6 patients per group) of the Boston study population. (A) Most microRNAs are downregulated in CLI samples compared to controls. (B) A subset of microRNAs is upregulated in CLI samples compared to control samples. Data are shown as mean ± stdev.

Validation of differential 14q32 microRNA expression

Previously, we have shown that inhibition of several 14q32 microRNAs has positive effects on blood flow recovery in a mouse model of CLI[25]. We performed individual microRNA rt/qPCRs to confirm the differential expression of 14q32 microRNAs miR-127, miR-134, miR-370, miR-376c, miR-411 and miR-539 in all SAT samples of CLI and control groups in the Boston study population. We confirmed significantly elevated expression levels of miR-127, miR-134, miR-370, miR-376c, miR-411 and miR-539 in adipose tissue of patients that underwent major amputation due to severe CLI (Figure 3). Expression of miR-127, miR-370 and miR-539 was approximately four-fold greater in CLI patients,

whereas miR-134, miR-376c and miR-411 showed over two-fold greater expression in these patients compared to controls.

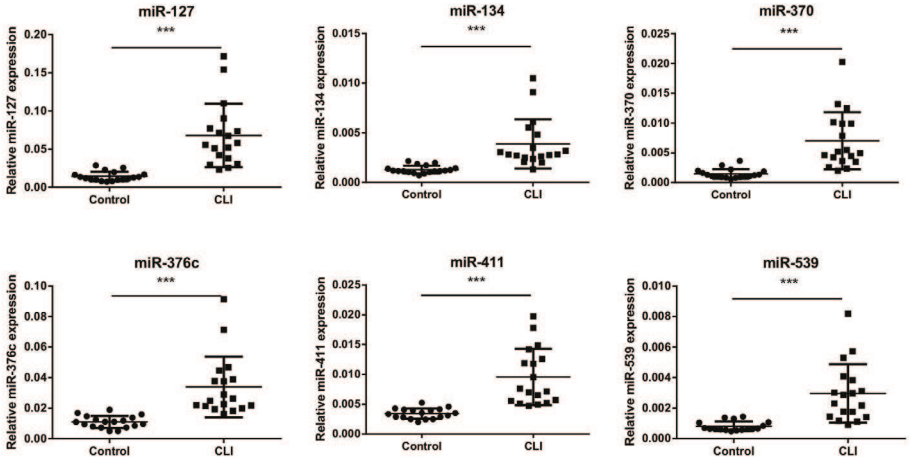

Figure 3. Upregulation of 14q32 microRNAs in amputation patients. Individual rt/qPCR measurements were performed to determine 14q32 microRNA expression in SAT samples of CLI and control samples (n=18 patients per group) in the Boston study population. Data are shown as mean ± stdev. ***P < 0.001

14q32 microRNAs as biomarkers for risk of limb loss

To determine the ability of each upregulated microRNA to predict the CLI in patients, we performed Receiver Operator Characteric (ROC) curve analysis. Using this method, all analysed 14q32 microRNAs significantly predicted CLI (P<0.01 for all microRNAs). Area under the curve (AUC) was greater than 0.96 for all examined microRNAs (Figure 4).

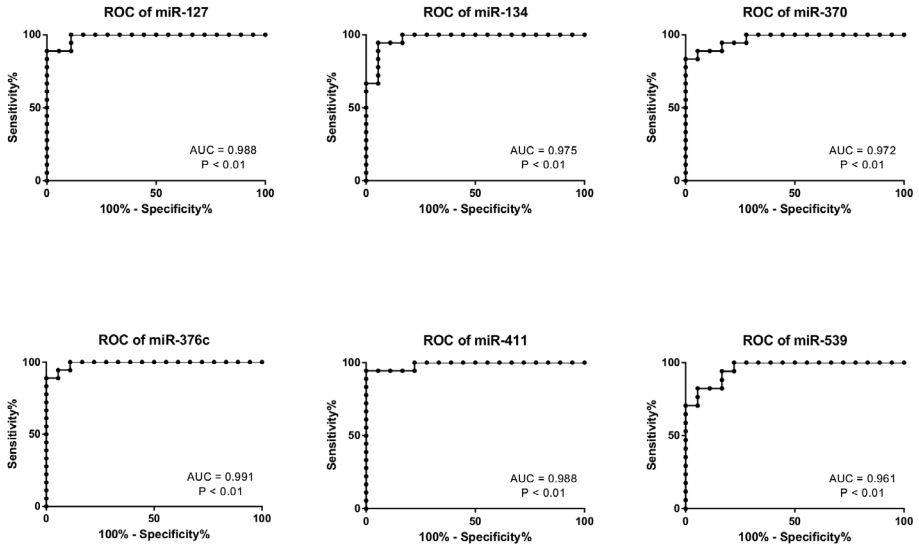

Figure 4. Diagnostic potential of 14q32 microRNAs. Receiver Operation Characteristic (ROC) curve analysis of individual microRNAs (miR-127, miR-134, miR-370, miR-376c, miR-411 and miR-539) to discriminate between CLI and control patients in the Boston study population.

Confirmation of 14q32 microRNA upregulation in a second study population

In order to validate whether upregulation of 14q32 microRNAs in SAT samples of CLI patients is independent of the studied patient population and demographics, we measured expression of 14q32 microRNAs in a second study population of patients (the Leiden study population) that underwent major lower limb amputation due to CLI. In addition, expression of 14q32 microRNAs was measured in PVAT of these patients. Similarly to the Boston study cohort, 14q32 microRNAs miR-127, miR-134, miR-370, miR-376c, miR-411 and miR-539 were significantly upregulated in SAT samples of CLI patients compared to controls (Figure 5A). Expression of 14q32 microRNAs was also upregulated in PVAT samples of these patients (Figure 5A). ROC curve analysis conducted on this subset of amputation samples from the Leiden study cohort confirmed that elevated expression of miR-127, miR-134, miR-370, miR-376c, miR-411 and miR-539 in SAT is a significant predictor of CLI (Figure 5B). All microRNAs showed an AUC of greater than 0.78 (Figure 5B).

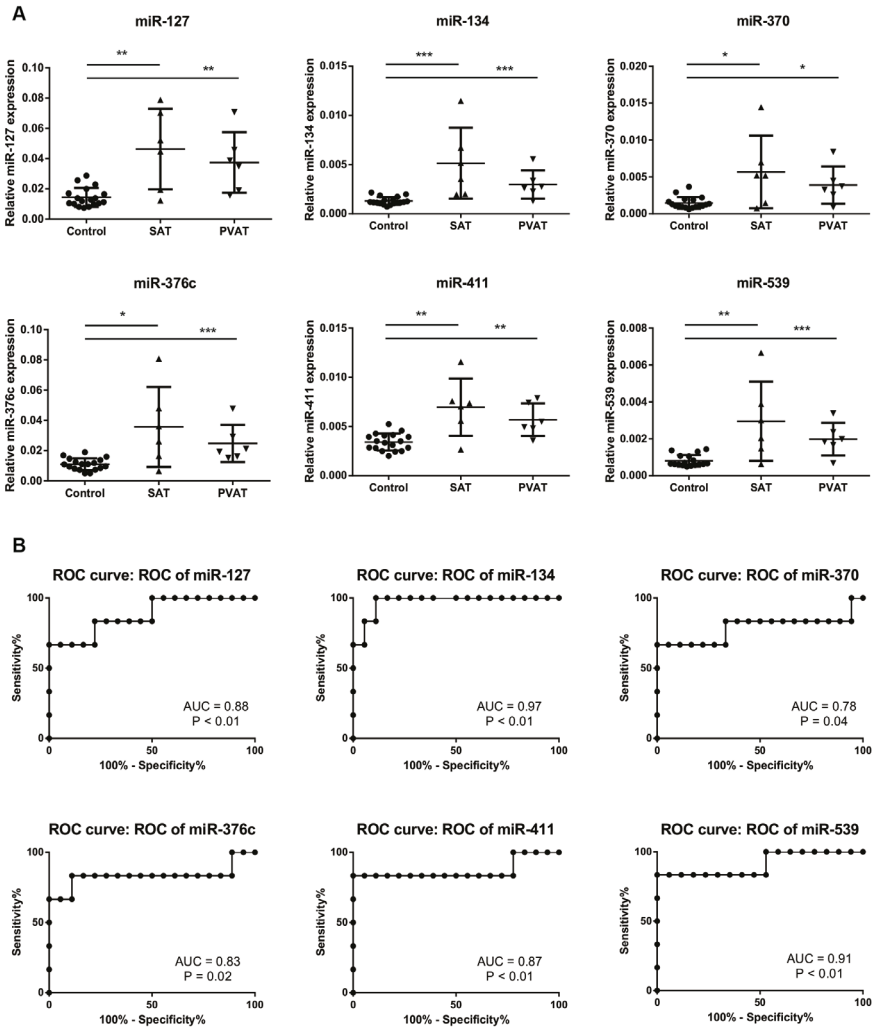

Figure 5. 14q32 microRNA upregulation in the Leiden study population. Rt/qPCR was performed on SAT and PVAT samples of CLI patients (n=6 patients) from the Leiden study population. (A) Upregulation of 14q32 microRNAs was observed in both SAT and PVAT of CLI patients compared to controls. (B) ROC curve analysis was performed to confirm the discriminative power of 14q32 microRNAs to identify CLI patients in this second study population. Data are shown as mean ± stdev. *P < 0.05; **P< 0.01; ***P < 0.001.

Discussion

The present study shows upregulation of 14q32 microRNAs miR-370, miR-539, miR-134, miR-411, miR-127 and miR-376c in the SAT of CLI patients that underwent major amputation. This study demonstrates that expression of these microRNAs in SAT may be used as biomarkers to identify CLI patients who are at risk of major amputation. These findings were confirmed in a second study population.

Previous studies have shown that SAT of CLI patients that underwent major amputation displays a distinct pro-inflammatory signature compared to SAT samples of control patients[22]. This dysregulation of inflammatory mediators was also observed in adipose tissue of patients with metabolic syndrome[23]. Here, we investigated differential expression of microRNAs in SAT of amputated CLI patients compared to control patients. Although generally microRNA expression in SAT was downregulated in CLI patients, a small group of microRNAs was upregulated in these patients. Six out of the eight upregulated microRNAs belong to the 14q32 microRNA gene cluster. Previously, we have shown involvement of several 14q32 microRNAs in post-ischemic neovascularization as well as atherosclerotic plaque formation and stability[25, 26]. Of the upregulated microRNAs reported here, several have also been implicated within cardiovascular disease and lipid metabolism. For example, miR-370 was reported to control expression of carnitine palmitoyltransferase 1A (Cpt1α) expression and fatty acid β-oxidation in liver cells. In addition, miR-370, via miR-122, controlled sterol-regulatory element binding protein 1c (SREBP-1c) and diacylglycerol acyltransferase-2 (DGAT2) expression and lipid metabolism[27, 28]. MiR-134 was shown to target angiopoietin-like 4 (ANGPTL4) and via this mechanism regulated lipoprotein lipase activity and ultimately oxLDL uptake by THP-1 macrophages[29]. Moreover, circulating miR-134 was significantly upregulated and correlated with coronary artery calcifications in patients with obstructive coronary disease[30]. Another study demonstrated elevated expression of both miR-134 and miR-370 in peripheral blood mononuclear cells (PBMCs) of patients with unstable angina pectoris compared to stable patients, suggesting that these microRNAs could be used to identify patients at risk for acute coronary syndromes[31]. Circulating miR-411 was differentially expressed in men with an abdominal aortic aneurysm compared to healthy controls, as well as in men with PAD[32]. Expression of miR-127 was elevated in symptomatic versus asymptomatic carotid plaques of patients undergoing carotid endarterectomy for atherosclerotic stenosis[33]. In most studies discussed here, microRNA expression was upregulated in patients compared to controls. These findings are in line with our data, where we show upregulation of 14q32 microRNAs miR-127, miR-134, miR-370, miR-376c, miR-411 and miR-539 in SAT samples of CLI patients at risk of amputation due to CLI. To our knowledge, there is no direct information linking miR-376c and miR-539 to PAD or CLI yet.

Most studies where microRNAs are evaluated as potential biomarker are based on the measurement of these microRNAs in serum or plasma. Rather than circulating plasmatic, we show here that local microRNA expression in adipose tissue can be used as biomarker. This provides direct local information on microRNA expression, whereas microRNAs detected in serum or plasma provides systemic

information and does not give information on the source of these microRNAs. The tight interaction between both the quantity and composition of adipose tissue and cardiovascular disease development and progression would require local evaluation of microRNA expression to accurately predict disease outcome.

Perivascular adipose tissue, which lines the blood vessels, has been shown to have local effects on the vasculature and influences both vascular health and disease[34]. Compared to other adipose tissue depots, PVAT has been reported to display a distinct (inflammatory) phenotype[35-38]. Therefore, we were also interested whether PVAT harvested from CLI patients that underwent major amputation would display a different microRNA signature than SAT of these patients. In this study, the increased expression of 14q32 microRNAs miR-127, miR-134, miR-370, miR-376c, miR-411 and miR-539 was comparable in PVAT and SAT samples of amputation patients. The increased expression of 14q32 microRNAs in PVAT of CLI patients not only supports for their role as biomarker, but also suggests an active role for 14q32 microRNAs in the interplay between PVAT and the vasculature.

Clinical Implications and Study Limitations

Although the sample size used for this study was relatively small and amputation and control cohorts were not perfectly matched for sex and age, we were able to identify several microRNAs that could be used to identify CLI patients at risk of amputation, in two different study populations. In a previous study, we also demonstrated upregulation of 14q32 microRNAs upon ischemia in a mouse model for CLI[25]. It should be noted that although we observe a profound difference between severe CLI patients that underwent an amputation and controls, we cannot exclude the possibility that these microRNAs are also upregulated in CLI patients which are not at risk of amputation. Future studies will have to investigate whether these microRNAs can be used to discriminate between patients with CLI which are at a high risk of amputation and patients which are treatable for CLI.

Conflict of interest

None declared.

Funding

This work was supported by the Netherlands Institute for Regenerative Medicine (NIRM, FES0908), the LUF-Gratama stichting (2014-05) and the Dutch Heart Foundation (Dr. E. Dekker Senior Postdoc, 2014T102). This work was also supported by the National Heart, Lung, and Blood Institute (1R01HL133500, R01HL079135 and 1R01HL079135-06S1), the American Heart Association (12GRNT9510001 and 16GRNT27090006), the Carl and Ruth Shapiro Family Foundation and the Swiss National Science Foundation (PILAP3_158895).

References

1. Ouriel K. Peripheral arterial disease. *Lancet* 2001 Oct 13;358(9289):1257-64.
2. Varu VN, Hogg ME, Kibbe MR. Critical limb ischemia. *J Vasc Surg* 2010 Jan;51(1):230-41.
3. Hirsch AT, Haskal ZJ, Hertzer NR, Bakal CW, Creager MA, Halperin JL, et al. ACC/AHA 2005 Practice Guidelines for the management of patients with peripheral arterial disease (lower extremity, renal, mesenteric, and abdominal aortic): a collaborative report from the American Association for Vascular Surgery/Society for Vascular Surgery, Society for Cardiovascular Angiography and Interventions, Society for Vascular Medicine and Biology, Society of Interventional Radiology, and the ACC/AHA Task Force on Practice Guidelines (Writing Committee to Develop Guidelines for the Management of Patients With Peripheral Arterial Disease): endorsed by the American Association of Cardiovascular and Pulmonary Rehabilitation; National Heart, Lung, and Blood Institute; Society for Vascular Nursing; TransAtlantic Inter-Society Consensus; and Vascular Disease Foundation. *Circulation* 2006 Mar 21;113(11):e463-e654.
4. Santilli JD, Santilli SM. Chronic critical limb ischemia: diagnosis, treatment and prognosis. *Am Fam Physician* 1999 Apr 1;59(7):1899-908.
5. Wang GK, Zhu JQ, Zhang JT, Li Q, Li Y, He J, et al. Circulating microRNA: a novel potential biomarker for early diagnosis of acute myocardial infarction in humans. *Eur Heart J* 2010 Mar;31(6):659-66.
6. Widera C, Gupta SK, Lorenzen JM, Bang C, Bauersachs J, Bethmann K, et al. Diagnostic and prognostic impact of six circulating microRNAs in acute coronary syndrome. *J Mol Cell Cardiol* 2011 Nov;51(5):872-5.
7. Tijsen AJ, Creemers EE, Moerland PD, de Windt LJ, van der Wal AC, Kok WE, et al. MiR423-5p as a circulating biomarker for heart failure. *Circ Res* 2010 Apr 2;106(6):1035-9.
8. Zampetaki A, Kiechl S, Drozdov I, Willeit P, Mayr U, Prokopi M, et al. Plasma microRNA profiling reveals loss of endothelial miR-126 and other microRNAs in type 2 diabetes. *Circ Res* 2010 Sep 17;107(6):810-7.
9. Li T, Cao H, Zhuang J, Wan J, Guan M, Yu B, et al. Identification of miR-130a, miR-27b and miR-210 as serum biomarkers for atherosclerosis obliterans. *Clin Chim Acta* 2011 Jan 14;412(1-2):66-70.
10. Fichtlscherer S, Zeiher AM, Dimmeler S. Circulating microRNAs: biomarkers or mediators of cardiovascular diseases? *Arterioscler Thromb Vasc Biol* 2011 Nov;31(11):2383-90.
11. Hakimzadeh N, Nossent AY, van der Laan AM, Schirmer SH, de Ronde MW, Pinto-Sietsma SJ, et al. Circulating MicroRNAs Characterizing Patients with Insufficient Coronary Collateral Artery Function. *PLoS One* 2015;10(9):e0137035.
12. Welten SM, Goossens EA, Quax PH, Nossent AY. The multifactorial nature of microRNAs in vascular remodelling. *Cardiovasc Res* 2016 Feb 23.
13. Mitchell PS, Parkin RK, Kroh EM, Fritz BR, Wyman SK, Pogosova-Agadjanyan EL, et al. Circulating microRNAs as stable blood-based markers for cancer detection. *Proc Natl Acad Sci U S A* 2008 Jul 29;105(30):10513-8.
14. Lavie CJ, Milani RV, Ventura HO. Obesity and cardiovascular disease: risk factor, paradox, and impact of weight loss. *J Am Coll Cardiol* 2009 May 26;53(21):1925-32.
15. Romero-Corral A, Montori VM, Somers VK, Korinek J, Thomas RJ, Allison TG, et al. Association of bodyweight with total mortality and with cardiovascular events in coronary artery disease: a systematic review of cohort studies. *Lancet* 2006 Aug 19;368(9536):666-78.
16. Horwich TB, Fonarow GC, Hamilton MA, MacLellan WR, Woo MA, Tillisch JH. The relationship between obesity and mortality in patients with heart failure. *J Am Coll Cardiol* 2001 Sep;38(3):789-95.
17. Oga EA, Eseyin OR. The Obesity Paradox and Heart Failure: A Systematic Review of a Decade of Evidence. *J Obes* 2016;2016:9040248.
18. Kershaw EE, Flier JS. Adipose tissue as an endocrine organ. *J Clin Endocrinol Metab* 2004 Jun;89(6):2548-56.
19. Lapidus L, Bengtsson C, Larsson B, Pennert K, Rybo E, Sjostrom L. Distribution of adipose tissue and risk of cardiovascular disease and death: a 12 year follow up of participants in the population study of women in Gothenburg, Sweden. *Br Med J (Clin Res Ed)* 1984 Nov 10;289(6454):1257-61.
20. Xu H, Barnes GT, Yang Q, Tan G, Yang D, Chou CJ, et al. Chronic inflammation in fat plays a crucial role in the development of obesity-related insulin resistance. *J Clin Invest* 2003 Dec;112(12):1821-30.
21. Claria J, Nguyen BT, Madenci AL, Ozaki CK, Serhan CN. Diversity of lipid mediators in human adipose tissue depots. *Am J Physiol Cell Physiol* 2013 Jun 15;304(12):C1141-C1149.
22. Mauro CR, Nguyen BT, Yu P, Tao M, Gao I, Seidman MA, et al. Inflammatory “adiposopathy” in major amputation patients. *Ann Vasc Surg* 2013 Apr;27(3):346-52.
23. Bremer AA, Devaraj S, Afify A, Jialal I. Adipose tissue dysregulation in patients with metabolic syndrome. *J Clin Endocrinol Metab* 2011 Nov;96(11):E1782-E1788.
24. Meijer RI, Serne EH, Smulders YM, van Hinsbergh VW, Yudkin JS, Eringa EC. Perivascular adipose tissue and its role in type 2 diabetes and cardiovascular disease. *Curr Diab Rep* 2011 Jun;11(3):211-7.
25. Welten SM, Bastiaansen AJ, de Jong RC, de Vries MR, Peters EA, Boonstra MC, et al. Inhibition of 14q32 MicroRNAs miR-329, miR-487b, miR-494, and miR-495 increases neovascularization and blood flow recovery after ischemia. *Circ Res* 2014 Sep 26;115(8):696-708.
26. Wezel A, Welten SM, Razawy W, Lagraauw HM, de Vries MR, Goossens EA, et al. Inhibition of MicroRNA-494 Reduces Carotid Artery Atherosclerotic Lesion Development and Increases Plaque Stability. *Ann Surg* 2015 Nov;262(5):841-7.
27. Iliopoulos D, Drosatos K, Hiyama Y, Goldberg IJ, Zannis VI. MicroRNA-370 controls the expression of microRNA-122 and Cpt1alpha and affects lipid metabolism. *J Lipid Res* 2010 Jun;51(6):1513-23.

28. Gao W, He HW, Wang ZM, Zhao H, Lian XQ, Wang YS, et al. Plasma levels of lipometabolism-related miR-122 and miR-370 are increased in patients with hyperlipidemia and associated with coronary artery disease. *Lipids Health Dis* 2012;11:55.
29. Lan G, Xie W, Li L, Zhang M, Liu D, Tan YL, et al. MicroRNA-134 Actives lipoprotein lipase-mediated Lipid Accumulation and Inflammatory Response by Targeting Angiopoietin-Like 4 in THP-1 Macrophages. *Biochem Biophys Res Commun* 2015 Nov 4.
30. Liu W, Ling S, Sun W, Liu T, Li Y, Zhong G, et al. Circulating microRNAs correlated with the level of coronary artery calcification in symptomatic patients. *Sci Rep* 2015;5:16099.
31. Hoekstra M, van der Lans CA, Halvorsen B, Gullestad L, Kuiper J, Aukrust P, et al. The peripheral blood mononuclear cell microRNA signature of coronary artery disease. *Biochem Biophys Res Commun* 2010 Apr 9;394(3):792-7.
32. Stather PW, Sylvius N, Sidloff DA, Dattani N, Verissimo A, Wild JB, et al. Identification of microRNAs associated with abdominal aortic aneurysms and peripheral arterial disease. *Br J Surg* 2015 Jun;102(7):755-66.
33. Maitrias P, Metzinger-Le Meuth V, Massy ZA, M'Baya-Moutoula E, Reix T, Caus T, et al. MicroRNA deregulation in symptomatic carotid plaque. *J Vasc Surg* 2015 Nov;62(5):1245-50.
34. Brown NK, Zhou Z, Zhang J, Zeng R, Wu J, Eitzman DT, et al. Perivascular adipose tissue in vascular function and disease: a review of current research and animal models. *Arterioscler Thromb Vasc Biol* 2014 Aug;34(8):1621-30.
35. Mauro CR, Ilonzo G, Nguyen BT, Yu P, Tao M, Gao I, et al. Attenuated adiposopathy in perivascular adipose tissue compared with subcutaneous human adipose tissue. *Am J Surg* 2013 Aug;206(2):241-4.
36. Chatterjee TK, Aronow BJ, Tong WS, Manka D, Tang Y, Bogdanov VY, et al. Human coronary artery perivascular adipocytes overexpress genes responsible for regulating vascular morphology, inflammation, and hemostasis. *Physiol Genomics* 2013 Aug 15;45(16):697-709.
37. Chatterjee TK, Stoll LL, Denning GM, Harrelson A, Blomkalns AL, Idelman G, et al. Proinflammatory phenotype of perivascular adipocytes: influence of high-fat feeding. *Circ Res* 2009 Feb 27;104(4):541-9.
38. Omar A, Chatterjee TK, Tang Y, Hui DY, Weintraub NL. Proinflammatory phenotype of perivascular adipocytes. *Arterioscler Thromb Vasc Biol* 2014 Aug;34(8):1631-6.

Part IV

Summary and Future Perspectives

Nederlandse Samenvatting
List of Publications
Curriculum Vitae

Chapter 9

Summary and Future Perspectives

Summary and Future Perspectives

Rationale

Cardiovascular disease is a general term used for diseases that affect the heart and blood vessels. The term includes (amongst other) coronary artery disease (CAD), cerebrovascular disease (CBVD) and peripheral arterial disease (PAD). The underlying cause for these diseases is atherosclerosis, which involves the gradual build-up of cholesterol-rich plaques in the arterial wall that eventually lead to narrowing and ultimately occlusion of arteries supplying blood to the heart, brain or extremities[1]. Patients with cardiovascular disease benefit from therapies that restore blood flow through (or around) these arteries. Unfortunately, endovascular interventions such as balloon angioplasty often result in the rapid re-narrowing of the affected arteries, called restenosis[2]. An alternative strategy could be to stimulate the endogenous formation of new blood vessels (i.e. neovascularization) in these patients. Angiogenesis and arteriogenesis are both neovascularization processes. Angiogenesis involves the sprouting of new capillaries towards an ischemic area. Arteriogenesis is the formation of collateral arteries from pre-existent arterioles[3]. Of course, it is also important to stop the progression of atherosclerosis in these patients.

The term vascular remodelling is a general term to describe all processes that involve remodelling of the vasculature leading to changes in blood flow. Atherosclerosis, restenosis, arteriogenesis and angiogenesis are thus all processes of vascular remodelling.

MicroRNAs are short, non-coding RNA molecules capable of regulating the expression of numerous genes. A single microRNA is able to downregulate the expression of numerous target genes, and by doing so, that single microRNA can regulate complex, multifactorial physiological processes, such as vascular remodelling processes[4]. In this thesis, the role of microRNAs in vascular remodelling was investigated, in particular that of microRNAs from the 14q32 microRNA cluster.

This Thesis

The aim of this thesis was to investigate the involvement of a specific microRNA cluster, located on human chromosome 14 (14q32; chromosome 12 in mice) in vascular remodelling. Many studies have reported on the role of microRNAs in the pathophysiology of these processes. Their findings are reviewed in **Chapter 2**, which focuses on the multifactorial nature of microRNAs. MicroRNAs are capable of regulating the expression of many genes that are involved in vascular remodelling and by doing so these microRNAs can either promote or inhibit structural changes of the vessel wall. As vascular remodelling processes are often regulated by similar mechanisms and factors, both positive and negative vascular remodelling can be affected by the same microRNA. In the past, this has been illustrated by the observation that interventions designed to stimulate arteriogenesis also increased atherosclerosis and vice versa. We discuss several microRNAs which were reported to have multiple roles in at least two of the following processes: atherosclerosis and/or restenosis, angiogenesis and/or arteriogenesis and aneurysm formation. MicroRNAs discussed in this review included the individual

microRNAs miR-126 and miR-155 and microRNA gene clusters 17-92, 23/24/27, 143/145 and 14q32. Interestingly, several microRNAs that were shown to increase neovascularization after ischemia also decreased lesion formation in models for atherosclerosis or vice versa. These studies call for the use of these particular microRNAs as therapeutic targets in treatment of cardiovascular disease.

14q32 microRNAs in vascular remodelling

Chapter 3 zooms in on the role of 14q32 microRNAs in post-ischemic neovascularization. In order to identify microRNAs that could influence post-ischemic neovascularization, we made use of a 'Reverse Target Prediction' model. Using this unique strategy, we started by generating a list of neovascularization related genes (i.e. genes involved in the regulation of angiogenesis and arteriogenesis). Next, we determined which microRNAs were predicted to target these neovascularization related genes. Interestingly, we observed enrichment of binding sites for multiple microRNAs from the same microRNA gene cluster located on human chromosome 14 (14q32 locus in humans, 12F1 in mice). We followed expression of 14q32 microRNAs after single ligation of the femoral artery as a model for effective neovascularization and observed three distinct expression patterns. MicroRNAs of the 14q32 cluster could be categorized into early responders, meaning their expression was rapidly upregulated within 24 hours after single ligation of the femoral artery; late-responders, meaning microRNA expression was not upregulated until 72 hours after ischemia induction; non-responders, microRNAs whose expression was not regulated at all after ischemia. Four microRNAs were selected for further evaluation, based on their expression during effective neovascularization and on the number of predicted neovascularization target genes. Early responder miR-494, late responder miR-329 and non-responder miR-495 were included for further analysis. In addition, miR-487b was selected, as we had previously shown a role for this microRNA in the outward remodelling of the aorta and it was the second-most significantly upregulated microRNA (early-responder). These microRNAs were inhibited using Gene Silencing Oligonucleotides (GSOs), which are a type of microRNA inhibitor made up by two synthetic DNA strands that are reverse complementary in sequence to the microRNA of interest[5]. The GSOs were injected one day prior to double ligation of the left femoral artery in mice. Using fluorescently labelled GSOs we studied uptake of these microRNA inhibitors, which were clearly visible in the ligated adductor and calf muscles, 24 hours after animals were subjected to hind limb ischemia but not in the unligated hind limb. When given a single injection of GSOs against miR-329, miR-487b, miR-494 or miR-495, mice showed an improved blood flow recovery compared to control treated animals. This increase in blood flow recovery was accompanied by an increase in collateral artery formation in the adductor muscle and increased capillary density in the ischemic soleus muscle of GSO treated animals. Multiple putative pro-arteriogenic and pro-angiogenic target genes of miR-329 and miR-494 were upregulated, both *in vivo* and *in vitro*. In addition, inhibition of 14q32 microRNAs increased *in vitro* proliferation of primary endothelial cells and primary myofibroblasts and increased sprouting from *ex vivo* aortic rings.

These data demonstrate a role for the 14q32 microRNAs miR-329, miR-487b, miR-494 and miR-495 in post-ischemic neovascularization and may offer future targets for therapeutic neovascularization.

Stimulation of arteriogenesis and angiogenesis is generally accompanied by an inflammatory reaction which is also in important contributor to atherosclerotic plaque formation. Factors that were shown to stimulate post-ischemic neovascularization in the past, often also led to the stimulation of the underlying cause of ischemia, atherosclerosis[6]. Also known as the 'Janus phenomenon', referring to the two-faced Roman god Janus, this phenomenon is a major drawback of translation towards the clinic for this research field[7]. Using the same 'Reverse Target Prediction' analysis as described in Chapter 3, we looked for microRNA binding sites within the 3'UTR of atherosclerosis related genes in **Chapter 4**. Intriguingly, we observed enrichment of binding sites for multiple microRNAs of the same 14q32 microRNA gene cluster as described in Chapter 3. Expression of 14q32 microRNAs miR-329, miR-494 and miR-495 was measured in human atherosclerotic plaques, as well as in murine organs involved in atherosclerosis. MiR-494 was abundantly expressed in human atherosclerotic plaques, particularly in unstable lesions. In addition, miR-494 was highly expressed in murine organs involved in atherosclerosis and therefore selected for further analysis. To study the effects of miR-494 on atherosclerotic plaque formation, atherosclerotic lesions were induced in hypercholesterolemic ApoE$^{-/-}$ mice by placement of perivascular collars around the carotid arteries. Four days after collar placement, mice were injected with GSO-494. Uptake of GSOs into the affected areas of the carotid arteries was visualized by the use of fluorescently labelled GSOs. Treatment with GSO-494 resulted in decreased lesion formation in treated animals, which was accompanied by an increase in lesion stability. Inhibition of miR-494 also reduced cholesterol levels in these animals and led to upregulation of several predicted target genes *in vivo*.

In this study we demonstrate that inhibition of miR-494, which we previously showed to have positive effects on post-ischemic neovascularization, does not negatively affect atherosclerosis formation but instead decreases lesion formation and increases plaque stability.

In **Chapter 5** we investigated the role of 14q32 microRNAs miR-329, miR-494 and miR-495 in restenosis. Restenosis comprises both intimal hyperplasia as well as accelerated atherosclerosis. Intimal hyperplasia is characterized by extracellular matrix rearrangements, smooth muscle cell proliferation and inflammation. On top of that, accelerated atherosclerosis is observed, especially under hypercholesterolemic conditions. Based on the results described in Chapter 3 and Chapter 4, we expected that 14q32 microRNA inhibition would reduce lesion formation in experimental restenosis mouse models. Using the femoral artery cuff model, intimal hyperplasia was studied in C57BL/6 mice treated with GSO-329, GSO-494 or GSO-495. Inhibition of miR-495 reduced intimal hyperplasia, decreased the influx of macrophages into the intima and decreased proliferation of smooth muscle cells. Inhibition of miR-494 had no effect on intimal hyperplasia, whereas inhibition of miR-329 showed a non-significant reduction of intimal hyperplasia. To investigate the effects of miR-329 and miR-495 inhibition on accelerated atherosclerosis development, collars were placed around the carotid arteries of hypercholesterolemic ApoE$^{-/-}$ mice. Inhibition of miR-329 again resulted in a non-significant reduction of atherosclerotic plaque size. GSO-495 treatment however, significantly reduced atherosclerotic plaque size and increased plaque stability in treated animals. Cholesterol levels were also decreased in GSO-495 treated animals compared to controls. Upregulation of multiple putative

target genes for miR-495 was observed in the carotid arteries and spleen of mice treated with GSO-495.

In summary, inhibition of miR-495 reduced lesion formation in experimental mouse models for restenosis. Using different mouse models, we studied the role of miR-495 in intimal hyperplasia and accelerated atherosclerosis, the two major contributors to restenosis. This study demonstrated the multifactorial nature of microRNAs in processes of vascular remodelling (in this case on restenosis) as the sum of the multiple (modest) effects of microRNA inhibition described here on target gene expression, cholesterol levels, smooth muscle cell proliferation and macrophage influx together were found to have profound effects on experimental restenosis. These findings could have future clinical implications for treatment of patients with coronary artery disease and peripheral artery disease. Treatment with microRNA inhibitors could be started before or directly after endovascular intervention, reducing the risk of restenosis. Nonetheless, extrapolation of these results should be done with care, as man and mice are not the same[8].

(Post-)transcriptional regulation of 14q32 microRNA expression

A recent study demonstrated that the Myocyte Enhancer Factor 2a (MEF2A) regulates transcription of (several microRNAs of) the 14q32 microRNA cluster[9]. In **Chapter 6,** we investigated the role of Mef2a in post-ischemic neovascularization and studied transcriptional regulation of several 14q32 microRNAs via Mef2a. We hypothesized that inhibition of Mef2a would lead to repression of the 14q32 microRNAs and therefore have beneficial effects on neovascularization after ischemia. Indeed, inhibition of Mef2a using GSOs improved post-ischemic blood flow recovery in a hind limb ischemia model. Both arteriogenesis in the adductor muscle as well as angiogenesis in the ischemic soleus muscle were increased in GSO-Mef2a treated animals compared to GSO-Control treated animals. However, when we measured expression of 14q32 microRNAs miR-329, miR-487b, miR-410, miR-494 and miR-495 in adductor muscle tissue of these animals, only miR-329 and miR-494 were decreased after Mef2a inhibition, while the other 14q32 microRNAs showed no difference in expression between GSO-Mef2a and GSO-Control treated animals. To determine whether Mef2a indeed affects transcription of 14q32 microRNAs miR-329, miR-487b, miR-494 and miR-495, we measured expression levels of primary (pri-microRNA) and precursor (pre-microRNA) microRNAs in GSO-Mef2a and GSO-Control treated animals. No differences were observed in the pri-microRNA and pre-microRNA levels of miR-329, miR-487b, miR-494 and miR-495 between GSO-treated groups. Since pri-microRNA transcript levels were not different between GSO-Mef2a and GSO-Control animals, the effects on miR-329 and miR-494 levels were most likely achieved via other mechanisms than transcription. Preliminary experiments suggest that Mef2a is involved in post-transcriptional regulation of 14q32 microRNAs. Using RNA binding protein immunoprecipitation (RIP) assays, we observed specific binding of Mef2a to the pri-microRNA transcript of miR-494, but not to pri- or pre-microRNAs of miR-487b, one of the microRNAs that was not affected by inhibition of Mef2a

In conclusion, inhibition of Mef2a improved post-ischemic neovascularization in mice and reduced expression of miR-329 and miR-494 in these animals, partially explaining the observed effects. These data show for the first time that Mef2a may function as RNA binding protein in the posttranscriptional

regulation of microRNAs.

In **Chapter 7** we further explore the post-transcriptional mechanisms that regulate expression of 14q32 microRNAs. There are several clues that 14q32 microRNAs are regulated at the post-transcriptional level. First, 14q32 microRNAs are regulated following three different expression patterns during vascular remodelling, as was discussed in Chapter 3. These 14q32 microRNA expression patterns are independent of their chromosomal location, as the genes that encode these early, late and non-responding microRNAs are randomly distributed along this genomic region. Not only temporal expression levels, but also basal expression levels of 14q32 microRNAs varied greatly. Moreover, basal and temporal expression of the -3p and -5p microRNAs coming from the same pre-microRNA were found to differ. RNA-binding proteins (RBPs) are able to influence processing of microRNAs[10]. MicroRNAs are first transcribed as pri-microRNAs, cleaved to form pre-microRNAs and subsequently processed to form mature microRNAs[11]. RBPs can either promote or inhibit pri- to pre-microRNA and pre- to mature microRNA processing. Using specific primers for each of the microRNA processing steps, we found that increased expression of 14q32 microRNAs after hind limb ischemia is not determined by increased transcription, but likely results from increased processing of pre-microRNA to mature microRNA. Differential expression of 14q32 microRNAs during ischemia was mimicked using an *in vitro* model in which 3T3 cells were serum-starved. Using Stable Isotope Labelling of Amino Acids (SILAC) on these cells, followed by RNA pull down and Mass Spectometry, we investigated which RBPs could bind to pre-microRNA transcripts of 14q32 microRNAs. When comparing late-responder miR-329 with non-responder miR-495, we observed specific binding of RNA binding proteins CIRBP and HADHB to pre-microRNA-329. Immunohistochemical staining confirmed expression of both CIRBP and HADHB in the adductor muscle of mice and expression of both CIRBP and HADHB was significantly upregulated in ischemic muscle tissue of mice at 72 hours after hind limb ischemia. Furthermore, using RBP immunoprecipitation experiments, we show specific binding of CIRBP to the pre-microRNA transcript of miR-329, but not the pri-microRNA transcript.

These data demonstrate a role for CIRBP in the post-transcriptional regulation of 14q32 microRNA miR-329 and miR-329 expression levels after induction of ischemia. Further studies will have to determine the nature of interaction between CIRBP and pre-microRNA-329 and whether CIRBP, and HADHB, also regulate other (late-responding) microRNAs during ischemia and vascular remodelling.

14q32 microRNA expression in subcutaneous adipose tissue

Biomarkers are measurable indicators of a disease state or disease progression, which can be used to predict disease development, progression and outcome[12]. A subset of patients with peripheral arterial disease develops critical limb ischemia (CLI), which is characterized by rest pain, ischemic ulceration and/or gangrene of the lower limb. One year survival in these patients is only 75% and within three years, 30 to 40% of patients will have undergone major amputation. For this group of patients, there are limited treatment options and to date, there is no reliable biomarker to predict PAD development and progression, which could be useful in treatment choices for this group of patients. In **Chapter 8**, we evaluated the expression of microRNAs in subcutaneous and perivascular adipose tissues of

patients that underwent amputation as a result of severe CLI, compared to microRNA expression in subcutaneous adipose tissue of healthy control patients that underwent elective orthopaedic surgery. Comparing microRNA expression in adipose tissues of amputation patients with controls, we observed a general downregulation of microRNA expression in adipose tissue of amputation patients. However, increased expression of miR-127, miR-134, miR-370, miR-376c, miR-411, miR-539, miR-886-3p and miR-146b was observed in amputation samples compared to samples of the control group. Notably, six out of eight upregulated microRNAs belong to the 14q32 microRNA cluster. We confirmed significant upregulation of 14q32 microRNAs miR-127, miR-134, miR-370, miR-376c, miR-411 and miR-539 in subcutaneous and perivascular adipose tissue of amputation patients in two different study populations.

We showed that local expression of 14q32 microRNAs in adipose tissue could be used as suitable biomarker to identify CLI patients at risk of amputation. Future studies will have to investigate whether these microRNAs can be used to discriminate between patients with CLI which are at a high risk of amputation and patients that are treatable for CLI. In addition, the interaction between local microRNA expression in adipose tissue and the vasculature should be investigated to gain more insight in the complex interplay between adipose and vascular organs in health and disease.

Future perspectives

In this thesis, the role of the 14q32 microRNA cluster in vascular remodelling has been investigated. Our data provide new mechanistic insights, as well as possible therapeutic targets for the treatment of cardiovascular diseases. MicroRNAs have the unique ability to target numerous genes and we have identified microRNAs that, by targeting multiple vascular remodelling related genes, have a broad effect on these processes. We have shown that inhibition of several 14q32 microRNAs improved blood flow recovery after induction of ischemia, while also reducing atherosclerotic lesion development and increasing plaque stability. In addition, restenosis was reduced after inhibition of 14q32 microRNAs. These studies demonstrate the possible use of 14q32 microRNAs as therapeutic target for cardiovascular diseases. The first clinical trials using a microRNA inhibitor (miR-122) as drug target for the treatment of hepatitis C are currently performed. Both miravirsen, a specific miR-122 inhibitor developed by Roche (formerly Santaris Pharma) and RG-101, a miR-122 antagonist developed by Regulus therapeutics, are currently monitored in phase II studies to asses safety and tolerability of the drugs[13, 14].

MicroRNA-based therapeutics for the treatment of cardiovascular disease have not yet entered clinical trials, but several microRNAs that gave promising results as therapeutic targets in murine models of cardiovascular disease have or are currently being studied in larger animal models. Therapeutic modulation of microRNA expression can either be achieved via overexpression of microRNAs that have a beneficial effect on the disease or by inhibition of microRNAs that drive disease progression. The development of microRNA mimics has lagged behind from the development of microRNA inhibitors due to technical challenges with their design and delivery[15]. For the inhibition of microRNAs, chemically engineered oligonucleotides have become available. In this thesis, we made use of Gene

Silencing Oligonucleotides (GSOs) for the inhibition of 14q32 microRNAs. GSOs are 3rd generation antisense oligonucleotides, developed by Idera pharmaceuticals. Each GSO molecule contains two identical DNA segments complementary to the target microRNA on a phosphorothioate backbone, which are linked together at the 5' end. By linking the 5' ends, these 5' ends are made inaccessible for TLR activation and immune activation which interferes with gene-silencing efficiency. In addition, each GSO has two free 3'ends, which are required for optimal gene-silencing[5]. The specific oligonucleotide chemistry used for the development of microRNA inhibitors affects binding affinity binding with the target microRNA, confers resistance to nucleases and improves cellular uptake. Although systemic inhibition of GSOs resulted in improved outcomes in the experimental models used to study vascular remodelling, additional studies are required to exclude off target effects. In addition, future studies will have to determine the mechanism of uptake of GSOs and the duration of microRNA inhibition *in vivo*, as well as to determine the optimal dose needed.

MicroRNA expression can be controlled at different levels. We investigated transcriptional regulation of 14q32 microRNAs via Mef2a. Inhibition of Mef2a improved post-ischemic blood flow recovery and indeed reduced expression of 14q32 microRNA miR-329 and miR-494, but not of other studied 14q32 microRNAs. We observed specific binding of Mef2a to pri-microRNA-494, revealing a possible role for Mef2a as RNA binding protein. RNA binding proteins have been found to enhance or inhibit microRNA processing from pri- to pre-microRNA and pre- to mature microRNA. We further examined which RBPs are responsible for post-transcriptional regulation of 14q32 microRNAs. We identified two RNA binding proteins, CIRBP and HADHB, which were upregulated after induction of ischemia and were also specifically bound to 14q32 microRNA pre-microRNA-329. Future studies will have to determine the nature of the interaction between these RBPs and pre-microRNA-329 and whether CIRBP and HADHB also regulate other microRNAs during ischemia. Understanding the regulatory mechanisms behind 14q32 microRNA expression may provide therapeutic targets. Regulation of RNA binding proteins that control expression of 14q32 microRNAs would mean that we could influence 14q32 microRNA expression even higher up the regulatory cascade of vascular remodelling, possibly having more profound therapeutic effects.

In the past, microRNAs have been reported as suitable biomarkers for the diagnosis and prognosis of cardiovascular disease including acute myocardial infarction, heart failure and peripheral arterial disease. Their small size protects microRNAs from endogenous RNase activity and contributes to the high stability of microRNA expression[16]. We determined the expression of microRNAs in subcutaneous and perivascular adipose tissues of patients that underwent major amputation as a result of severe critical limb ischemia and in subcutaneous adipose tissue of control orthopaedic patients. We showed specific upregulation of 14q32 microRNAs in adipose tissues of amputation patients in two different study populations. These results demonstrate the potential of 14q32 microRNAs as biomarkers for the identification of patients at risk of major amputation. However, before these microRNAs can be used in the clinic as biomarker, these findings will have to be confirmed in studies with larger patient populations. Also, expression of 14q32 microRNAs in adipose tissue of amputation patients should be compared to 14q32 microRNA expression in adipose tissue of critical limb ischemia patients without

(the need for) major amputation to confirm whether 14q32 microRNA expression can be used to discriminate between critical limb ischemia patients at risk or not at risk of amputation. Nonetheless, this study demonstrates that local evaluation of microRNA expression can be used to predict disease outcome and these findings also suggest a role for 14q32 microRNAs in the complex interplay between adipose tissues and the vasculature.

In addition to the role of 14q32 microRNAs in processes of vascular remodelling, we should keep an open mind to the possible role of other non-coding RNAs from the 14q32 cluster in these processes. Besides the 54 microRNAs, the 14q32 region also encodes genes for other non-coding RNAs, namely long non coding RNAs (lncRNAs) and small nucleolar RNAs (snoRNAs).

LncRNAs are non-coding RNA transcripts, typically more than 200 nucleotides in length, that are involved in (amongst other) processes of epigenetic and transcriptional regulation[17, 18]. One of the 14q32 lncRNAs, Maternally Expressed Gene 3 (MEG3), is thought to control the imprinted expression of this cluster[20]. Using Meg3$^{-/-}$ models and case reports in humans, it has been suggested that MEG3 controls transcription of downstream microRNAs (and perhaps also lncRNAs and snoRNAs). Moreover, MEG3 was found to be upregulated in activated endothelial cells under hypoxia[19]. The function of MEG8 is less clear, whereas the small nucleolar RNA host gene 23 (SNHG23) is thought to give rise to the snoRNAs witin the 14q32 cluster.

SnoRNAs represent a class of non-coding RNA molecules which are located within the nucleoli of the cell or within specialized bodies called Cajal bodies[21]. SnoRNAs are typically between 60 and 300 nucleotides in length. Broadly, snoRNAs can be grouped into two different categories, based on their sequence and secondary structure. H/ACA box snoRNAs contain two conserved sequence motifs named the 'H-box' and 'AHA-box'. C/D box snoRNAs contain the conserved 'C-box' at their 5'end and a so called 'D-box' at their 3'end[22]. Generally, H/AHA box snoRNAs guide pseudouridylation of their target RNAs, while C/D box snoRNAs guide 2'O-methylation. In addition to these classical functions, snoRNAs have also been found to exert non-classical functions. These snoRNAs are referred to as 'orphan snoRNAs'. Within the cardiovascular field, snoRNAs were shown to influence metabolic stress, lipotoxicity and cholesterol transport[23, 24]. The function of 14q32 snoRNAs is still unknown. Although 14q32 snoRNAs have the conserved sequence motifs of 'C/D box' snoRNAs, these snoRNAs have no known RNA targets and thus belong to the category of 'orphan snoRNAs'. In humans, the 14q32 locus contains three highly related copy sets of SNORD112 (1 copy), SNORD113 (9 copies) and SNORD114 (31 copies). In mice, there are 7 equivalents for the 41 human snoRNAs, namely DQ267100, DQ267101, DQ267102, AF357355, AF357359, AF357425, and AF357426. Conservation between human and murine 14q32 snoRNAs is lower than for the 14q32 microRNAs. Preliminary data showed that murine 14q32 snoRNAs, like 14q32 microRNAs, follow distinct expression patterns after induction of ischemia and could be categorized into early responders, late responders and non-responders. Moreover, inhibition of murine snoRNAs DQ267100, DQ267102 and AF357426 using GSOs resulted in increased sprouting from aortic rings. These data suggest a role for 14q32 snoRNAs in vascular remodelling. Indeed, other studies have also demonstrated non-canonical roles for snoRNAs in procesess involved

in cardiovascular disease, namely metabolic stress, lipotoxicity and cholesterol trafficking[23, 24]. Future experiments will have to elucidate the role of 14q32 snoRNAs in vascular remodelling and their possible mechanisms of action.

In conclusion, this thesis provides novel insights on the role of 14q32 microRNAs in processes of vascular remodelling. Experimental studies have identified 14q32 microRNAs as potential therapeutic targets for treatment and prevention of atherosclerosis, restenosis and peripheral arterial disease.

Reference List

1. Hansson GK. Inflammation, atherosclerosis, and coronary artery disease. *N Engl J Med* 2005 Apr 21;352(16):1685-95.
2. Bennett MR. In-stent stenosis: pathology and implications for the development of drug eluting stents. *Heart* 2003 Feb;89(2):218-24.
3. Buschmann I, Schaper W. Arteriogenesis Versus Angiogenesis: Two Mechanisms of Vessel Growth. *News Physiol Sci* 1999 Jun;14:121-5.
4. Bartel DP. MicroRNAs: genomics, biogenesis, mechanism, and function. *Cell* 2004 Jan 23;116(2):281-97.
5. Bhagat L, Putta MR, Wang D, Yu D, Lan T, Jiang W, et al. Novel oligonucleotides containing two 3'-ends complementary to target mRNA show optimal gene-silencing activity. *J Med Chem* 2011 Apr 28;54(8):3027-36.
6. van Royen N, Hoefer I, Bottinger M, Hua J, Grundmann S, Voskuil M, et al. Local monocyte chemoattractant protein-1 therapy increases collateral artery formation in apolipoprotein E-deficient mice but induces systemic monocytic CD11b expression, neointimal formation, and plaque progression. *Circ Res* 2003 Feb 7;92(2):218-25.
7. Epstein SE, Stabile E, Kinnaird T, Lee CW, Clavijo L, Burnett MS. Janus phenomenon: the interrelated tradeoffs inherent in therapies designed to enhance collateral formation and those designed to inhibit atherogenesis. *Circulation* 2004 Jun 15;109(23):2826-31.
8. Schaper W, Winkler B. Of mice and men--the future of cardiovascular research in the molecular era. *Cardiovasc Res* 1998 Jul;39(1):3-7.
9. Snyder CM, Rice AL, Estrella NL, Held A, Kandarian SC, Naya FJ. MEF2A regulates the Gtl2-Dio3 microRNA mega-cluster to modulate WNT signaling in skeletal muscle regeneration. *Development* 2013 Jan 1;140(1):31-42.
10. Siomi H, Siomi MC. Posttranscriptional regulation of microRNA biogenesis in animals. *Mol Cell* 2010 May 14;38(3):323-32.
11. Krol J, Loedige I, Filipowicz W. The widespread regulation of microRNA biogenesis, function and decay. *Nat Rev Genet* 2010 Sep;11(9):597-610.
12. Fichtlscherer S, Zeiher AM, Dimmeler S. Circulating microRNAs: biomarkers or mediators of cardiovascular diseases? *Arterioscler Thromb Vasc Biol* 2011 Nov;31(11):2383-90.
13. Gebert LF, Rebhan MA, Crivelli SE, Denzler R, Stoffel M, Hall J. Miravirsen (SPC3649) can inhibit the biogenesis of miR-122. *Nucleic Acids Res* 2014 Jan;42(1):609-21.
14. Regulus Therapeutics. All HCV Patients Treated with a Single SC Administration of 4 mg/kg of RG-101 Responded with Mean Viral Load Reduction of 4.8 log10 at Day 29 and 9/14 Patients are Below the Limit of Quantification at Day 57; http://ir.regulusrx.com/releasedetail.cfm?ReleaseID=895314. 2015.
15. van Rooij E., Olson EN. MicroRNA therapeutics for cardiovascular disease: opportunities and obstacles. *Nat Rev Drug Discov* 2012 Nov;11(11):860-72.
16. Mitchell PS, Parkin RK, Kroh EM, Fritz BR, Wyman SK, Pogosova-Agadjanyan EL, et al. Circulating microRNAs as stable blood-based markers for cancer detection. *Proc Natl Acad Sci U S A* 2008 Jul 29;105(30):10513-8.
17. Mercer TR, Mattick JS. Structure and function of long noncoding RNAs in epigenetic regulation. *Nat Struct Mol Biol* 2013 Mar;20(3):300-7.
18. Rinn JL, Chang HY. Genome regulation by long noncoding RNAs. *Annu Rev Biochem* 2012;81:145-66.
19. Michalik KM, You X, Manavski Y, Doddaballapur A, Zornig M, Braun T, et al. Long noncoding RNA MALAT1 regulates endothelial cell function and vessel growth. *Circ Res* 2014 Apr 25;114(9):1389-97.
20. Gordon FE, Nutt CL, Cheunsuchon P, Nakayama Y, Provencher KA, Rice KA, et al. Increased expression of angiogenic genes in the brains of mouse meg3-null embryos. *Endocrinology* 2010 Jun;151(6):2443-52.
21. Kiss T. Small nucleolar RNA-guided post-transcriptional modification of cellular RNAs. *EMBO J* 2001 Jul 16;20(14):3617-22.
22. Filipowicz W, Pogacic V. Biogenesis of small nucleolar ribonucleoproteins. *Curr Opin Cell Biol* 2002 Jun;14(3):319-27.
23. Michel CI, Holley CL, Scruggs BS, Sidhu R, Brookheart RT, Listenberger LL, et al. Small nucleolar RNAs U32a, U33, and U35a are critical mediators of metabolic stress. *Cell Metab* 2011 Jul 6;14(1):33-44.
24. Brandis KA, Gale S, Jinn S, Langmade SJ, Dudley-Rucker N, Jiang H, et al. Box C/D small nucleolar RNA (snoRNA) U60 regulates intracellular cholesterol trafficking. *J Biol Chem* 2013 Dec 13;288(50):35703-13.

Nederlands Samenvatting

Introductie

Hart- en vaatziekten is een algemene term voor aandoeningen aan het hart en de bloedvaten. Hieronder vallen ziekten die een vernauwing van de bloedvaten tot gevolg hebben, zoals coronair vaatlijden (bij bloedvaten rondom het hart), cerebrovasculaire ziekten (bij bloedvaten in de hersenen) of perifeer vaatlijden (bij bloedvaten in de benen). De meest voorkomende oorzaak voor hart- en vaatziekten is atherosclerose of aderverkalking. Aderverkalking ontstaat doordat er in de loop van de jaren ophopingen (plaques) van cholesterol en ontstekingscellen verzamelen in de vaatwand. Dit leidt tot vernauwingen en uiteindelijk zelfs tot afsluitingen van de bloedvaten die de hersenen, hart of ledematen van bloed voorzien.

Patiënten met hart- en vaatziekten zijn erbij gebaat dat deze vernauwingen worden behandeld zodat de bloedtoevoer naar achterliggende weefsels weer hersteld wordt. Naast een gezonde levensstijl en de behandeling met medicijnen die de bloeddruk en het cholesterol verlagen, zijn er verschillende mogelijkheden om deze patiënten te behandelen. Dotteren is het oprekken van een bloedvat door middel van een ballonnetje. Hierdoor wordt de plaque weggedrukt en kan er weer bloed door het bloedvat stromen. Om te voorkomen dat het bloedvat na het oprekken weer terugveert, wordt er meestal een stent geplaatst. Een nadeel van deze ingreep is dat het dotteren leidt tot beschadiging van de vaatwand. Hierdoor ontstaat er een ontstekingsreactie waardoor de atherosclerotische plaque weer snel terug kan komen. Dit noemt men restenose. Een andere behandelmogelijkheid is een bypass operatie. Bij deze operatie wordt er door middel van een ander bloedvat een omleiding om de vernauwing geplaatst. Maar ook zo'n omleiding gaat bij sommige patiënten helaas snel weer dicht zitten.

Een alternatieve manier om de bloedstroom in patiënten te herstellen is door de vorming van bloedvaten door het lichaam zelf te stimuleren. Hierdoor ontstaan er 'natuurlijke' bypasses of omleidingen, zonder dat de patiënt geopereerd hoeft te worden. De vorming van nieuwe bloedvaten noemen we neovascularisatie. Er zijn verschillende manieren waarop bloedvaten kunnen ontstaan. Angiogenese en arteriogenese zijn de twee belangrijkste vormen van neovascularisatie. Bij angiogenese ontstaan er nieuwe bloedvaten uit bestaande bloedvaten. Angiogenese vindt plaats in gebieden met weinig zuurstof, zogenaamde ischemische gebieden. Bij arteriogenese ontstaan er geen nieuwe bloedvaten maar groeien bestaande kleine bloedvaten uit tot grote bloedvaten (collateralen). Deze collateralen kunnen meer bloed vervoeren dan de kleine bloedvaten.
Vaatwand remodellering is de algemene term waarmee processen beschreven worden die een verandering in de vaatwand (en vaak ook de bloedstroom) tot gevolg hebben. Hieronder vallen dus arteriogenese en angiogenese, maar ook atherosclerose en restenose.

MicroRNAs zijn kleine, niet-coderende RNA moleculen die de expressie van vele genen kunnen reguleren. Eén enkel microRNA kan de expressie van zijn targetgenen verlagen en op die manier complexe, fysiologische processen aansturen. Zo kunnen microRNAs ook processen van vaatwand remodellering reguleren. In dit proefschrift is de rol van één specifiek cluster van microRNAs, het 14q32 microRNA cluster, in vaatwand remodellering onderzocht.

Dit proefschrift

Het doel van dit proefschrift was om de rol van één specifiek microRNA cluster, welke in mensen gelegen is op chromosoom 14 (14q32; chromosoom 12F1 in muizen), in vaatwand remodellering te onderzoeken. MicroRNAs spelen een belangrijke rol bij vaatwand remodellering en eerdere studies hebben de rol van microRNAs in de pathofysiologie van deze processen beschreven. In **Hoofdstuk 2**

wordt een overzicht gegeven van de multifactoriële aard van microRNAs in processen van vaatwand remodellering. MicroRNAs kunnen de expressie van vele genen reguleren die belangrijk zijn voor vaatwand remodellering en op die manier veranderingen in de vaatwand stimuleren of remmen. Bij processen van vaatwand remodellering liggen vaak dezelfde onderliggende mechanismen en factoren ten grondslag. Dit is in het verleden aangetoond door de observatie dat interventies bedacht om arteriogenese te stimuleren, ook leidden tot het stimuleren van atherosclerose en andersom. Dit betekent dat meerdere processen van vaatwand remodellering beïnvloed zouden kunnen worden door hetzelfde microRNA. In Hoofdstuk 2 worden de microRNAs besproken die beschreven zijn een rol te spelen in minstens twee van de volgende processen: atherosclerose en/of restenose, angiogenese en/of arteriogenese en aneurysma vorming. De microRNAs die in dit hoofdstuk besproken worden zijn de individuele microRNAs miR-126 en miR-155 en de microRNA clusters 17-92, 23/24/27, 143/145 en 14q32. Het is interessant om op te merken dat enkele microRNAs waarvan beschreven is dat ze neovascularisatie stimuleren na ischemie, ook een remming van plaque formatie lieten zien in modellen voor atherosclerose. Deze eigenschap maakt die specifieke microRNAs een geschikte kandidaat als target voor de behandeling van cardiovasculaire ziekten.

14q32 microRNAs in vaatwand remodellering

In **Hoofdstuk 3** wordt de rol van 14q32 microRNAs in neovascularisatie na ischemie onderzocht. Om microRNAs te identificeren die een rol kunnen spelen bij post-ischemische neovascularisatie hebben wij gebruik gemaakt van een 'Reverse Target Prediction' model. Hiertoe zijn wij begonnen met het opstellen van een lijst met genen waarvan al bekend was dat ze een rol spelen in post-ischemische neovascularisatie (zowel arteriogenese als angiogenese). MicroRNAs binden aan specifieke locaties van hun target genen, de zogenaamde 3' untranslated region (3'UTR). Vervolgens hebben we bepaald welke microRNAs een mogelijke bindingsplaats voor deze genen hadden. Voor meerdere microRNAs van het 14q32 microRNA cluster vonden we een verrijking van voorspelde bindingsplaatsen in neovascularisatie-gerelateerde genen. In een *in vivo* muismodel voor neovascularisatie, waarbij ligatie van de arteria femoralis plaatsvindt, hebben wij de expressie van 14q32 microRNAs over de tijd vervolgd. MicroRNAs van het 14q32 cluster volgden drie verschillende expressie patronen tijdens neovascularisatie. De 14q32 microRNAs kunnen onderverdeeld worden in vroege responders, late responders en non-responders. Vroege responders waren binnen 24 uur na ligatie van de arteria femoralis opgereguleerd. Late responders werden pas72 uur na ligatie opgereguleerd , terwijl non-responders niet gereguleerd werden. Drie microRNAs, onder andere miR-329 (late responder), miR-494 (vroege responder) en miR-495 (non-responder), werden geselecteerd voor verder onderzoek op basis van hun expressie patroon en het aantal voorspelde neovascularisatie targetgenen. Als vierde microRNA werd miR-487b geselecteerd voor verder onderzoek, aangezien wij in een eerdere studie hebben laten zien dat dit microRNA een belangrijke rol speelt tijdens vaatwand remodellering van de aorta vaatwand.

De geselecteerde microRNAs werden vervolgens geremd door middel van zogenaamde Gene Silencing Oligonucleotides (GSOs). GSOs zijn een type microRNA-remmer, bestaande uit twee synthetische DNA strengen die omgekeerd complementair zijn aan het volwassen microRNA van interesse. GSOs werden geïnjecteerd in muizen 24 uur voordat dubbele ligatie van de arteria femoralis (achterpoot ischemie model) plaatsvond. Met behulp van fluorescent gelabelde GSOs hebben wij laten zien dat dit type microRNA-remmer in het spierweefsel van de aangedane achterpoot komt. Eén enkele injectie met GSOs tegen miR-329, miR-487b, miR-494 en miR-495 resulteerde in een beter en versneld herstel van de bloedtoevoer naar de achterpoot in vergelijking met controle dieren. Zowel arteriogenese als angiogenese werden gestimuleerd in de spierweefsels van GSO-behandelde muizen. Daarnaast

hebben wij *in vitro* en *in vivo* de regulatie van meerdere neovascularisatie targetgenen laten zien na microRNA remming. Tenslotte hebben wij *in vitro* bevestigd dat remming van 14q32 microRNAs miR-329, miR-487b, miR-494 en miR-495 leidt tot meer angiogenese en meer proliferatie van vasculaire celtypen.

Deze data bevestigen een rol voor 14q32 microRNAs miR-329, miR-487b, miR-494 en miR-495 in post-ischemische neovascularisatie en bieden mogelijke therapeutische targets om neovascularisatie te stimuleren.

Het is bekend dat het stimuleren van arteriogenese en angiogenese gepaard gaat met een inflammatoire reactie. Inflammatie is ook een belangrijk proces bij atherosclerose. In het verleden is aangetoond dat factoren die post-ischemische neovascularisatie stimuleren, ook de vorming van atherosclerotische plaques stimuleren. Dit ongewenste effect is beter bekend als het 'Janus fenomeen', refererend aan de gelijknamige Romeinse god met twee gezichten. Dit fenomeen is een ongewenst effect voor de ontwikkeling van therapieën die bedoeld zijn om de bloedtoevoer in patiënten met coronair of perifeer vaatlijden te herstellen (de andere kant van de medaille). Met behulp van dezelfde 'Reverse Target Prediction' methode zoals beschreven in Hoofdstuk 3, hebben wij in **Hoofdstuk 4** gezocht naar microRNAs die een rol spelen bij het ontstaan van atherosclerose. Wij observeerden wederom een groot aantal voorspelde bindingsplaatsen in atherosclerose-gerelateerde genen voor microRNAs van het 14q32 cluster. Vervolgens hebben wij, zoals beschreven in Hoofdstuk 3, de expressie van een aantal dezelfde 14q32 microRNAs, miR-329, miR-494 en miR-495, gemeten in humane atherosclerotische plaques. De expressie van vooral miR-494 was hoog in de atherosclerotische plaques, voornamelijk in plaques met een onstabiel fenotype. Daarnaast was miR-494 duidelijk aanwezig in verschillende organen van de muis die belangrijk zijn voor atherosclerose. MiR-494 werd daarom geselecteerd voor verder onderzoek in atherosclerose. Om dit te bestuderen werd de vorming van atherosclerotische plaques geïnduceerd in $ApoE^{-/-}$ muizen. Remming van miR-494 in deze muizen resulteerde in kleinere atherosclerotische plaques in vergelijking met controle muizen. Nog belangrijker is dat deze atherosclerotische plaques stabieler waren. Dit is gunstig aangezien stabiele plaques een kleinere kans hebben om te scheuren en zo de slagader af te sluiten. Remming van miR-494 zorgde verder voor een verlaging van het cholesterol in de behandelde dieren en leidde tot opregulatie van meerdere voorspelde target genen *in vivo*.

In deze studie laten wij zien dat remming van miR-494, waarvan we in een eerdere studie hebben laten zien dat dit post-ischemische neovascularisatie stimuleert, niet leidt tot een verergering van atherosclerose maar in plaats daarvan leidt tot kleinere en stabielere atherosclerotische plaques.

In **Hoofdstuk 5** hebben we de rol van 14q32 microRNAs miR-329, miR-494 en miR-495 in restenose onderzocht, ook een proces van vaatwand remodellering. Restenose bestaat uit door twee processen: intimale hyperplasie en versnelde atherosclerose. Intimale hyperplasie wordt gekarakteriseerd door veranderingen in de extracellulaire matrix, proliferatie van gladde spiercellen en inflammatie. Daarbovenop wordt versnelde atherosclerose waargenomen, voornamelijk onder hypercholesterolemische condities. Op basis van de studies beschreven in Hoofdstuk 3 en 4 verwachtten wij dat remming van 14q32 microRNAs tot minder restenose zou leiden in experimentele muis modellen. Intimale hyperplasie werd daarom bestudeerd in C57BL/6 muizen behandeld met GSOs tegen miR-329, miR-494 en miR-495. Remming van miR-495 zorgde voor minder intimale hyperplasie, minder influx van macrofagen (ontstekingscellen) en minder proliferatie van gladde spiercellen in de vaatwand vergeleken met controle muizen. Remming van miR-329 zorgde voor een

niet-significante vermindering van intimale hyperplasie, terwijl remming van miR-494 geen effect had op intimale hyperplasie. Vervolgens bestudeerden wij de rol van miR-329 en miR-495 remming op versnelde atherosclerose in ApoE$^{-/-}$ muizen. Remming van miR-329 leidde weer tot een niet-significante reductie van de atherosclerotische plaque, terwijl remming van GSO-495 resulteerde in significant kleinere atherosclerotische plaques in vergelijking met controle muizen. Hierbij observeerden wij regulatie van miR-495 target genen in zowel de carotiden als de milt van GSO-495 behandelde dieren. Tot slot zorgde remming van miR-495 voor een verlaging van de cholesterol spiegels in het bloed van behandelde dieren.

Samenvattend laat deze studie zien dat remming van miR-495 leidt tot minder restenose in experimentele muismodellen. Door twee verschillende muismodellen te gebruiken, konden wij de rol van miR-495 in zowel intimale hyperplasie als versnelde atherosclerose bestuderen. Hoewel de effecten beschreven in deze studie bescheiden zijn, laat deze studie juist zien dat de opsomming van al deze kleine veranderingen in gen expressie, maar ook gladde spiercel proliferatie, macrofaag influx en cholesterol levels, uiteindelijk een groot effect teweeg kan brengen.

(Post-)transcriptionele regulatie van 14q32 microRNA expressie

Een recente studie heeft laten zien dat expressie van enkele 14q32 microRNAs gereguleerd wordt door de transcriptiefactor Mef2a. In **Hoofdstuk 6** hebben wij de rol van Mef2a in post-ischemische neovascularisatie onderzocht en daarbij de transcriptionele regulatie van meerdere 14q32 microRNAs bestudeerd. Onze hypothese was dat remming van Mef2a zou leiden tot remming van 14q32 microRNAs en dus een positief effect zou hebben op post-ischemische neovascularisatie. Na remming van Mef2a met GSOs observeerden wij inderdaad een verbeterd herstel van de bloedtoevoer na dubbele ligatie van de arteria femoralis. Arteriogenese en angiogenese waren beide gestimuleerd in de spierweefsels van GSO-Mef2a behandelde dieren. Echter, alleen expressie van miR-329 en miR-494 bleek geremd na remming van Mef2a, terwijl miR-487b, miR-410 en miR-495 geen verschil in expressie vertoonden na Mef2a remming. Om te bepalen of Mef2a inderdaad de transcriptie van 14q32 microRNAs beïnvloedt, hebben wij de expressie levels van microRNA voorlopers bepaald. Daarvoor hebben wij de expressie van primaire microRNAs (pri-microRNAs) en precursor microRNAs (pre-microRNAs) gemeten. Er werden geen verschillen geobserveerd in de pri-microRNA en pre-microRNA levels van miR-329, miR-487b, miR-494 en miR-495 tussen GSO-Mef2a en controle behandelde dieren. Aangezien de pri-microRNA levels gelijk waren tussen GSO-Mef2a en GSO-controle behandelde dieren, vermoedden wij dat de effecten op miR-329 en miR-494 levels kwamen door andere mechanismen dan via regulatie van transcriptie. Preliminaire experimenten wekken de suggestie dat Mef2a betrokken is bij post-transcriptionele regulatie van 14q32 microRNAs. Met behulp van RNA-binding protein (RBP) immunoprecipitation (RIP) assays, observeerden wij binding van Mef2a aan pri-microRNA transcripten van miR-494. Binding van Mef2a zagen wij niet aan pri- of pre-microRNAs van miR-487b, één van de microRNAs die geen verschil liet zien in expressie levels na Mef2a remming.

In Hoofdstuk 6 laten laten wij zien dat remming van Mef2a het herstel van bloedtoevoer in muizen na inductie van ischemie bevordert. De expressie levels van miR-329 en miR-494 gaan omlaag na Mef2a remming. Het lijkt erop dat deze remming wordt bewerkstelligd door post-transcriptionele regulatie van deze microRNAs door Mef2a. Wij laten hier voor de eerste keer zien dat Mef2a kan functioneren als RNA-binding protein bij de post-transcriptionele regulatie van 14q32 microRNAs.

In **Hoofdstuk 7** gaan wij verder in op de mechanismen die expressie van 14q32 microRNAs kunnen reguleren. Er zijn enkele aanwijzingen dat 14q32 microRNAs gereguleerd worden op post-

transcriptioneel niveau. Zoals beschreven in Hoofdstuk 3, worden 14q32 microRNAs gereguleerd volgens drie verschillende expressie-patronen tijdens vaatwand remodellering. Deze expressie-patronen zijn onafhankelijk van de locatie van de microRNA genen op het chromosoom, aangezien de genen die coderen voor vroege, late en non-responders op dit genomische gebied allemaal door elkaar liggen. Daarnaast zijn er ook grote verschillen in de basale expressie levels van 14q32 microRNAs.

RNA-binding proteins (RBPs) zijn eiwitten die een rol kunnen spelen bij de vorming van microRNAs. MicroRNAs worden afgeschreven van microRNA genen en vormen zo eerst primaire microRNAs (pri-microRNAs). Deze pri-microRNAs worden geknipt tot precursor microRNAs (pre-microRNAs). In een volgende stap wordt dit pre-microRNA geknipt tot een (volwassen) microRNA. RBPs kunnen de knip-stappen van pri-microRNA tot pre-microRNA en pre-microRNA tot microRNA beïnvloeden. In dit hoofdstuk laten wij zien dat expressie van 14q32 microRNAs waarschijnlijk voornamelijk gereguleerd wordt in de pre-microRNA naar volwassen microRNA stap. Met daaropvolgende experimenten demonstreerden wij dat twee RBPs, genaamd CIRBP en HADHB, binden aan pre-microRNA-329. Met behulp van immunohistochemische kleuring konden wij de aanwezigheid van deze eiwitten in spierweefsel van muizen bevestigen. Daarnaast observeerden wij een verhoogde expressie van CIRBP en HADHB in ischemisch spierweefsel, 72 uur na inductie van ischemie door middel van dubbele ligatie van de arteria femoralis. Met behulp van RIP-experimenten demonstreerden wij tot slot dat CIRBP specifiek bindt aan het pre-microRNA van miR-329 maar niet aan het pri-microRNA. Deze data demonstreren een rol voor CIRBP in de post-transcriptionele regulatie van het 14q32 microRNA miR-329.

Deze studie laat zien dat 14q32 microRNAs gereguleerd worden op post-transcriptioneel niveau door twee RBPs, CIRBP en HADHB. Hiermee biedt deze studie nieuwe inzichten in de regulatie van expressie van 14q32 microRNAs na ischemie.

14q32 microRNA expressie in subcutaan vetweefsel

Biomarkers zijn (makkelijk) meetbare stoffen die een indicatie geven over de aanwezigheid of ernst/stadium van een bepaalde ziekte. Dergelijke markers kunnen gebruikt worden om ziekten in een vroeg stadium op te sporen maar ook om de ziekteprogressie en uitkomst te voorspellen.

Perifeer vaatlijden zal zich in een deel van de patiënten verder ontwikkelen tot kritieke ischemie. Bij kritieke ischemie zijn er pijnklachten in de voet of been bij rust en is er sprake van slechte wondgenezing. Een deel van deze patiënten ondergaat binnen enkele jaren amputatie van het onderbeen. Voor deze groep patiënten is het aantal behandelingsopties beperkt. Daarnaast is er vooralsnog geen betrouwbare biomarker om het ontstaan en het verloop van perifeer vaatlijden te voorspellen. In **Hoofdstuk 8** hebben wij expressie van microRNAs in zowel subcutaan als perivasculair vetweefsel bepaald van patiënten die een onderbeenamputatie ondergingen als gevolg van kritieke ischemie. MicroRNA expressie in deze weefsels werd vergeleken met de expressie in subcutaan vetweefsel van gezonde controle patiënten die electieve orthopedische chirurgie ondergingen. Expressie van microRNAs was voornamelijk verlaagd in vetweefsel van kritieke ischemie patiënten in vergelijking met gezonde controles. Echter, een aantal microRNAs liet juist een verhoogde expressie zien in vetweefsels van patiënten met kritieke ischemie in vergelijking met gezonde controles. Deze microRNAs waren miR-127, miR-134, miR-370, miR-376c, miR-411, miR-539, miR-886-3p en miR-146b. Opvallend was dat zes van de acht microRNAs die verhoogd waren behoren tot het 14q32 microRNA cluster. Tevens konden wij significante verhoging van deze 14q32 microRNAs miR-127, miR-134, miR-370, miR-376c, miR-411 en miR-539 bevestigen in zowel subcutaan als perivasculair vetweefsel in twee onafhankelijke studie populaties.

Met deze studie laten we zien dat de lokale expressie van microRNAs in vetweefsel gebruikt kan worden als biomarker om patiënten met kritieke ischemie te identificeren. Vervolgstudies moeten uitwijzen of deze microRNAs gebruikt kunnen worden om onderscheid te maken tussen patiënten met kritieke ischemie die het risico lopen om amputatie te ondergaan en patiënten met kritieke ischemie die nog verder behandeld kunnen worden.

Conclusie

In dit proefschrift laat ik de rol van 14q32 microRNAs in verschillende processen van vaatwand remodellering zien. De experimentele data leveren nieuwe inzichten en kennis in de regulatie van 14q32 microRNAs en demonstreren de mogelijkheid om 14q32 microRNAs te gebruiken als potentiële therapeutische targets voor de behandeling en preventie van atherosclerose, restenose en perifeer vaatlijden.

List of Publications

Oleaga C, Welten S, Belloc A, Solé A, Rodriguez L, Mencia N, Selga E, Tapias A, Noé V, Ciudad CJ. Identification of novel Sp1 targets involved in proliferation and cancer by functional genomics. *Biochem Pharmacol.* 2012 Dec 15;84(12):1581-91.

Bastiaansen AJ, Ewing MM, de Boer HC, van der Pouw Kraan TC, de Vries MR, Peters EA, Welten SM, Arens R, Moore SM, Faber JE, Jukema JW, Hamming JF, Nossent AY, Quax PH. Lysine acetyltransferase PCAF is a key regulator of arteriogenesis. *Arterioscler Thromb Vasc Biol.* 2013 Aug;33(8):1902-10.

Nossent AY, Eskildsen TV, Andersen LB, Bie P, Brønnum H, Schneider M, Andersen DC, Welten SM, Jeppesen PL, Hamming JF, Hansen JL, Quax PH, Sheikh SP. The 14q32 microRNA-487b targets the antiapoptotic insulin receptor substrate 1 in hypertension-induced remodeling of the aorta. *Ann Surg.* 2013 Nov;258(5):743-51

Bastiaansen AJ, Karper JC, Wezel A, de Boer HC, Welten SM, de Jong RC, Peters EA, de Vries MR, van Oeveren-Rietdijk AM, van Zonneveld AJ, Hamming JF, Nossent AY, Quax PH. TLR4 accessory molecule RP105 (CD180) regulates monocyte-driven arteriogenesis in a murine hind limb ischemia model. *PLoS One.* 2014 Jun 19;9(6):e99882.

Welten SM, Bastiaansen AJ, de Jong RC, de Vries MR, Peters EA, Boonstra MC, Sheikh SP, La Monica N, Kandimalla ER, Quax PH, Nossent AY. Inhibition of 14q32 MicroRNAs miR-329, miR-487b, miR-494, and miR-495 increases neovascularization and blood flow recovery after ischemia. Circ Res. 2014 Sep 26;115(8):696-708.

Wezel A, Welten SM, Razawy W, Lagraauw HM, de Vries MR, Goossens EA, Boonstra MC, Hamming JF, Kandimalla ER, Kuiper J, Quax PH, Nossent AY, Bot I. Inhibition of MicroRNA-494 Reduces Carotid Artery Atherosclerotic Lesion Development and Increases Plaque Stability. Ann Surg. 2015 Nov;262(5):841-7; discussion 847-8.

Welten SM, Quax PH, Nossent AY. Letter regarding article, "MicroRNA-155 exerts cell-specific antiangiogenic but proarteriogenic effects during adaptive neovascularization". *Circulation.* 2015 Dec 8;132(23):e375.

Welten SM, Goossens EA, Quax PH, Nossent AY. The multifactorial nature of microRNAs in vascular remodelling. *Cardiovasc Res.* 2016 May 1;110(1):6-22

Inhibition of 14q32 microRNA miR-495 reduces lesion formation, intimal hyperplasia and plasma cholesterol levels in experimental restenosis. Welten SM, de Jong RC, Wezel A, de Vries MR, Boonsta MC, Peters HA, Jukema JW, van der Sluis TC, Arens R, Bot I, Agrawal S, Quax PH, Nossent AY. *Submitted for publication.*

Welten SM, de Vries MR, Peters HA, Agrawal S, Quax PH, Nossent AY. Inhibition of Mef2a enhances post-ischemic neovascularization via 14q32 microRNAs miR-329 and miR-494. *Submitted for publication.*

Welten SM, Longchamp A, Tao M, Kielbasa SM, Quax PH, Ozaki CK, Nossent AY. Upregulation of 14q32 microRNAs in human subcutaneous adipose tissue samples of patients with critical limb ischemia undergoing major amputation. *Submitted for publication.*

de Vries MR, Trompet S, Welten SM, van der Kwast RV, Boon RA, Agrawal S, Jukema JW, Quax PH, Nossent AY. Evidence for an Independent Role of 14q32 snoRNAs in Human Cardiovascular Disease. *Submitted for publication.*

Nossent AY, Bastiaansen AJ, Peters HA, de Vries MR, Aref Z, Welten SM, de Jager SC, van der Pouw Kraan TC, Quax PH. The CCR7-CCL19/CCL21 Axis is Essential for Effective Arteriogenesis in a Murine Model of Hindlimb Ischemia *Submitted for publication*

Welten SM, Downie Ruiz Velasco A, Quax PH, Michlewski G, Nossent AY. Posttranscriptional regulation of 14q32 microRNA miR-329 during vascular regeneration after ischemia. *Manuscript in preparation.*

Curriculum Vitae

Sabine Marlies Janine Welten werd geboren op 5 januari 1988 in Amsterdam. Na het cum laude behalen van haar VWO diploma in 2006 aan het Bernardinus College te Heerlen startte zij met haar studie Biomedische Wetenschappen in Leiden. Gedurende haar studie heeft zij aan diverse medisch wetenschappelijke onderzoeken meegewerkt, zowel binnen verschillende afdeling van het Leids Universitair Medisch Centrum als in het buitenland. In 2009 ging zij voor twee maanden naar Taiwan voor een onderzoeksstage aan het National Defense Medical Center in Taipei. In augustus 2010 behaalde zij haar Bachelor diploma. September 2010 tot Januari 2011 deed zij haar eerste masterstage aan de afdeling Moleculaire Biologie en Biochemie van de Universiteit van Barcelona onder begeleiding van Prof. C. Ciudad. Dit resulteerde in haar eerste wetenschappelijke publicatie. Van September 2011 tot Mei 2012 deed zij haar afstudeerstage op de afdeling Vaatchirurgie van het Leids Universitair Medisch Centrum. In mei 2012 studeerde zij af als Master of Science. Aansluitend startte zij haar promotieonderzoek op de afdeling Vaatchirurgie van het LUMC onder leiding van dr. A.Y. Nossent en Prof. P.H.A. Quax, waar zij het onderzoek van haar afstudeerstage heeft voortgezet en waarvan de resultaten in dit proefschrift beschreven zijn. Dit onderzoek was onderdeel van een door het ‘ Netherlands Institute for Regenerative Medicine’ (NIRM) gefinancierd project. Tijdens haar promotietraject heeft Sabine meegewerkt aan het organiseren van de LUMC PhD day 2013, een carriere dag voor promovendi. Van Juni 2016 tot en met Augustus 2016 was Sabine werkzaam bij de Commissie Medische Ethiek van het Leids Universitair Medisch Centrum gewerkt. In dezelfde periode rondde zij haar proefschrift af. Sinds September 2016 is Sabine werkzaam als Consultant Life Sciences bij ttopstart BV, te Bilthoven. In Juni 2017 zal zij met haar verloofde Peter trouwen en zullen zij hun eerst gekochte huis in Breukelen betrekken.